VNIVERSITAT DE VALÈNCIA

Departamento de Física Teórica, UV – IFIC (CSIC)

Neutrino masses and dark matter: a path to new physics

PhD thesis by

Juan Andrés Herrero García

Under the supervision of

Nuria Rius Dionis

Arcadi Santamaria i Luna

Valencia, June 2014

NURIA RIUS DIONIS, profesora titular del Departamento de Física Teórica de la Universidad de Valencia, y

ARCADI SANTAMARIA I LUNA, catedrático del Departamento de Física Teórica de la Universidad de Valencia,

Certifican:

Que la presente memoria, "NEUTRINO MASSES AND DARK MATTER: A PATH TO NEW PHYSICS" ha sido realizada bajo su dirección en el Instituto de Física Corpuscular, centro mixto de la Universidad de Valencia y del CSIC, por JUAN ANDRÉS HERRERO GARCÍA, y constituye su Tesis para optar al grado de Doctor en Ciencias Físicas.

Y para que así conste, en cumplimiento de la legislación vigente, presenta en el Departamento de Física Teórica de la Universidad de Valencia la referida Tesis Doctoral, y firman el presente certificado, en

Valencia, 10 de Mayo de 2014

Nuria Rius Dionis

Arcadi Santamaria i Luna

A mis padres

If you can dream - and not make dreams your master...
If you can meet with Triumph and Disaster
and treat those two impostors just the same...
If you can talk with crowds and keep your virtue,
or walk with kings - nor lose the common touch...
Yours is the Earth and everything that is in it,
And -which is more- you will be a Man my son!

Rudyard Kipling

Every man dies, not every man really lives.

William Wallace - Braveheart

El cerebro no está para descubrir la verdad, sino para hacer predicciones para poder sobrevivir.

Richard Gregory, profesor emérito de neuropsicología de la U. Bristol.

El destino es el que baraja las cartas, pero somos nosotros los que jugamos.

Shakespeare

Nada más cumplir siete tuve que interrumpir mi educación para ir a la escuela.

Bernard Shaw

Es mejor tener la boca cerrada y parecer estúpido que abrirla y disipar la duda.

Mark Twain

La edad de piedra no se acabó porque se acabaran las piedras.

Jeque Yamani

Es más fácil desintegrar un átomo que un prejuicio.
No entiendes realmente algo a menos que seas capaz de explicárselo a tu abuela.

Albert Einstein

Jamás diga una mentira que no pueda probar.

Millor Fernandes

Sólo creo en las estadísticas que yo mismo falsifico.

Winston Churchill

Robar un banco no es nada comparado con fundarlo.

Bertolt Brecht

Gasté mucho dinero en licor, mujeres, juergas y coches deportivos. El resto, lo desperdicié.

George Best

En aprender cómo se juega al póker se tarda un minuto, en controlar los aspectos del juego toda una vida.

Mike Sexton

Y ganar, ganar, ganar, y volver a ganar, ganar ganar, y volver a ganar, ganar, ganar...

Luis Aragonés

List of publications

This PhD thesis is based on the following publications:

- *On the nature of the fourth generation neutrino and its implications* [1]
  A. Aparici, J. Herrero-Garcia, N. Rius and A. Santamaria.
  JHEP **1207** (2012) 030

- *Neutrino masses from new generations* [2]
  A. Aparici, J. Herrero-Garcia, N. Rius and A. Santamaria.
  JHEP **1107** (2011) 122

- *The Zee-Babu model revisited in light of new data* [3]
  J. Herrero-Garcia, M. Nebot, N. Rius and A. Santamaria.
  sent to NPB

- *On the annual modulation signal in dark matter direct detection* [4]
  J. Herrero-Garcia, T. Schwetz and J. Zupan.
  JCAP **1203** (2012) 005

- *Astrophysics independent bounds on the annual modulation of dark matter signals'* [5]
  J. Herrero-Garcia, T. Schwetz and J. Zupan.
  Phys.Rev.Lett. 109 141301

- *Halo-independent methods for inelastic dark matter scattering* [6]
  N. Bozorgnia, J. Herrero-Garcia, T. Schwetz and J. Zupan.
  JCAP **1307** (2013) 049

and the following contributions to proceedings:

- *Can New Generations Explain Neutrino Masses?* [7]
  A. Aparici, J. Herrero-Garcia, N. Rius and A. Santamaria.
  Moriond proceedings

- *Implications of new generations on neutrino masses* [8]
  A. Aparici, J. Herrero-Garcia, N. Rius and A. Santamaria.
  J.Phys.Conf.Ser. 408 012030 (2013)

Other works not included in this thesis:

- *Neutrino masses, Grand Unification, and Baryon Number Violation* [9]
  A. de Gouvea, J. Herrero-Garcia and A. Kobach.
  sent to PRD

Abbreviations

The following abbreviations have been used throughout the text:

SM Standard Model

BSM beyond the Standard Model

HEP high energy physics

SSB spontaneous symmetry breaking

VEV vacuum expectation value

EFT effective field theory

EWS electroweak scale

EWSB electroweak symmetry breaking

LFV lepton flavour violation

LN lepton number

LNV lepton number violation

NP new physics

QCD Quantum Chromodynamics

QED Quantum Electrodynamics

QFT Quantum Field Theory

0$\nu\beta\beta$ neutrinoless double beta decay

CL confidence level

LHC Large Hadron Collider

PMNS Pontecorvo-Maki-Nagakawa-Sakata (or lepton mixing) matrix

NH Normal Hierarchy

IH Inverted Hierarchy

QD quasi-degenerate spectrum

CKM Cabibbo-Kobayashi-Maskawa (or quark mixing) matrix

DM dark matter

CDM cold dark matter

WDM warm dark matter

DE dark energy

ΛCDM Cosmological Model (Λ: cosmological constant, **CDM**: cold dark matter)

FLRW metric Friedmann-Lemaitre-Robertson-Walker metric

GR General Relativity

RD radiation-domination

MD matter-domination

MW Milky Way

MOND Modified Newtonian Dynamics

f.o. freeze-out

WIMP Weakly Interacting Massive Particle

SHM Standard Halo Model

SI spin-independent

SD spin-dependent

IV isospin-violating

SHM Standard Halo Model

Resumen

Resumimos aquí en castellano la investigación realizada en esta tesis doctoral, las principales conclusiones obtenidas y la estructura de la misma.

Esta tesis doctoral se ha centrado en dos de las evidencias más convincentes para la necesidad de física más allá del Modelo Estándar (SM): las masas de los neutrinos y la materia oscura (DM). La escala de esta nueva física (NP) es completamente desconocida, por lo que hemos adoptado un enfoque fenomenológico, con su testabilidad como un objetivo primordial. En este sentido, nos hemos centrado en los modelos radiativos de masas de neutrinos, a la escala del TeV, y se ha supuesto que la materia oscura es una partícula masiva de interacción débil (WIMP), de masa $\mathcal{O}(1 - 10^3)$ GeV.

La primera parte de la tesis se dedica al estudio de modelos de masas de neutrinos generadas radiativamente. Éstos explican por qué las masas de los neutrinos son mucho menores que las del resto de los fermiones: los neutrinos no tienen masa a nivel árbol, siendo su masa generada radiativamente a uno, dos o tres loops (más loops típicamente producen masas de los neutrinos demasiado pequeñas y/o tienen problemas con las restricciones que vienen de no observar procesos que violen sabor (LFV) en leptones cargados). Además, gracias a la supresión de los loops y a la presencia obligatoria de varios acoplamientos para violar número leptónico (LN), estos modelos tienen partículas a una escala lo suficientemente baja como para dar señales en colisionadores, como el LHC, y en los experimentos de baja energía como los que buscan $\mu \to e\gamma$ o $0\nu\beta\beta$.

En esta tesis se ha estudiado la generación de la masa de los neutrinos radiativamente a dos loops, tanto a través de nuevos fermiones (nuevas familias) como de nuevos escalares (el modelo Zee-Babu). También se estudió la conexión de estos modelos de masas de neutrinos con otras ramas de física de altas energías, como la física del Higgs, ya sea indirectamente, por ejemplo a través de modificaciones de la señal de $H \to \gamma\gamma$, o directamente, a través de la detección de las nuevas partículas.

En los primeros trabajos, se estudió en detalle la posibilidad de la existencia de una cuarta generación secuencial del SM, abordando en particular las

propiedades de los neutrinos ligeros y su naturaleza [1]. El neutrino de la cuarta generación debe ser mucho más pesado que los otros, por lo que la opción más plausible es la existencia de un neutrino dextrógiro para darle masa. Nos dimos cuenta de que si los neutrinos ligeros son partículas de Majorana, hay una contribución a la masa de Majorana de este neutrino dextrógiro a dos loops. Por lo tanto, el neutrino de la cuarta generación también debe ser Majorana, a menos que se imponga cierta simetría en los leptones de la cuarta generación.

Se analizaron en detalle las posibles implicaciones de tener un neutrino pesado de Majorana de la cuarta generación. En particular, se generan masas de los neutrinos ligeros a dos loops, y esta contribución puede superar fácilmente el límite cosmológico de la escala de masa absoluta de los neutrinos.

Sin embargo, incluso si hay una contribución a las masas de los neutrinos ligeros, su espectro no se puede explicar con una única familia adicional. Por lo tanto, en un trabajo diferente, se estudió la posibilidad de que los neutrinos ligeros fueran sin masa a nivel árbol, con sus masas generadas a dos loops por la acción de los nuevos fermiones, por ejemplo, con dos generaciones adicionales [2].

Actualmente, gracias al LHC, la existencia de nuevas generaciones secuenciales de partículas ha sido descartada, al menos si el sector escalar comprende sólo el bosón de Higgs del SM, debido al hecho de que la producción del bosón de Higgs aumenta con la presencia de los nuevos fermiones (y también sus desintegraciones varían significativamente si existe una nueva familia). Existen algunas posibilidades que pueden salvar a la cuarta generación, como un sector escalar mayor, por ejemplo, con un doblete de Higgs adicional que sólo se acopla a la cuarta familia [10]. Aun así, cotas a los fermiones de la cuarta generación están muy cerca del límite perturbativo: en el caso de los quarks $\gtrsim 600$ GeV, véase, por ejemplo, [11].

En otro trabajo hemos revisado el modelo de Zee-Babu [3] a la luz de los nuevos datos, por ejemplo, el ángulo de mezcla θ_{13}, el nuevo bound de $\mu \to e\gamma$ y los resultados del LHC. También se analiza la posibilidad de explicar las desviaciones respecto al SM en $H \to \gamma\gamma$ vista por ATLAS (aunque no es una desviación significativa).

Nos encontramos con que los datos de oscilación de neutrinos y las restricciones de bajas energías siguen siendo compatibles con masas de los nuevos escalares accesibles al LHC. Si alguno de los escalares es descubierto, el modelo puede ser falsable por la combinación de información sobre los modos de desintegración con los datos de neutrinos. Por el contrario, si se encuentra que el espectro de neutrinos es invertido y la fase CP δ es muy diferente de $\sim \pi$, las masas de los escalares cargados estarán fuera del alcance del LHC.

En un sentido amplio, se ha tratado de arrojar algo de luz sobre las diferentes formas de generar masas de los neutrinos radiativamente, centrándonos en que fueran comprobables, siempre con la mirada puesta en las posibles señales en el LHC, y en su conexión con otras ramas de la física de altas energías. Esperemos que, con más información experimental, la naturaleza nos ayude a averiguar de qué forma entre la larga lista de posibilidades ganan masa los neutrinos. Por el momento, podemos decir que las familias adicionales se encuentran *en muy mal estado*, mientras que el modelo de Zee-Babu sigue *vivo* y listo para ser descubierto en el LHC!

Respecto a la DM, nos hemos dedicado al estudio de los límites que pueden ponerse en su modulación anual. Si la DM son partículas que interaccionan débilmente con el SM (WIMPs), pueden ser observadas en experimentos de detección directa. Éstos son muy difíciles de realizar, ya que el número de eventos esperado de la DM es muy bajo y las señales del fondo son muy grandes, incluso cuando los experimentos se colocan en laboratorios a mucha profundidad y debidamente blindados.

La modulación anual que debe estar presente en la señal de experimentos de detección directa, debido al movimiento relativo de la Tierra alrededor del Sol, podría ayudar a discriminar una señal de DM del fondo (algunas señales de fondo modulan, como los muones, pero la fase no tiene por qué coincidir con la esperada de DM, ver capítulo 6).

Un punto importante a tener en cuenta en la interpretación de una señal DM es que las tasas de eventos están sujetas a incertidumbres astrofísicas, como la distribución de velocidades de la DM, la densidad local o la velocidad de escape, por lo que es importante ser lo más independiente de los parámetros astrofísicos como sea posible. Ésto se puede hacer representando la integral de la distribución de velocidades dividida entre la velocidad ($\eta(v_m, t)$, dónde v_m es la mínima velocidad necesaria para producir un retroceso nuclear de una energía dada, véase eq. 6.10) de los diferentes experimentos en el mismo rango de velocidades (v_m).

En esta tesis, hemos deducido restricciones a la modulación anual en términos de la tasa total de eventos (no modulada), que son casi independientes de las incertidumbres astrofísicas, mediante el desarrollo de $\eta(v_m, t)$ a primer orden en la velocidad, $v_e(t)/v$, donde $v_e(t)$ es la velocidad de la Tierra alrededor del Sol y v es la velocidad de la DM. Este test es una prueba importante que cualquier señal de modulación anual tiene que pasar.

Aplicamos estos límites a las modulaciones vistas por DAMA y CoGeNT [4], y obtuvimos que la modulación de DAMA es compatible con su tasa constante, mientras que la de CoGeNT está excluida para halos típicos de DM a $\gtrsim 90\%$ CL.

En un segundo trabajo demostramos como las cotas de la modulación

de un experimento en función de su tasa constante, obtenidas en el anterior trabajo, pueden aplicarse entre experimentos diferentes, en el mismo rango de velocidades (v_m). Los aplicamos a la modulación de DAMA frente a los resultados nulos de XENON, CDMS y otros experimentos [5]. Una interpretación en términos de DM de la modulación de DAMA está desfavorecida por al menos un experimento en más de 4σ, para una masa de la DM $\lesssim 15$ GeV, para todo tipo de interacciones.

También hemos ampliado el análisis al caso de dispersión inelástica [6], mostrando como DAMA es incompatible con XENON 100 también en este caso.

En un sentido amplio, hemos hallado límites independientes de la astrofísica que las modulaciones anuales tienen que cumplir. Con suerte, este tipo de pruebas va a ayudar a discriminar entre señales verdaderas de DM y fondos. Es importante destacar que es una condición necesaria para que la modulación sea de DM, pero no suficiente. Después de aplicar los límites a las modulaciones anuales de DAMA y CoGeNT y compararlos con los otros experimentos que no ven DM, éstas están muy desfavorecidas interpretadas como debidas a DM. Esperamos que en los próximos años más datos experimentales ayuden a clarificar la actual situación, que es confusa, y esperemos que la DM esté allí fuera lista para ser descubierta de una manera u otra!

La tesis (ya en inglés, el lenguaje científico por excelencia) está estructurada de la siguiente forma. Comienza con la motivación de la necesidad de nueva física (NP) en la parte I. Como los dos temas principales de esta tesis, las masas de los neutrinos y la materia oscura, aunque son dos de las formas más interesantes para buscar NP, son muy diferentes en la naturaleza[1], hemos dividido la tesis en dos partes independientes.

En la parte II damos una introducción al tema de la masa de los neutrinos. Después de una breve introducción al SM en el capítulo 1, y al uso de teorías efectivas (EFT) con el Operador Weinberg en mente, se estudia la fenomenología de neutrinos en el capítulo 2, dando una introducción a la violación de número leptónico (LNV). Antes de proponer cualquier cosa, uno tiene que saber lo que hay ya propuesto, y el capítulo 3 intenta realizar esta tarea, con una revisión de algunos de los modelos más populares de la literatura.

La parte III es una introducción al tema de la materia oscura (DM). Tras una corta descripción del modelo cosmológico en el capítulo 4, motivamos la necesidad de materia oscura, enumerando sus propiedades y revisando brevemente la posibilidad de detectarla de forma indirecta y en colisionadores

[1] Al menos en principio, aunque puede haber conexiones entre ellos, véase el modelo del doblete inerte en el capítulo 3, sección 3.6.2.

en el capítulo 5. En el capítulo 6 nos centramos en la detección directa de la DM, en su modulación anual, presentando un análisis de la distribución de velocidades y una forma de presentar los datos que es independiente de la astrofísica, y terminando con un breve resumen de la situación experimental en detección directa de DM.

En la parte IV, hacemos un resumen de los resultados obtenidos y algunas observaciones finales sobre la investigación realizada. Por último, en la parte V presentamos una copia de los artículos de investigación realizados para esta tesis, tal y como se publican en las diferentes revistas. Estos artículos resumen la principal labor de investigación realizada estos años, y la discusión, la interpretación de los resultados y las conclusiones de cada uno de los trabajos presentados son de importancia, siendo lo presentado aquí (y en la parte IV) únicamente un conciso resumen de las mismas.

Preface

In this doctoral thesis we have focused on two of the most compelling evidences for physics beyond the Standard Model (SM): neutrino masses and dark matter (DM). The new physics scale regarding these two topics is completely unknown, so we have adopted a phenomenological approach, with testability as a prime goal. In this sense, we have focused on TeV scale neutrino mass models (radiative) and we have assumed that DM is a Weakly Interacting Massive Particle, WIMP, with mass $\mathcal{O}(1 - 10^3)$ GeV.

We start the thesis by motivating the need for new physics (NP) in part I. As the two main topics of this thesis, neutrino masses and DM, while being two of the more interesting ways to look for NP, are quite different in nature[2], we have divided the thesis into two independent parts.

In part II we give an introduction to the topic of neutrino masses. After a brief introduction to the SM in chapter 1, and the use of effective theories (EFT) with the Weinberg Operator in mind, we study the phenomenology of neutrinos in chapter 2, giving an introduction to the topic of lepton number violation (LNV). Before proposing a new model, one needs to know what has already been studied in the literature, and chapter 3 tries to accomplish this task, with a review of some of the most popular models.

In part III we give an introduction to the topic of DM. After a brief introduction to the Cosmological Model in chapter 4, we motivate the need for DM, enumerating its properties and reviewing briefly the possibility of detecting it indirectly and in colliders in chapter 5. In chapter 6 we focus on direct detection of DM, introducing the concepts of event rate and annual modulation signal, and discussing the velocity distribution and how data can be presented in an astrophysics-independent way. We finish by discussing the experimental results of DM direct detection.

Regarding the research done on neutrino masses, we have analysed radiative neutrino mass models with extra fermions/scalars (in the context of new generations and the Zee-Babu model), looking for connections with other NP

[2]At least in principle, although there are several proposed connections and interplays between them. As a nice example, see the inert doublet model in chapter 3, section 3.6.2.

scenarios. With respect to DM, we have focused on one of the fundamental ways to discover it, which is its direct detection, and, in particular, we have studied the annual modulation signal and bounds that can be placed on it. In part IV, we give a summary of the results obtained and some concluding remarks on the research done.

Finally, in part V we present a copy of the research articles done for this thesis, as published in the different journals. This is the main research done in this thesis, and the discussion, interpretation of the results and the conclusions of each of the works presented are of relevance, with the conclusions presented in IV being a concise summary of them.

Contents

Part I

Introduction: new physics is needed

From $\sim 10^{-10}$ s up to today, at $\sim 10^{17}$ s, (or equivalently in energy, from the ∼TeV to the current temperature, given by the Cosmic Microwave Background (CMB), $\sim 10^{-4}$ eV) the history of the Universe is based on well known laws of physics[3]. Before $\sim 10^{-10}$ s, or equivalently above the TeV, up to the Planck scale at $\sim 10^{16}$ TeV, almost nothing is known.[4]

At low scales (high energies, but below the electroweak scale (EWS), $\sim \mathcal{O}(100)$ GeV), the Standard Model (SM) of particle physics, which we will review in chapter 1, section 1.1, describes almost all known particle physics processes, and has been tested with great accuracy both in the quark and in the lepton sectors. In addition, with the discovery of the Higgs boson [13, 14], its missing piece responsible for the breaking of electroweak symmetry (EWSB), it seems a complete theory.

At large scales (low energies), the ΛCDM Model, based on General Relativity and on the Cosmological Principle, that we will review in chapter 4, section 4.1, is a very successful framework that describes the evolution of the Universe. Large scale observations, like the Cosmic Microwave Background (CMB), or the abundances of light elements (Nucleosynthesis), are extremely strong evidences of a Hot Big Bang.

However, the truth is that we have both in particle physics and in cosmology many unsolved questions. The SM is far from describing all the micro-physics we know of, and we think of it as just a low energy effective theory (EFT) valid at energies below the scale of new physics (NP) Λ where a more fundamental description will kick in (the use of EFT will be reviewed in section 1.4 of chapter 1). In a similar way, ΛCDM describes the dynamics of the Universe with a few parameters, but unfortunately in many cases it is just a parametrization of the new physics (NP) by just giving it a name and some very basic properties, like the cosmological constant (Λ) or cold dark matter (CDM), but we are far from knowing which new particles and interactions describe this NP.

As the author thinks that it is of uttermost importance to examine deeply *why* we study something, let us devote some time to analyse why we think NP is needed, explaining in more detail the drawbacks of the SM and the ΛCDM model, before focusing on the main topics of this thesis. The main reasons coming from experimental observations are the following:

- Dark energy (DE). DE is responsible for the accelerated expansion of

[3] Although some like dark energy and dark matter are still mysteries.

[4] With the discovery of cosmological B-modes made by BICEP2 [12], which are the imprint of the gravitational waves of inflation, and that should be confirmed by Planck, we are in fact reaching much earlier times in our knowledge of the History of the Universe, times as early as $\sim 10^{-36}$ s, or energies of $\sim 10^{16}$ GeV.

the Universe, as observed in 1998 using Type Ia Supernovae [15, 16]. As will be shown in chapter 4, different observations have revealed that only about $\sim 5\%$ of the Universe is described by the SM, the rest being dark matter ($\sim 26\%$) and DE ($\sim 69\%$), for which we don't have yet an accepted fundamental theory. One option is that it is just a cosmological constant (see [17] for a review), a fluid with negative pressure, with equation of state $p = -\rho$. However, the value of Λ is much smaller than the one expected in QFT, a possible reason being some unknown symmetry. It could also happen that DE is due to some dynamical mechanism [18, 19], for instance with a quintessence field with time-dependent w, or a modified theory of gravity [20].

- Dark matter (DM). There is compelling evidence of the existence of non-luminous non-baryonic matter in the Universe. A substantial part of this thesis will be devoted to DM and its direct detection. We leave to chapters 5 and 6 an overview of these topics.

- The baryon asymmetry of the Universe (BAU). In the Universe there are more baryons (b) than anti-baryons ($\bar{b}$); annihilations have not erased all particles, so fortunately matter is present, with a small baryon to photon ratio, $\eta = \frac{n_b - n_{\bar{b}}}{n_\gamma} \sim 10^{-10}$. This BAU should be generated dynamically, because even if there was a preexisting asymmetry, fine-tuned to the present value, it would have been diluted after inflation. Several mechanisms exist, like leptogenesis [21], which for instance can occur via decays of heavy right-handed neutrinos (with masses larger than 10^9 GeV [22]) that violate lepton number (LN), and this asymmetry can be transferred to the baryons via sphaleron processes, which preserve $B - L$. Note that in general three conditions [23] must be satisfied to generate the BAU: violation of B, violation of C and CP (otherwise processes involving $\bar{b}$ would generate the same BAU but opposite in sign as the one generated by b) and departure from thermal equilibrium. The SM has all the ingredients, however the amount of CP violation is too small and the transition is not strongly first order.

- Neutrino masses. In the SM (defined without right-handed neutrinos), neutrinos are massless. However, we know that neutrinos oscillate and are therefore massive particles that mix. A substantial part of this thesis will be devoted to neutrino masses and models, so we refer to chapters 2 and 3 for an overview.

From theoretical arguments, we have that the SM is not satisfactory in the following points:

- The so-called flavour puzzle. There is no explanation for the number of families[5], the masses or the mixings of the leptons and quarks. In particular, there is a hierarchy in masses between particles of the different families, which is not understood at all. Many free parameters (~ 20) are needed to explain all the low-energy data and at the moment no compelling theory of flavour is able to explain why they take the values we have measured. In addition, indirect constraints on flavour changing neutral currents (FCNC) and other LFV processes have pushed the NP scale to be in most cases far away from the EWS.

- The strong CP problem. A term in the Lagrangian $\theta\epsilon^{\mu\nu\rho\sigma}G_{\mu\nu}G_{\rho\sigma}$, which is a relevant operator, is perfectly allowed by the SM symmetry and violates T and CP. However, bounds from neutron electric dipole moments yield $\theta \lesssim 10^{-9}$, and the common lore is that Lagrangian parameters should be $\mathcal{O}(1)$ unless a symmetry protects them (this is known as *naturality*). A solution is to promote θ to a field, the axion, charged under the Peccei-Quinn symmetry [24–27]. In addition, it can constitute the DM of the Universe, with a mass around $\sim 10^{-5}$ eV.

- The Hierarchy problem. It is not a problem of the SM, but a problem that the SM has in the presence of NP at a high scale Λ. The Higgs mass is not protected by any symmetry (unlike fermions, protected by chiral symmetry, or gauge bosons, whose mass is protected by the gauge symmetry) and receives quadratic corrections, $\propto \Lambda^2$, which yield the presence of a weak-scale Higgs boson ($m_h \sim 125$ GeV) unnatural.[6] In principle, this problem could be solved if, like the pions in QCD, the Higgs boson is no longer an elementary scalar particle but a condensate of fermions, like in Technicolor models (see [28] for a classic review). Another possibility is Supersymmetry (see [29–31] for some reviews), where fermions and bosons are related to each other. One should always keep in mind that, if no high energy NP exists, as stated at the beginning, there is no Hierarchy Problem. However, gravity is always there, although we do not know how to construct a renormalizable quantum field theory (QFT) of it.

- Unification of interactions. The SM group is the direct product of three gauge groups. It would be desirable if these were unified in a unique

[5] In this thesis we present some works regarding possibility of the existence of a fourth generation. The new experimental evidence with the discovery of the Higgs boson strongly disfavours the presence of extra families.

[6] Another way to pose the problem is that a large amount of cancellations between the bare mass and the loop corrections is needed, i.e., a high degree of fine-tuning is necessary.

group at a higher scale.[7] In fact, anomaly cancellation within each family makes clear that leptons *know about* quarks and viceversa, so the fact that at some point they are unified in the same representation should not surprise anyone. In addition, we know that couplings run with energy, and in the SM, the gauge couplings point to a high-scale around 10^{15} GeV where they would unify. However, in the SM they don't perfectly unify, so NP between the EW and the GUT scales is needed to help them converge.[8]

- Charge quantization. It is not understood why protons ($q_p = +e$, with e the magnitude of the electron charge) and electrons ($q_e = -e$) have opposite electric charges. At a more fundamental level, quarks come in either $+2/3\,e$ or $-1/3\,e$. There is no explanation for this in the SM, while there is in some GUTs, like SU(5) [33].

- Gravity. We describe micro-physics with QFT. However, when one tries to quantize gravity, we are dealt with a non-renormalizable theory. This makes the unification of gravity with the other SM interactions one of the most important theoretical problem (if not the most). There have been attempts to go beyond QFT, such as String Theory, with however limited predictive power. An important fact is to note that gravity involves the presence of a new energy scale, the Planck scale ($m_p = \sqrt{\hbar\, c/G} \approx 10^{19}$ GeV), and therefore the Hierarchy problem seems a real concern, unless the NP makes the existence of very different scales *natural*.

- Inflation. In the Standard Cosmological Model ΛCDM, with a Hot Big Bang, which will be reviewed in chapter 4, there are some problems (the horizon problem, the flatness problem, the problem of structure formation, or the absence of monopoles and domain walls hypothesized in some SM extensions...) which are solved by having a period of accelerated expansion in the very early Universe ($t \sim 10^{-34}$ s), called inflation. After the discovery of primordial B-modes caused by primordial gravitational waves, made by BICEP2 [12], and which should be confirmed independently by other experiments, like Planck, the SM needs to be extended to accommodate inflation. In the literature there are many testable inflationary models and more data should shed light

[7] These theories are called Grand Unified Theories (GUTs), and SO(10) is a very nice example, whose irreducible representation is the **16** and contains the ν_R as a fundamental component. Lower bounds to the GUT scale exist from proton decay [32].

[8] In Supersymmetry, depending on the scale of SUSY breaking, unification can be achieved (typically it should kick in below $\mathcal{O}(10)$ TeV).

on which is the one chosen by Nature. The interested reader is referred to [34] for a nice review on inflation.

From all these reasons, we know that NP, possibly in many different scales $\Lambda_{\rm NP}$ and forms, is needed:

- If $\Lambda_{\rm NP} \sim \mathcal{O}(1)$ TeV, it may be tested at the Large Hadron Collider (LHC) in its second run at $13 - 14$ TeV, but this does not need to be the case.
- If $\Lambda_{\rm NP} \ll$ EWS (like the axion, that solves the strong CP problem and is a good DM candidate), the SM would not even be a good EFT, and it may be tested in other type of experiments.
- If $\Lambda_{\rm NP} \gg \mathcal{O}(1)$ TeV, we may never be able to detect the new particles directly, and we may just have to gather indirect evidence via effects of them in other low-energy processes, and by falsifying other possibilities.[9] However, as we have seen, there are *naturality* arguments to expect that if the NP is roughly above $\mathcal{O}(10)$ TeV, some mechanism is needed to solve the Hierarchy Problem.

In this thesis we focus on NP scenarios with testable scales, at $\sim \mathcal{O}(1)$ TeV, that try to shed some light on neutrino masses and dark matter.

[9] This may be the case for SO(10) well-motivated seesaw type I, to be studied in chapter 3, section 3.1, which seems a very reasonable explanation to neutrino masses, but very difficult to test.

Part II

Neutrino masses

Chapter 1

The Standard Model in a nutshell

The Standard Model (SM) describes our current knowledge of particle physics. It is a quantum field theory (QFT) that successfully describes the electromagnetic, the weak and the strong interactions [35–46]. However, it does not describe all known phenomena and we know that new physics (NP) is needed, as has been argued in the introduction, part I. In this chapter we will briefly review the basic components of the SM.

1.1 The gauge group and the fermion content

The SM is based on the gauge group $\mathrm{SU(3)_c} \times \mathrm{SU(2)_L} \times \mathrm{U(1)_Y}$, with the messengers of the interactions being the gauge bosons associated with the generators of each group:

- 8 gluons G^μ for the strong interactions based on $\mathrm{SU(3)_c}$, Quantum Chromodynamics (QCD), with g_s being the strong coupling.

- The charged W^μ, the neutral Z^μ and the photon A^μ for the unified electroweak interactions, based on the product group $\mathrm{SU(2)_L} \times \mathrm{U(1)_Y}$, with g being the coupling of the $\mathrm{SU(2)_L}$ interactions and g' the coupling of the $\mathrm{U(1)_Y}$ ones.[1]

[1] After spontaneous symmetry breaking (SSB) the third real gauge boson W^3_μ of SU(2) and the hypercharge one of $\mathrm{U(1)_Y}$, B_μ, mix to yield the Z and the photon, the force carrier of Quantum Electrodynamics (QED).

	$\ell = \begin{pmatrix}\nu_L \\ e_L\end{pmatrix}$	$e_{\rm R}$	$\nu_{\rm R}?$	$Q = \begin{pmatrix}u_L \\ d_L\end{pmatrix}$	$u_{\rm R}$	$d_{\rm R}$	ϕ
$\mathrm{SU(3)_c}$	1	1	1	3	3	3	1
$\mathrm{SU(2)_L}$	2	1	1	2	1	1	2
$\mathrm{U(1)_Y}$	$-1/2$	-1	0	$+1/6$	$+2/3$	$-1/3$	$+1/2$

Table 1.1: The Standard Model particle content of one family (quarks and leptons, $\psi_\alpha = (Q, d_{\rm R}, u_{\rm R}, \ell, e_{\rm R})$) and its representation under $\mathrm{SU(3)_c} \times \mathrm{SU(2)_L} \times \mathrm{U(1)_Y}$. Also shown the Higgs field ϕ. The existence of right-handed neutrinos $\nu_{\rm R}$ is at this moment completely hypothetical, only based on simplicity, aesthetic and theoretical reasons.

The covariant derivatives take into account the transformation properties of the fields under the SM gauge group:

$$D_\mu = \partial_\mu - i g_s \frac{\lambda_a}{2} G^a_\mu - i g\, T_a W^a_\mu - i g'\, Y\, B_\mu, \tag{1.1}$$

for a general field that transforms non-trivially under $\mathrm{SU(3)_c}$ and $\mathrm{SU(2)_L}$, and has hypercharge Y. T_a are the generators of weak isospin $\mathrm{SU(2)_L}$, with $T_a = \frac{1}{2}\sigma_a$ for the SM $\mathrm{SU(2)_L}$ doublets, where σ_a ($a = 1, 2, 3$) are the Pauli matrices. $\frac{\lambda_a}{2}$ ($a = 1, 2, ..., 8$) are the generators of $\mathrm{SU(3)_c}$, with λ_a the Gell-Mann matrices, which take care of the transformation of quarks as color triplets.

The kinetic terms for the gauge bosons are:

$$\mathcal{L}_{\text{kin gauge}} = -\frac{1}{4} G^a_{\mu\nu} G^{\mu\nu}_a - \frac{1}{4} W^a_{\mu\nu} W^{\mu\nu}_a - \frac{1}{4} B_{\mu\nu} B^{\mu\nu}, \tag{1.2}$$

with the field strength tensors given by:

$$W^a_{\mu\nu} \equiv \partial_\mu W^a_\nu - \partial_\nu W^a_\mu + g\, \epsilon^{abc}\, W^b_\mu W^c_\nu, \tag{1.3}$$

$$G^a_{\mu\nu} \equiv \partial_\mu G^a_\nu - \partial_\nu G^a_\mu + g_s\, f^{abc}\, G^b_\mu G^c_\nu, \tag{1.4}$$

$$B_{\mu\nu} \equiv \partial_\mu B_\nu - \partial_\nu B_\mu, \tag{1.5}$$

where ϵ^{abc} (f^{abc}) are the structure constants of $\mathrm{SU(2)_L}$ ($\mathrm{SU(3)_c}$), i.e., for instance for $\mathrm{SU(2)_L}$, $[T^a, T^b] = i\epsilon^{abc} T^c$.

The fermions come in three generations or families, with identical quantum numbers, but different masses.[2] Let us focus for the moment on just the first family, which makes up all the visible matter of the Universe. Table 1.1 summarizes the particle content of one SM family.

The $\mathrm{SU(2)_L}$ charge is called *weak isospin* T. The SM doublets (left-handed, $\psi_\mathrm{L} = \frac{1}{2}(1-\gamma_5)\psi$), ℓ and Q, have isospin 1/2. The third component of isospin is $T_3 = +1/2$ for the up components of the doublets, ν_L and u_L, ($T_3 = -1/2$ for the down ones, d_L and e_L). The right-handed components ($\psi_\mathrm{R} = \frac{1}{2}(1+\gamma_5)\psi$) of the SM fermions, e_R, u_R and d_R, are singlets, i.e., they don't transform under $\mathrm{SU(2)_L}$. Note that in the original SM (built when neutrinos where thought to be massless) right-handed partners (ν_R) for the left-handed neutrinos are absent. This is fine for anomaly cancellation within each family, as the hypercharge of the hypothetical ν_R is zero.[3] However, one may wonder why wouldn't neutrinos have right-handed partners.

The kinetic terms for the fermions are:

$$\mathcal{L}_{\text{kin fermions}} = \sum_\alpha i\,\bar{\psi}^\alpha\,\gamma^\mu D_\mu\,\psi_\alpha, \tag{1.6}$$

where $\psi_\alpha = (Q, d_\mathrm{R}, u_\mathrm{R}, \ell, e_\mathrm{R})$.

1.2 The Higgs mechanism

Gauge symmetry explicitly forbids a mass term for bosons and fermions. These can be generated via spontaneous symmetry breaking (SSB) of the EW symmetry. This is known as *the Higgs mechanism*. In the simplest version, a Higgs field $\phi = \begin{pmatrix}\phi^+\\ \phi^0\end{pmatrix}$ is introduced as a complex scalar doublet under $\mathrm{SU(2)_L}$. The most general Lagrangian for the Higgs field is:

$$\mathcal{L}_\text{Higgs} = (D_\mu\phi)^\dagger D^\mu\phi + \mu^2\,\phi^\dagger\phi - \lambda\,(\phi^\dagger\phi)^2\,, \tag{1.7}$$

where $\mu^2 > 0$ gives a Mexican-hat type potential.

To find the minimum of the Lagrangian, which will be at zero kinetic energy, one minimizes the scalar potential $V(|\phi|) = -\mu^2|\phi|^2 + \lambda\,|\phi|^4$. $\phi = 0$ is not a minimum of the scalar potential due to the negative sign of μ^2. $V(|\phi|)$ is minimised for $|\phi| = \sqrt{\mu^2/2\lambda} \equiv \frac{v}{\sqrt{2}}$. The measured VEV of the Standard Model

[2] Really at this point we are in the flavour basis, so only after diagonalising (going to the mass basis), can one really speak about the masses of the fields. In other words, the down quark with definite mass is a combination of the down quarks of the three families.

[3] If $B-L$ is to be a gauge symmetry, ν_R are needed, as then the $B-L$ gauge symmetry is no longer non-anomalous.

is $v \simeq 246$ GeV [47]. Now we can rewrite the Higgs field, as an excitation around this minimum:

$$\phi(x) = \frac{v + H(x)}{\sqrt{2}} e^{i \frac{\sigma^a}{2} \theta^a(x)/v} \begin{pmatrix} 0 \\ 1 \end{pmatrix} , \tag{1.8}$$

with $a = 1, 2, 3$. The H component of the field ϕ is the Higgs boson, the only physical particle of the scalar doublet, with mass $m_{\mathrm{H}}^2 = 2\lambda v^2$. It has been recently discovered at the LHC, with a mass around 125 GeV [13, 14].

The θ's are the would-be Goldstone bosons, which become the longitudinal degrees of freedom the massive gauge fields, the Z and the W.

If we substitute eq. 1.8 into the kinetic term of the Higgs, $(D_\mu \phi)^\dagger D^\mu \phi$, we obtain the masses of the gauge bosons. The W boson, $W^\pm \equiv \frac{1}{\sqrt{2}} (W_1 \mp i W_2)$, has a mass $m_{\mathrm{W}}^2 \equiv g^2 \frac{v^2}{4}$. However, there is mixing between B_μ and W_μ^3, so to obtain the physical spectrum we have to diagonalize their mass matrix:

$$\frac{v^2}{4} \begin{pmatrix} W_\mu^3 & B_\mu \end{pmatrix} \begin{pmatrix} g^2 & -gg' \\ -gg' & g'^2 \end{pmatrix} \begin{pmatrix} W_3^\mu \\ B^\mu \end{pmatrix} , \tag{1.9}$$

with the following rotation (using the short-hand notation $s_\theta \equiv \sin\theta$ and so on):

$$\begin{pmatrix} W_\mu^3 \\ B_\mu \end{pmatrix} = \begin{pmatrix} c_{\theta_W} & s_{\theta_W} \\ -s_{\theta_W} & c_{\theta_W} \end{pmatrix} \begin{pmatrix} Z_\mu \\ A_\mu \end{pmatrix} ,$$

with $t_{\theta_W} \equiv g'/g$, where θ_{W} is the *Weinberg angle*.

This matrix has a zero eigenvalue, which corresponds to the photon mass, the other massive particle being the Z, with mass $m_{\mathrm{Z}}^2 \equiv \left(g^2 + g'^2\right) \frac{v^2}{4}$.

The photon is the only massless gauge boson, associated with an unbroken subgroup of $\mathrm{SU(2)_R} \times \mathrm{U(1)_Y}$: QED, $\mathrm{U(1)_{em}}$. From the covariant derivative we can relate the electric charge Q to the third component of isospin T_3 and to the hypercharge Y:

$$\begin{aligned} D_\mu \supset & -i \frac{g}{\sqrt{2}} \left(\sigma^+ W_\mu + \sigma^- W_\mu^* \right) \\ & - i \left(g\, c_{\theta_W}\, T_3 - g' Y\, s_{\theta_W} \right) Z_\mu \\ & - i \frac{gg'}{\sqrt{g^2 + g'^2}} \left(T_3 + Y \right) A_\mu , \end{aligned}$$

where we assumed it acts on a SM $\mathrm{SU(2)_L}$ doublet, with $\sigma^+ = \sigma^1 + i\,\sigma^2$, $\sigma^- = (\sigma^+)^\dagger$.

As we know from QED that the photon couples to the electron with strenght e (for $Q = -1$), we have that $Q = T_3 + Y$ and $e = \frac{gg'}{\sqrt{g^2 + g'^2}}$.

1.3 Flavour: masses and mixings

Charged (only for non-trivial representations of $\mathrm{SU(2)_L}$, like the doublets of the SM) and neutral currents arise from the fermion kinetic terms, eq. 1.6.

For a general doublet $\Psi_{\mathrm{L}}^{\mathrm{T}} = \begin{pmatrix} U_{\mathrm{L}} & D_{\mathrm{L}} \end{pmatrix}$, the neutral currents (NC) are:

$$\mathcal{L}_{\mathrm{NC}} = g\, T^3_\psi\, \overline{\psi_{\mathrm{L}}}\, \gamma_\mu\, \psi_{\mathrm{L}}\, W_3^\mu + g'(Q_\psi - T^3_\psi)\, \overline{\psi_{\mathrm{L}}}\, \gamma_\mu\, \psi_{\mathrm{L}}\, B^\mu + g' Q_\psi\, \overline{\psi_{\mathrm{R}}}\, \gamma_\mu\, \psi_{\mathrm{R}}\, B^\mu =$$

$$= e\, \bar{\psi}\, \gamma_\mu \left[\frac{T^3_\psi}{s_{\theta_W} c_{\theta_W}} \frac{1}{2}(1-\gamma_5) - Q_\psi t_{\theta_W} \right] \psi\, Z^\mu \;+\; e Q_\psi\, \bar{\psi} \gamma_\mu \psi\, A^\mu\,,$$

where ψ_{L} represents either U_{L} or D_{L}. The last term is just the QED Lagrangian.

And the charged currents (CC) are of the form:

$$\mathcal{L}_{\mathrm{CC}} = g\, \overline{\Psi_{\mathrm{L}}}\, \gamma_\mu \left(T^1 W_1^\mu + T^2 W_2^\mu \right)\, \Psi_{\mathrm{L}} = \frac{e}{\sqrt{2}\, s_{\theta_W}}\, \overline{U_{\mathrm{L}}} \gamma_\mu D_{\mathrm{L}}\, W^\mu \;+\; \mathrm{H.c.}, \quad (1.10)$$

where notice that $U_{\mathrm{L}}, D_{\mathrm{L}}$ are not the physical (massive) up- or down-type fermions.

The Higgs field provides fermion mass terms. With the following definitions $\tilde{\phi} \equiv i\sigma_2\, \phi^*$, $\tilde{\ell} \equiv i\sigma_2\, \ell^{\mathrm{c}}$, $\ell^{\mathrm{c}} \equiv C\, \overline{\ell^{\mathrm{T}}}$ [4] we can add to the SM Lagrangian (in fact we have to add, as they are allowed by the symmetries) the following interactions:

$$\mathcal{L}_{\mathrm{Yukawa}} = \bar{\ell} Y_e e_{\mathrm{R}}\, \phi \;+\; \bar{\ell} Y_\nu \nu_{\mathrm{R}}\, \tilde{\phi} \;+\; \overline{Q}\, Y_u u_{\mathrm{R}}\, \tilde{\phi} \;+\; \overline{Q}\, Y_d\, d_{\mathrm{R}}\, \phi \;+ \mathrm{H.c.} \quad (1.11)$$

The Yukawa matrices Y_e, Y_ν, Y_u, Y_d are 3×3 complex matrices. After SSB, for each fermion f, with $M_f = Y_f v/\sqrt{2}$, we get:

$$\mathcal{L}_{\text{fermion mass}} = \sum_f \left(1 + \frac{H}{v} \right) \bar{f}_{\mathrm{L}} M_f f_{\mathrm{R}} + \mathrm{H.c.}\,, \quad (1.12)$$

with $f = u, d, e$ (and ν if ν_{R} are present), and each of the fields understood as a vector in family or flavour space, i.e., $u = (u, c, t)$, $d = (d, s, b)$, $e = (e, \mu, \tau)$ (and $= (\nu_e, \nu_\mu, \nu_\tau)$ if ν_{R} are present). The VEV sets the common scale for the masses of the gauge bosons and the fermions, and the gauge and individual Yukawa couplings provide the different hierarchies in mass between the different particles (some of them like the top or the electron Yukawas span ~ 5 orders of magnitude!).

[4] Let us notice that the fundamental representation of SU(2) is pseudoreal.

We need to diagonalize these mass matrices. For the quark sector, for instance for the up-type quarks we can perform the rotations $u_{\rm L}^m = V_{u_{\rm L}} u_{\rm L}$ and $u_{\rm R}^m = V_{u_{\rm R}} u_{\rm R}$, where the superscript m refers to mass eigenstates, such that we diagonalise the mass matrix: $M_u = V_{u_{\rm L}} D_u V_{u_{\rm R}}^\dagger$. And similarly for the down-type quarks: $M_d = V_{d_{\rm L}} D_d V_{d_{\rm R}}^\dagger$, with $d_{\rm L}^m = V_{d_{\rm L}} d_{\rm L}$ and $d_{\rm R}^m = V_{d_{\rm R}} d_{\rm R}$. After this diagonalization, an extra matrix, the Cabibbo-Kobayashi-Maskawa (CKM) quark mixing matrix, $V_{\rm CKM}$, will appear in the CC interactions:

$$\mathcal{L}_{\rm CC}^{\rm quark\,sector} = \frac{e}{\sqrt{2}\, s_{\theta_W}} \overline{u_{\rm L}} \gamma_\mu \, V_{\rm CKM} d_{\rm L} \, W^\mu + \text{H.c.} \tag{1.13}$$

where $V_{\rm CKM} = V_{u_{\rm L}}^\dagger V_{d_{\rm L}}$.[5] Therefore, in the SM, while CC change flavour at tree level, there are no tree level flavour changing neutral currents (FCNC).

For massless neutrinos, the equivalent lepton mixing matrix disappears. For instance, we can diagonalize the electron mass matrix trivially: $M_e = V_L D_e V_R^\dagger$, $e_{\rm R} = V_R \, e_{\rm R}$ and $\ell = V_L \ell$.

However, for massive neutrinos, equivalently to the situation just described for the quark sector, CC that change flavour appear:

$$\mathcal{L}_{\rm CC}^{\rm lepton\,sector} = \frac{e}{\sqrt{2}\, s_{\theta_W}} \overline{e_{\rm L}} \gamma_\mu U_{\rm PMNS} \nu_{\rm L} \, W^\mu \; + \; \text{H.c.}, \tag{1.14}$$

with $U_{\rm PMNS}$ the Pontecorvo-Maki-Nagakawa-Sakata (PMNS) lepton mixing matrix.

For 3 generations, a 3×3 unitary matrix has 3 angles and 6 phases. However, 5 of the phases can be removed, as field redefinitions like $f \to e^{i\alpha_f} f$ leave the Lagrangian invariant. One cannot be removed (transforming all fields with the same phase, α), as it is associated to the conservation of baryon number. This way only 1 phase remains, is physical, and appears in the CKM matrix. Regarding the lepton sector, the situation is analogous if neutrinos are Dirac particles, with only one phase present. If, however, neutrinos are Majorana particles, 2 extra physical phases appear in the PMNS mixing matrix (see section 2.2, chapter 2).

As a summary, the SM final Lagrangian before SSB, which has all terms permitted by the gauge symmetry, particle content and renormalizability,[6] is given by:

$$\mathcal{L}_{\rm SM} = \mathcal{L}_{\rm kin\,fermions} + \mathcal{L}_{\rm kin\,bosons} + \mathcal{L}_{\rm Yukawa} + \mathcal{L}_{\rm Higgs}, \tag{1.15}$$

[5] One can always start, for instance, in the up-quarks mass basis, as before SSB one can perform independent unitary transformations in the $\ell_{\rm L}$ and $u_{\rm L}$, and in this case $V_{\rm CKM} \equiv V_{d_{\rm L}}$.

[6] As said in the introduction in part I, a term like $\theta \, \epsilon_{\mu\nu\rho\sigma} \, G^{\mu\nu} G^{\rho\sigma}$ is allowed and violates CP.

where different terms are given in eqs. 1.2, 1.6, 1.7 and 1.11. As explained before, after SSB, charged and neutral currents, as well as mass terms for fermions and gauge bosons, are present.

1.4 Effective Field Theory

Effective field theory (EFT) is based on the well-tested principle that dynamics at low energies (large distances) does not depend on the details of the dynamics at high energies (short distances), up to a given accuracy.

The SM operators have dimension four or less, and are renormalizable. With EFT one can parametrize any high-energy physics at a high scale Λ by using non-renormalizable operators, whose validity is restricted to energies smaller than Λ. All the effective operators must respect Lorentz invariance and gauge symmetries, but do not need to respect global accidental symmetries of the SM, like baryon and lepton number. The predictivity of the EFT, of course, is restricted to some precision: we have to stop at some dimension, as the number of possible efective operators is infinite. However, this does not pose any problem, as experimental signatures are also restricted to a given precision.

The Lagrangian of the effective operators can be parametrized as:

$$\mathcal{L}_{\text{eff}} = \mathcal{L} + \sum_{n=5} \sum_{i} \left(\frac{C_i^n}{\Lambda^{n-4}} \mathcal{O}_i^n + \text{H.c.} \right) , \tag{1.16}$$

where n indicates the dimension of the operator and i labels the different operators of a given dimension. The operators of dimension n have dimensionful couplings with dimensions of inverse mass to the power $n-4$, with the coefficients C_i^n being dimensionless.[7]

EFT will prove to be a very useful tool to analise Majorana neutrino masses, i.e., lepton number violation (LNV) via effective operators. For instance, the Weinberg operator, which is the only dimension 5 operator with the SM fields and violates lepton number (LN), and will be explained in detail in chapter 2, can be generated by different complete theories, such as the seesaw models. In this way, we can be very general in parameterizing different Majorana neutrino mass models by making use of the Weinberg operator.

If one knows the full theory, the equivalence of both the effective theory and the complete description, at the energy scale of the new particles (say the mass of right-handed neutrinos in seesaw type I), is known as *matching*.

At dimension 6 there are many four fermion operators, and some of them lead to flavor changing neutral currents (FCNC), like the process $b \to s\gamma$, to

[7] The separation between Λ and C is arbitrary, of course.

CP-violating electric dipole moments or to baryon number violating processes, like proton decay. To date none of these processes have been observed, setting the scale of new physics Λ to be very high, depending on the particular operator. If one assumes order one coefficients, from neutrino masses typically one gets $\Lambda_{\nu\,\text{masses}} \sim \mathcal{O}(10^{13}\,\text{GeV})$, from FCNC $\Lambda_{\text{FCNC}} \geq \mathcal{O}(10 - 10^3\,\text{TeV})$, while from proton decay $\Lambda_{\text{p decay}} \geq \mathcal{O}(10^{16}\,\text{GeV})$. These predictions are valid for a large class of NP models, and demonstrate the power of EFT. Of course, it could happen that the coefficients are not order one but suppressed (for instance if they are generated at loops, or for some reason of the order of the Yukawa of the electron), and then, for instance if one thinks of the Weinberg operator as a parameterization of radiative and seesaw models, the LNV scale in these cases can be much lower.

This poses a problem of *naturalness* with the relevant operators of the SM:

- the Higgs mass, $m_{\text{H}} \approx 125$ GeV.
- the cosmological constant, observed to correspond to a vacuum energy density $\rho_\Lambda \sim 10^{-11}\text{eV}^4$).[8]

Another place where *naturality* may play a role is the hypothetical right-handed mass m_R, although this case is slightly different as it is protected by LN, i.e., in its absence LN is a good symmetry, so it could be small in the t'Hooft sense (quantum corrections are proportional to itself, so if small at tree level, it can be kept small naturally). However, if one thinks that it is not protected by any gauge symmetry, it could be as large as the largest scale present in the theory, for instance the GUT scale, motivated by $SO(10)$.

Let us notice that all mass terms are in fact protected by another symmetry, scale invariance, that is anomalous, i.e., broken at the quantum level by the running of the couplings.

[8] Any QFT estimation yields a value $60 - 120$ orders of magnitude larger!, the worst discrepancy between theory and experiment in physics [48].

Chapter 2

Neutrino masses

We briefly review in this chapter the key facts about neutrinos, focusing on their masses. We refer the interested reader to [47, 49–51] for some more extended reviews on neutrino physics and to [52] for a mandatory reference on neutrino physics.

2.1 Brief history of neutrino oscillations

In 1930, neutrinos were proposed by Pauli as neutral fermions with spin 1/2 as an explanation to the apparent energy and spin non-conservation in nuclear β decay, which had a continuum spectrum typical of a two-body decay[1] [53].

25 years later, Reines and Cowan discovered neutrinos escaping from a nuclear reactor in Savannah River [54–56].[2]

In the late sixties, the Homestake experiment [57], directed by Davis, observed a discrepancy between the expected solar neutrino flux and the one detected that led to the hypothesis that neutrinos are massive particles that mix as a possible explanation [58].

In 1998, Super-Kamiokande reported evidence of neutrino oscillations in the atmospheric neutrino flux and later SNO and KamLAND confirmed solar neutrino oscillations.

So the last two decades can be thought of as the *neutrino golden era*, with confirmation that neutrinos are massive particles that mix thanks to the results obtained with solar [57, 59–62] and atmospheric [63–65] neutrinos, confirmed with man-made sources: nuclear reactors [66] and accelerators [67, 68].

However, currently the origin and nature of the neutrinos tiny mass is still a mystery. Just one thing is known: the original SM with massless neutrinos

[1] We detect the electrons emitted, the electron anti-neutrinos are not detected.

[2] Electron anti-neutrinos to be more precise.

needs to be extended.

2.2 Neutrino parameters

Neutrino oscillations require mixing among the three flavour states ν_α, with $\alpha = e, \mu, \tau$, which can be expressed as quantum superpositions of three massive states ν_i, with $i = 1, 2, 3$. The PMNS mixing matrix that appears in charged current interactions, eq. 1.14, relates both basis (in the following $U_{\rm PMNS} \equiv U$ for simplicity), i.e., $\nu_\alpha = \sum_i U_{\alpha i}\nu_i$. It can be parametrized in terms of three Euler angles $\theta_{12}, \theta_{13}, \theta_{23}$ and just a CP violating phase δ if neutrinos are Dirac. However, there are two extra physical Majorana phases α_1, α_2 if neutrinos are Majorana particles. The explicit realization of the lepton mixing matrix is: $U = \mathcal{R} \cdot \mathcal{D}$, with $\mathcal{D} = \mathrm{diag}(e^{i\,\alpha_1/2}, e^{i\,\alpha_2/2}, 1)$ and, using the short-hand notation $\cos\theta_{ij} \equiv c_{ij}$ and so on, $\mathcal{R}$ is given by:

$$\mathcal{R} = \begin{pmatrix} c_{12}c_{13} & s_{12}c_{13} & s_{13}e^{-i\delta} \\ -s_{12}c_{23} - c_{12}s_{23}s_{13}e^{i\delta} & c_{12}c_{23} - s_{12}s_{23}s_{13}e^{i\delta} & s_{23}c_{13} \\ s_{12}s_{23} - c_{12}c_{23}s_{13}e^{i\delta} & -c_{12}s_{23} - s_{12}c_{23}s_{13}e^{i\delta} & c_{23}c_{13} \end{pmatrix}.$$

Oscillation experiments are only sensitive to mass-squared splittings ($\Delta m^2_{ij} \equiv m^2_i - m^2_j$). Currently, there are two possible choices of the sign of $\Delta m^2_{31} \equiv \Delta m^2_{atm}$, while $\Delta m^2_{21} \equiv \Delta m^2_{sol}$ is known to be positive. Therefore the ordering of the masses is compatible with:

- $m_1 \lesssim m_2 < m_3$ - Normal Hierarchy (NH).
- $m_3 < m_1 \lesssim m_2$ - Inverted Hierarchy (IH).
- $m_1 \approx m_2 \approx m_3$ - quasi-degenerate spectrum (QD). Notice that QD is still allowed depending on the cosmological assumptions used to derive the bound on the sum of the neutrino masses.

The minimum value for the sum of the masses from oscillation experiments is ~ 0.06 eV (~ 0.1 eV) for NH (IH), while for QD it is larger.

So to describe neutrinos we need ≥ 6 different parameters: at least 2 masses (data are still compatible with one being massless), 3 mixing angles and 1 phase (2 more phases in the case of Majorana neutrinos). Notice that recently the neutrino mixing angle θ_{13} has been measured [71–73]. We present in figure 2.1 the current values for the oscillation parameters, which are extracted from a global fit from [69] (see also [74, 75] for other global fits).

Regarding the absolute neutrino mass scale, the so-called effective electron neutrino mass, $m^2_{\nu_e} \equiv \sum_i m^2_i |U_{ei}|^2$, is constrained by Tritium β-decay.

NuFIT 1.2 (2013)

	Free Fluxes + RSBL		Huber Fluxes, no RSBL	
	bfp $\pm 1\sigma$	3σ range	bfp $\pm 1\sigma$	3σ range
$\sin^2\theta_{12}$	$0.306^{+0.012}_{-0.012}$	$0.271 \to 0.346$	$0.313^{+0.013}_{-0.012}$	$0.277 \to 0.355$
$\theta_{12}/^\circ$	$33.57^{+0.77}_{-0.75}$	$31.37 \to 36.01$	$34.02^{+0.79}_{-0.76}$	$31.78 \to 36.55$
$\sin^2\theta_{23}$	$0.446^{+0.008}_{-0.008} \oplus 0.593^{+0.027}_{-0.043}$	$0.366 \to 0.663$	$0.444^{+0.037}_{-0.031} \oplus 0.592^{+0.028}_{-0.042}$	$0.361 \to 0.665$
$\theta_{23}/^\circ$	$41.9^{+0.5}_{-0.4} \oplus 50.3^{+1.6}_{-2.5}$	$37.2 \to 54.5$	$41.8^{+2.1}_{-1.8} \oplus 50.3^{+1.6}_{-2.5}$	$36.9 \to 54.6$
$\sin^2\theta_{13}$	$0.0231^{+0.0019}_{-0.0019}$	$0.0173 \to 0.0288$	$0.0244^{+0.0019}_{-0.0019}$	$0.0187 \to 0.0303$
$\theta_{13}/^\circ$	$8.73^{+0.35}_{-0.36}$	$7.56 \to 9.77$	$9.00^{+0.35}_{-0.36}$	$7.85 \to 10.02$
$\delta_{\rm CP}/^\circ$	266^{+55}_{-63}	$0 \to 360$	270^{+77}_{-67}	$0 \to 360$
$\frac{\Delta m^2_{21}}{10^{-5}\ \mathrm{eV}^2}$	$7.45^{+0.19}_{-0.16}$	$6.98 \to 8.05$	$7.50^{+0.18}_{-0.17}$	$7.03 \to 8.08$
$\frac{\Delta m^2_{31}}{10^{-3}\ \mathrm{eV}^2}$ (N)	$+2.417^{+0.014}_{-0.014}$	$+2.247 \to +2.623$	$+2.429^{+0.055}_{-0.054}$	$+2.249 \to +2.639$
$\frac{\Delta m^2_{32}}{10^{-3}\ \mathrm{eV}^2}$ (I)	$-2.411^{+0.062}_{-0.062}$	$-2.602 \to -2.226$	$-2.422^{+0.063}_{-0.061}$	$-2.614 \to -2.235$

Figure 2.1: Neutrino parameters from the global fit [69]. As the authors state, for *Free Fluxes + RSBL* reactor fluxes have been left free and short baseline reactor data (RSBL) ($\lesssim 100$ m) have been included included; for *Huber Fluxes, no RSBL* the flux predictions from [70] have been used, and RSBL data was not included.

However, cosmological observations provide the tightest constraints on the absolute scale of neutrino masses (in particular on the sum of the masses, $\sum_i m_i$), via their contribution to the energy density of the Universe and the growth of structure. In general these bounds depend on the assumptions made about the expansion history as well as on the cosmological data included in the analysis [76], but typically $\sum_i m_i < 1$ eV (and in most analysis stronger, see table 2.1).

Finally, if neutrinos are Majorana particles, complementary information on neutrino masses can be obtained from $0\nu2\beta$ decay. The contribution of the known light neutrinos to the $0\nu2\beta$ decay amplitude is proportional to the effective Majorana mass of ν_e, $m_{ee} \equiv |\sum_i m_i U_{ei}^2|$, which depends not only on the masses and mixing angles of the mixing matrix but also on the phases.

All the experimental constraints coming from cosmology, Tritium and $0\nu\beta\beta$ are summarized in table 2.1.

Tritium β decay		
m_{ν_e}	< 2.2 eV 95% CL	[77, 78]
m_{ν_e}	< 2 eV 95% CL	[79]
m_{ν_e} (future)	~ 0.2 eV 95% CL	[80]
$0\nu\beta\beta$		
m_{ee}	$< 0.2 - 0.4$ eV 90% CL	[81]
m_{ee}	$< 0.14 - 0.38$ eV 90% CL	[82]
m_{ee}	< 0.34 eV 90% CL	[83]
m_{ee} (future)	~ 0.01 eV 90% CL	[84]
Cosmology		
$\sum_i m_i$	< 0.23 eV 95% CL	[85]

Table 2.1: Current status and future prospects of the experimental constraints on neutrino parameters coming from cosmology, Tritium and $0\nu\beta\beta$ decay.

2.2.1 Unsolved questions in the neutrino sector

Even if it is true that in the last two decades there have been major discoveries in the field of neutrinos, we still need further input from experiments, whose next generation will try, among other things, to determine the following:

- The nature Dirac or Majorana of neutrinos, i.e., whether lepton number (LN) is a conserved symmetry or not (see next section). Observation of $0\nu\beta\beta$ would imply that LN is violated by two units, and therefore neutrinos are Majorana particles [86].
- The sign of Δm^2_{23}, i.e., whether the spectrum is NH or IH.
- The existence of CP violation in the lepton sector and its value.
- Lepton flavour violation (LFV) in the charged lepton sector, via observation of processes like $\mu \to e\gamma$ (the current limit is $5.7 \cdot 10^{-13}$ at 90% CL [87]).[3]

[3] As lepton flavour is violated in neutrinos (neutrino oscillations), it is also expected to be violated at some point in the charged lepton sector. In the SM $\nu_{\rm L}$ and $e_{\rm L}$ come in $SU(2)_{\rm L}$ doublets, and as neutrinos are massive, after diagonalization CC interactions appear, see 1.14.

- The absolute mass scale of neutrinos.

- If sterile neutrinos exist: LSND experiment reported evidence for the appearance of $\bar{\nu_e}$ in a $\bar{\nu_\mu}$ beam [88], that can be interpreted as oscillations with additional sterile neutrinos with a mass-squared difference $\Delta m^2 \sim 1\,\mathrm{eV}^2$. MiniBooNE neutrino and antineutrino data may be explained and be compatible with LSND with several sterile neutrinos, by allowing for CP violating effects between neutrino and antineutrino oscillations [89, 90].

The hope is that combining these (and other) experimental results the mechanism by which neutrino masses are generated will eventually be uncovered.

2.3 Dirac and Majorana masses

Fermions without electric charge, like neutrinos (only LN, which is a global symmetry in the SM), can have two classes of mass terms, Dirac and Majorana:

- The Dirac fermion has *four* internal degrees of freedom, describing particles and antiparticles with opposite charges, each of them with two different helicities. It is therefore appropriate for particles that carry internal charges (such as electric charge) which distinguish them from their counterparts, the antiparticles. The mass term connects opposite chirality fields (takes a left-handed particle ψ_L to a right-handed particle ψ_R) and it has the following form:

$$m_\mathrm{D}\,\overline{\psi_\mathrm{R}}\,\psi_\mathrm{L} + \mathrm{H.c.} \tag{2.1}$$

- A Majorana fermion has *two* degrees of freedom, without any internal (conserved) charge, i.e., it is its own antiparticle, $\psi^c = \psi$. The mass term takes a left-handed particle ψ_L to a right-handed antiparticle ψ^c_L, which is the CP conjugate of a left-handed particle, or takes a right-handed particle ψ_R to a left-handed antiparticle, ψ^c_R. It violates any $U(1)$ symmetry, like LN for the case of neutrinos, and it is of the form:

$$m_\mathrm{L}\,\overline{\psi^c_\mathrm{L}}\,\psi_\mathrm{L} + \mathrm{H.c.} \tag{2.2}$$

A theory can have only left-handed neutrinos and their CP conjugate states, without having right-handed neutrinos. In this case the neutrino could be massless or can have a Majorana mass m_L like in eq. 2.2, which violates

LN by two units. However, active neutrinos $\nu_{\rm L}$ come in $\mathrm{SU}(2)_{\rm L}$ doublets, ℓ, so with the SM content $m_{\rm L}\,\overline{\nu_{\rm L}^c}\,\nu_{\rm L}$ is not gauge invariant, and therefore $m_{\rm L}$ must come from a non-renormalizable operator, parametrized via the Weinberg operator, see section 2.4. If the SM particle content is extended, $m_{\rm L}$ can be generated, as will be shown in chapter 3, either at tree level (seesaw models) or at loop level (radiative models).

When both the left- and right-handed neutrinos, $\nu_{\rm L}$ and $\nu_{\rm R}$, are present, the most general mass terms are:

$$\mathcal{L}_M = -\frac{1}{2} m_{\rm L} \overline{\nu_{\rm L}^c} \nu_{\rm L} - \frac{1}{2} m_{\rm R} \overline{\nu_{\rm R}^c} \nu_{\rm R} - m_{\rm D} \overline{\nu_R} \nu_{\rm L} + \text{H.c.},$$

and there are several possibilities:

- if all mass terms vanish neutrinos are massless, so they are two Weyl spinors (ruled-out).
- If $m_{\rm L} = m_{\rm R} = 0$ the left-handed and the right-handed neutrinos combine to form a Dirac neutrino.[4]
- If $m_{\rm L} \neq 0$, $m_{\rm R} \neq 0$ and $m_{\rm D} = 0$, there are two Majorana neutrinos $\nu_{\rm L}$ and $\nu_{\rm R}$ with masses $m_{\rm L}$ and $m_{\rm R}$.
- If $m_{\rm L}$ or $m_{\rm R}$ or both are non-vanishing, and also $m_{\rm D}$, the physical states (which are Majorana) are admixtures of the states $\nu_{\rm L}$ and $\nu_{\rm R}$ with masses obtained by diagonalising the mass matrix, as will be shown in chapter 3, section 3.1.

So, if we add $\nu_{\rm R}$ to the SM, which seems well-motivated by the fact that all other fermions have left- and right-handed components, what is the most natural option, Dirac or Majorana masses? In QFT, we know that we have to add all gauge invariant renormalizable terms compatible with the field content of the theory, like $m_{\rm R}\,\overline{\nu_{\rm R}^c}\,\nu_{\rm R}$, so we find that LN, which was an accidental U(1) global symmetry of the SM, is violated.[5] Moreover, if $\nu_{\rm R}$ are added to the SM, as they are gauge singlets (sterile), $m_{\rm R}$ could be at an energy scale not related to the EWS: for instance much larger than the EWS, leading to the Seesaw mechanism that will be explained in sec. 3.1, but in principle there is no reason for $m_{\rm R}$ not to be, for example, at or below the EWS.

[4] Notice that a Dirac fermion can be regarded as two mass-degenerate Majorana fermions of opposite CP.

[5] Also baryon number and generational lepton numbers are accidental global symmetries of the SM. Any new neutrino mass model should violate generational lepton numbers, independently of their Dirac (LN conserving) or Majorana (lepton number violating, LNV) nature.

On the other hand, to have Dirac neutrinos like all other fermions, we have to forbid m_{R}, that is, LN (or B-L[6]) has to be imposed *by hand*. LN would be an exact symmetry, but not obtained accidentally from the gauge invariance and particle content as in the SM, but imposed *by hand*, which is theoretically not very rewarding. In this case, neutrinos would be Dirac particles ($\nu \equiv \nu_{\mathrm{L}} + \nu_{\mathrm{R}}$), like the rest of the fermions.

In addition, for Dirac neutrinos, one has to face the quantitative problem of the values of their masses. As neutrinos would acquire their masses after SSB like all other fermions, via the Higgs mechanism, their masses should be of the order of the vacuum expectation value (VEV) of the neutral component of the Higgs field, $\mathcal{O}(100\,\mathrm{GeV})$, but they are at least 12 orders of magnitude smaller! This problem of fine-tuning of Yukawas to give several orders of magnitude of difference in masses is also present for the other fermions, although quantitatively smaller.[7] In the case of neutrinos, it is difficult to imagine that 173 and 10^{-11} GeV particles (the top and the neutrinos) acquire their masses via the same mechanism. In addition, all other fermions range from the electron mass $\mathcal{O}(1\,\mathrm{MeV})$ up to the top mass, $\mathcal{O}(100\,\mathrm{GeV})$, while there would be a gap between neutrino masses $\mathcal{O}(1\,\mathrm{eV})$ and the electron mass.[8]

As will be explained in chapter 3, there can be explanations for the smallness of their mass, like seesaw models (a heavy particle explains neutrinos tiny mass) and radiative models (they are much lighter than other particles because they are massless at tree level, with their mass generated at loops). In the next section we will study how if neutrinos are Majorana particles, their masses can be generally parametrized by an effective operator.

2.4 The Weinberg operator

As we have argued in the previous section, it does not seem very natural that neutrinos are Dirac particles. LN is an accidental global symmetry of the SM (like baryon number) and if one thinks of the SM as a low-energy effective theory (see section 1.4 for a brief discussion of EFT), one finds that at dimension 5 there is only one effective operator, the Weinberg operator,

[6] Beyond perturbation theory LN is violated, however, B-L is preserved. Therefore, to avoid Majorana mass terms it is more appealing to impose *by hand* B-L, which is anomaly free.

[7] As already said in the introduction I, for example the electron and the top masses are ~ 5 orders of magnitude away and altogether this is known as the flavour problem: why three generations, why are the masses and mixings what they are...

[8] One can speculate whether it is the *perfect* range for $\mathcal{O}(1\,\mathrm{keV})$ right-handed neutrinos, which are in addition good warm dark matter candidates.

which happens to violate LN by two units:

$$\mathcal{L}_5 = \frac{1}{2}\frac{c_{\alpha\beta}}{\Lambda_{\rm W}}(\overline{\ell_\alpha}\tilde{\phi})\,(\phi^\dagger\tilde{\ell}_\beta) + \text{H.c.}\,, \tag{2.3}$$

where $\Lambda_W \gg v$ is the scale of new physics and $c_{\alpha\beta}$ are model-dependent coefficients. Upon electroweak symmetry breaking, the Weinberg operator leads to a Majorana mass matrix for the light neutrinos of the form

$$m_{\rm L} = c\,\frac{v^2}{\Lambda_W}\,. \tag{2.4}$$

Notice that $c_{\alpha\beta}$ have flavour structure, and in some models can carry additional suppression due to loop factors (as is the case in radiative mechanisms) and/or ratios of mass parameters (for instance in type II seesaw there is a suppression of the LNV parameter μ, see eq. 3.6, therefore $c \propto \mu/m_\chi$). In those cases one typically relates directly $\Lambda_{\rm W}$, which does not need to be extremely large, to the masses of the new particles and absorb all suppression factors in $c_{\alpha\beta}$.

By doing some SU(2) Fierz transformations one can rewrite the Weinberg operator in eq. (2.3):

$$\left(\overline{\ell_\alpha}\tilde{\phi}\right)\,\left(\phi^\dagger\tilde{\ell}_\beta\right) = -\left(\overline{\ell_\alpha}\,\vec{\sigma}\tilde{\phi}\right)\,\left(\phi^\dagger\,\vec{\sigma}\tilde{\ell}_\beta\right) = \frac{1}{2}\left(\overline{\ell_\alpha}\,\vec{\sigma}\,\tilde{\ell}_\beta\right)\,\left(\phi^\dagger\,\vec{\sigma}\,\tilde{\phi}\right),$$

where α and β are family indices and $\vec{\sigma} \equiv (\sigma_1, \sigma_2, \sigma_3)$ is a vector in the adjoint representation of SU(2) whose components are the 2×2 Pauli matrices. From the three explicit forms one can easily read the three different new particles that can generate the Weinberg operator at tree-level: a hyperchargeless heavy fermion singlet (triplet) for the first (second) expressions, and a $Y = 1$ heavy scalar triplet for the third one. These are precisely seesaw models: type I (III) and II respectively, which we discuss in more detail in chapter 3. This demonstrates the power of the Weinberg operator, which parametrizes Majorana neutrino masses of very different extensions of the SM.

Chapter 3

Neutrino mass models

There are many neutrino mass models on the market. In this chapter we briefly review some of the most popular ones. We start by discussing type I seesaw, which requires the addition of right-handed neutrinos to the SM, which was introduced in section 2.3 of chapter 2. We also summarize other types of seesaw models, before moving on to some of the best-motivated high-energy frameworks. We conclude with radiative models, which will be the main topic of this part of the thesis.

3.1 Type I: fermionic singlets

In type I seesaw [91–95], n SM fermionic singlets are added to the SM; these have the quantum numbers of right-handed neutrinos, and can be denoted by $\nu_{\mathrm{R}i}$. Note that to explain neutrino data, which requires al least two massive neutrinos, a minimum of two extra singlets are needed; however, $n = 3$ is aesthetically (and based on a possible $SO(10)$ unification) the most reasonable option. Having no charges under the SM, Majorana masses for right-handed neutrinos are allowed by gauge invariance, so the new terms in the Lagrangian are:

$$\mathcal{L}_{\nu_{\mathrm{R}}} = i\,\overline{\nu_{\mathrm{R}}}\gamma^{\mu}\partial_{\mu}\nu_{\mathrm{R}} - \left(\frac{1}{2}\overline{\nu_{\mathrm{R}}^{\mathrm{c}}}m_{\mathrm{R}}\nu_{\mathrm{R}} + \overline{\ell}\,\tilde{\phi}\,Y\,\nu_{\mathrm{R}} + \mathrm{H.c.}\right)\,, \tag{3.1}$$

where m_{R} is a $n \times n$ symmetric matrix, Y is a general $3 \times n$ matrix and we have omitted flavour indices for simplicity. After spontaneous symmetry breaking (SSB), the neutrino mass terms are given by (see the diagram of figure 3.1)

$$\mathcal{L}_{\nu\,\mathrm{mass}} = -\frac{1}{2}\begin{pmatrix}\overline{\nu_{\mathrm{L}}} & \overline{\nu_{\mathrm{R}}^{\mathrm{c}}}\end{pmatrix}\begin{pmatrix}0 & m_{\mathrm{D}} \\ m_{\mathrm{D}}^{\mathrm{T}} & m_{\mathrm{R}}\end{pmatrix}\begin{pmatrix}\nu_{\mathrm{L}}^{\mathrm{c}} \\ \nu_{\mathrm{R}}\end{pmatrix} + \mathrm{H.c.}\,, \tag{3.2}$$

where $m_{\mathrm{D}} = Y\frac{v}{\sqrt{2}}$.

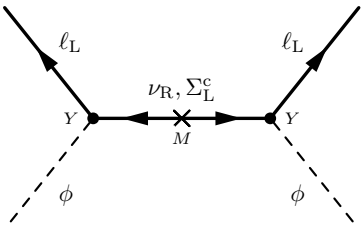

Figure 3.1: Seesaw type I neutrino mass diagram.

$m_{\rm R}$ is in principle free, however if $m_{\rm R} \gg m_{\rm D}$, upon block-diagonalization one obtains n heavy leptons which are mainly SM singlets, with masses $\sim m_{\rm R}$, and the well-known seesaw formula for the effective light neutrino Majorana mass matrix,

$$m_\nu \simeq -m_{\rm D}\, m_{\rm R}^{-1}\, m_{\rm D}^{\rm T}\,, \tag{3.3}$$

which naturally explains the smallness of light neutrino masses as a consequence of the presence of heavy SM singlet leptons. Notice that if one wants leptogenesis to be the source of the baryon asymmetry of the Universe, typically there is a lower bound on these right-handed neutrinos, $m_{\rm R} > 10^9$ GeV [22].

3.2 Type II: scalar triplet

The type II seesaw [96–100] only adds to the SM field content one scalar triplet with hypercharge $Y = 1$ and assigns to it lepton number $L = -2$. In the doublet representation of $\mathrm{SU}(2)_{\rm L}$, using $\vec{\sigma} = (\sigma^1, \sigma^2, \sigma^3)$ and $\vec{\chi} = (\chi_1, \chi_2, \chi_3)$, the triplet can be written as a 2×2 matrix, whose components are

$$\chi = \frac{1}{\sqrt{2}} \vec{\sigma} \cdot \vec{\chi} = \begin{pmatrix} \chi^+ & \chi^{++} \\ \chi_0 & -\chi^+ \end{pmatrix}\,, \tag{3.4}$$

where we defined $\chi^{++} \equiv \frac{\chi_1 - i\chi_2}{\sqrt{2}}$, $\chi^+ \equiv \frac{\chi_3}{\sqrt{2}}$ and $\chi^0 \equiv \frac{\chi_1 + i\chi_2}{\sqrt{2}}$, with third component of isospin $T_3 = 1, 0, -1$, as can be seen by computing $[\sigma_3/2, \chi]$.

Gauge invariance allows a Yukawa coupling of the scalar triplet to two lepton doublets,

$$\mathcal{L}_\chi = \left((Y_\chi^\dagger)_{\alpha\beta}\, \overline{\ell}_\alpha \chi \ell_\beta + \text{H.c.} \right) - V(\phi, \chi)\,, \tag{3.5}$$

where Y_χ is a symmetric matrix in flavour space. The scalar potential has, among others, the following terms:

$$V(\phi, \chi) = m_\chi^2\, \mathrm{Tr}[\chi\chi^\dagger] - \left(\mu\, \tilde{\phi}^\dagger \chi^\dagger \phi + \text{H.c.} \right) + \ldots \tag{3.6}$$

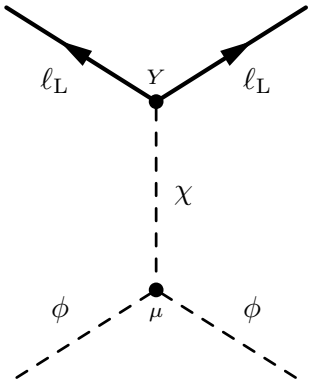

Figure 3.2: Seesaw type II neutrino mass diagram.

The μ coupling violates lepton number explicitly, and it induces a vacuum expectation value (VEV) for the triplet via the VEV of the doublet, even if $m_\chi > 0$. In the limit $m_\chi \gg v$ this VEV can be approximated by:

$$\langle \chi \rangle \equiv v_\chi \simeq \frac{\mu v^2}{2\, m_\chi^2}; \tag{3.7}$$

then, the Yukawa couplings in equation (3.5) lead to a Majorana mass matrix for the left-handed neutrinos via the diagram of figure 3.2:

$$m_\nu = 2 Y_\chi v_\chi = Y_\chi \frac{\mu v^2}{m_\chi^2}. \tag{3.8}$$

The dependence of neutrino masses on Y_χ and μ can be understood from the Lagrangian, since the breaking of LN results from the simultaneous presence of the Yukawa and μ couplings. As long as m_χ^2 is positive and large, v_χ will be small, in agreement with the constraints from the ρ parameter, $v_\chi \lesssim 6$ GeV [101]. Moreover, the parameter μ, which has dimensions of mass, can be naturally small, because in its absence LN is recovered, increasing the symmetry of the model.

3.3 Type III: fermionic triplets

In the type III seesaw model [102,103], the SM is extended by fermion $SU(2)_{\rm L}$ triplets Σ_α with zero hypercharge. As in type I, at least two fermion triplets are needed to have two non-vanishing light neutrino masses. We choose the spinors Σ_α to be right-handed under Lorentz transformations and write

them in SU(2) Cartesian components $\vec{\Sigma}_\alpha = (\Sigma^1_\alpha, \Sigma^2_\alpha, \Sigma^3_\alpha)$. The Cartesian components can be written in terms of charge eigenstates as usual

$$\Sigma^+_\alpha = \frac{1}{\sqrt{2}}(\Sigma^1_\alpha - i\Sigma^2_\alpha) \,, \qquad \Sigma^0_\alpha = \Sigma^3_\alpha \,, \qquad \Sigma^-_\alpha = \frac{1}{\sqrt{2}}(\Sigma^1_\alpha + i\Sigma^2_\alpha) \,, \tag{3.9}$$

and the charged components can be further combined into negatively charged Dirac fermions $E_\alpha = \Sigma^-_\alpha + \Sigma^{+\mathrm{c}}_\alpha$. Using standard four-component notation the new terms in the Lagrangian are given by

$$\mathcal{L}_\Sigma = i\,\overline{\vec{\Sigma}_\alpha}\gamma^\mu D_\mu \cdot \vec{\Sigma}_\alpha - \left(\frac{1}{2}(m_\mathrm{R})_{\alpha\beta}\overline{\vec{\Sigma}^\mathrm{c}_\alpha}\cdot\vec{\Sigma}_\beta + Y_{\alpha\beta}\,\overline{\ell_\alpha}\,\left(\vec{\sigma}\cdot\vec{\Sigma}_\beta\right)\tilde{\phi} + \mathrm{H.c.}\right) , \tag{3.10}$$

where Y is the Yukawa coupling of the fermion triplets to the SM lepton doublets and the Higgs, and m_R their Majorana mass matrix, which can be chosen to be diagonal and real in flavour space.

After SSB the neutrino mass matrix can be written as

$$\mathcal{L}_{\nu\,\mathrm{mass}} = -\frac{1}{2}\begin{pmatrix}\overline{\nu_\mathrm{L}} & \overline{\Sigma^{0\mathrm{c}}}\end{pmatrix}\begin{pmatrix}0 & m_\mathrm{D}\\ m_\mathrm{D}^\mathrm{T} & m_\mathrm{R}\end{pmatrix}\begin{pmatrix}\nu^\mathrm{c}_\mathrm{L}\\ \Sigma^0\end{pmatrix} + \mathrm{H.c.}\,, \tag{3.11}$$

which is the same as in the type I seesaw just replacing $\nu_{\mathrm{R}i}$ by Σ^0_α, and therefore leads to a light neutrino Majorana mass matrix

$$m_\nu \simeq -m_\mathrm{D}\, m_\mathrm{R}^{-1}\, m_\mathrm{D}^\mathrm{T}\,. \tag{3.12}$$

However, since the triplet has also charged components with the same Majorana mass, in this case there are stringent lower bounds on the new mass scale from direct searches, so $m_\mathrm{R} \gtrsim 100$ GeV.

3.4 Inverse seesaw

In inverse and linear seesaw models, one can have much lighter right-handed neutrinos masses than in type I seesaw (although in that case right-handed neutrinos can also be light if their Yukawas are small) and still get the correct neutrino mass scale [104]. In these models, LN is slightly broken by a small parameter protected from radiative corrections, and flavour and CP violation effects are not suppressed by light neutrino masses. The model incorporates two singlet fermions, N and S, per generation, to which we assign LN one. In the (ν_L, N^c, S) basis the 9×9 mass matrix Ω of the neutral sector after SSB has this form:

$$\Omega = \begin{pmatrix} 0 & m_{\rm D} & M_{\rm L}^T \\ m_{\rm D}^T & 0 & M^T \\ M_{\rm L} & M & \mu \end{pmatrix},$$

where $m_{\rm D} = Y\, v/\sqrt{2}$, M are 3×3 arbitrary complex matrices in flavour space and μ is complex and symmetric. If $M_{\rm L} = 0$ and $\mu \neq 0$, the models is called *inverse seesaw*, while if $M_{\rm L} \neq 0$ and $\mu = 0$ it is called *linear seesaw*. LN is violated in the μ and or $M_{\rm L}$ terms.[1]

Let us focus on the *inverse seesaw limit*, $M_{\rm L} = 0$. If we assume $m_{\rm D}$, $\mu \ll M$, the matrix Ω can be diagonalized by a unitary transformation leading to 9 mass eigenstates: three light neutrinos, while the other three pairs of two-component leptons combine to form three quasi-Dirac leptons. We can block-diagonalize first the $2-3$ sub-matrix, and then the $1-2$. The effective Majorana mass matrix for the light neutrinos is approximately given by:

$$m_\nu = m_{\rm D}^T (M^T)^{-1} \mu\, M^{-1} m_{\rm D}, \tag{3.13}$$

while the three pairs of heavy neutrinos have masses of order M, and the admixture among singlet and doublet $SU(2)$ states is suppressed by $m_{\rm D}/M$. Although M is a large Dirac ($\Delta L = 0$) mass scale suppressing the light neutrino masses, it can be much smaller than in type I seesaw, as there is the further suppression of the LNV scale μ/M. In the limit $\mu = 0$, LN would be conserved, and the three light neutrinos would be massless Weyl particles, while the six heavy neutral leptons will combine to form three Dirac fermions.

3.5 High-energy frameworks

3.5.1 Left-right symmetric models

Some possible high energy well-motivated theories that embed seesaw mechanisms are left-right (LR) symmetric models, which restore parity at high energies [95, 105, 106], based on the group $SU(2)_{\rm L} \times SU(2)_{\rm R} \times U(1)_{\rm B-L}$.

In LR symmetric models, the right-handed fermion fields are doublets under $SU(2)_{\rm R}$. There are both $W_{\rm L}$ and $W_{\rm R}$, and left- and right-handed neutrinos, $\nu_{\rm L}$ and $\nu_{\rm R}$, so neutrinos become massive.

The minimal model involves a bi-doublet $\phi(2,2,0)$ and a pair of triplets $\Delta_{\rm L}(3,1,2)$ and $\Delta_{\rm R}(1,3,2)$. When the LR and the EW symmetries are broken, the bidoublets provide fermion masses, while the triplets provide Majorana mass terms for $\nu_{\rm L}$ and ν_R.

[1] If LN was spontaneously broken by the VEV of a singlet $\langle\sigma\rangle$, $\mu = y\,\langle\sigma\rangle$.

The minimum of the potential is achieved for $v^2 \sim v_{\rm L} v_{\rm R}$ [107], with $v_{\rm L}$ ($v_{\rm R}$) the VEV of the triplet scalar $\Delta_{\rm L}$ ($\Delta_{\rm R}$). Thus, if $v_{\rm R} \gg v_{\rm L}$ (in agreement with the ρ parameter, see discussion on $v_\chi \equiv v_L$ in section 3.2) the Majorana mass term for $\nu_{\rm R}$ ($m_{\rm R} = f\, v_{\rm R}$) is large and the Majorana mass term for the left-handed neutrinos ($m_{\rm L} = f\, v_{\rm L}$) is small, where the couplings f are the same as there is a left-right symmetry. Therefore, the neutrino masses are given by:

$$m_\nu = f\, v_{\rm L} - m_{\rm D}\, (f\, v_{\rm R})^{-1}\, m_{\rm D}^T, \tag{3.14}$$

and can be naturally small.

3.5.2 Supersymmetric models

There is an intrinsically supersymmetric way of breaking LN by breaking the so-called R parity, which is defined as $\mathrm{R} = (-1)^{3\mathrm{B}+\mathrm{L}+2\mathrm{S}}$, with B (L) the baryon (lepton) number and S the spin, so SM (supersymmetric) particles have $R = 1(-1)$ [108–117] (for a review see [118]). In this scenario, the SM doublet neutrinos mix with the neutralinos, i.e., the supersymmetric (fermionic) partners of the neutral gauge and Higgs bosons. As a consequence, Majorana masses for neutrinos (generated at tree level and at one loop) are naturally small because they are proportional to the small R-parity-breaking parameters.

3.5.3 Grand Unified Theories

Some of these left-right models and supersymmetric extensions of the SM are naturally embedded in Grand Unified Theories (GUTs) like SO(10) or SU(5) [33], although this is not needed. It is remarkable the fact that the hypothetical right-handed neutrinos, $\nu_{\rm R}$, would complete the representation 16 of SO(10), so that all fermions of each family are contained in a single representation of the unifying group. This looks too impressive not to be significant.

We refer the reader to [52] for a more thorough discussion on how to accommodate neutrino masses in high energy frameworks.

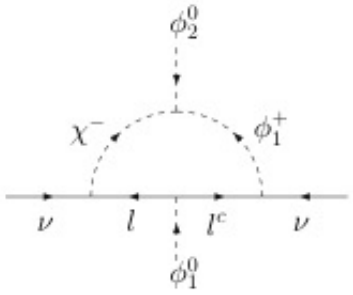

Figure 3.3: The Zee model diagram contributing to neutrino masses.

3.6 Radiative models

Small Majorana neutrino masses may also be induced by radiative corrections. Typically, on top of loop factors of at least $1/(4\pi)^2$,[2] there are additional suppressions due to couplings and/or ratios of masses, leading to the observed light neutrino masses with a NP scale not far above the EWS, so in principle these models can be tested at the LHC.

In this thesis we will analyse in detail various radiative models, like the Zee-Babu model [119, 120], and another two-loop mechanism [121], by adding new generations (see the scientific research, part V). Therefore, here we just give a brief introduction to two other examples: the Zee model [119, 122] and the Inert Doublet Model [123–125].

3.6.1 The Zee Model

The Zee model [119, 122] uses the fact that $\bar{\tilde{\ell}}\ell$ couples to a charged scalar singlet χ^+ with $Y = 1$. This coupling, call it f, is anti-symmetric. Two Higgs doublets are needed so the LNV term $\widetilde{\phi_2}\phi_1\,\chi^-$ exists.

If ϕ_2 does not couple to leptons, the diagram shown in figure 3.3 gives neutrino masses at one loop, and the final expression of the neutrino mass matrix can be written as [126]:

$$(m_\nu)_{ij} = C\, f_{ij}(m_{\ell i}^2 - m_{\ell j}^2), \tag{3.15}$$

where C is some constant that includes the loop factor and m_ℓ are the charged leptons masses. Therefore, the mass matrix is symmetric, as it has to be, and the ee element is suppressed with respect to the other ones, which renders in general a tiny rate of $0\nu\beta\beta$. The reader is referred to [127] for a recent analysis of the model.

[2] More than three loops typically yield too light neutrino masses or have problems with LFV.

3.6.2 The Scotogenic model

The Scotogenic model[3] (see for instance [128] for the original proposal, and [123–125, 129–136] for some among the long list of different studies of the model, some of them with just a inert doublet and no inert singlet fermions) is an extension of the SM which provides both neutrino masses and a dark matter (DM) candidate.

The SM is extended with a second scalar doublet η and at least two right-handed singlet (or triplet) fermions $\nu_{\mathrm{R}i}$[4] (or $\overline{\Sigma}_i$) with masses $m_{\mathrm{R}i}$ are needed to give masses to the two known active massive neutrinos.[5]

All of the new fields are odd under a discrete symmetry Z_2, while the SM particles are even. The lightest of them is stable, so if it is the neutral component and if its mass and interactions are the correct ones to have the measured relic abundance, it could provide the DM of the Universe.

First of all, let us briefly explain how a discrete symmetry can be motivated, although in principle it looks ad hoc. A Z_{N} discrete symmetry can be gauged in a $\mathrm{U}(1)_{\mathrm{D}}$ group. For example, consider matter fields χ with $\mathrm{U}(1)_{\mathrm{D}}$ charge $Q_\chi = -1$ and Higgs field ϕ with charge $Q_\phi = N$. Let us call v the VEV of this Higgs field which breaks spontaneously the symmetry. Then we can have that the symmetry is broken by the VEV:

$$\mathcal{L} = \phi\chi^N + \mathrm{H.c.} \to v\chi^N + \mathrm{H.c.}, \tag{3.16}$$

and we see how the Lagrangian has a discrete remnant Z_{N} symmetry:

$$\chi \to e^{i2\pi/N}\chi,$$

that it is exactly conserved due to its gauge origin.

The new interactions of the model that are added to the SM are:

$$\mathcal{L}_{\nu_{\mathrm{R}}} = i\,\overline{\nu_{\mathrm{R}}}\gamma^\mu\partial_\mu\nu_{\mathrm{R}} - \left(\frac{1}{2}\overline{\nu_{\mathrm{R}}^c}m_{\mathrm{R}}\nu_{\mathrm{R}} + \overline{\ell}\,\tilde{\eta}\,Y\,\nu_{\mathrm{R}} + \mathrm{H.c.}\right), \tag{3.17}$$

and the most general scalar potential $V(\eta, \phi)$ is:

$$V(\eta,\phi) = m_1^2\,\phi^\dagger\phi + m_2^2\,\eta^\dagger\eta + \frac{1}{2}\lambda_1(\phi^\dagger\phi)^2 + \frac{1}{2}\lambda_2(\eta^\dagger\eta)^2 +$$

[3] Also sometimes known as the Inert Doublet Model (IDM).

[4] We call them $\nu_{\mathrm{R}i}$, although they are not what one normally means by right-handed neutrinos: they do not couple to the lepton doublets via the Higgs, i.e., there is no Dirac mass after SSB.

[5] If the three of them are massive we would need to add three right-handed singlets, as in seesaw models.

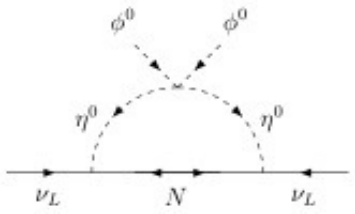

Figure 3.4: Scotogenic model diagram contributing to neutrino masses. The N represent either right-handed neutrinos, $\nu_{\mathrm{R}i}$, or the neutral component of fermion triplets, Σ^0.

$$+ \lambda_3(\phi^\dagger\phi)(\eta^\dagger\eta) + \lambda_4(\phi^\dagger\eta)(\eta^\dagger\phi) + \frac{1}{2}\lambda_5\Big((\phi^\dagger\eta)^2 + \text{H.c.}\Big). \tag{3.18}$$

Notice that there is a U(1) global symmetry (LN) violated by the simultaneous presence of m_{R}, λ_5 and Y. If we assume $m_2^2 > 0$ so $\langle\eta\rangle = 0$, the Z_2 is exactly conserved and neutrinos remain massless at tree level. The masses of the scalar particles in this model are:

$$m_H^2 = -2\,m_1^2 = 2\,\lambda_1 v^2, \tag{3.19}$$

$$m_{\eta^+}^2 = m_2^2 + \lambda_3\, {}^{v^2}\!/_2, \tag{3.20}$$

$$m_{\eta_1^0}^2 = m_2^2 + (\lambda_3 + \lambda_4 + \lambda_5)\, {}^{v^2}\!/_2, \tag{3.21}$$

$$m_{\eta_2^0}^2 = m_2^2 + (\lambda_3 + \lambda_4 - \lambda_5)\, {}^{v^2}\!/_2, \tag{3.22}$$

where H is the SM Higgs and the rest are the components of η. The lightest of η_1^0, η_2^0 can serve as a DM candidate (if all $\nu_{\mathrm{R}i}$ are heavier). Notice that the mass splitting between η_1^0 and η_2^0 is proportional to λ_5, which is naturally small, as in its absence LN is conserved.

The one-loop diagram that contributes to neutrino masses from η_1^0 and η_2^0 exchange is shown in figure 3.4, and its exact contribution is given by:

$$(m_\nu)_{ij} = \sum_k \frac{Y_{ik}\,Y_{jk}\,m_{\mathrm{R}k}}{16\,\pi^2}\left[\frac{m_{\eta_1^0}^2}{m_{\eta_1^0}^2 - m_{\mathrm{R}k}^2}\ln\frac{m_{\eta_1^0}^2}{m_{\mathrm{R}k}^2} - \frac{m_{\eta_2^0}^2}{m_{\eta_2^0}^2 - m_{\mathrm{R}k}^2}\ln\frac{m_{\eta_2^0}^2}{m_{\mathrm{R}k}^2}\right]. \tag{3.23}$$

In the limit $m_{\eta_1^0}^2 - m_{\eta_2^0}^2 = \lambda_5 v^2 \ll m_0^2 = (m_{\eta_1^0}^2 + m_{\eta_2^0}^2)/2$, we get:

$$(m_\nu)_{ij} = \frac{\lambda_5 v^2}{16\,\pi^2}\sum_k \frac{Y_{ik}\,Y_{jk}\,m_{\mathrm{R}k}}{m_0^2 - m_{\mathrm{R}k}^2}\left[1 - \frac{m_{\mathrm{R}k}^2}{m_0^2 - m_{\mathrm{R}k}^2}\ln\frac{m_0^2}{m_{\mathrm{R}k}^2}\right]. \tag{3.24}$$

There are some limiting cases:

- For $m_{\mathrm{R}k}^2 \ll m_0^2$:

$$(m_\nu)_{ij} = \frac{\lambda_5 v^2}{8\,\pi^2 m_0^2} \sum_k Y_{ik}\, Y_{jk}\, m_{\mathrm{R}k}. \tag{3.25}$$

- For $m_{\mathrm{R}k}^2 \gg m_0^2$:

$$(m_\nu)_{ij} = \frac{\lambda_5 v^2}{8\,\pi^2} \sum_k \frac{Y_{ik}\, Y_{jk}}{m_{\mathrm{R}k}} \left[-1 - \ln \frac{m_0^2}{m_{\mathrm{R}k}^2} \right]. \tag{3.26}$$

- For $m_{\mathrm{R}k}^2 \simeq m_0^2$:

$$(m_\nu)_{ij} = \frac{\lambda_5 v^2}{16\,\pi^2} \sum_k \frac{Y_{ik}\, Y_{jk}}{m_{\mathrm{R}k}}. \tag{3.27}$$

So the typical seesaw scale is reduced by $\sim \frac{\lambda_5}{(4\,\pi)^2}$. This means that for $\lambda_5 Y^2 \simeq 10^{-8}$, we can have neutrino masses with a NP scale at the TeV.

If we consider $\nu_{\mathrm{R}i}$ lighter than the η's and we want it to be a DM candidate and at the same time to give the right order of magnitude of neutrino masses, there are strong constraints coming from LFV processes such as $\mu \to e\,\gamma$.

However, as studied in [129, 130] it is still possible to find compatible points that satisfy all constraints (for instance with $\lambda_5 \sim 10^{-9}$). Recently, it was also studied in [136] the possibility that the lightest right-handed singlet does not reach thermal equilibrium in the early Universe so that it behaves as a Feebly Interacting Massive Particle (FIMP). For the case of fermion triplets, as they have gauge interactions, it is in principle much easier to satisfy the three constraints: neutrino masses, DM abundance and the LFV constraints.

For η lighter than $\nu_{\mathrm{R}i}$, as it is a doublet, it is possible to satisfy the strong constraints coming from relic abundance, LFV, direct detection and so on [131, 132]. In this case, there are also constraints on λ_5 coming from DM relic abundance and direct detection bounds, see for instance [133]. Studies of the scotogenic model in the context of leptogenesis and baryogenesis can be found in [134] and [135], respectively.

We emphasize here that the Scotogenic model is a nice example of a radiative model that connects issues in principle disconnected such as neutrinos masses and DM, with a powerful phenomenology.

Part III

Dark matter

Chapter 4

The Cosmological Model in a nutshell

In this chapter we briefly review the Cosmological Model, before focusing on dark matter (DM) in the next chapter.

4.1 The basic ingredients of the ΛCDM model

The Cosmological Model is also known as the ΛCDM model, where Λ refers to the cosmological constant, which causes the accelerated expansion of the Universe we have observed, and CDM stands for cold dark matter (it could also be warm, see chapter 5), which is an extra matter component in addition to the luminous one, that we *observe* via its gravitational effects.

These are the basic ingredients of the ΛCDM model:

- The *Cosmological Principle*. By assuming that the symmetries of the Universe, thought of as a perfect fluid, are isotropy (invariance under rotations) and homogeneity (invariance under translations), on scales larger that ~ 100 Mpc, one obtains that the metric $g_{\mu\nu}$, known as the Friedmann-Lemaitre-Robertson-Walker (FLRW) metric, is:[1]

$$ds^2 \equiv g_{\mu\nu}dx^\mu dx^\nu = -dt^2 + a^2(t)\Big[\frac{dr^2}{1-kr^2} + r^2 d\Omega\Big], \tag{4.2}$$

[1] Recall Minkowski's metric for a flat space-time:

$$ds^2 = -dt^2 + dr^2 + r^2 d\Omega^2. \tag{4.1}$$

with $d\Omega = d\theta^2 + \sin^2\theta d\phi^2$, $a(t)$ the *scale factor* which parametrizes the evolution of space-time and k the curvature of space-time ($k = 0$, see below).

- *Einsteins' Field Equations of General Relativity (GR)*, invariant under general transformations of coordinates, which are:

$$R_{\mu\nu} - \frac{1}{2}g_{\mu\nu}R + \Lambda g_{\mu\nu} = \frac{8\pi G}{c^4}T_{\mu\nu}, \tag{4.3}$$

where $g_{\mu\nu}$ is the space-time metric, $R_{\mu\nu}$ is the Ricci tensor, $R = g_{\mu\nu}R^{\mu\nu}$ the Ricci scalar and $T_{\mu\nu}$ is the energy-momentum tensor, constructed in terms of the matter Lagrangian density. As already mentioned, Λ is the cosmological constant, which parametrizes the accelerated expansion of the Universe. A pictorial representation of GR is that *energy (matter) tells space-time how to curve, while space-time tells matter how to move.*

Eq. 4.3 can be derived from the Hilbert-Einstein action (with $g = \det g_{\mu\nu}$):

$$S = \int \sqrt{-g}d^4x\Big(\frac{c^4}{16\pi G}(R - 2\Lambda) + \mathcal{L}_m\Big), \tag{4.4}$$

through the *Principle of Least Action* ($\delta S = 0$). $\mathcal{L}_\mathrm{m}$ is the matter content of the theory, whose variation with respect to the metric gives rise to the energy-momentum tensor $T_{\mu\nu}$ of eq. 4.3.

In principle $\mathcal{L}_\mathrm{m}$ can be associated to the content of the Standard Model (SM) of particle physics, plus any beyond the SM (BSM) physics, such as dark matter (DM), neutrino masses, inflation and so on, i.e.:[2]

$$\mathcal{L}_\mathrm{m} = \mathcal{L}_\mathrm{SM} + \mathcal{L}_\mathrm{BSM} = \mathcal{L}_\mathrm{SM} + \mathcal{L}_{\nu\,\mathrm{masses}} + \mathcal{L}_\mathrm{DM} + ... \tag{4.5}$$

However, in general, the different energy components are interpreted as forming a fluid, and are divided in matter and radiation. For a perfect fluid we have that:

$$T^{\mu\nu} = (\rho + p)U^\mu U^\nu + pg^{\mu\nu}, \tag{4.6}$$

with ρ and p the energy density and the pressure and U^μ the four-velocity vector of the fluid. In an homogeneous and isotropic Universe, it is given by:

$$T^\mu_\nu = \mathrm{diag}(-\rho, p, p, p). \tag{4.7}$$

[2]Let us notice that GR, encoded in eq. 4.3, is a classical theory, while the SM is a Quantum Field Theory (QFT). A more complete theory which would unify both gravity and and gauge interactions is still missing, as quantization of GR yields a non-renormalizable theory. String Theory, that goes beyond QFT, is the most popular candidate.

- The *equation of state* of different energy components, that relates their pressure and their density: $p_i = w_i \rho_i$. From the *First Law of Thermodynamics*, $dE_i + dW_i = 0$, with the energy being $E_i = \rho_i V$ and the work done by the system $dW_i = p_i dV$, with $V = a^3$, we get:

$$\frac{\dot{\rho}_i}{\rho_i} = -3(1 + w_i)\frac{\dot{a}}{a}, \tag{4.8}$$

  which can be integrated to obtain:

$$\rho_i \propto a^{-3(1+w_i)} \ . \tag{4.9}$$

  Matter has $w_{\text{matter}} = 0$, so $\rho_{\text{matter}} \propto a^{-3}$. For radiation $w_{\text{rad}} = 1/3$ and therefore $\rho_{\text{rad}} \propto a^{-4}$, and for the cosmological constant $w_\Lambda = -1$ and trivially $\rho_\Lambda = \text{constant}$.

4.2 Friedmann equations

Using the metric $g_{\mu\nu}$ of eq. 4.2 in *Einsteins equations* of GR, eq. 4.3, together with eq. 4.7, one obtains the *Friedmann equations*, which describe the evolution of the Universe in terms of the energy content:

$$\left(\frac{\dot{a}}{a}\right)^2 = \frac{8\pi G}{3}\rho_{\text{tot}}(t) - \frac{k}{a^2} \tag{4.10}$$

and

$$\left(\frac{\ddot{a}}{a}\right)^2 = -\frac{4\pi G}{3}(\rho_{\text{tot}}(t) + 3p_{\text{tot}}), \tag{4.11}$$

where $\rho_{\text{tot}} = \sum_i \rho_i$ and $p_{\text{tot}} = \sum_i p_i$. Using eq. 4.9 (which can also be obtained combining eqs. 4.10 and 4.11) in eq. 4.10 ($k = 0$), one obtains the time evolution of the scale factor:

$$a(t) \propto t^{1/2}, \tag{4.12}$$

for the epoch of radiation domination (RD), i.e., when the energy density of the Universe was dominated by radiation, at $T > T_{\text{M-R equality}} \sim 1$ eV, and

$$a(t) \propto t^{2/3} \tag{4.13}$$

for the matter-dominated epoch (MD), i.e., when the energy density of the Universe was dominated by matter.

For a cosmological constant (that dominates today), $\omega = -1$, one gets:

$$a(t) \propto e^{H_0 t}. \tag{4.14}$$

Similarly, an accelerated expansion happens during inflation, see section 4.5.

The left-hand side of eq. 4.10 is the square of the *Hubble parameter*, $H(t) \equiv \frac{\dot{a}}{a}$. Its value today is $H_0 = (73.8 \pm 2.4)\ \mathrm{km\,s^{-1}\,Mpc^{-1}}$ as measured by the Hubble Space Telescope [137][3]; recently, however, the Planck satellite has measured a smaller value: $H_0 = (67.3 \pm 1.2)\ \mathrm{km\,s^{-1}\,Mpc^{-1}}$ [85].

From observations of the Cosmic Microwave Background (CMB) - the relic photons that were released when electrons and protons combined to form hydrogen atoms - made by the Planck satellite [85], we know that the energy density is to a great accuracy equal to the *critical density*, ρ_{crit}: the energy density needed to have a flat Universe ($k = 0$), defined from eq. 4.10 as:

$$\rho_{\mathrm{crit}} \equiv \frac{3H_0^2}{8\pi G} \sim 10^4\, h^2 \frac{\mathrm{eV}}{\mathrm{cm}^3} \sim 3 \cdot 10^{10} \frac{\mathrm{M_{Sun}}}{\mathrm{Mpc}^3} \sim 10^{-30} \frac{\mathrm{g}}{\mathrm{cm}^3} \sim 10^{-6} \frac{\mathrm{GeV}}{\mathrm{cm}^3}, \quad (4.15)$$

i.e., in the Universe is almost empty ($\sim$ one Hydrogen atom per cubic metre).[4]

Different energy components are expressed as ratios with respect to ρ_{crit}, that can be thought of, in a hand-waving fashion, as a measure of the different weights of kinetic $K_i \sim \frac{1}{2} m_i \dot{a}^2$ and potential energy $U_i \sim \frac{GMm_i}{a}$ for a particle of mass m_i, as can be trivially seen using $V \sim \frac{4}{3}\pi a^3$:

$$\Omega_i \equiv \frac{\rho_i}{\rho_{\mathrm{crit}}} \sim \frac{U_i}{K_i}. \quad (4.16)$$

Using $\Omega_{\mathrm{tot}} = \sum_i \Omega_i$, eq. 4.10 can be expressed in the following compact and nice form:

$$\Omega_{\mathrm{tot}} - 1 = \frac{k}{a^2\, H^2}. \quad (4.17)$$

4.3 Hubble's Law and other cosmological parameters

Let us introduce a few important cosmological concepts and parameters. *Redshift* is defined as

$$z \equiv \frac{\lambda_0 - \lambda_e}{\lambda_e} = \frac{a_0}{a_e} - 1\ , \quad (4.18)$$

[3]The subscript 0 always denotes current values. Sometimes h is used, which is today's Hubble constant, H_0, in units of $100\,\mathrm{km\,s^{-1}\,Mpc^{-1}}$. A useful quantity to keep in mind is $h^2 \simeq 0.5$.

[4]Notice the overdensity at our location in the Milky Way (MW), where $\rho_{\mathrm{local}} \approx 0.3\,\mathrm{GeV\,cm^{-3}}$.

where λ_0 is the observed wavelength of the radiation at a time t_0 and λ_e is the wavelength emitted at a time t_e by the source which is at a *comoving coordinate* r. The convention is to take $a_0 = 1$.

The length of the spatial geodesic at a fixed time, $dt = 0$, is the *proper distance* d_p. Along a radial geodesic $d\Omega = 0$, so we get from eq. 4.2:

$$d_p(t) = a(t)\, r. \tag{4.19}$$

Differentiating with respect to time, we get:

$$v_r = H_0\, d_p, \tag{4.20}$$

where for simplicity we have taken the *peculiar velocities* of the galaxies to be zero, i.e., $v_p \equiv a\dot{r} = 0$. Therefore galaxies expand with *recessional velocities* v_r proportional to their proper distances. This is known as *Hubble's Law* and has been tested to a great accuracy (for large values of redshift there are deviations, see below).

The *luminosity distance* is defined as

$$d_L^2 = \frac{L}{4\pi F}\ , \tag{4.21}$$

where L is the luminosity of the source and F the flux received by the observer.

In an expanding Universe one obtains from energy conservation that the flux received at our position, whose photons are redshifted by a factor $1 + z \equiv a_0/a$, is:

$$F = \frac{L}{4\pi a_0^2 r^2 (1+z)^2}. \tag{4.22}$$

So from eqs. 4.21 and 4.23, we get that:

$$d_L = d_p(1+z)\ . \tag{4.23}$$

The *deceleration parameter* is defined as:

$$q = -\frac{a\ddot{a}}{\dot{a}^2}\ . \tag{4.24}$$

To connect observations (*redshift, luminosity distances*) and the cosmological parameters (H_0, q_0) let us consider the path travelled by light in a null-geodesic. From eq. 4.2:

$$0 = ds^2 = -dt^2 + \frac{a^2}{1-kr^2}dr^2, \tag{4.25}$$

and taking $k = 0$, we can integrate it from a time t_1 to the current time, t_0:

$$r = \int_{t_1}^{t_0} \frac{dt}{a(t)}. \tag{4.26}$$

For small enough redshifts, we can expand the scale factor in a Taylor series around its actual value a_0:

$$a(t_1) = a_0 + (\dot{a})_0 \Delta t + \frac{1}{2}(\ddot{a})_0 (\Delta t)^2 + \ldots, \tag{4.27}$$

where $\Delta t = t_1 - t_0$. Then, eq. 4.26 becomes:

$$r = a_0^{-1} \left[-\Delta t + \frac{1}{2} H_0 \Delta t^2 + \ldots. \right]. \tag{4.28}$$

Substituting eq. 4.27 in eq. 4.18, we get:

$$\frac{1}{1+z} = 1 + H_0 \Delta t - \frac{1}{2} q_0 H_0^2 \Delta t^2 + \ldots, \tag{4.29}$$

from which Δt can be obtained by expanding in z:

$$\Delta t = H_0^{-1} \left[-z + \left(1 + \frac{q_0}{2} \right) z^2 + \ldots \right]. \tag{4.30}$$

Replacing eq. 4.30 in eq. 4.28 it is straightforward to obtain

$$r = \frac{1}{a_0 H_0} \left[z - \frac{1}{2} \left(1 - q_0 \right) z^2 + \ldots \right]. \tag{4.31}$$

Finally, using eq. 4.23, we get:

$$d_L = H_0^{-1} \left[z + \frac{1}{2}(1 + q_0) z^2 + \ldots \right]. \tag{4.32}$$

For $z \ll 1$, we have that $z = H_0 \, d_L$. Using that for low enough redshifts the *recessional velocity* is $v_r \approx cz$ and $d_L \approx d_p$, we get *Hubble's Law*. At larger redshifts we will have deviations from this law that are connected with the *deceleration parameter*, as can be seen in eq. 4.32.

4.4 The energy content of the Universe

In 1998, by using type Ia Supernovae, which are *standard candles*, i.e., their luminosity profiles (L) are known, measurements of d_L (see eq. 4.21) showed that the expansion of the Universe in recent epochs is accelerating [15, 16]. A cosmological constant Λ could provide the repulsive force needed to accelerate the expansion, with $\rho_\Lambda = -p = \frac{\Lambda}{8\pi G}$, but this does not have to be the case, and in general we refer to this mysterious component with negative pressure as dark energy (DE). From these Supernovae luminosity distances, a combination

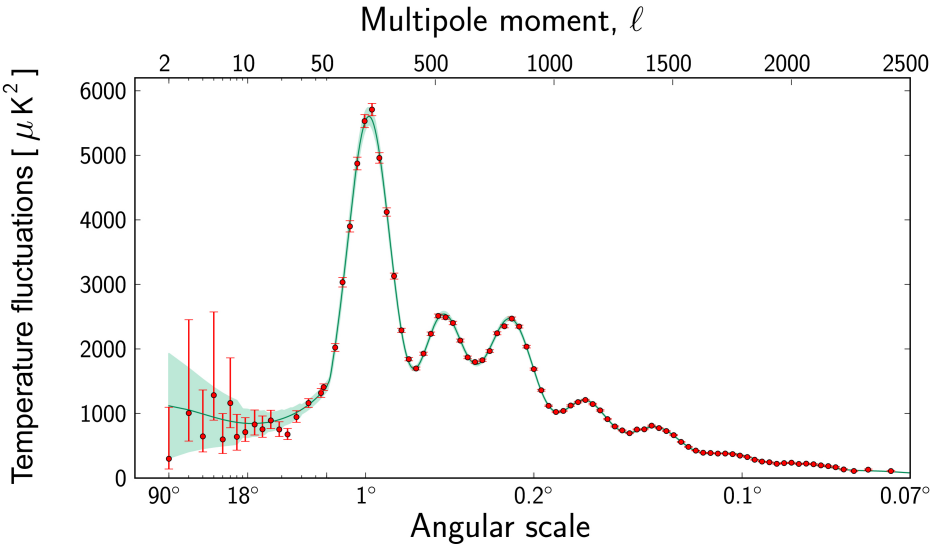

Figure 4.1: The temperature fluctuations of the CMB observed by Planck [85].

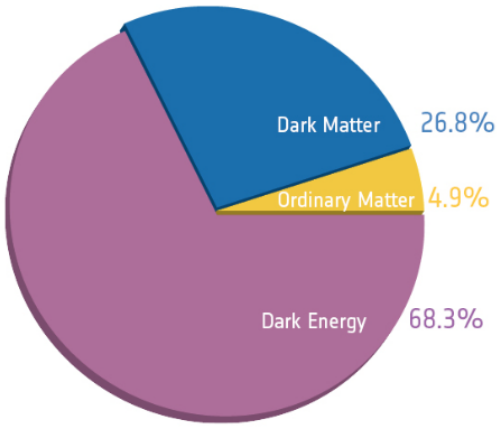

Figure 4.2: The energy content of the Universe by Planck [85].

of the total energy density in matter, $\Omega_{\rm matter}$, and that in dark energy, $\Omega_{\rm DE}$, can be inferred.[5]

We show in figure 4.1 the CMB temperature fluctuations as a function of the angular scale [85]. Depending on the content of baryons, DM and DE, the shape, position and height of the CMB peaks vary. For instance, the position of the first peak of the CMB tells us that the Universe is flat, $\Omega_{\rm total} = 1$. Using latest Planck results [85], we know the following facts about the energy content of the Universe today, illustrated in figure 4.2:

- It is dominated by DE, with $\Omega_{\rm DE} \sim 0.68$. If the current acceleration is understood as being caused by a cosmological constant Λ, which has been negligible throughout the entire history of the Universe, this poses the question of *why precisely now* $\Omega_{\rm matter} \sim \Omega_\Lambda$.
- DM constitutes a significant fraction of the energy density in the Universe, $\Omega_{\rm DM} \sim 0.27$.
- Visible matter, which is described by the first family of the SM (atoms) (see chapter 1) represents just a tiny fraction of the total, $\Omega_{\rm b} \approx 0.05$.[6]
- The photon and the neutrino energy densities are almost negligible.

So we have that:

$$\Omega_{\rm total} = \Omega_{\rm b} + \Omega_{\rm DM} + \Omega_{\rm DE} = 1. \tag{4.33}$$

The baryon density $\Omega_{\rm b}$ has also been measured and agrees well with the synthesis of elements in the Early Universe (a few seconds after the *Big Bang*), known as *Big Bang Nucleosynthesis* (BBN) [138–142]. At temperatures ~ 1 MeV, the light elements were produced with mass abundances of $\sim 75\%$ (^{1}H), $\sim 25\%$ $^4_2$He, $\sim 0.01\%$ deuterium ($^2_1$H) and $^3_2$He, and $\sim 10^{-10}\%$ $^7_3$Li. For instance, a somewhat hand-waving computation of the Helium mass abundance is rather straightforward. Calling n_n (n_p) the number density of neutrons (protons), roughly the final number of He nuclei is $1/2\, n_n$, as two neutrons per He atom are needed. The mass is $m_{\rm He} \sim 4m_n$, so $\rho_{\rm He} \approx 2n_n m_n$ and the total mass is $\rho_{\rm tot} \approx (n_n + n_p)m_n$, where we took $m_n \sim m_p$. The final mass fraction of Helium $Y_{\rm He}$ is therefore given by:

$$Y_{\rm He} \equiv \frac{\rho_{\rm He}}{\rho_{\rm tot}} = \frac{2(n_n/n_p)}{1 + (n_n/n_p)}, \tag{4.34}$$

[5] Λ can be also interpreted as entering on the left-hand side of the GR equations, eq. 4.3, forming part of the *geometry of the Universe*, although it is probably easier to think of it as an extra energy component.

[6] There is no better *lesson in humility* towards our knowledge of the Universe as this piece of data.

which just depends on the neutron to proton fraction at the moment of Nucleosynthesis, given by their equilibrium distributions:

$$\frac{n_n}{n_p} \sim e^{\frac{-(m_n - m_p)}{T_{\rm Nucl}}}. \tag{4.35}$$

Neutrons interact with positrons or electron neutrinos to create protons and other products, until the expansion of the Universe is larger than these rates, moment at which they freeze-out. If Nucleosynthesis occurred very early, $T_{\rm Nucl} \gg 10$ MeV, then $n_n/n_p \sim 1$ and $Y_{\rm He} \to 1$. If too late, $T_{\rm Nucl} \ll 1$ MeV, then $n_n/n_p \sim 0$ and $Y_{\rm He} \to 0$. At $T_{\rm Nucl} \sim 0.7$ MeV which is the correct freeze-out temperature, $n_n/n_p \sim 1/6$[7], and at $T_{\rm Nucl} \sim 0.1$ MeV, when the Universe had cooled sufficiently to allow deuterium nuclei to survive disruption by high-energy photons, $n_n/n_p \sim 1/7$, for which one gets $Y_{\rm He} \sim 0.25$, in agreement with observations.

The excellent agreement between the theoretical computations and the observations is one of the main evidences of a *Hot Big Bang*, together with the observation of the CMB.

Analysis of *Large Scale Structure* (LSS), like the study of the photon-baryon fluid before recombination, where the competition between gravity and radiation pressure produces oscillations in the plasma which propagate as acoustic waves, known as *Baryon Acoustic Oscillations* (BAO), can be used to infer the cosmic expansion. Also from observations of clusters of galaxies, for instance, via *gravitational lensing*, one gets information on $\Omega_{\rm matter}$.

For a mass density $\rho(\mathbf{r})$, one can define the density contrast $\delta(\mathbf{r}) \equiv {}^{(\rho(\mathbf{r})-\rho_0)}/_{\rho_0}$, where ρ_0 is the mean value of the matter density. The *matter power spectrum*, $P(\mathbf{k})$, is just the Fourier transform of the correlation function of the matter density contrast, $\xi(\mathbf{r}) = \langle \delta(\mathbf{r_1})\delta(\mathbf{r_1}+\mathbf{r})\rangle$, i.e.:

$$P(\mathbf{k}) = \int \xi(\mathbf{r})\, \mathbf{e^{i\,k\cdot r}}\, \mathbf{d^3 r}, \tag{4.36}$$

and can be reconstructed from different observations, as shown in figure 4.3. As will be discussed in chapter 5, if DM was hot, $P(\mathbf{k})$ at low scales would be suppressed (also warm dark matter modifies it, but it is compatible).

The different cosmological observations from CMB, BAO and Supenovae agree very well, as can be seen in figure 4.4, and it is sometimes known as *the Concordance Model* (another name of the ΛCDM model).

[7] This fraction is not constant, as the neutron decays.

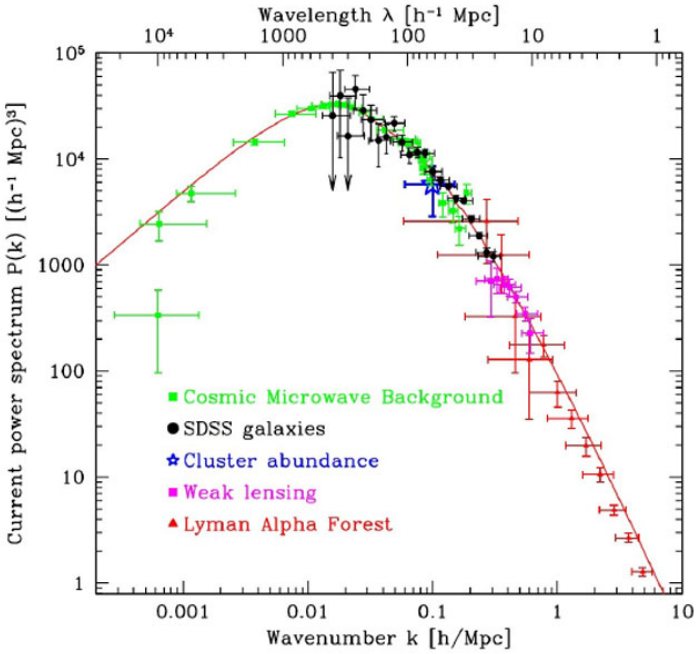

Figure 4.3: The matter power spectrum $P(\mathbf{k})$ reconstructed from different observations [143].

4.5 An inflationary epoch

The evidence for an inflationary epoch in the first stages of the Universe, at $t \sim 10^{-34}$ s, is very strong. Looking at eq. 4.11, we see that to have an accelerated expansion, $\ddot{a} > 0$, we need that, if the component i dominates the energy density, $\rho_i(t) + 3p_i < 0$ (i.e., $\omega_i < -1/3$).

This is equivalent to demanding that the comoving *Hubble radius* decreases with time:

$$\frac{d}{dt}\left(\frac{1}{a\,H}\right) \equiv \frac{-\ddot{a}}{a\,H} < 0. \tag{4.37}$$

One of the most important pieces of evidence for an epoch of accelerated expansion comes from the CMB. As shown in figure 4.1, where the CMB temperature fluctuations are plotted as a function of the angular scale [85], the CMB is extremely homogeneous, with temperature fluctuations $\delta T/T \sim 10^{-5}$. The problem is that within the standard *Big Bang* paradigm, these regions were never causally connected. This is known as *the horizon problem* and it is easy to show how inflation solves it by looking at figure 4.5 (from [34]), which shows the evolution of the comoving Hubble radius, $1/(aH(t))$, which is the maximum distance between causally connected regions (the maximum

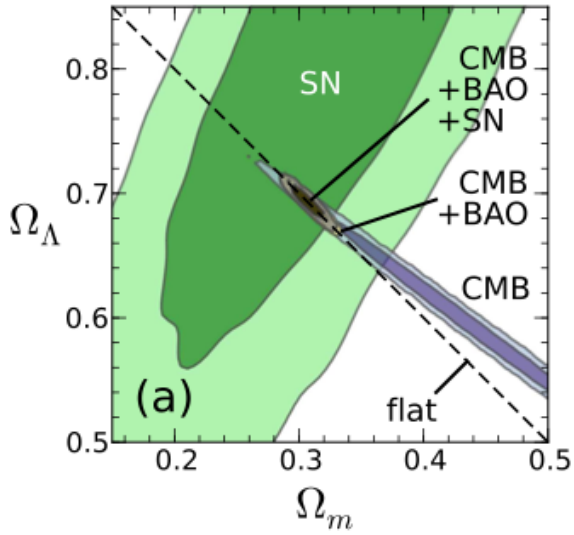

Figure 4.4: The concordance within the ΛCDM model of the different cosmological observations coming from the CMB (Planck and WP), BAO (SDSS-II, BOSS and 6dFGS) and Supernovae (Union2), from [144]. Dark and light regions indicate 68.3% and 95.4% CL.

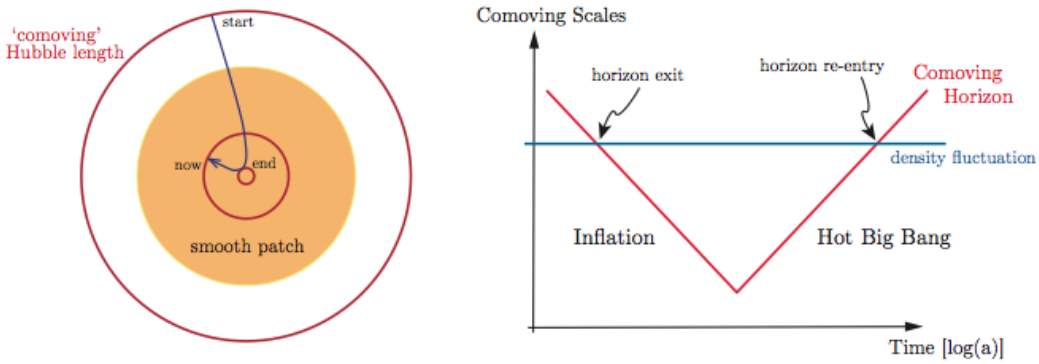

Figure 4.5: Left: The comoving Hubble sphere shrinks during inflation and expands after inflation. Right: all scales relevant to cosmological observations today were larger than the comoving *Hubble radius* until recently (came back within the *Hubble radius* at relatively recent times). However, at sufficiently early times, these scales were smaller than the *Hubble radius* and therefore causally connected.

distance light has had time to travel), shrinking during inflation and expanding afterwards.

All scales that are relevant to cosmological observations today were larger than the Hubble radius until recently - having reentered the Hubble radius at relatively recent times. However, at sufficiently early times, these scales were smaller than the Hubble radius and therefore causally connected if inflation happened.

As has been already said, current observations of the CMB by the Planck satellite [85] tell us that the Universe is flat, i.e., $k = 0$ in eq. 4.2, and therefore $\Omega_{\text{total}} \equiv \frac{\rho_{\text{total}}}{\rho_{\text{crit}}} = 1$.[8] In the standard picture, the right-hand side of eq. 4.17 always grows with time ($\propto t$ in RD ($\propto t^{2/3}$ in MD)), and therefore Ω would have to be severely fine-tuned to one in the past to be observed today as having a value equal to one. This is known as *the flatness problem*, and a period of accelerated expansion is able to solve it, as can be clearly deduced from eq. 4.37. Last but not least, the density fluctuations that we see in the CMB, from which structures grew, are caused by the primordial fluctuations of the inflationary field Φ and the metric $g_{\mu\nu}$ ($\Phi(\vec{x}, t) \equiv \Phi(t) + \delta\Phi(\vec{x}, t)$, $g_{\mu\nu}(\vec{x}, t) \equiv g_{\mu\nu}(t) + \delta g_{\mu\nu}(\vec{x}, t)$).

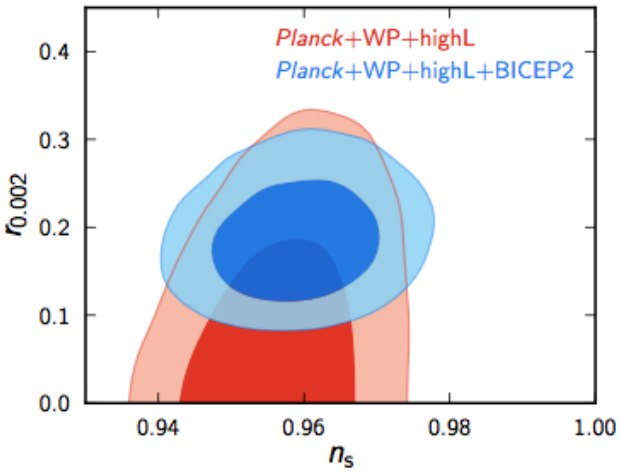

Figure 4.6: Contours showing the 68% and 95% CL regions for r and the scalar spectral index n_s, from [12].

Inflation implies that the quantization of the gravitational field coupled to the exponential expansion produces a primordial background of stochastic

[8] The first acoustic peak determines the size of the horizon at the time of decoupling, and therefore the geometry of the Universe.

gravitational waves, that would give a unique signature on the CMB via local quadrupole anisotropies, that include a *curl* or B-mode component at degree angular scales, which depends on the tensor-to-scalar ratio, r. Recently, the first detection of primordial B-modes was made by BICEP2 [12], in the range $30 < l < 150$, inconsistent with the null hypothesis at several standard deviations. They give a tensor-to-scalar ratio of $r = 0.20^{+0.07}_{-0.05}$. This ratio in the simplest models tells us that the typical energy scale of inflation is similar to the GUT scale, $\sim 10^{16}$ GeV. In figure 4.6 from [12] are shown contours in the tensor (r) and the scalar spectral index (n_s) plane. As scalars do not produce B-modes while tensors do, the detection of B-modes is a smoking gun of tensor modes, and therefore of inflation. This discovery, which as always in physics should be confirmed by other independent experiments, like Planck, is to date the most compelling evidence of a nearly exponential expansion which sets the initial conditions for the subsequent *Hot Big Bang*, understood as the creation of particles from inflaton decays, not as the initial singularity.

For different inflationary models and a more extense discussion, the reader is referred to [34], a nice review of the topic.

Chapter 5

Dark matter

In this chapter we discuss the evidence and properties of DM. We will then focus on Weakly Interacting Massive Particles (WIMPs) and detection prospects via indirect searches, colliders and cosmological imprints. We leave direct detection, which is the focus of this thesis, to chapter 6.

5.1 Evidence of dark matter

There is plenty of evidence for the existence of some extra matter in the Universe, whose properties we will detail in the next section. The most important pieces of evidence are the following:

1. Rotation curves of spiral galaxies.

   Like the planets rotating around the Sun, one would expect that luminous matter in the galaxies, basically Hydrogen, should have a rotation speed that would decrease with the distance to the galactic centre as $1/\sqrt{r}$.[1] However, one observes[2] that the rotation velocity remains practically constant ($v_{rot} \sim v_{Sun} \sim 220$ km/s) up to large distances, see figure 5.1. This can not be understood with just the luminous matter, which decreases exponentially with the distance: there must be a much larger gravitational potential than that created by luminous matter.

   There are non-DM possibilities to explain this piece of evidence, for instance if we modify gravity at these scales (Modified Newtonian Dynamics, MOND [145, 146] or its relativistic version [147]). Its basic

[1] In reality there are two components of luminous matter with different behaviours, the bulge and the disc, as can be seen looking at figure 5.3.

[2] In the Milky Way (MW) we can measure its rotation curve using the Hydrogen 21 cm line, as there is too much dust to observe X-rays.

assumption is that *Newton's Second Law* has only been tested at large accelerations. The new modified equation would be:

$$F = m\,\mu[a/a_0]\,a, \tag{5.1}$$

where $\mu = 1$ for $a \gg a_0$, recovering *Newton's Second Law*, and $\mu = a/a_0$ if $a \ll a_0$. Therefore, for a star of mass m far away from the galaxy of mass M at a distance r, we have:

$$F = \frac{GMm}{r^2} = m\,\mu[a/a_0]\,a, \tag{5.2}$$

and we get for $a \ll a_0$:

$$a = \frac{\sqrt{GMa_0}}{r} \;\rightarrow\; v = (GMa_0)^{1/4} = \text{constant}. \tag{5.3}$$

The only parameter of the theory, a_0, is similar for all galaxies and has a curious value, $a_0 \sim 1.2 \cdot 10^{-10}\,\mathrm{m\,s^{-2}} \sim c\,H_0$.

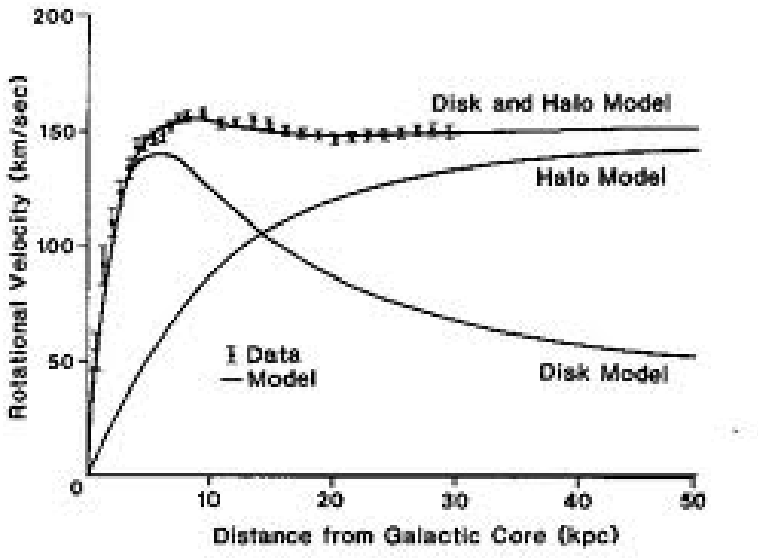

Figure 5.1: Rotation velocity as a function of distance. It can be seen how the sum of the disc and the halo components give the observed final constant speed.

2. Mass-to-light ratio of galaxy clusters.

One can apply the Virial Theorem ($2T + V = 0$) to galaxy clusters, which are gravitationally bounded systems. From X-rays one gets the temperature of the baryons in the gas, and therefore their velocities, from which the mass of the cluster can be inferred. In the 1930's, F. Zwicky applied this procedure to the galaxies inside the *Coma Cluster*, and obtained a very large mass-to-light ratio of ~ 400 (in solar units)[3]: more matter than the luminous one is present.

3. Collisions of clusters, like the Bullet Cluster.

   In figure 5.2 [148] we see the result of the merging of two galaxy clusters. Via gravitational lensing we can infer that most of the matter of the cluster is located in the blue regions, while from X-rays observations we see that the luminous matter, basically the gas of the clusters that collided, is located in the red regions. It is very difficult to conceive how gravity in a modified theory will point to regions (the blue ones) where no matter is present.

Figure 5.2: Picture of the Bullet Cluster. In blue the matter component, inferred from gravitational lensing; in red, the luminous component, from X-rays.

4. The anisotropies of the Cosmic Microwave Background (CMB).

   As was discussed in chapter 4, by measuring the positions and relative heights of the acoustic peaks of the CMB [85,149], see figure 4.1, one can deduce the energy content of the Universe. There are two competing forces in the photon-baryon-dark matter plasma: radiation pressure that acts as a repulsive force, and gravity that is an attractive force. DM

[3]Currently typical values of the total matter density in clusters are $\Omega_M \sim 0.2 - 0.3$.

does not couple to photons, while baryons do, and therefore the relative heights of the peaks give us information about the relative amount of DM (mainly the third peak) compared to baryonic matter (mainly the second peak).

5. The growth of structure.

   From N-body simulations we infer that the growth of structures in the Universe is a hierarchical process. During radiation domination the growth is slow; clustering becomes more efficient when matter dominates. As DM does not dissipate energy, it seeds large potential wells, where baryonic matter becomes gravitationally trapped, forming therefore small scales that are gravitationally bound and decouple from the overall expansion. This leads to a picture of hierarchical structure formation with small-scale structures (like stars and galaxies) forming first and then merging into larger structures (clusters and superclusters of galaxies).

6. Globular Clusters.

   These are regions of $\sim 10^5$ stars, very old, that would escape the galaxy, as they are moving very fast, if the galactic potential well was just the one created by the luminous matter.

7. Other cosmological observations, like the matter power spectrum, BBN and gravitational lensing tell us that the amount of matter is not compatible with the luminous one.

5.2 Properties of dark matter

Although there are exceptions, the main properties that DM particle χ should have are the following:

- It interacts gravitationally.
- Collision-less, it does not dissipate. This is the main reason why DM does not lose energy and therefore forms ellipsoidal haloes (see figure 5.3 for our halo in the Milky Way), unlike baryonic matter, that forms discs due to energy losses and angular momentum conservation.
- Cold (or warm) at the time of decoupling, i.e., $m_\chi > T_{\rm dec}$, otherwise it would have free-streamed erasing the smaller structures. The matter power spectrum $P(\mathbf{k})$, as shown in figure 4.3, gives us very valuable

information about the type of DM particle. For typical CDM, the smaller scales that can be formed are $\sim 10^{-6}\, M_S$, while for typical WDM (HDM) these are $\sim 10^{9}\, M_S$ [150] ($\sim 10^{15}\, M_S$), yielding for them a non-hierarchical growth of structure. This rules-out HDM as a primary component, as $P(\mathbf{k})$ would be suppressed at the smaller scales, while WDM is still allowed, even as the dominant component.

- Neutral (no tree level EW interactions). It does not emit or absorb light. Otherwise the CMB as well as the matter spectrum would be different. In addition, bounds on charged DM (CHAMPs) [151] from looking for heavy isotopes or heavy water are very strong, see for instance [152].

- Colorless (no tree level color interactions). In general, DM that is strongly interacting with nucleons is severely constrained, for instance from measurements of the Earth's heat flow [153].

- Long-lived with respect to the age of the Universe (or stable), so it is present today with the observed abundance. Light DM candidates, such as the axion or the sterile neutrino, are naturally long-lived as their lifetimes are inversely proportional to the mass to the fifth power. For the case of WIMPs, however, some symmetry is usually needed.

- It may interact weakly with the SM. If it is a thermal relic, in principle it is hoped that it *talks* to the SM, see section 5.3, although this does not have to be the case.

- It has to be a new particle not present in the SM: baryonic objects such as interstellar gas, massive compact halo objects (MACHOs) or primordial black holes [154] are ruled-out as a significant component. MACHOs are ruled-out by gravitational lensing searches [155] and black holes in several mass ranges are severy constrained, see for instance [156]. In addition, BBN imposes severe constraints on the amount of light elements, which matches the amount of gas (basically Hydrogen and Helium) observed [157]. Neutrinos (HDM) are also ruled-out as the primary component: we know that relic neutrinos are part of the DM energy density, but not a significant fraction as they are hot. Well-motivated non-baryonic candidates include axions (can explain the CP problem of the SM) or neutralinos (SUSY solves theoretically the Hierarchy Problem).[4]

[4]For more information on WIMP candidates (among other DM topics, such as the evidence and properties of DM) the reader is referred to the review [158]. For a minimalistic approach, see [159], where the different multiplets with their assignments that can be added

- It can have whatever spin: $0, 1/2, 1...$

- There could be more than one non-baryonic DM particle, i.e., contributing significantly to the DM energy density of the Universe. Why would there just be one stable DM? In the SM there are a few stable (or extremely long-lived) particles: electrons (lightest electrically charged particle), protons (lightest particle carrying baryon number, which could decay only by higher-dimensional operators), photons (massless, by kinematics), gluons (lightest colored states) and the lightest fermion, which is the lightest neutrino, stable thanks to angular momentum conservation.

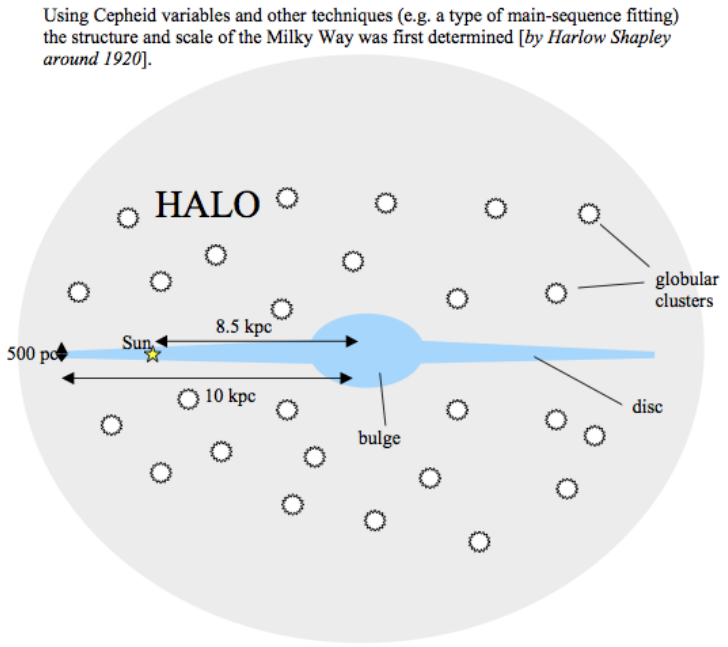

Figure 5.3: Pictorical view of the Milky Way (MW), with the disc, the bulge and the DM halo. Figure taken from the lecture notes "Galaxies", by Phil Uttley.

to the SM to provide a neutral stable particle, that is a viable DM candidate, are studied (like a spin 1/2 $Y = 0$ $SU(2)_{\rm L}$ quintuplet which has a stable particle).

5.3 Thermal freeze-out and the WIMP paradigm

In the *Hot Big Bang* paradigm, basic ingredient of the ΛCDM model, the Early Universe is a hot and dense *soup* of particles in thermal equilibrium. The particle interaction rate, $\Gamma \sim n \langle \sigma v \rangle$, is initially, when the temperature is very high, much larger than the Hubble expansion rate, H. Thermal decoupling happens at $T = T_{\text{f.o.}}$, when the particle interaction rate becomes of the same order of the Hubble expansion rate, $\Gamma(T_{\text{f.o.}}) \sim H(T_{\text{f.o.}})$. To compute relic densities one should solve Boltzmann equations, that describe the evolution of the number densities, $n(t)$:

$$\frac{dn}{dt} + 3Hn = -\langle \sigma_{ann} v \rangle [(n)^2 - (n^{eq})^2], \tag{5.4}$$

where n^{eq} is the equilibrium number density. However, here we will just discuss what happens qualitatively.

If this freeze-out (f.o.) occurs in the radiation-dominated era, $T_{\text{f.o.}} > T_{\text{M-R equality}} \sim 1$ eV, we can use that ($n_{\text{hot}} \propto T^3$)

$$\rho \sim \rho_{\text{rad}} = \frac{\pi^2}{30} g_* T^4, \tag{5.5}$$

with g_* the number of relativistic degrees of freedom at $T_{\text{f.o.}}$. Therefore, using eq. 4.10 (setting $k = 0$), we can approximate:

$$H = \left(\frac{8\pi G}{3}\rho\right)^{1/2} \simeq \frac{T^2}{M_p}, \tag{5.6}$$

where we used that $M_p = \sqrt{\frac{1}{8\pi G}}$.

Depending on whether the particle decoupling happens while being relativistic ($T_{\text{f.o.}} > m_\chi$) or non-relativistic ($T_{\text{f.o.}} < m_\chi$), it is called a *hot* or *cold* relic.

Neutrinos, that are non-relativistic today (at least two of them)[5], but are relativistic (hot) when they decouple at $T^\nu_{\text{f.o.}} \simeq 1$ MeV, have a relic density given by:[6]

$$\Omega_\nu h^2 \simeq \frac{\sum_i m_{\nu i}}{93\,\text{eV}} \lesssim 10^{-2}, \tag{5.7}$$

where we have used the approximate upper bound on the sum of neutrino masses coming from different cosmological observations, $\sum m_{\nu i} \lesssim 1$ eV. As

[5] If there is a relativistic neutrino today, its contribution to the energy density is $\Omega_\nu h^2 \sim 5.6 \cdot 10^{-5}$.

[6] Before knowing the upper bound on neutrino masses that comes from cosmology, for instance from not erasing the smaller scales of the Universe, one could set a limit on $\sum m_{\nu i} \lesssim \mathcal{O}(20)$ eV so the Universe was not over-closed.

we know from neutrino oscillations (see chapter 2) that $\sum m_{\nu i} \gtrsim 0.06\,(0.1)$ eV for NH (IH), there are also lower bounds for their contribution to the energy density: $\Omega_\nu h^2 \gtrsim 6 \cdot 10^{-4}\,(\sim 10^{-3})$.

WIMPs are DM particles with weak scale masses, $m_\chi = \mathcal{O}(1 - 10^3)$ GeV, and interactions, $\sigma_\chi = \mathcal{O}(10^{-8})\,\text{GeV}^{-2}$. They are among the most popular candidates (several examples exist, such as the neutralino in Supersymmetry), and in principle they can be detected.

When the temperature of the Universe was larger than their mass, $T > m_\chi$, the number densities of photons and WIMPs were similar and $n_\chi \sim n_\gamma \propto T^3$ and WIMPs annihilated into lighter particles and viceversa. But when the temperature dropped below their mass, their number density was reduced exponentially, $n_\chi \propto e^{\frac{-m_\chi}{T}}$. As a consequence, $\Gamma < H$ and they froze-out. With their weak scale values, the final relic abundance is found to be roughly the observed one. This is called the WIMP miracle, as the final abundance is proportional to the one at the equilibrium, which for CDM (non-relativistic) depends exponentially on the temperature at freeze-out $T_{\text{f.o.}}$ and on the mass (it is Boltzmann suppressed). The freeze-out temperature $T_{\text{f.o.}}$ depends on the DM mass and only logarithmically on the cross-section..., yielding a final value of $m_\chi/T_{\text{f.o.}} \approx 20 - 25$, quite insensitive to the particular kind of the DM interactions and masses.

Neglecting decays of the DM particles[7], the final expression for the current number density is:

$$n_{\text{today}} = n_{\text{fo}} = \frac{H_{\text{f.o.}}}{\langle \sigma_{\text{ann}} v \rangle_{\text{f.o.}}}\,, \tag{5.8}$$

and the relic density can be easily computed to be:

$$\Omega_{\text{DM}} h^2 \propto \frac{3 \times 10^{-27}\,\text{cm}^3\,\text{s}^{-1}}{\langle \sigma_{\text{ann}} v \rangle_{\text{f.o.}}}, \tag{5.9}$$

where one can see that for weak scale couplings it is easy to achieve the observed value, $\Omega_{\text{DM}} h^2 \sim 0.1$.

There is an allowed range in masses for CDM relics: $\mathcal{O}(10)\text{GeV} \leq m_\chi \leq \mathcal{O}(100)\text{TeV}$. The upper bound comes from the fact that couplings cannot be arbitrarily large, while the lower bound, known as the Lee-Weinberg limit [160], comes from not over-closing the Universe for weak scale cross-section ($\sigma \sim G_F^2 m_\chi^2$) DM particles.

Exceptions of this typical thermal freeze-out exist [161], the most relevant ones being the existence of resonances (with mass $m_R \simeq 2m_\chi$), threshold effects (which imply that $\sigma_{\text{f.o.}} > \sigma_{\text{today}}$) and co-annihilations (for various DM particles with similar masses, $m_{\text{heavy}} - m_{\text{light}} \lesssim T_{\text{f.o.}}$).

[7] There could be entropy injections from relic decays, for instance, which would dilute the final densities.

5.4 Asymmetric dark matter

In the standard paradigm for DM via thermal freeze-out, the DM and baryon relic densities arise from completely different mechanisms, and the fact that their densities are of the same order of magnitude is a coincidence. Asymmetric DM (see for instance [162–164], [165] for a nice implementation and [166] for a recent review on the topic) proposes that, similarly to baryons, a particle-antiparticle asymmetry of DM particles is left over, linked to the ordinary baryonic one. Therefore, the number densities are similar, $n_\chi \sim n_{\text{baryons}}$, and the masses fulfill $m_\chi \sim 5\, m_{\text{baryons}} \sim 5\,\text{GeV}$.

The two basic ingredients an asymmetric DM model needs to have are:

- a conserved (or approximately-conserved) dark global quantum number, so that a dark asymmetry exists.
- an interaction that erases the symmetric part, just as in the SM the strong and electroweak interactions annihilate the symmetric component of the SM into photons.

Apart from these, the new dark sector could be as complicated (or more) as the SM.

In addition to being theoretically very appealing, asymmetric DM models recently gain attention as an explanation for the low DM mass hints observed by some direct detection experiments, as will be shown in chapter 6. A special feature is that indirect detection through DM particle-antiparticle annihilations is absent, because there are no DM antiparticles left to annihilate with, so direct detection seems in principle a more promising way to test this hypothesis.

5.5 Dark matter searches

In this thesis we focus on direct detection, therefore we next briefly review the status of other interesting ways to search for DM: indirect detection, collider searches and via cosmological measurements, and leave direct detection to chapter 6. These searches assume (*hope*) that DM interacts at some point with the SM.

5.5.1 Dark matter indirect detection

In principle, one could observe the annihilation and decay products of DM particles: neutrinos, photons (gamma rays, X-rays, synchrotron radiation),

electrons and positrons, protons and antiprotons, anti-deuterons (bound states of $\bar{p}$ and $\bar{n}$)...

These two different processes are given in general by the following expressions:

- Particle decay:

$$\Gamma_{\text{decay}} = \int n_\chi \, dV \cdot \frac{1}{\tau_{\text{decay}}} \cdot N_{\text{SM}}^{\text{decay}}. \tag{5.10}$$

- Particle annihilation:

$$\Gamma_{\text{ann}} = \int n_\chi^2 \, dV \cdot \sigma_{\text{ann}} \, v \cdot N_{\text{SM}}^{\text{ann}}. \tag{5.11}$$

In both cases the first term is the number of particles in the volume V, the second is the decay/annihilation rate and the third is the flux of SM particles per event.

WIMPs are therefore expected to annihilate very efficiently in regions with high densities, such as the galactic centre, galaxy clusters, dwarf spheroidals, the Sun... Of course, separating astrophysical origins (cosmic rays) from true DM particle decays is very challenging, and therefore anti-particles rather than particles, and heavy nuclei, which have much smaller backgrounds, are commonly searched for.

One of the *smoking guns* of DM would be for instance high energy neutrinos pointing directly to the Sun or a gamma ray line coming from the galactic centre, as they are not deflected by the magnetic fields of the galaxy.

The experimental situation is controversial, and although there is no confirmed DM discovery, there have been several claims in the past years. For example, Pamela, ATIC and Fermi have shown an excess with respect to the background of positrons in the ∼tens to ∼hundreds of GeV.

A DM explanation of the PAMELA excess faces the problem that no antiproton excess is observed (and no excess of radio emission or gamma rays). In addition, the DM particle should have an annihilation cross-section much larger than the one needed to explain the observed abundance.[8] All in all, pulsars seem to be a plausible explanation for this excess.

[8]The annihilation cross-section, σ_{ann}, does not have to be the same at freeze-out and at current times. If it is dominated by the p-wave contribution, it may happen that $\sigma_{\text{ann}}^{\text{f.o.}} > \sigma_{\text{ann}}^{\text{now}}$. Therefore, the $\sigma_{\text{ann}}^{\text{now}}$ extracted from absence of indirect signals constitutes a lower bound for $\sigma_{\text{ann}}^{\text{f.o.}}$.

5.5.2 Collider searches

DM particles, being very-weakly interacting and stable, are expected to escape detection at colliders, yielding large amounts of missing energy and other particles (for instance a jet or a photon) [167–169]. The limits set by these kind of searches at the Tevatron and LHC are competitive with those coming from direct searches, especially for spin-dependent interactions and light DM masses.

An important caveat to discover DM at colliders is that one can never say that they are stable enough, nor that their annihilation cross-section is such that, they are present today with the correct relic abundance and therefore constitute the DM of the Universe. Therefore, even if a stable neutral particle is observed at a collider, direct and indirect detection of it are needed before claiming it is the DM.

5.5.3 Imprints in BBN and in the CMB

DM annihilations and decays *inject* energy and particles, changing the history and properties of the Universe at different epochs. These energy injections can change the formation of light nuclei (BBN) (see for instance [170, 171]) or the anisotropies of the CMB (see for instance [172, 173] and more recently [174, 175]), yielding very strong constraints on the annihilation cross-section, especially in the case of the CMB.

A word of caution is in order in all indirect searches: in almost every analysis, the rates (and therefore the final constraints) depend crucially on the channel, and are therefore model-dependent.

Chapter 6

Direct detection of dark matter

We know that DM interacts gravitationally. A fundamental question is whether DM interacts also non-gravitationally. We review in this chapter direct detection: experiments that are looking for the scattering of DM particles from the galactic halo in underground detectors.

6.1 The event rate

As seen in chapter 5, particles that freeze-out with weak scale masses and couplings, or Weakly Interacting Massive Particles (WIMPs), are among the most interesting candidates, and at some level we expect that they interact with the SM.[1] If DM is a WIMP it may induce an observable signal in underground detectors by depositing a tiny amount of energy after scattering with a nucleus in the detector material [176]. Many experiments are currently exploring this possibility and delivering a wealth of data.

A useful picture to visualize direct detection is illustrated in figure 6.1, where one sees that, in our reference frame, as we move through the galactic halo, there is a DM flux of particles that goes through the Earth.

This flux gives rise to a differential event rate. The rate for a DM particle χ to scatter off a nucleus (A, Z) and deposit the nuclear recoil energy E_{nr} in the detector is given by $R(E_{nr}, t)$:

$$R(E_{nr}, t) = \frac{\rho_\chi}{m_\chi} \frac{1}{m_A} \int_{v>v_m} d^3v \frac{d\sigma_A}{dE_{nr}} v f_{\rm det}(\mathbf{v}, t), \tag{6.1}$$

and it is measured in events/keV/kg/day. m_A and m_χ are the nucleus and DM masses, σ_A the DM–nucleus scattering cross section and $\mathbf{v}$ the 3-vector

[1] Really, *we just hope* that they do interact with the SM, as there could be just an independent dark sector with no interactions with the SM.

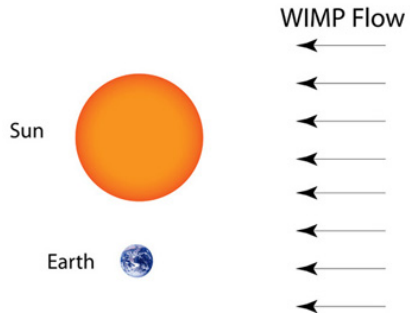

Figure 6.1: The WIMP flow in our rest-frame.

relative velocity between DM and the nucleus, with $v \equiv |\mathbf{v}|$.

In direct detection, only the DM density at our location in the MW matters, ρ_χ. It has some uncertainty, but it affects all experiments by a global factor. Typical values are $\rho_\chi \simeq 0.3\,\mathrm{GeV/cm^3}$. There are many different DM density profiles of our galaxy in the literature, one of the most popular ones being the Navarro-Frenk-White (NFW) (see [177] for a discussion on CDM haloes):

$$\rho(r) \propto \frac{1}{r(1+r/r_s)^2}, \tag{6.2}$$

with $r_s \sim 20$ kpc.

$f_{\mathrm{det}}(\mathbf{v}, t)$ describes the distribution of DM particle velocities in the detector rest frame, with $f_{\mathrm{det}}(\mathbf{v}, t) \geq 0$ and $\int d^3v f_{\mathrm{det}}(\mathbf{v}, t) = 1$, and it is related to the velocity distribution in the rest frame of the Sun, f_{sun} and at the galaxy, f_{gal}, by:

$$f_{\mathrm{det}}(\mathbf{v}, t) = f_{\mathrm{sun}}(\mathbf{v} + \mathbf{v}_e(t)) = f_{\mathrm{gal}}(\mathbf{v} + \mathbf{v}_e(t) + \mathbf{v}_{\mathrm{sun}}), \tag{6.3}$$

with $\mathbf{v}_{\mathrm{sun}} \approx (0, 220, 0)\,\mathrm{km/s} + \mathbf{v}_{\mathrm{pec}}$ and $\mathbf{v}_{\mathrm{pec}} \approx (10, 13, 7)$ km/s the peculiar velocity of the Sun. We are using galactic coordinates where x points towards the galactic center, y in the direction of the galactic rotation, and z towards the galactic north, perpendicular to the disc.

The velocity vector of the Earth, $\mathbf{v}_e(t)$, is relevant for the annual modulation signal, which will be described in the following section, and can be written as [178]

$$\mathbf{v}_e(t) = v_e[\mathbf{e}_1 \sin\lambda(t) - \mathbf{e}_2, \cos\lambda(t)] \tag{6.4}$$

with $v_e = 29.8$ km/s, and $\lambda(t) = 2\pi(t - 0.218)$ with t in units of 1 year and $t = 0$ at January 1st, while $\mathbf{e}_1 = (-0.0670, 0.4927, -0.8676)$ and $\mathbf{e}_2 = (-0.9931, -0.1170, 0.01032)$ are orthogonal unit vectors spanning the plane of the Earth's orbit, assumed to be circular. As shown in [179], eq. (6.4) provides

an excellent approximation to describe the annual modulation signal. For more information on the relevance of the Earth's velocity for direct detection experiments we recommend the recent analysis [180].

The integral of the velocity distribution enters in $R(E_{nr}, t)$ because DM scattering at different angles probes different DM velocities even for fixed E_{nr}. For a DM particle to deposit a recoil energy E_{nr} in the detector, a minimal velocity v_m is required by kinematics, restricting the integral over velocities in eq. (6.1).

For inelastic scattering between two DM particles close in mass, we have that the minimal velocity required for a recoil of energy E_{nr} is:

$$v_m = \sqrt{\frac{1}{2m_A E_{nr}}} \left(\frac{m_A E_{nr}}{\mu_{\chi A}} + \delta \right), \tag{6.5}$$

where $\mu_{\chi A}$ is the reduced mass of the DM-nucleus system, and δ is the mass splitting between the two DM states. For each value of E_{nr} there is a corresponding v_m while the converse is not always true: certain values of v_m correspond to two values of E_{nr}. We study inelastic scattering in detail in [6], where this simple observation gave rise to *shape test* explained there.

For elastic scattering, $\delta = 0$, eq. 6.5 reduces to

$$v_m = \sqrt{\frac{m_A E_{nr}}{2\mu_{\chi A}^2}}. \tag{6.6}$$

It is interesting to notice that for light DM particles, i.e., in the limit $m_\chi \ll m_A$, $v_m \propto 1/m_\chi$, and therefore we are probing the tail of the velocity distribution. In principle, the integral is extended up to arbitrarily large velocities, however, there is a maximum speed that DM particles can have to be gravitationally bound to the galaxy, known as the escape velocity, $v_{\rm esc}$ (more on it later).

The particle physics enters in eq. (6.1) through the differential cross section. For direct detection to make sense, DM should couple at some level to up and/or down quarks and/or electrons. Of course, it could happen that DM interacts with these first-family fermions via loops.

For the standard spin-independent (SI) and spin-dependent (SD) scattering the differential cross section has the form

$$\frac{d\sigma_A}{dE_{nr}} = \frac{m_A}{2\mu_{\chi A}^2 v^2} \sigma_A^0 F^2(E_{nr}), \tag{6.7}$$

where σ_A^0 is the total DM–nucleus scattering cross section at zero momentum transfer, and $F(E_{nr})$ is the nuclear form factor, different for SI and SD. If DM is composite, a DM form factor $F_{DM}(E_{nr})$ appears here, but we neglect this possibility for the rest of the thesis.

SI interactions arise from scalar and vector couplings to quarks, and σ_A^0 can be written for them as

$$\sigma_A^{\rm SI} = \sigma_p[Z + (A-Z)(f_n/f_p)]^2 \mu_{\chi A}^2/\mu_{\chi p}^2\,, \tag{6.8}$$

where σ_p is the DM–proton cross-section and $f_{n,p}$ are coupling strengths to neutron and proton, respectively. If $f_n \neq f_p$ the interactions are isospin-violating (IV).

SD interactions arise from axial-vector couplings to quarks, and σ_A^0 can be written for them as

$$\sigma_A^{\rm SD} = \frac{32\mu_{\chi A}^2}{\pi} G_F^2 \frac{(J+1)}{J}(a_p\overline{S_p} + a_n\overline{S_n})^2, \tag{6.9}$$

where J is the spin of the nucleus, $\overline{S_p}$ ($\overline{S_n}$) are the average spin contributions from the proton (neutron) groups and a_p (a_n) are the effective couplings to the proton (neutron).

In general both interactions contribute, although for nuclei with mass number $A > 20$ the SI contribution usually dominates.

It will be very useful for the rest of the thesis to define the halo integral

$$\eta(v_m, t) \equiv \int_{v>v_m} d^3v \frac{f_{\rm det}(\mathbf{v}, t)}{v}\,, \tag{6.10}$$

using which the event rate is given by

$$R(E_{nr}, t) = C\, F^2(E_{nr})\, \eta(v_m, t) \qquad \text{with} \qquad C = \frac{\rho_\chi \sigma_A^0}{2 m_\chi \mu_{\chi A}^2}. \tag{6.11}$$

The coefficient C contains the particle physics dependence, while $\eta(v_m, t)$ encodes the astrophysics dependence.

6.2 The annual modulation signal

The direct detection experiments measure the nuclear recoils via light, charge and/or heat. Some of them are capable of measuring two of these signals, which allow them to discriminate between electron (expected for backgrounds) and nuclear recoils (expected for DM interactions). In addition, DM will scatter at most once, and this is used to discriminate between nuclear recoils coming from DM and those coming from, for instance, neutrons, which could scatter more than once. Of course, going under mountains or to abandoned mines, using radiopure materials and building shieldings is of uttermost importance to be able to reject the environmental backgrounds.

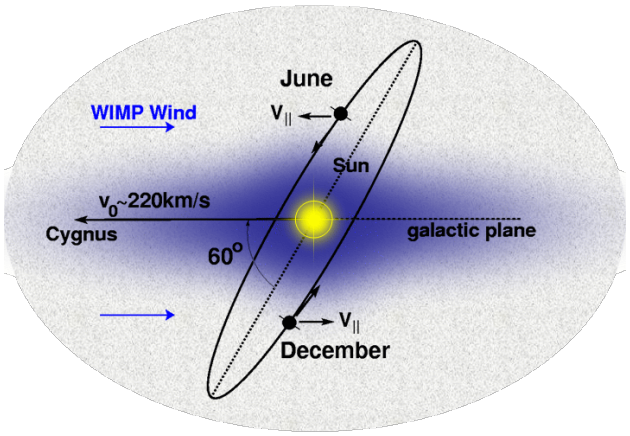

Figure 6.2: Representation of the Earth's orbit around the Sun that gives rise to the annual modulation signal of DM.

One of the most powerful ways to discriminate between backgrounds (not all unfortunately, as will be explained below) and DM signals is observing an annual modulation.

As can be seen in figure 6.2, due to the motion of the Earth around the Sun, the velocity of the DM will be different throughout the year. Qualitatively, the maximum will be in June, when $v^{June}_{\text{WIMP wind}} \sim v_{sun} + \frac{v_e}{2}$, and the minimum in December, when $v^{Dec}_{\text{WIMP wind}} \sim v_{sun} - \frac{v_e}{2}$. This is known as the *annual modulation signal* of DM, and it is a very useful discriminant of backgrounds. We recommend the reader the interesting review on the annual modulation [181].

The halo integral, eq. 6.10, and thus the rate, eq. 6.11, will have time-independent and time-dependent components

$$\eta(v_m, t) = \overline{\eta}(v_m) + \delta\eta(v_m, t)\,, \tag{6.12}$$

In general, one can expand $\eta(v_m, t)$ as a Fourier series

$$\eta(v_m, t) = \sum_{n=0} A^{(n)}_\eta(v_m) \cos 2n\pi(t - t_n), \tag{6.13}$$

where $A^{(0)}_\eta \equiv \bar{\eta}(v_m)$ is the time averaged rate, $A^{(1)}_\eta \equiv A_\eta(v_m)$ is the amplitude of the annual modulation signal, $A^{(2)}_\eta$ the amplitude of the semi-annual modulation, and so on.

In the work included in this thesis [4], we were able to bound A_η in terms

of $\eta(v_m)$, by doing an expansion in v_e. The bounds have the form

$$\int_{v_1}^{v_2} dv_m A_\eta(v_m) \leq v_e \, \overline{\eta}(v_1) \,, \tag{6.14}$$

and are almost independent of astrophysics.

6.3 The velocity distribution and the η-$v_{\rm min}$ plot

Astrophysical uncertainties are very relevant to direct detection experiments (see for instance [182–184]).

While stars (baryons) travel together in roughly circular orbits with small velocity dispersion, and therefore have roughly the same velocity in the galactic frame, $\sim 220\,\mathrm{km\,s^{-1}}$, DM particles travel individually with no circular dependence in general and therefore have a large velocity dispersion, with a wide velocity distribution.

When presenting results of DM direct detection experiments, it has become customary to use the Standard Halo Model (SHM), i.e., a Maxwellian DM velocity distribution, in order to show the constraints on the plane scattering cross section versus DM mass. This assumes an isotropic, isothermal sphere for the DM distribution. In the galactic rest frame (truncated at the galaxy escape velocity $v_{\rm esc}$ to account for the fact that very high velocity WIMPs escape the Galaxy's potential and therefore the tail of the distribution is depleted) it is given by:

$$f_{\rm gal}(\mathbf{v}) \propto [e^{-\frac{\mathbf{v}^2}{\bar{v}^2}} - e^{-\frac{v_{\rm esc}^2}{\bar{v}^2}}]\Theta(v_{\rm esc} - v) \,, \tag{6.15}$$

where the second term is just to smoothen the transition near the escape velocity. Typically one uses $\bar{v} = 220\,\mathrm{km\,s^{-1}}$ and $v_{\rm esc} = 550\,\mathrm{km\,s^{-1}}$. This is an extra source of uncertainty, giving the maximum speed of DM particles in the detector rest frame:

$$v_{\rm maximum} \sim v_{\rm sun} + v_{\rm esc}. \tag{6.16}$$

There is some uncertainty in $v_{\rm sun}$, but most of it comes from $v_{\rm esc}$, which recent measurements from RAVE [186] set to $533^{+54}_{-41}\,\mathrm{km\,s^{-1}}$. It is important to notice that, as we saw, for light WIMPs $v_m \propto 1/m_\chi$ and therefore $v_{\rm esc}$ can affect the limits of heavy targets on light WIMPs.

However, the most important astrophysical uncertainties do not come from ρ_χ or $v_{\rm esc}$, but from the velocity distribution $f_{\rm gal}(\mathbf{v})$. This SHM is clearly

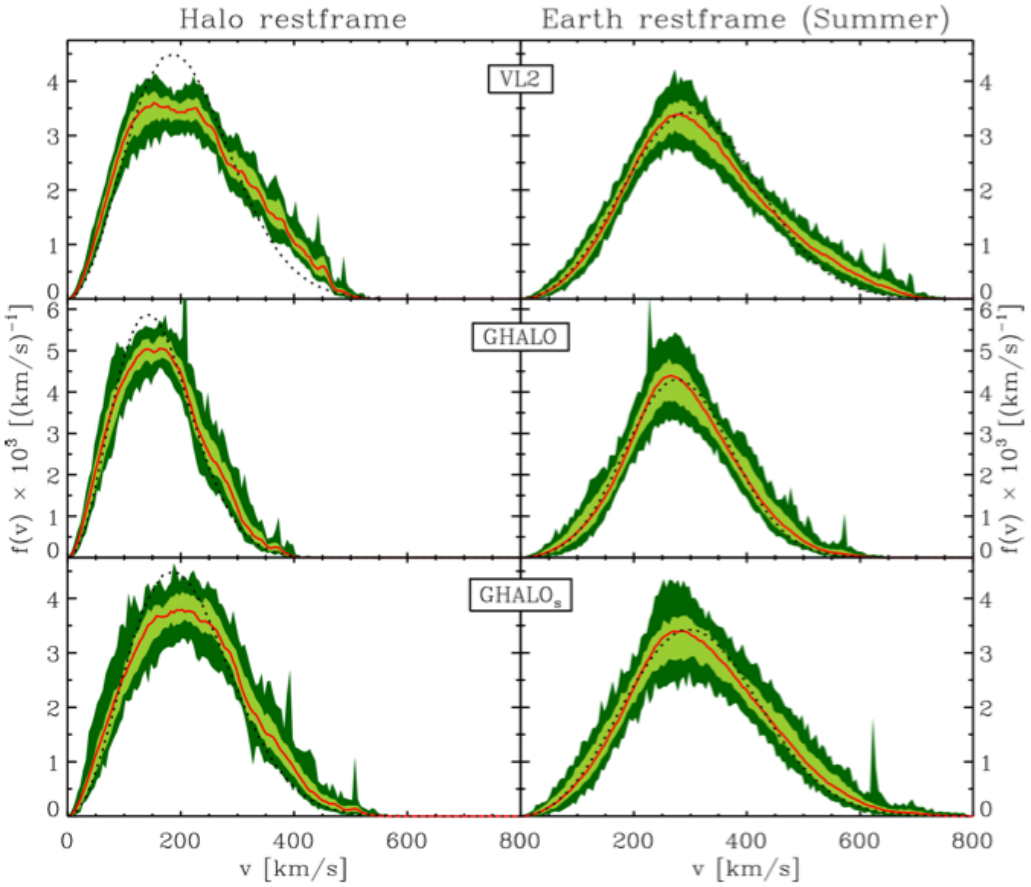

Figure 6.3: Velocity distribution function from N-body simulations of *Via Lactea II* (from [185]). The right (left) panels are in the restframe of the Earth on June 2nd, when the Earth's velocity relative to Galactic DM halo is maximum (of the galaxy). The solid red line is the average distribution, the light and dark green shaded regions denote the 68% scatter around the median and the minimum and maximum values over the samples, and the dotted line represents the best-fitting Maxwell-Boltzmann distribution.

an oversimplification, with N-body simulations indicating a more complicated structure of the DM halo, see e.g., fig. 6.3 (from [185]). In fact, from N-body simulations, we know that, in the tail of the DM velocity distribution, halo-substructures such as tidal streams [178, 187–189]- regions with very small velocity dispersions, not spatially mixed (they can be parametrized by $\delta^3(\vec{v}-\vec{v_s})$)- or debris flows [190], spatially homogeneous regions with constant speed (which can be parametrized by $\delta(v-v_s)$) are expected. The true

distribution is thus quite sensitive to the exact history of the MW, mergers, etc, and significantly depends on the halo properties, for instance with the presence of a dark disk [191] or extragalactic components [192].

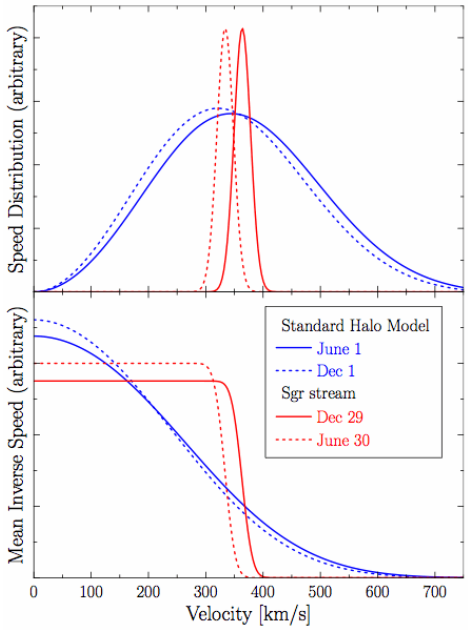

Figure 6.4: $f(v)$ (top) and $\eta(v_m)$ (bottom) versus velocity for the Maxwellian and for a stream (taken from [181]).

The dependence of the WIMP signals on the velocity distribution has been studied for instance in [179, 193–196]. In the constant rate, the velocity distribution is integrated over v, so it is not so much dependent. However, the annual modulation signals can be greatly modified.

We show in figures 6.4, 6.5 and 6.6 (from [181]) the differences both in the rate and in the annual modulation expected depending on the very different forms of $f(v)$.

Figure 6.4 plots $f(v)$ (top) and $\eta(v_m)$ (bottom) versus velocity, for a Maxwellian velocity distribution and for a stream, while figure 6.5 plots the rate $\eta(v_m)$ and the modulation amplitude $A_\eta(v_m)$ versus the recoil energy E_{nr} for the Maxwellian, for a stream and for a debris flow. One can see in figure 6.5 that there is a sign flip in $A_\eta(v_m)$ for the SHM (and also for debris flows and for the stream, although for this last case only at the particular velocity of the stream the modulation is significant) at some particular recoil energy E_{nr}^{flip}: that is a clear sign of DM, as backgrounds are not expected to show such behaviour.

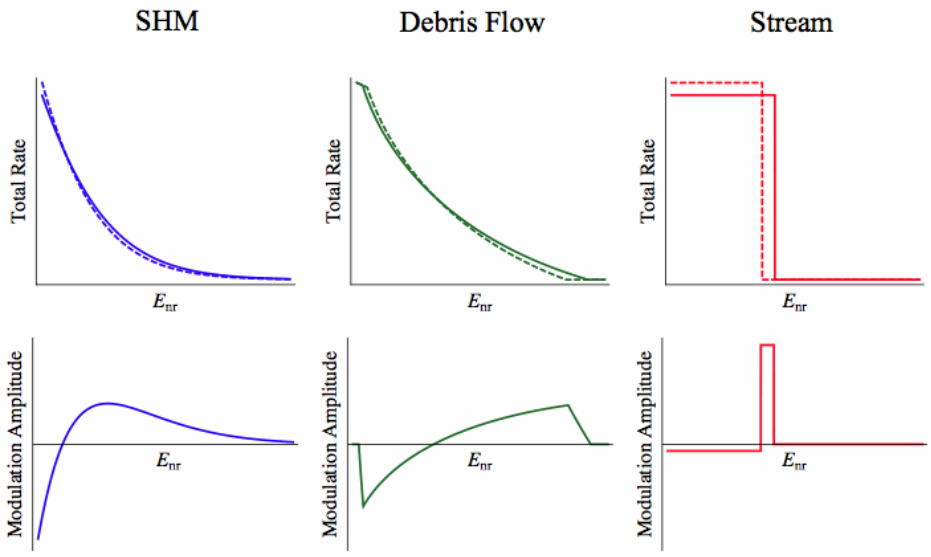

Figure 6.5: The constant rate $\eta(v_m)$ (top) and the modulation amplitude $A_\eta(v_m)$ (bottom) versus recoil energy E_{nr} for the Maxwellian, for a stream and for a debris flow, shown at the times when the rate is minimized and maximized (taken from [181]).

In figure 6.6, the fractional modulation (modulation over constant rate) is plotted versus time for the Maxwellian, for a stream (reduced by $\sim 1/10$) and for the sum of both contributions. Non-sinusoidal behaviours are expected when one considers a non SHM. From the recoil energy at which the flip occurs, E_{nr}^{flip}, related to the minimum velocity at which it occurs, that for the SHM is $v_m^{\text{flip}} \sim 200\,\text{km}\,\text{s}^{-1}$, one can infer the DM mass m_χ via eq. 6.6.

Presumably, the true velocity distribution is a mixture of different contributions, i.e., a SHM with some streams and debris here and there, and one should try to be completely independent of it when comparing different experiments, which in addition are sensitive to different velocity space regions of $f(v)$ (their v_m ranges can be completely different).

Therefore, showing the experimental data in an astrophysics - independent fashion is of uttermost interest. The halo integral $\eta(v_m, t)$, eq. 6.10, is the basis for the astrophysics-independent comparison of experiments [197, 198]. It uses an extremely simple and useful observation: one can translate different energy ranges $E_{nr\,i}$ of different experiments i into a v_m range common to all of them, and plot their corresponding $\eta(v_m, t)$, which encodes the astrophysics uncertainty on v_{esc} and $f(\vec{v})$ and has to be the same for all experiments. In [199], this halo-independent method to compare data from DM direct

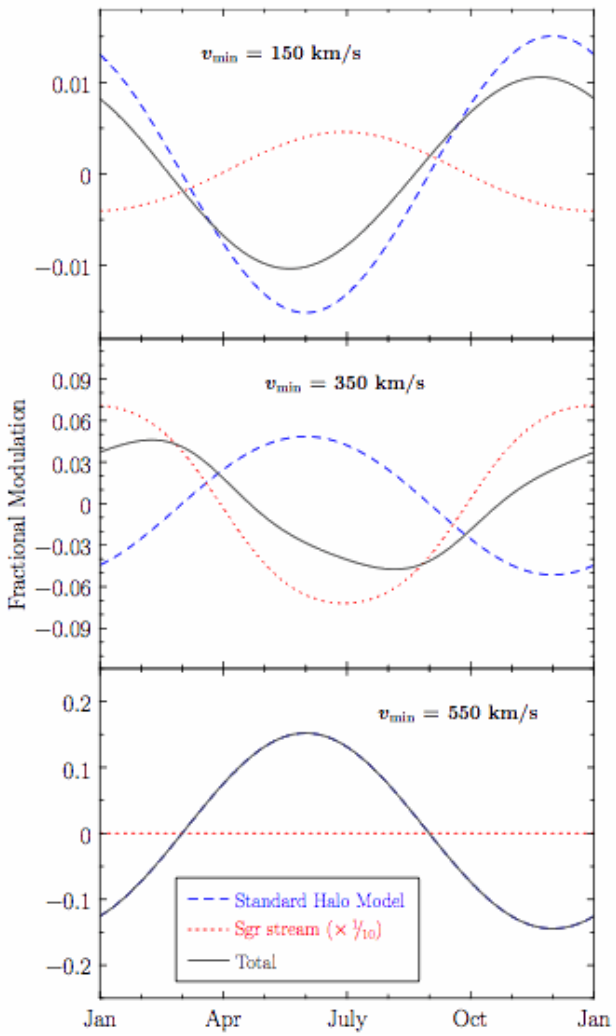

Figure 6.6: The fractional modulation versus time for the Maxwellian, for a stream (reduced by $\sim 1/10$ and for the sum of both contributions (taken from [181]).

detection was extended to any type of interaction, like magnetic moment ones.

In the work included in this thesis [5], using this fact and applying the astrophysics-independent bounds derived in our first work [4], we were able to bound the modulation amplitude of one experiment, $A_\eta^{\exp 1}$, in terms of the constant rate of another experiment, $\eta(v_m)^{\exp 2}$. In [6] we extended the study to inelastic scattering.

6.4 Current experimental situation

For SD the leading constraints come from SIMPLE [200], PICASSO [201], and COUPP [202] and for SI from CDMS-Ge [203, 204], XENON100 [205], and more recently LUX [206], which has put the most stringent bounds on SI interactions of DM.

Some experiments have found anomalies that may be due to a DM particle with a low mass ($\lesssim 10$ GeV), like DAMA [207], CoGeNT [208], and CRESST [209]. The situation is also controversial with CDMS Si [210], which has three events that can be interpreted as DM. All of these are in strong tension (if not excluded) with several of the previous null-results.

The two experiments that see an annual modulation are DAMA [207], at $\sim 9\sigma$ and CoGeNT [208], at 2.2σ, with compatible phases between themselves. However, the amplitude of the modulation in the CoGeNT is much larger than its rate, pointing if interpreted as DM to a non-Maxwellian halo or non-standard DM interactions. We analysed the compatibility of modulations and rates within the same experiment in great detail in the research done in [4].

The DAMA/LIBRA results [207] have a total exposure of 1.17 ton yr over 13 years with a modulation claimed to be compatible with DM at the $\sim 9\sigma$ level. This annual modulation can be explained under standard assumptions regarding the DM halo (SHM) and WIMP interactions (elastic, SI) with a DM mass of either ~ 10 scattering primarily on Na nuclei or of 80 GeV scattering primarily on I nuclei, see Figure 6.7, from [211] (and also for instance [196, 212]),[2] with this last solution being excluded by LUX by several orders of magnitude [206]. DAMA claims that no modulating background satisfies having a sinusoidal one-year period rate with the proper phase and amplitude, and present only in a definite low energy range.

Note also that gravitational focusing of the Sun affects the phase of the modulation [213–216], especially at low velocities (large DM masses), and the modulation caused just by this effect has minima (maxima) when the Earth is behind (in front of) the Sun, which occurs in March (September). Therefore the standard modulation phase caused by the Earth's velocity predicted in the SHM, June 1$^{\text{st}}$, changes due to gravitational focusing. For DAMA, in the energy ranges $2-4, 2-5, 2-6$ keVee were data is available, it changes by a few days for an 80 GeV DM mass, being predicted to be around May 20$^{\text{th}}$ [216], which is compatible with the one observed by the collaboration.

[2] Really there are in both cases more scatterings on iodine due to the A^2 enhancement in the cross section, however for a 10 GeV particle these are below the energy threshold. Lowering the threshold of the DAMA experiment would in principle allow to distinguish between both solutions [212].

Many explanations have been proposed in the literature for the DAMA signal:

- Radon abundance, with an increase in the summer and a decrease in the winter.
- Neutron flux, that modulates due to the water and snow present in the overburden (in winter the water absorbs more neutrons than in the summer) or the change in density of the upper atmosphere. For instance, in [217], neutron data were extrapolated to the DAMA region, and in principle could give such an annual modulation.
- Cosmic muons. For instance, in [218], using muon data from MACRO, LVD and Borexino, the muon phase is found to be incompatible with that of the DAMA at $5.2\,\sigma$.

A possibility is that DAMA might be seeing a combination of these effects, and therefore observing a mixed phase, quite close to the SHM DM one.

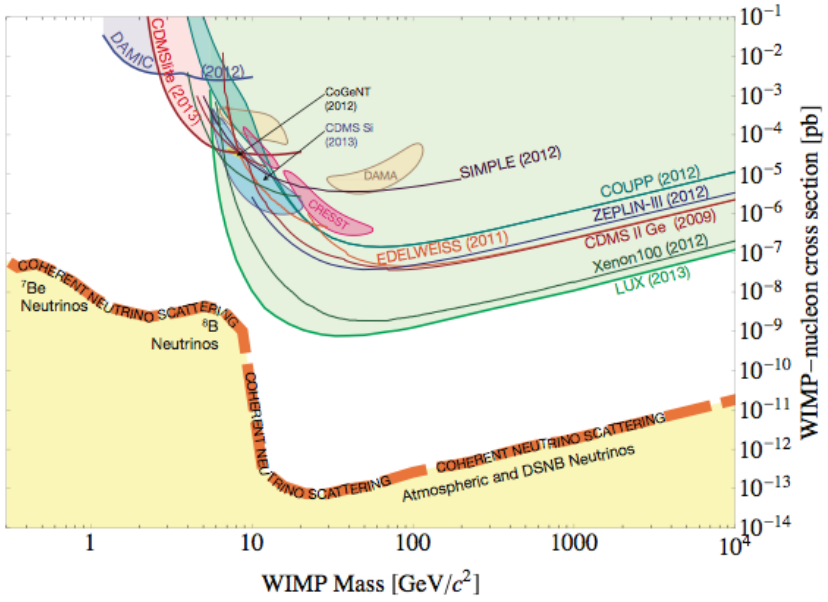

Figure 6.7: WIMP discovery limit (thick dashed orange) compared with current limits and regions of interest from [211]. The dominant neutrino components for different WIMP mass regions are labeled. The regions and bounds shown are at 90% C.L.

In fig. 6.7, taken from [211], the current experimental limits are summarized, together with the irreducible neutrino background that next generation

experiments will be facing. Progress beyond the cross sections of this neutrino background will require discriminating it from DM via annual modulation (although it also modulates) or directional detection signals.

Part IV

Final remarks and conclusions

On radiative neutrino mass models

We summarize in this section the results presented in the first part of the thesis, which is devoted to the study of neutrino masses via radiative models.

As has been argued in chapters 2 and 3, there are several mechanisms proposed to give masses to neutrinos. A very appealing option are radiative models, which explain why neutrino masses are much smaller than the masses of the rest of the fermions: neutrinos are massless at tree level, with their mass being generated radiatively at one, two or three loops (more loops typically yield too light neutrino masses and/or are generally incompatible with low-energy constraints, like charged LFV constraints). In addition, thanks to the loop suppression and the mandatory presence of a few couplings to violate lepton number (LN), these models have particles at a scale low enough to be produced at colliders, in particular in our case, at the LHC, and in low-energy experiments, giving signals in lepton flavour violating (LFV) processes like $\mu \to e\gamma$ or LNV ones, such as $0\nu\beta\beta$.

In this thesis we have studied radiative generation of neutrino masses at two-loops both through new fermions (new families) and new scalars (the Zee-Babu model). We also studied the implications of these models to other HEP scenarios, either indirectly, such as Higgs physics, for instance via modifications of the $H \to \gamma\gamma$ signal, or directly, detecting the new particles.

In the first works, we studied in detail the possibility of the existence of a fourth SM sequential generation, addressing in particular the light neutrino properties and their nature [1]. The fourth generation neutrino must be much heavier than the light ones, $m_4 \gtrsim m_{\rm Z}/2$, and a right-handed neutrino is very likely needed to provide a mass for it. We realised that if light neutrinos are Majorana particles, as LN is then violated, in all types of seesaw models there is a contribution to the Majorana mass of this right-handed neutrino at two loops. Therefore, the fourth generation neutrino should also be Majorana, unless some symmetry is imposed on the leptons of the fourth generation.

We analysed in detail the possible implications of having a heavy fourth-generation Majorana neutrino. In particular, it generates light neutrino masses at two loops and this contribution can easily exceed the cosmological bound on the absolute mass scale of the light neutrinos. There can also be extra contributions from the heavy states to $0\nu\beta\beta$, which, however, when one imposes that light neutrino masses do not exceed the cosmological scale, are in most regions of the parameter space smaller than the usual contribution from light neutrinos. We also studied possible signals in LFV processes and other rare processes.

However, even if there is a contribution to the light neutrino masses, their spectrum cannot be explained with just an extra family. Therefore, in a

different work, we studied the possibility that light neutrinos were massless at tree level, with their masses being generated at two loops by the action of two extra generations [2].

Currently, thanks to the LHC the existence of extra sequential generations of particles has now been ruled out, at least if the scalar sector comprises just the SM Higgs boson, due to the fact that the Higgs boson production is enhanced in the presence of new fermions (and also its decays vary significantly if a new family exists). Other possibilities arise which may save the fourth generation, such as an extended scalar sector, for instance with an extra Higgs doublet that only couples to the fourth family [10]. Limits on fourth generation fermions are, however, very close to the perturbative limit in the case of the quarks $\gtrsim 600$ GeV, see for instance [11],

In another work [3], we updated the current status of the Zee-Babu model in the light of new data, e.g., the mixing angle θ_{13}, the rare decay $\mu \to e\gamma$ and the LHC results. We also analysed the possibility of accommodating the deviations in $\Gamma(H \to \gamma\gamma)$ hinted by the LHC experiments (an enhanced Higgs diphoton decay rate in the ZB model is compatible with current data only in a small part of the parameter space), and the stability of the scalar potential, as well as restrictions that can be placed on the trilinear coupling from charge conservation.

We found that neutrino oscillation data and low energy constraints are still compatible with masses of the extra charged scalars accessible to LHC. We also studied the decays of the doubly-charged singlets, which could be detected at LHC-14 and may help to discriminate this model from others. Moreover, if any of the scalars is discovered, the model can be falsified by combining the information on the singly and doubly charged scalar decay modes with neutrino data. Conversely, if the neutrino spectrum is found to be inverted and the CP phase δ is quite different from $\sim \pi$, the masses of the charged scalars will be well outside the LHC reach.

In a broad sense, we have tried to shed some light on different forms to generate neutrino masses radiatively, focusing on their testability, always with an eye on possible signals at the LHC, and their connection to other HEP branches. Hopefully, with more experimental input, nature will help us disentangle between the overwhelming list of possibilities. For the moment, we can say that extra families are in a very bad shape, while the Zee-Babu is still alive and *ready* to be discovered at LHC-14!

On bounds on the DM annual modulation signal

We summarize in this section the results presented in the second part of the thesis, which is devoted to the study of bounds on the annual modulation signal.

As has been argued in chapter 5, Weakly Interacting Massive Particles (WIMPs) are well-motivated dark matter (DM) candidates which are expected to *talk* to the SM, as their relic abundance comes from thermal freeze-out. In this sense, a signal in direct detection experiments could be possible and probably expected, as discussed in chapter 6, as well as signals in colliders, in indirect detection and in other cosmological observables.

Direct detection experiments are very difficult to perform, as the expected DM signals are very low and the backgrounds are very large, even when the experiments are placed, shielded, in deep-underground laboratories. In fact, as we saw in figure 6.7, we will be reaching the irreducible neutrino background in the future.

The annual modulation that should be present in the signal of direct detection experiments, due to the relative motion of the Earth around the Sun, could help discriminate a DM signal from the background (some can modulate, like muons, but the phase does not have to coincide with the expected one from DM).

An important point to keep in mind when interpreting a DM signal is that the rates are subject to astrophysical uncertainties, such as the velocity distribution of the DM particles, the local density or the escape velocity, so it is important to be as independent of the astrophysical parameters as possible. This can be done by plotting their corresponding inverse mean velocity $\eta(v_m, t)$ in the same range of v_m.

In this thesis, we bounded the annual modulation in terms of the unmodulated event rate, which is almost independent from astrophysical uncertainties, by expanding to first order the rate (really $\eta(v_m, t)$, see eq. 6.10) in powers of $v_e(t)/v$, where $v_e(t)$ is the velocity of the Earth around the Sun and v is the DM velocity in the halo. The method is an important test that any annually-modulated DM signal has to pass.

We applied these bounds to DAMA and CoGeNT, comparing their modulations and rates [4]. DAMA's modulation is compatible with its own rate, while CoGeNT is excluded for typical DM haloes at $\gtrsim 90\%$ C.L.

In a second work we showed how the unmodulated rate of one experiment can bound the annual modulation seen in another experiment in the same v_m range. We applied it to DAMA's modulation versus null-results from

XENON, CDMS and other experiments, for the case of elastic scattering, with spin-independent (SI), spin-dependent (SD) and isospin violating (IV) interactions [5]. A DM interpretation of DAMA's modulation was disfavoured by at least one experiment at more than 4σ for a DM mass $\lesssim 15$ GeV, for all type of interactions.

In particular, for the case of spin-independent interactions, DAMA is excluded by XENON100 at more than 6σ for a DM mass larger or equal to 8 GeV. Of course, the CL of exclusion depends on systematic uncertainties, such as the sodium quenching factor, but even letting it vary, SI interactions are excluded at more than 5σ for a dark matter mass larger or equal to 10 GeV. For the case of SD or IV interactions, consistency can be achieved at about 3σ for this DM mass.

We have also extended the analysis to inelastic scattering [6], showing how DAMA is incompatible with XENON 100 null-results. This extension was not trivial, due to the fact that at larger velocities, where inelastic scattering is relevant, substructure in the DM halo, such as cold streams, may be present, and higher harmonics can become important. We also applied *the shape test* to DAMA, which comes from the fact that in inelastic scattering the rates of the two different energy branches within an experiment (for instance, DAMA), corresponding to the same v_m, should be equal. In some regions of the parameter space inelastic scattering for DAMA can be excluded just based on the energy spectrum of the modulation.

In a broad way, we have derived astrophysics-independent bounds that annual modulations have to fulfill. Hopefully, this kind of tests will help to discriminate between true DM signals and backgrounds. It is important to emphasize that it is a necessary condition for the modulation to be of DM origin, but not sufficient.

After applying our bounds to DAMA and CoGeNT annual modulations' and comparing them to other null-result experiments, they are in very bad shape. We expect that in future years more experimental input from direct detection experiments will help to clarify the currently confusing situation among these different experimental results, that look really incompatible, and let's hope that DM is out there ready to be discovered one way or another!

Bibliography

[1] A. Aparici, J. Herrero-Garcia, N. Rius, and A. Santamaria, *On the Nature of the Fourth Generation Neutrino and its Implications*, JHEP **1207**, 030 (2012), 1204.1021. Back to page i, vi, or 81

[2] A. Aparici, J. Herrero-Garcia, N. Rius, and A. Santamaria, *Neutrino masses from new generations*, JHEP **1107**, 122 (2011), 1104.4068. Back to page i, vi, or 82

[3] J. Herrero-Garcia, M. Nebot, N. Rius, and A. Santamaria, *The Zee-Babu Model revisited in the light of new data*, (2014), 1402.4491. Back to page i, vi, or 82

[4] J. Herrero-Garcia, T. Schwetz, and J. Zupan, *On the annual modulation signal in dark matter direct detection*, JCAP **1203**, 005 (2012), 1112.1627. Back to page i, vii, 69, 74, 75, or 83

[5] J. Herrero-Garcia, T. Schwetz, and J. Zupan, *Astrophysics independent bounds on the annual modulation of dark matter signals*, Phys.Rev.Lett. **109**, 141301 (2012), 1205.0134. Back to page i, viii, 74, or 84

[6] N. Bozorgnia, J. Herrero-Garcia, T. Schwetz, and J. Zupan, *Halo-independent methods for inelastic dark matter scattering*, JCAP **1307**, 049 (2013), 1305.3575. Back to page i, viii, 67, 74, or 84

[7] A. Aparici, J. Herrero-Garcia, N. Rius, and A. Santamaria, *Can New Generations Explain Neutrino Masses?*, (2011), 1106.0415. Back to page i

[8] A. Aparici, J. Herrero-Garcia, N. Rius, and A. Santamaria, *Implications of new generations on neutrino masses*, J.Phys.Conf.Ser. **408**, 012030 (2013), 1110.0663. Back to page i

[9] A. de Gouvea, J. Herrero-Garcia, and A. Kobach, *Neutrino Masses, Grand Unification, and Baryon Number Violation*, (2014), 1404.4057. Back to page ii

[10] M. Geller, S. Bar-Shalom, G. Eilam, and A. Soni, *The 125 GeV Higgs in the context of four generations with 2 Higgs doublets*, Phys.Rev. **D86**, 115008 (2012), 1209.4081. Back to page vi or 82

[11] CMS Collaborations, A. Ivanov, *Limits on Fourth Generation Fermions*, (2013), 1308.3084. Back to page 82

[12] BICEP2 Collaboration, P. A. R. Ade *et al.*, *BICEP2 I: Detection Of B-mode Polarization at Degree Angular Scales*, (2014), 1403.3985. Back to page 3, 6, 50, or 51

[13] CMS Collaboration, S. Chatrchyan *et al.*, *Observation of a new boson at a mass of 125 GeV with the CMS experiment at the LHC*, Phys.Lett. **B716**, 30 (2012), 1207.7235. Back to page 3 or 14

[14] ATLAS Collaboration, G. Aad *et al.*, *Observation of a new particle in the search for the Standard Model Higgs boson with the ATLAS detector at the LHC*, Phys.Lett. **B716**, 1 (2012), 1207.7214. Back to page 3 or 14

[15] Supernova Cosmology Project, S. Perlmutter *et al.*, *Measurements of Omega and Lambda from 42 high redshift supernovae*, Astrophys.J. **517**, 565 (1999), astro-ph/9812133. Back to page 4 or 44

[16] Supernova Search Team, A. G. Riess *et al.*, *Observational evidence from supernovae for an accelerating universe and a cosmological constant*, Astron.J. **116**, 1009 (1998), astro-ph/9805201. Back to page 4 or 44

[17] S. M. Carroll, *The Cosmological constant*, Living Rev.Rel. **4**, 1 (2001), astro-ph/0004075. Back to page 4

[18] P. Peebles and B. Ratra, *The Cosmological constant and dark energy*, Rev.Mod.Phys. **75**, 559 (2003), astro-ph/0207347. Back to page 4

[19] E. J. Copeland, M. Sami, and S. Tsujikawa, *Dynamics of dark energy*, Int.J.Mod.Phys. **D15**, 1753 (2006), hep-th/0603057. Back to page 4

[20] S. Nojiri and S. D. Odintsov, *Introduction to modified gravity and gravitational alternative for dark energy*, eConf **C0602061**, 06 (2006), hep-th/0601213. Back to page 4

[21] M. Fukugita and T. Yanagida, *Baryogenesis Without Grand Unification*, Phys.Lett. **B174**, 45 (1986). Back to page 4

[22] S. Davidson and A. Ibarra, *A Lower bound on the right-handed neutrino mass from leptogenesis*, Phys.Lett. **B535**, 25 (2002), hep-ph/0202239. Back to page 4 or 28

[23] A. Sakharov, *Violation of CP Invariance, c Asymmetry, and Baryon Asymmetry of the Universe*, Pisma Zh.Eksp.Teor.Fiz. **5**, 32 (1967). Back to page 4

[24] R. Peccei and H. R. Quinn, *CP Conservation in the Presence of Instantons*, Phys.Rev.Lett. **38**, 1440 (1977). Back to page 5

[25] R. Peccei and H. R. Quinn, *Constraints Imposed by CP Conservation in the Presence of Instantons*, Phys.Rev. **D16**, 1791 (1977). Back to page 5

[26] S. Weinberg, *A New Light Boson?*, Phys.Rev.Lett. **40**, 223 (1978). Back to page 5

[27] F. Wilczek, *Problem of Strong p and t Invariance in the Presence of Instantons*, Phys.Rev.Lett. **40**, 279 (1978). Back to page 5

[28] E. Farhi and L. Susskind, *Technicolor*, Phys.Rept. **74**, 277 (1981). Back to page 5

[29] H. E. Haber and G. L. Kane, *The Search for Supersymmetry: Probing Physics Beyond the Standard Model*, Phys.Rept. **117**, 75 (1985). Back to page 5

[30] H. P. Nilles, *Supersymmetry, Supergravity and Particle Physics*, Phys.Rept. **110**, 1 (1984). Back to page 5

[31] S. P. Martin, *A Supersymmetry primer*, (1997), hep-ph/9709356. Back to page 5

[32] P. Langacker, *Grand Unified Theories and Proton Decay*, Phys.Rept. **72**, 185 (1981). Back to page 6

[33] H. Georgi and S. Glashow, *Unity of All Elementary Particle Forces*, Phys.Rev.Lett. **32**, 438 (1974). Back to page 6 or 32

[34] D. Baumann, *TASI Lectures on Inflation*, (2009), 0907.5424. Back to page 7, 48, or 51

[35] S. Glashow, *Partial Symmetries of Weak Interactions*, Nucl.Phys. **22**, 579 (1961). Back to page 11

[36] P. W. Higgs, *Broken Symmetries and the Masses of Gauge Bosons*, Phys.Rev.Lett. **13**, 508 (1964). Back to page 11

[37] F. Englert and R. Brout, *Broken Symmetry and the Mass of Gauge Vector Mesons*, Phys.Rev.Lett. **13**, 321 (1964). Back to page 11

[38] G. Guralnik, C. Hagen, and T. Kibble, *Global Conservation Laws and Massless Particles*, Phys.Rev.Lett. **13**, 585 (1964). Back to page 11

[39] P. W. Higgs, *Spontaneous Symmetry Breakdown without Massless Bosons*, Phys.Rev. **145**, 1156 (1966). Back to page 11

[40] T. Kibble, *Symmetry breaking in nonAbelian gauge theories*, Phys.Rev. **155**, 1554 (1967). Back to page 11

[41] S. Weinberg, *A Model of Leptons*, Phys.Rev.Lett. **19**, 1264 (1967). Back to page 11

[42] A. Salam, *Weak and Electromagnetic Interactions*, Conf.Proc. **C680519**, 367 (1968). Back to page 11

[43] M. Han and Y. Nambu, *Three Triplet Model with Double SU(3) Symmetry*, Phys.Rev. **139**, B1006 (1965). Back to page 11

[44] H. Fritzsch, M. Gell-Mann, and H. Leutwyler, *Advantages of the Color Octet Gluon Picture*, Phys.Lett. **B47**, 365 (1973). Back to page 11

[45] M. Gell-Mann, *Quarks*, Acta Phys.Austriaca Suppl. **9**, 733 (1972). Back to page 11

[46] H. Fritzsch and M. Gell-Mann, *Current algebra: Quarks and what else?*, eConf **C720906V2**, 135 (1972), hep-ph/0208010. Back to page 11

[47] Particle Data Group, J. Beringer *et al.*, *Review of Particle Physics (RPP)*, Phys.Rev. **D86**, 010001 (2012). Back to page 14 or 19

[48] S. Weinberg, *The Cosmological Constant Problem*, Rev.Mod.Phys. **61**, 1 (1989). Back to page 18

[49] R. Mohapatra *et al.*, *Theory of neutrinos: A White paper*, Rept.Prog.Phys. **70**, 1757 (2007), hep-ph/0510213. Back to page 19

[50] M. Gonzalez-Garcia and M. Maltoni, *Phenomenology with Massive Neutrinos*, Phys.Rept. **460**, 1 (2008), 0704.1800. Back to page 19

[51] Intensity Frontier Neutrino Working Group, A. de Gouvea *et al.*, *Neutrinos*, (2013), 1310.4340. Back to page 19

[52] R. Mohapatra and P. Pal, *Massive neutrinos in physics and astrophysics. Second edition*, World Sci.Lect.Notes Phys. **60**, 1 (1998). Back to page 19 or 32

[53] W. Pauli, *Dear radioactive ladies and gentlemen*, Phys.Today **31N9**, 27 (1978). Back to page 19

[54] F. Reines and C. Cowan, *Detection of the free neutrino*, Phys.Rev. **92**, 830 (1953). Back to page 19

[55] F. Reines, C. Cowan, F. Harrison, A. McGuire, and H. Kruse, *Detection of the free anti-neutrino*, Phys.Rev. **117**, 159 (1960). Back to page 19

[56] C. Cowan, F. Reines, F. Harrison, H. Kruse, and A. McGuire, *Detection of the free neutrino: A Confirmation*, Camb.Monogr.Part.Phys.Nucl.Phys.Cosmol. **14**, 38 (2000). Back to page 19

[57] B. Cleveland *et al.*, *Measurement of the solar electron neutrino flux with the Homestake chlorine detector*, Astrophys.J. **496**, 505 (1998). Back to page 19

[58] V. Gribov and B. Pontecorvo, *Neutrino astronomy and lepton charge*, Phys.Lett. **B28**, 493 (1969). Back to page 19

[59] GALLEX, W. Hampel *et al.*, *GALLEX solar neutrino observations: Results for GALLEX IV*, Phys. Lett. **B447**, 127 (1999). Back to page 19

[60] GNO, M. Altmann *et al.*, *GNO solar neutrino observations: Results for GNO I*, Phys. Lett. **B490**, 16 (2000), hep-ex/0006034. Back to page 19

[61] SNO, Q. R. Ahmad *et al.*, *Direct evidence for neutrino flavor transformation from neutral-current interactions in the Sudbury Neutrino Observatory*, Phys. Rev. Lett. **89**, 011301 (2002), nucl-ex/0204008. Back to page 19

[62] The Borexino, G. Bellini *et al.*, *Measurement of the solar 8B neutrino rate with a liquid scintillator target and 3 MeV energy threshold in the Borexino detector*, Phys. Rev. **D82**, 033006 (2010), 0808.2868. Back to page 19

[63] KAMIOKANDE-II, K. S. Hirata *et al.*, *Experimental Study of the Atmospheric Neutrino Flux*, Phys. Lett. **B205**, 416 (1988). Back to page 19

[64] Super-Kamiokande, Y. Fukuda *et al.*, *Evidence for oscillation of atmospheric neutrinos*, Phys. Rev. Lett. **81**, 1562 (1998), hep-ex/9807003. Back to page 19

[65] Soudan-2, W. W. M. Allison *et al.*, *The atmospheric neutrino flavor ratio from a 3.9 fiducial kiloton-year exposure of Soudan 2*, Phys. Lett. **B449**, 137 (1999), hep-ex/9901024. Back to page 19

[66] KamLAND, K. Eguchi *et al.*, *First results from KamLAND: Evidence for reactor anti- neutrino disappearance*, Phys. Rev. Lett. **90**, 021802 (2003), hep-ex/0212021. Back to page 19

[67] K2K, E. Aliu *et al.*, *Evidence for muon neutrino oscillation in an accelerator- based experiment*, Phys. Rev. Lett. **94**, 081802 (2005), hep-ex/0411038. Back to page 19

[68] MINOS, P. Adamson *et al.*, *Search for muon-neutrino to electron-neutrino transitions in MINOS*, Phys. Rev. Lett. **103**, 261802 (2009), 0909.4996. Back to page 19

[69] M. Gonzalez-Garcia, M. Maltoni, J. Salvado, and T. Schwetz, *Global fit to three neutrino mixing: critical look at present precision*, JHEP **1212**, 123 (2012), 1209.3023. Back to page 20 or 21

[70] P. Huber, *On the determination of anti-neutrino spectra from nuclear reactors*, Phys.Rev. **C84**, 024617 (2011), 1106.0687. Back to page 21

[71] DOUBLE-CHOOZ Collaboration, Y. Abe *et al.*, *Indication for the disappearance of reactor electron antineutrinos in the Double Chooz experiment*, Phys.Rev.Lett. **108**, 131801 (2012), 1112.6353. Back to page 20

[72] DAYA-BAY Collaboration, F. An *et al.*, *Observation of electron-antineutrino disappearance at Daya Bay*, Phys.Rev.Lett. **108**, 171803 (2012), 1203.1669. Back to page 20

[73] RENO collaboration, J. Ahn *et al.*, *Observation of Reactor Electron Antineutrino Disappearance in the RENO Experiment*, Phys.Rev.Lett. **108**, 191802 (2012), 1204.0626. Back to page 20

[74] D. Forero, M. Tortola, and J. Valle, *Global status of neutrino oscillation parameters after Neutrino-2012*, Phys.Rev. **D86**, 073012 (2012), 1205.4018. Back to page 20

[75] G. Fogli *et al.*, *Global analysis of neutrino masses, mixings and phases: entering the era of leptonic CP violation searches*, Phys.Rev. **D86**, 013012 (2012), 1205.5254. Back to page 20

[76] J. Lesgourgues and S. Pastor, *Massive neutrinos and cosmology*, Phys. Rept. **429**, 307 (2006), astro-ph/0603494. Back to page 21

[77] J. Bonn *et al.*, *The Mainz neutrino mass experiment*, Nucl. Phys. Proc. Suppl. **91**, 273 (2001). Back to page 22

[78] V. M. Lobashev *et al.*, *Direct search for neutrino mass and anomaly in the tritium beta-spectrum: Status of 'Troitsk neutrino mass' experiment*, Nucl. Phys. Proc. Suppl. **91**, 280 (2001). Back to page 22

[79] Troitsk Collaboration, V. Aseev *et al.*, *An upper limit on electron antineutrino mass from Troitsk experiment*, Phys.Rev. **D84**, 112003 (2011), 1108.5034. Back to page 22

[80] KATRIN, A. Osipowicz *et al.*, *KATRIN: A next generation tritium beta decay experiment with sub-eV sensitivity for the electron neutrino mass*, (2001), hep-ex/0109033. Back to page 22

[81] GERDA Collaboration, M. Agostini *et al.*, *Results on neutrinoless double beta decay of 76Ge from GERDA Phase I*, Phys.Rev.Lett. **111**, 122503 (2013), 1307.4720. Back to page 22

[82] EXO Collaboration, M. Auger *et al.*, *Search for Neutrinoless Double-Beta Decay in ^{136}Xe with EXO-200*, Phys.Rev.Lett. **109**, 032505 (2012), 1205.5608. Back to page 22

[83] H. V. Klapdor-Kleingrothaus *et al.*, *Latest Results from the Heidelberg-Moscow Double Beta Decay Experiment*, Eur. Phys. J. **A12**, 147 (2001), hep-ph/0103062. Back to page 22

[84] F. T. Avignone, III, S. R. Elliott, and J. Engel, *Double Beta Decay, Majorana Neutrinos, and Neutrino Mass*, Rev. Mod. Phys. **80**, 481 (2008), 0708.1033. Back to page 22

[85] Planck Collaboration, P. Ade *et al.*, *Planck 2013 results. XVI. Cosmological parameters*, (2013), 1303.5076. Back to page 22, 42, 45, 46, 48, 50, or 55

[86] J. Schechter and J. Valle, *Neutrinoless Double beta Decay in SU(2) x U(1) Theories*, Phys.Rev. **D25**, 2951 (1982). Back to page 22

[87] MEG Collaboration, J. Adam *et al.*, *New constraint on the existence of the $\mu \to e\gamma$ decay*, Phys.Rev.Lett. **110**, 201801 (2013), 1303.0754. Back to page 22

[88] LSND Collaboration, A. Aguilar-Arevalo *et al.*, *Evidence for neutrino oscillations from the observation of anti-neutrino(electron) appearance in a anti-neutrino(muon) beam*, Phys.Rev. **D64**, 112007 (2001), hep-ex/0104049. Back to page 23

[89] MiniBooNE Collaboration, A. Aguilar-Arevalo *et al.*, *A Search for electron neutrino appearance at the $\Delta m^2 \sim 1eV^2$ scale*, Phys.Rev.Lett. **98**, 231801 (2007), 0704.1500. Back to page 23

[90] MiniBooNE Collaboration, A. Aguilar-Arevalo *et al.*, *Improved Search for $\bar{\nu}_\mu \to \bar{\nu}_e$ Oscillations in the MiniBooNE Experiment*, Phys.Rev.Lett. **110**, 161801 (2013), 1207.4809. Back to page 23

[91] P. Minkowski, *$\mu \to e\gamma$ at a Rate of One Out of 1-Billion Muon Decays?*, Phys.Lett. **B67**, 421 (1977). Back to page 27

[92] P. Ramond, *The Family Group in Grand Unified Theories*, p. 265 (1979), hep-ph/9809459, Retro-Preprint (1979 unpublished Caltech preprint no: CALT-68-709). Invited talk at the Sanibel Symposia, Feb 1979. Back to page 27

[93] M. Gell-Mann, P. Ramond, and R. Slansky, *Complex Spinors and Unified Theories*, Conf.Proc. **C790927**, 315 (1979), Published in Supergravity, P. van Nieuwenhuizen and D.Z. Freedman (eds.), North Holland Publ. Co., 1979. Back to page 27

[94] T. Yanagida, *Horizontal Symmetry and Masses of Neutrinos*, Conf.Proc. **C7902131**, 95 (1979). Back to page 27

[95] R. N. Mohapatra and G. Senjanovic, *Neutrino Mass and Spontaneous Parity Violation*, Phys.Rev.Lett. **44**, 912 (1980). Back to page 27 or 31

[96] W. Konetschny and W. Kummer, *Nonconservation of Total Lepton Number with Scalar Bosons*, Phys.Lett. **B70**, 433 (1977). Back to page 28

[97] T. Cheng and L.-F. Li, *Neutrino Masses, Mixings and Oscillations in SU(2) x U(1) Models of Electroweak Interactions*, Phys.Rev. **D22**, 2860 (1980). Back to page 28

[98] G. Lazarides, Q. Shafi, and C. Wetterich, *Proton Lifetime and Fermion Masses in an SO(10) Model*, Nucl.Phys. **B181**, 287 (1981). Back to page 28

[99] M. Magg and C. Wetterich, *Neutrino Mass Problem and Gauge Hierarchy*, Phys.Lett. **B94**, 61 (1980). Back to page 28

[100] J. Schechter and J. Valle, *Neutrino Masses in SU(2) x U(1) Theories*, Phys.Rev. **D22**, 2227 (1980). Back to page 28

[101] S. Kanemura and K. Yagyu, *Radiative corrections to electroweak parameters in the Y=1 Higgs triplet model and implication with the recent Higgs boson searches at the CERN LHC*, (2012), 1201.6287. Back to page 29

[102] R. Foot, H. Lew, X. He, and G. C. Joshi, *Seesaw Neutrino Masses Induced by a Triplet of Leptons*, Z.Phys. **C44**, 441 (1989). Back to page 29

[103] E. Ma and D. Roy, *Heavy triplet leptons and new gauge boson*, Nucl.Phys. **B644**, 290 (2002), hep-ph/0206150. Back to page 29

[104] R. Mohapatra and J. Valle, *Neutrino Mass and Baryon Number Nonconservation in Superstring Models*, Phys.Rev. **D34**, 1642 (1986). Back to page 30

[105] R. N. Mohapatra and G. Senjanovic, *Neutrino Masses and Mixings in Gauge Models with Spontaneous Parity Violation*, Phys.Rev. **D23**, 165 (1981). Back to page 31

[106] G. Senjanovic and R. N. Mohapatra, *Exact Left-Right Symmetry and Spontaneous Violation of Parity*, Phys.Rev. **D12**, 1502 (1975). Back to page 31

[107] N. Deshpande, J. Gunion, B. Kayser, and F. I. Olness, *Left-right symmetric electroweak models with triplet Higgs*, Phys.Rev. **D44**, 837 (1991). Back to page 32

[108] C. Aulakh and R. N. Mohapatra, *Neutrino as the Supersymmetric Partner of the Majoron*, Phys.Lett. **B119**, 136 (1982). Back to page 32

[109] L. J. Hall and M. Suzuki, *Explicit R-Parity Breaking in Supersymmetric Models*, Nucl.Phys. **B231**, 419 (1984). Back to page 32

[110] I.-H. Lee, *Lepton Number Violation in Softly Broken Supersymmetry*, Phys.Lett. **B138**, 121 (1984). Back to page 32

[111] I.-H. Lee, *Lepton Number Violation in Softly Broken Supersymmetry. 2.*, Nucl.Phys. **B246**, 120 (1984). Back to page 32

[112] J. R. Ellis, G. Gelmini, C. Jarlskog, G. G. Ross, and J. Valle, *Phenomenology of Supersymmetry with Broken R-Parity*, Phys.Lett. **B150**, 142 (1985). Back to page 32

[113] G. G. Ross and J. Valle, *Supersymmetric Models Without R-Parity*, Phys.Lett. **B151**, 375 (1985). Back to page 32

[114] S. Dawson, *R-Parity Breaking in Supersymmetric Theories*, Nucl.Phys. **B261**, 297 (1985). Back to page 32

[115] A. Santamaria and J. Valle, *Spontaneous R-Parity Violation in Supersymmetry: A Model for Solar Neutrino Oscillations*, Phys.Lett. **B195**, 423 (1987). Back to page 32

[116] A. Masiero and J. Valle, *A Model for Spontaneous R Parity Breaking*, Phys.Lett. **B251**, 273 (1990). Back to page 32

[117] M. Hirsch, M. Diaz, W. Porod, J. Romao, and J. Valle, *Neutrino masses and mixings from supersymmetry with bilinear R parity violation: A Theory for solar and atmospheric neutrino oscillations*, Phys.Rev. **D62**, 113008 (2000), hep-ph/0004115. Back to page 32

[118] R. Barbier *et al.*, *R-parity violating supersymmetry*, Phys.Rept. **420**, 1 (2005), hep-ph/0406039. Back to page 32

[119] A. Zee, *Quantum Numbers of Majorana Neutrino Masses*, Nucl.Phys. **B264**, 99 (1986). Back to page 33

[120] K. Babu, *Model of 'Calculable' Majorana Neutrino Masses*, Phys.Lett. **B203**, 132 (1988). Back to page 33

[121] K. Babu and E. Ma, *Natural Hierarchy of Radiatively Induced Majorana Neutrino Masses*, Phys.Rev.Lett. **61**, 674 (1988). Back to page 33

[122] A. Zee, *A Theory of Lepton Number Violation, Neutrino Majorana Mass, and Oscillation*, Phys.Lett. **B93**, 389 (1980). Back to page 33

[123] E. Ma and D. Suematsu, *Fermion Triplet Dark Matter and Radiative Neutrino Mass*, Mod.Phys.Lett. **A24**, 583 (2009), 0809.0942. Back to page 33 or 34

[124] J. Kubo, E. Ma, and D. Suematsu, *Cold Dark Matter, Radiative Neutrino Mass, $\mu \to e\gamma$, and Neutrinoless Double Beta Decay*, Phys.Lett. **B642**, 18 (2006), hep-ph/0604114. Back to page 33 or 34

[125] L. Lopez Honorez, E. Nezri, J. F. Oliver, and M. H. Tytgat, *The Inert Doublet Model: An Archetype for Dark Matter*, JCAP **0702**, 028 (2007), hep-ph/0612275. Back to page 33 or 34

[126] L. Wolfenstein, *A Theoretical Pattern for Neutrino Oscillations*, Nucl.Phys. **B175**, 93 (1980). Back to page 33

[127] X.-G. He and S. K. Majee, *Implications of Recent Data on Neutrino Mixing and Lepton Flavour Violating Decays for the Zee Model*, JHEP **1203**, 023 (2012), 1111.2293. Back to page 33

[128] E. Ma, *Verifiable radiative seesaw mechanism of neutrino mass and dark matter*, Phys.Rev. **D73**, 077301 (2006), hep-ph/0601225. Back to page 34

[129] D. Schmidt, T. Schwetz, and T. Toma, *Direct Detection of Leptophilic Dark Matter in a Model with Radiative Neutrino Masses*, Phys.Rev. **D85**, 073009 (2012), 1201.0906. Back to page 34 or 36

[130] T. Toma and A. Vicente, *Lepton Flavor Violation in the Scotogenic Model*, JHEP **1401**, 160 (2014), 1312.2840. Back to page 34 or 36

[131] A. Goudelis, B. Herrmann, and O. Stål, *Dark matter in the Inert Doublet Model after the discovery of a Higgs-like boson at the LHC*, JHEP **1309**, 106 (2013), 1303.3010. Back to page 34 or 36

[132] A. Arhrib, Y.-L. S. Tsai, Q. Yuan, and T.-C. Yuan, *An Updated Analysis of Inert Higgs Doublet Model in light of the Recent Results from LUX, PLANCK, AMS-02 and LHC*, (2013), 1310.0358. Back to page 34 or 36

[133] R. Barbieri, L. J. Hall, and V. S. Rychkov, *Improved naturalness with a heavy Higgs: An Alternative road to LHC physics*, Phys.Rev. **D74**, 015007 (2006), hep-ph/0603188. Back to page 34 or 36

[134] T. Hambye, F.-S. Ling, L. Lopez Honorez, and J. Rocher, *Scalar Multiplet Dark Matter*, JHEP **0907**, 090 (2009), 0903.4010. Back to page 34 or 36

[135] J. Racker, *Mass bounds for baryogenesis from particle decays and the inert doublet model*, (2013), 1308.1840. Back to page 34 or 36

[136] E. Molinaro, C. E. Yaguna, and O. Zapata, *FIMP realization of the scotogenic model*, (2014), 1405.1259. Back to page 34 or 36

[137] A. G. Riess *et al.*, *A 3Hubble Space Telescope and Wide Field Camera 3*, Astrophys.J. **730**, 119 (2011), 1103.2976. Back to page 42

[138] R. Alpher, H. Bethe, and G. Gamow, *The origin of chemical elements*, Phys.Rev. **73**, 803 (1948). Back to page 46

[139] R. A. Alpher, J. W. Follin, and R. C. Herman, *Physical Conditions in the Initial Stages of the Expanding Universe*, Phys.Rev. **92**, 1347 (1953). Back to page 46

[140] R. V. Wagoner, W. A. Fowler, and F. Hoyle, *On the Synthesis of elements at very high temperatures*, Astrophys.J. **148**, 3 (1967). Back to page 46

[141] P. Peebles, *Primordial Helium Abundance and the Primordial Fireball. 2*, Astrophys.J. **146**, 542 (1966). Back to page 46

[142] P. J. E. Peebles, *Primeval Helium Abundance and the Primeval Fireball*, Phys. Rev. Lett. **16**, 410 (1966). Back to page 46

[143] M. Tegmark and M. Zaldarriaga, *Separating the early universe from the late universe: Cosmological parameter estimation beyond the black box*, Phys.Rev. **D66**, 103508 (2002), astro-ph/0207047. Back to page 48

[144] M. J. Mortonson, D. H. Weinberg, and M. White, *Dark Energy: A Short Review*, (2013), 1401.0046. Back to page 49

[145] M. Milgrom, *A Modification of the Newtonian dynamics as a possible alternative to the hidden mass hypothesis*, Astrophys.J. **270**, 365 (1983). Back to page 53

[146] J. Bekenstein and M. Milgrom, *Does the missing mass problem signal the breakdown of Newtonian gravity?*, Astrophys.J. **286**, 7 (1984). Back to page 53

[147] J. D. Bekenstein, *Relativistic gravitation theory for the MOND paradigm*, Phys.Rev. **D70**, 083509 (2004), astro-ph/0403694. Back to page 53

[148] D. Clowe *et al.*, *A direct empirical proof of the existence of dark matter*, Astrophys.J. **648**, L109 (2006), astro-ph/0608407. Back to page 55

[149] WMAP, G. Hinshaw *et al.*, *Nine-Year Wilkinson Microwave Anisotropy Probe (WMAP) Observations: Cosmological Parameter Results*, Astrophys.J.Suppl. **208**, 19 (2013), 1212.5226. Back to page 55

[150] M. R. Lovell *et al.*, *The properties of warm dark matter haloes*, (2013), 1308.1399. Back to page 57

[151] A. De Rujula, S. Glashow, and U. Sarid, *CHARGED DARK MATTER*, Nucl.Phys. **B333**, 173 (1990). Back to page 57

[152] S. Dimopoulos, D. Eichler, R. Esmailzadeh, and G. D. Starkman, *Getting a Charge Out of Dark Matter*, Phys.Rev. **D41**, 2388 (1990). Back to page 57

[153] G. D. Mack, J. F. Beacom, and G. Bertone, *Towards Closing the Window on Strongly Interacting Dark Matter: Far-Reaching Constraints from Earth's Heat Flow*, Phys.Rev. **D76**, 043523 (2007), 0705.4298. Back to page 57

[154] P. Ivanov, P. Naselsky, and I. Novikov, *Inflation and primordial black holes as dark matter*, Phys.Rev. **D50**, 7173 (1994). Back to page 57

[155] MACHO Collaboration, C. Alcock *et al.*, *The MACHO project: Microlensing results from 5.7 years of LMC observations*, Astrophys.J. **542**, 281 (2000), astro-ph/0001272. Back to page 57

[156] B. Carr, K. Kohri, Y. Sendouda, and J. Yokoyama, *New cosmological constraints on primordial black holes*, Phys.Rev. **D81**, 104019 (2010), 0912.5297. Back to page 57

[157] S. F. Anderson, C. J. Hogan, B. F. Williams, and R. F. Carswell, *Mapping Low-Density Intergalactic Gas: a Third Helium Lyman-alpha Forest*, Astron.J. **117**, 56 (1999), astro-ph/9808105. Back to page 57

[158] G. Bertone, D. Hooper, and J. Silk, *Particle dark matter: Evidence, candidates and constraints*, Phys.Rept. **405**, 279 (2005), hep-ph/0404175. Back to page 57

[159] M. Cirelli, N. Fornengo, and A. Strumia, *Minimal dark matter*, Nucl.Phys. **B753**, 178 (2006), hep-ph/0512090. Back to page 57

[160] B. W. Lee and S. Weinberg, *Cosmological Lower Bound on Heavy Neutrino Masses*, Phys.Rev.Lett. **39**, 165 (1977). Back to page 60

[161] K. Griest and D. Seckel, *Three exceptions in the calculation of relic abundances*, Phys.Rev. **D43**, 3191 (1991). Back to page 60

[162] D. B. Kaplan, *A Single explanation for both the baryon and dark matter densities*, Phys.Rev.Lett. **68**, 741 (1992). Back to page 61

[163] D. E. Kaplan, M. A. Luty, and K. M. Zurek, *Asymmetric Dark Matter*, Phys.Rev. **D79**, 115016 (2009), 0901.4117. Back to page 61

[164] H. Davoudiasl and R. N. Mohapatra, *On Relating the Genesis of Cosmic Baryons and Dark Matter*, New J.Phys. **14**, 095011 (2012), 1203.1247. Back to page 61

[165] M. Blennow, B. Dasgupta, E. Fernandez-Martinez, and N. Rius, *Aidnogenesis via Leptogenesis and Dark Sphalerons*, JHEP **1103**, 014 (2011), 1009.3159. Back to page 61

[166] K. Petraki and R. R. Volkas, *Review of asymmetric dark matter*, Int.J.Mod.Phys. **A28**, 1330028 (2013), 1305.4939. Back to page 61

[167] E. A. Baltz, M. Battaglia, M. E. Peskin, and T. Wizansky, *Determination of dark matter properties at high-energy colliders*, Phys.Rev. **D74**, 103521 (2006), hep-ph/0602187. Back to page 63

[168] M. Beltran, D. Hooper, E. W. Kolb, Z. A. Krusberg, and T. M. Tait, *Maverick dark matter at colliders*, JHEP **1009**, 037 (2010), 1002.4137. Back to page 63

[169] A. Birkedal, K. Matchev, and M. Perelstein, *Dark matter at colliders: A Model independent approach*, Phys.Rev. **D70**, 077701 (2004), hep-ph/0403004. Back to page 63

[170] K. Jedamzik, *Big bang nucleosynthesis constraints on hadronically and electromagnetically decaying relic neutral particles*, Phys.Rev. **D74**, 103509 (2006), hep-ph/0604251. Back to page 63

[171] K. Jedamzik and M. Pospelov, *Big Bang Nucleosynthesis and Particle Dark Matter*, New J.Phys. **11**, 105028 (2009), 0906.2087. Back to page 63

[172] T. R. Slatyer, N. Padmanabhan, and D. P. Finkbeiner, *CMB Constraints on WIMP Annihilation: Energy Absorption During the Recombination Epoch*, Phys.Rev. **D80**, 043526 (2009), 0906.1197. Back to page 63

[173] S. Galli, F. Iocco, G. Bertone, and A. Melchiorri, *CMB constraints on Dark Matter models with large annihilation cross-section*, Phys.Rev. **D80**, 023505 (2009), 0905.0003. Back to page 63

[174] R. Diamanti, L. Lopez-Honorez, O. Mena, S. Palomares-Ruiz, and A. C. Vincent, *Constraining Dark Matter Late-Time Energy Injection: Decays and P-Wave Annihilations*, JCAP **1402**, 017 (2014), 1308.2578. Back to page 63

[175] L. Lopez-Honorez, O. Mena, S. Palomares-Ruiz, and A. C. Vincent, *Constraints on dark matter annihilation from CMB observationsbefore Planck*, JCAP **1307**, 046 (2013), 1303.5094. Back to page 63

[176] M. W. Goodman and E. Witten, *Detectability of Certain Dark Matter Candidates*, Phys.Rev. **D31**, 3059 (1985). Back to page 65

[177] J. F. Navarro, C. S. Frenk, and S. D. White, *The Structure of cold dark matter halos*, Astrophys.J. **462**, 563 (1996), astro-ph/9508025. Back to page 66

[178] G. Gelmini and P. Gondolo, *WIMP annual modulation with opposite phase in Late-Infall halo models*, Phys.Rev. **D64**, 023504 (2001), hep-ph/0012315. Back to page 66 or 71

[179] A. M. Green, *Effect of realistic astrophysical inputs on the phase and shape of the WIMP annual modulation signal*, Phys. Rev. **D68**, 023004 (2003), astro-ph/0304446. Back to page 66 or 72

[180] C. McCabe, *The Earth's velocity for direct detection experiments*, JCAP **1402**, 027 (2014), 1312.1355. Back to page 67

[181] K. Freese, M. Lisanti, and C. Savage, *Annual Modulation of Dark Matter: A Review*, (2012), 1209.3339. Back to page 69, 72, 73, or 74

[182] C. McCabe, *The Astrophysical Uncertainties Of Dark Matter Direct Detection Experiments*, Phys.Rev. **D82**, 023530 (2010), 1005.0579. Back to page 70

[183] M. T. Frandsen, F. Kahlhoefer, C. McCabe, S. Sarkar, and K. Schmidt-Hoberg, *Resolving astrophysical uncertainties in dark matter direct detection*, JCAP **1201**, 024 (2012), 1111.0292. Back to page 70

[184] M. Fairbairn, T. Douce, and J. Swift, *Quantifying Astrophysical Uncertainties on Dark Matter Direct Detection Results*, Astropart.Phys. **47**, 45 (2013), 1206.2693. Back to page 70

[185] M. Kuhlen *et al.*, *Dark Matter Direct Detection with Non-Maxwellian Velocity Structure*, JCAP **1002**, 030 (2010), 0912.2358. Back to page 71

[186] T. Piffl *et al.*, *The RAVE survey: the Galactic escape speed and the mass of the Milky Way*, (2013), 1309.4293. Back to page 70

[187] C. Savage, K. Freese, and P. Gondolo, *Annual Modulation of Dark Matter in the Presence of Streams*, Phys.Rev. **D74**, 043531 (2006), astro-ph/0607121. Back to page 71

[188] S. Chang, A. Pierce, and N. Weiner, *Using the Energy Spectrum at DAMA/LIBRA to Probe Light Dark Matter*, Phys.Rev. **D79**, 115011 (2009), 0808.0196. Back to page 71

[189] A. Natarajan, C. Savage, and K. Freese, *Probing dark matter streams with CoGeNT*, Phys.Rev. **D84**, 103005 (2011), 1109.0014. Back to page 71

[190] M. Kuhlen, M. Lisanti, and D. N. Spergel, *Direct Detection of Dark Matter Debris Flows*, Phys.Rev. **D86**, 063505 (2012), 1202.0007. Back to page 71

[191] T. Bruch, J. Read, L. Baudis, and G. Lake, *Detecting the Milky Way's Dark Disk*, Astrophys.J. **696**, 920 (2009), 0804.2896. Back to page 72

[192] K. Freese, P. Gondolo, and L. Stodolsky, *On the direct detection of extragalactic WIMPs*, Phys.Rev. **D64**, 123502 (2001), astro-ph/0106480. Back to page 72

[193] N. Fornengo and S. Scopel, *Temporal distortion of annual modulation at low recoil energies*, Phys. Lett. **B576**, 189 (2003), hep-ph/0301132. Back to page 72

[194] M. Fairbairn and T. Schwetz, *Spin-independent elastic WIMP scattering and the DAMA annual modulation signal*, JCAP **0901**, 037 (2009), 0808.0704. Back to page 72

[195] A. M. Green, *Dependence of direct detection signals on the WIMP velocity distribution*, JCAP **1010**, 034 (2010), 1009.0916. Back to page 72

[196] N. Bozorgnia, R. Catena, and T. Schwetz, *Anisotropic dark matter distribution functions and impact on WIMP direct detection*, (2013), 1310.0468. Back to page 72 or 75

[197] P. J. Fox, J. Liu, and N. Weiner, *Integrating Out Astrophysical Uncertainties*, Phys.Rev. **D83**, 103514 (2011), 1011.1915. Back to page 73

[198] P. J. Fox, G. D. Kribs, and T. M. Tait, *Interpreting Dark Matter Direct Detection Independently of the Local Velocity and Density Distribution*, Phys.Rev. **D83**, 034007 (2011), 1011.1910. Back to page 73

[199] E. Del Nobile, G. Gelmini, P. Gondolo, and J.-H. Huh, *Generalized Halo Independent Comparison of Direct Dark Matter Detection Data*, JCAP **1310**, 048 (2013), 1306.5273. Back to page 73

[200] M. Felizardo *et al.*, *Final Analysis and Results of the Phase II SIMPLE Dark Matter Search*, Phys.Rev.Lett. **108**, 201302 (2012), 1106.3014. Back to page 75

[201] PICASSO Collaboration, S. Archambault *et al.*, *Constraints on Low-Mass WIMP Interactions on ^{19}F from PICASSO*, Phys.Lett. **B711**, 153 (2012), 1202.1240. Back to page 75

[202] COUPP Collaboration, E. Behnke *et al.*, *First Dark Matter Search Results from a 4-kg CF_3I Bubble Chamber Operated in a Deep Underground Site*, Phys.Rev. **D86**, 052001 (2012), 1204.3094. Back to page 75

[203] CDMS-II Collaboration, Z. Ahmed *et al.*, *Dark Matter Search Results from the CDMS II Experiment*, Science **327**, 1619 (2010), 0912.3592. Back to page 75

[204] CDMS-II Collaboration, Z. Ahmed *et al.*, *Results from a Low-Energy Analysis of the CDMS II Germanium Data*, Phys.Rev.Lett. **106**, 131302 (2011), 1011.2482. Back to page 75

[205] XENON100 Collaboration, E. Aprile *et al.*, *Dark Matter Results from 225 Live Days of XENON100 Data*, Phys.Rev.Lett. **109**, 181301 (2012), 1207.5988. Back to page 75

[206] LUX Collaboration, D. Akerib *et al.*, *First results from the LUX dark matter experiment at the Sanford Underground Research Facility*, (2013), 1310.8214. Back to page 75

[207] DAMA Collaboration, LIBRA Collaboration, R. Bernabei *et al.*, *New results from DAMA/LIBRA*, Eur.Phys.J. **C67**, 39 (2010), 1002.1028. Back to page 75

[208] C. Aalseth *et al.*, *Search for An Annual Modulation in Three Years of CoGeNT Dark Matter Detector Data*, (2014), 1401.3295. Back to page 75

[209] G. Angloher *et al.*, *Results from 730 kg days of the CRESST-II Dark Matter Search*, Eur.Phys.J. **C72**, 1971 (2012), 1109.0702. Back to page 75

[210] CDMS Collaboration, R. Agnese *et al.*, *Silicon Detector Dark Matter Results from the Final Exposure of CDMS II*, Phys.Rev.Lett. (2013), 1304.4279. Back to page 75

[211] J. Billard, L. Strigari, and E. Figueroa-Feliciano, *Implication of neutrino backgrounds on the reach of next generation dark matter direct detection experiments*, (2013), 1307.5458. Back to page 75 or 76

[212] C. Kelso, P. Sandick, and C. Savage, *Lowering the Threshold in the DAMA Dark Matter Search*, JCAP **1309**, 022 (2013), 1306.1858. Back to page 75

[213] K. Griest, *Effect of the Sun's Gravity on the Distribution and Detection of Dark Matter Near the Earth*, Phys.Rev. **D37**, 2703 (1988). Back to page 75

[214] P. Sikivie and S. Wick, *Solar wakes of dark matter flows*, Phys.Rev. **D66**, 023504 (2002), astro-ph/0203448. Back to page 75

[215] M. S. Alenazi and P. Gondolo, *Phase-space distribution of unbound dark matter near the Sun*, Phys.Rev. **D74**, 083518 (2006), astro-ph/0608390. Back to page 75

[216] S. K. Lee, M. Lisanti, A. H. G. Peter, and B. R. Safdi, *Effect of Gravitational Focusing on Annual Modulation in Dark-Matter Direct-Detection Experiments*, Phys.Rev.Lett. **112**, 011301 (2014), 1308.1953. Back to page 75

[217] J. P. Ralston, *One Model Explains DAMA/LIBRA, CoGENT, CDMS, and XENON*, (2010), 1006.5255. Back to page 76

[218] E. Fernandez-Martinez and R. Mahbubani, *The Gran Sasso muon puzzle*, JCAP **1207**, 029 (2012), 1204.5180. Back to page 76

Part V

Scientific Research

FTUV-14-0214, IFIC/14-13

The Zee-Babu Model revisited in the light of new data

Juan Herrero-Garcia[a], Miguel Nebot[b], Nuria Rius[a] and Arcadi Santamaria[a]

[a] *Departament de Física Teòrica, Universitat de València and*

IFIC, Universitat de València-CSIC

Dr. Moliner 50, E-46100 Burjassot (València), Spain and

[b] *Centro de Física Teórica de Partículas,*

Instituto Superior Técnico – Universidade de Lisboa

Av. Rovisco Pais 1, 1049-001 Lisboa, Portugal

Abstract

We update previous analyses of the Zee-Babu model in the light of new data, e.g., the mixing angle θ_{13}, the rare decay $\mu \to e\gamma$ and the LHC results. We also analyse the possibility of accommodating the deviations in $\Gamma(H \to \gamma\gamma)$ hinted by the LHC experiments, and the stability of the scalar potential. We find that neutrino oscillation data and low energy constraints are still compatible with masses of the extra charged scalars accessible to LHC. Moreover, if any of them is discovered, the model can be falsified by combining the information on the singly and doubly charged scalar decay modes with neutrino data. Conversely, if the neutrino spectrum is found to be inverted and the CP phase δ is quite different from π, the masses of the charged scalars will be well outside the LHC reach.

I. INTRODUCTION

The observed pattern of neutrino masses and mixing remains one of the major puzzles in particle physics. Moreover, massive neutrinos provide irrefutable evidence for physics beyond the Standard Model (SM) and many theoretical possibilities have been proposed to account for the lightness of neutrinos (see [1–4] for some reviews). With the running of the LHC, it is timely to explore neutrino mass models in which the scale of new physics is close to the TeV. In particular, radiative mechanisms are especially appealing, since small neutrino masses are generated naturally due to loop factors. On the other hand, new physics effects can be sizable also in low energy experiments, for instance lepton flavour violating rare decays of charged leptons, $\ell_\alpha \to \ell_\beta \gamma$, providing complementary probes for such models.

In this paper we consider the Zee-Babu model (ZB) of neutrino masses[1], which just adds two (singly and doubly) charged scalar singlets to the SM. Neutrino masses are generated at two loops and are proportional to the Yukawa couplings of the new scalars and inversely proportional to the square of their masses. This is phenomenologically quite interesting because the new scalars cannot be very heavy or have very small Yukawa couplings, otherwise neutrino masses would be too small. As a consequence, such scalars may be accessible at the LHC, and in principle they could explain the slight excess over the SM prediction found by ATLAS in the diphoton Higgs decay channel $H \to \gamma\gamma$ (currently CMS does not see any excess, see section III for the latest data). They also mediate a variety of lepton flavour violating (LFV) processes, leading to rates measurable in current experiments.

The phenomenology of the ZB model has been widely analyzed: neutrino oscillation data was used to constrain the parameter space of the model, LFV charged lepton decay rates calculated and collider signals discussed [10–12]. Non-standard neutrino interactions in the ZB model have also been thoroughly studied, in correlation with possible LHC signals and LFV processes [13]. In [12], some of us performed an exhaustive numerical study of the full parameter space of the model using Monte Carlo Markov Chain (MCMC) techniques, which allow to efficiently explore high-dimensional spaces. However, in the last few years there

[1] The model was first proposed in [5] and studied carefully in [6]. Similar models with a doubly charged scalar and masses generated at two loops were discussed in [7] (two-loop neutrino mass models containing doubly-charged singlets have also been recently discussed in connection with neutrinoless double beta decay [8, 9]).

have been several experimental results which motivate an up-to-date analysis including all relevant data currently available. Therefore, in this work we update previous analysis in the light of the recent measurement of the neutrino mixing angle θ_{13} [14–16], the new MEG limits on $\mu \to e\gamma$ [17], the lower bounds on doubly-charged scalars coming from LHC data [18, 19], and, of course, the discovery of a 125 GeV Higgs boson by ATLAS and CMS [20, 21]. Moreover, we also study the possibility of accommodating deviations from the SM prediction for the Higgs diphoton decay channel, and the effects of the new couplings of the model in the stability of the scalar potential. A possible enhancement of the Higgs diphoton decay rate in the ZB model together with the vacuum stability of the scalar potential has been studied in [22], however a consistent updated analysis including all constraints is lacking.

The outline of the paper is the following. In section II we briefly review the main features of the ZB model, discussing perturbativity and naturality estimates for the allowed ranges of the free parameters of the model. We summarize present constraints from recent neutrino oscillation data, low energy lepton-flavour violating processes, universality and stability of the scalar potential. We also review the collider phenomenology of the ZB model, discussing current limits from LHC, and briefly comment on the prospects for non-standard neutrino interactions. In section III we analyze in detail the contributions of the ZB charged scalars to both, $\Gamma(H \to \gamma\gamma)$ and $\Gamma(H \to Z\gamma)$. After some analytic estimates in section IV, we present the results of our MCMC numerical analysis in section V and we conclude in section VI. Renormalization group equations for the ZB model and relevant loop functions are collected in the appendices.

II. THE ZEE-BABU MODEL

We follow the notation of [12]. As mentioned above, the Zee-Babu model only contains, in addition to the SM, two charged singlet scalar fields

$$h^{\pm}, \qquad k^{\pm\pm}\,, \tag{1}$$

with weak hypercharges ± 1 and ± 2 respectively (we use the convention $Q = T_3 + Y$).

The scalar potential is given by

$$\begin{aligned} V \;=\; & m_H'^2 H^\dagger H + m_h'^2 |h|^2 + m_k'^2 |k|^2 + \lambda_H (H^\dagger H)^2 + \lambda_h |h|^4 + \lambda_k |k|^4 \\ & + \; \lambda_{hk} |h|^2 |k|^2 + \lambda_{hH} |h|^2 H^\dagger H + \lambda_{kH} |k|^2 H^\dagger H + \left(\mu h^2 k^{++} + \text{h.c.}\right)\,, \end{aligned} \tag{2}$$

being H the $SU(2)$ doublet Higgs boson, while the leptons have Yukawa couplings to both H and the new charged scalars:

$$\mathcal{L}_Y = \overline{L_L}\, Y e H + \overline{\tilde{L}_L} f \ell h^+ + \overline{e^c} g\, e\, k^{++} + \text{h.c.}\,, \tag{3}$$

where L_L and e are the SM $SU(2)$ lepton doublets and singlets, respectively, and $\tilde{L}_L \equiv i\tau_2 L_L^c = i\tau_2 C \overline{L_L}^T$, with τ_2 Pauli's second matrix. Due to Fermi statistics, f_{ab} is an antisymmetric matrix in flavour space while g_{ab} is symmetric.

Notice that we can assign lepton number -2 to both scalars, h^+ and k^{++}, in such a way that total lepton number L (or $B-L$) is conserved in the complete Lagrangian, except for the trilinear coupling μ of the scalar potential; thus, lepton number is explicitly broken by the μ-coupling. It is important to remark that lepton number violation requires the simultaneous presence of the four couplings Y, f, g and μ, because if any of them vanishes one can always assign quantum numbers in such a way that there is a global $U(1)$ symmetry. This means that neutrino masses will require the simultaneous presence of the four couplings.

Regarding the physical free parameters in the ZB model, our convention is the following: without loss of generality, we choose the 3×3 charged lepton Yukawa matrix Y to be diagonal with real and positive elements. We also use fermion field rephasings to remove three phases from the elements of the matrix g and charged scalar rephasings to set μ real and positive, and to remove one phase from f. In summary we have 12 moduli (3 from Y, 3 from f and 6 from g_{ab}), 5 phases (3 from g and 2 from f) and the real and positive parameter μ, plus the rest of real parameters in the scalar potential. As discussed in [12], this choice is compatible with the standard parametrization of neutrino masses and mixings.

After electroweak symmetry breaking, the masses of charged leptons are $m_a = Y_{aa} v$, with $v \equiv \langle H^0 \rangle = 174\,\text{GeV}$, the VEV of the standard Higgs doublet, while the physical charged scalar masses are given by

$$m_h^2 = m_h'^2 + \lambda_{hH} v^2\,, \qquad m_k^2 = m_k'^2 + \lambda_{kH} v^2\,. \tag{4}$$

In principle, the scale of the new mass parameters of the ZB model (m_h, m_k and μ) is arbitrary. However from the experimental point of view it is interesting to consider new scalars light enough to be produced in the second run of the LHC. Also theoretical arguments suggest that the scalar masses should be relatively light (few TeV), to avoid unnaturally large one-loop corrections to the Higgs mass which would introduce a hierarchy

problem. Therefore, in this paper we will focus on the masses of the new scalars, m_h, m_k, below 2 TeV.

The Yukawa couplings of the new scalars of the model enter in the neutrino mass formula and in several LFV processes, and are strongly bounded for the scalar masses we are considering except in a few corners of the parameter space where we require that the theory remains perturbative. Since one-loop corrections to Yukawa couplings are order

$$\delta f \sim \frac{f^3}{(4\pi)^2}\,, \qquad \delta g \sim \frac{g^3}{(4\pi)^2}\,. \tag{5}$$

one expects from perturbativity $f, g \ll 4\pi$, although, as we will see, for the scalar masses considered here, phenomenological constraints are always stronger.

The couplings of the charged scalars in the scalar potential, apart from the stability constraints described in section II E, are essentially free. However, for the theory to make sense as a perturbative theory we also impose the limit[2] $\lambda_{h,k,kH,hH,hk} < 4\pi$.

The trilinear coupling among charged scalars μ, on the other hand, is different, for it has dimensions of mass and it is insensitive to high energy perturbative unitarity constraints. However, it induces radiative corrections to the masses of the charged scalars of order

$$\delta m_k^2, \delta m_h^2 \sim \frac{\mu^2}{(4\pi)^2}\,. \tag{6}$$

Requiring that the corrections in absolute value are much smaller than the masses we can derive a naive upper bound for this parameter, $\mu \ll 4\pi \min(m_h, m_k)$, but it is difficult to fix an exact value of μ for which the contributions to the scalar masses are unacceptably large, leading to a highly fine-tuned scenario.

A large value of μ, as compared with scalar masses, is also disfavoured because it could lead to a deeper minimum of the scalar potential for non-vanishing values of the charged fields, therefore breaking charge conservation. This phenomenon has also been studied in the context of supersymmetric theories (see for instance [25–27]). As an example, by looking at the particular direction $|H| = |h| = |k| = r$, and requiring that the charge breaking minimum is not a global minimum, $V(r \neq 0) > 0$, one obtains

$$\mu^2 < (\lambda_H + \lambda_h + \lambda_k + \lambda_{hH} + \lambda_{kH} + \lambda_{hk}) \left(m_H'^2 + m_h'^2 + m_k'^2\right). \tag{7}$$

[2] Notice that there could be order one differences in the perturbativity constraints on the different couplings λ_i from perturbative unitarity of the matrix elements [23, 24]. We can neglect them for the purpose of this work, keeping in mind that they could be relevant when perturbativity is "pushed" to the limit (as needed to explain $H \to \gamma\gamma$ enhancement, see sec. III).

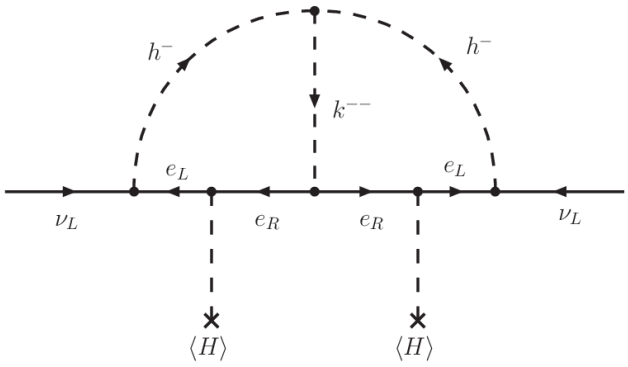

Figure 1: Diagram contributing to the neutrino Majorana mass at two loops.

Assuming no cancellations between the λ's or mass terms, neglecting λ_H and $m_H'^2$, and using the perturbative limit for the rest of the couplings $\lambda_i \lesssim 4\pi$ one finds a very conservative bound on μ

$$\mu \lesssim \sqrt{20\pi}\,\max(m_k, m_h) \sim 8\,\max(m_k, m_h) \tag{8}$$

Tighter limits can be obtained by looking at all directions in the potential and/or allowing for cancellations.

Given that the neutrino masses depend linearly on the parameter μ, as we will see in the next section, the ability of the model to accommodate all present data is quite sensitive to the upper limit allowed for μ. Thus we choose to implement such limit in terms of a parameter κ,

$$\mu < \kappa\,\min(m_h, m_k)\,, \tag{9}$$

and discuss our results for different values of $\kappa = 1, 5, 4\pi$. Notice that we are using the naturality upper bound (expressed in terms of $\min(m_h, m_k)$), which in general is much more restrictive than the upper bound obtained by requiring that the minimum of the potential does not break charge conservation (expressed in terms of $\max(m_h, m_k)$).

A. Neutrino masses.

The lowest order contribution to neutrino masses involving the four relevant couplings appears at two loops [5, 6] and its Feynman diagram is depicted in fig. 1.

The calculation of this diagram gives the following mass matrix for the neutrinos (defined

as an effective term in the Lagrangian $\mathcal{L}_\nu \equiv -\frac{1}{2}\overline{\nu_L^c}\mathcal{M}_\nu\nu_L + \text{h.c.}$)

$$(\mathcal{M}_\nu)_{ij} = 16\mu f_{ia} m_a g^*_{ab} I_{ab} m_b f_{jb}\,, \tag{10}$$

where I_{ab} is the two-loop integral, which can be calculated analytically [28]. However, since m_c, m_d are the masses of the charged leptons, necessarily much lighter than the charged scalars, we can neglect them and obtain a much simpler form

$$I_{cd} \simeq I = \frac{1}{(16\pi^2)^2}\frac{1}{M^2}\frac{\pi^2}{3}\tilde{I}(r) \quad , \quad M \equiv \max(m_h, m_k)\,, \tag{11}$$

where $\tilde{I}(r)$ is a function of the ratio of the masses of the scalars $r \equiv m_k^2/m_h^2$,

$$\tilde{I}(r) = \begin{cases} 1 + \frac{3}{\pi^2}(\log^2 r - 1) & \text{for } r \gg 1 \\ 1 & \text{for } r \to 0 \end{cases}\,, \tag{12}$$

which is close to one for a wide range of scalar masses. Within this approximation the neutrino mass matrix can be directly written in terms of the Yukawa coupling matrices, f, g, and Y

$$\mathcal{M}_\nu = \frac{v^2\mu}{48\pi^2 M^2}\tilde{I}\, f\, Y\, g^\dagger Y^T f^T\,. \tag{13}$$

A very important point is that since f is a 3×3 antisymmetric matrix, $\det f = 0$ (for 3 generations), and therefore $\det \mathcal{M}_\nu = 0$. Thus, at least one of the neutrinos is exactly massless at this order.

The neutrino Majorana mass matrix $\mathcal{M}_\nu$ can be written as

$$\mathcal{M}_\nu = U D_\nu U^T\,, \tag{14}$$

where D_ν is a diagonal matrix with real positive eigenvalues, and U is the Pontecorvo-Maki-Nakagawa-Sakata (PMNS) leptonic mixing matrix. We are left with only two possibilities for the neutrino masses, m_i:

- Normal hierarchy (NH): the solar squared mass difference is $\Delta_S = m_2^2$, the atmospheric mass splitting $\Delta_A = m_3^2$ and $m_1 = 0$, with $m_3 \gg m_2$.
- Inverted hierarchy (IH): $\Delta_S = m_2^2 - m_1^2$, $\Delta_A = m_1^2$ and $m_3 = 0$, with $m_1 \approx m_2$.

The standard parametrization for the PMNS matrix is

$$U = \begin{pmatrix} c_{13}c_{12} & c_{13}s_{12} & s_{13}e^{-i\delta} \\ -c_{23}s_{12} - s_{23}s_{13}c_{12}e^{i\delta} & c_{23}c_{12} - s_{23}s_{13}s_{12}e^{i\delta} & s_{23}c_{13} \\ s_{23}s_{12} - c_{23}s_{13}c_{12}e^{i\delta} & -s_{23}c_{12} - c_{23}s_{13}s_{12}e^{i\delta} & c_{23}c_{13} \end{pmatrix} \begin{pmatrix} 1 & & \\ & e^{i\phi/2} & \\ & & 1 \end{pmatrix}\,, \tag{15}$$

Process	Experiment (90% CL)	Bound (90% CL)
$\mu^- \to e^+e^-e^-$	BR$< 1.0 \times 10^{-12}$	$\lvert g_{e\mu}g^*_{ee}\rvert < 2.3 \times 10^{-5} \left(\frac{m_k}{\text{TeV}}\right)^2$
$\tau^- \to e^+e^-e^-$	BR$< 2.7 \times 10^{-8}$	$\lvert g_{e\tau}g^*_{ee}\rvert < 0.009 \left(\frac{m_k}{\text{TeV}}\right)^2$
$\tau^- \to e^+e^-\mu^-$	BR$< 1.8 \times 10^{-8}$	$\lvert g_{e\tau}g^*_{e\mu}\rvert < 0.005 \left(\frac{m_k}{\text{TeV}}\right)^2$
$\tau^- \to e^+\mu^-\mu^-$	BR$< 1.7 \times 10^{-8}$	$\lvert g_{e\tau}g^*_{\mu\mu}\rvert < 0.007 \left(\frac{m_k}{\text{TeV}}\right)^2$
$\tau^- \to \mu^+e^-e^-$	BR$< 1.5 \times 10^{-8}$	$\lvert g_{\mu\tau}g^*_{ee}\rvert < 0.007 \left(\frac{m_k}{\text{TeV}}\right)^2$
$\tau^- \to \mu^+e^-\mu^-$	BR$< 2.7 \times 10^{-8}$	$\lvert g_{\mu\tau}g^*_{e\mu}\rvert < 0.007 \left(\frac{m_k}{\text{TeV}}\right)^2$
$\tau^- \to \mu^+\mu^-\mu^-$	BR$< 2.1 \times 10^{-8}$	$\lvert g_{\mu\tau}g^*_{\mu\mu}\rvert < 0.008 \left(\frac{m_k}{\text{TeV}}\right)^2$
$\mu^+e^- \to \mu^-e^+$	$G_{M\bar{M}} < 0.003 G_F$	$\lvert g_{ee}g^*_{\mu\mu}\rvert < 0.2 \left(\frac{m_k}{\text{TeV}}\right)^2$

Table I: Constraints from tree-level lepton flavour violating decays [3].

where $c_{ij} \equiv \cos\theta_{ij}$, $s_{ij} \equiv \sin\theta_{ij}$ and since one of the neutrinos is massless, there is only one physical Majorana phase, ϕ, in addition to the Dirac phase δ.

B. Low energy constraints.

In order to provide neutrino masses compatible with experiment, the Yukawa couplings of the charged scalars cannot be too small and their masses cannot be too large. This immediately gives rise to a series of flavour lepton number violating processes, as for instance $\mu^- \to e^-\gamma$ or $\mu^- \to e^+e^-e^-$, with rates which can be, in some cases, at the verge of the present experimental limits. Therefore, we can use these processes to obtain information about the parameters of the model and hopefully to confirm or to exclude the model in a near future by exploiting the synergies with direct searches for the new scalars at LHC.

In this section we follow the notation of [12], where all the relevant formulae can be found, and update the new bounds. We collect the relevant tree-level lepton flavour violating constraints, from $\ell_a^- \to \ell_b^+\ell_c^-\ell_d^-$ decays and $\mu^+e^- \leftrightarrow \mu^-e^+$ transitions, in table I.

Universality constraints are summarized in table II where we have combined the measurements presented in [29] for the different couplings. There seems to be a 2σ discrepancy in G_τ^{exp}/G_e^{exp}, which we interpret as a bound. If confirmed and interpreted within the ZB model, one obtains that $|f_{\mu\tau}|^2 - |f_{e\mu}|^2 = 0.05\,(m_h/\text{TeV})^2$. As we will see in section IV, for NH spectrum $f_{e\mu} \sim f_{\mu\tau}/2$, therefore one needs $m_h \sim 4\,f_{\mu\tau}\text{TeV}$, which is easily achieved. For

SM Test	Experiment	Bound (90%CL)
lept./hadr. univ.	$\sum_{q=d,s,b} \lvert V_{uq}^{exp}\rvert^2 = 0.9999 \pm 0.0006$	$\lvert f_{e\mu}\rvert^2 < 0.007 \left(\frac{m_h}{\text{TeV}}\right)^2$
μ/e universality	$\frac{G_\mu^{exp}}{G_e^{exp}} = 1.0010 \pm 0.0009$	$\lvert\lvert f_{\mu\tau}\rvert^2 - \lvert f_{e\tau}\rvert^2\rvert < 0.024 \left(\frac{m_h}{\text{TeV}}\right)^2$
τ/μ universality	$\frac{G_\tau^{exp}}{G_\mu^{exp}} = 0.9998 \pm 0.0013$	$\lvert\lvert f_{e\tau}\rvert^2 - \lvert f_{e\mu}\rvert^2\rvert < 0.035 \left(\frac{m_h}{\text{TeV}}\right)^2$
τ/e universality	$\frac{G_\tau^{exp}}{G_e^{exp}} = 1.0034 \pm 0.0015$	$\lvert\lvert f_{\mu\tau}\rvert^2 - \lvert f_{e\mu}\rvert^2\rvert < 0.04 \left(\frac{m_h}{\text{TeV}}\right)^2$

Table II: Constraints from universality of charged currents obtained combining the experimental results compiled in table 2 of [29].

Experiment	Bound (90%CL)
$\delta a_e = (12 \pm 10) \times 10^{-12}$	$r\left(\lvert f_{e\mu}\rvert^2 + \lvert f_{e\tau}\rvert^2\right) + 4\left(\lvert g_{ee}\rvert^2 + \lvert g_{e\mu}\rvert^2 + \lvert g_{e\tau}\rvert^2\right) < 5.5 \times 10^3\,(m_k/\text{TeV})^2$
$\delta a_\mu = (21 \pm 10) \times 10^{-10}$	$r\left(\lvert f_{e\mu}\rvert^2 + \lvert f_{\mu\tau}\rvert^2\right) + 4\left(\lvert g_{e\mu}\rvert^2 + \lvert g_{\mu\mu}\rvert^2 + \lvert g_{\mu\tau}\rvert^2\right) < 7.9\,(m_k/\text{TeV})^2$
$BR(\mu \to e\gamma) < 5.7 \times 10^{-13}$	$r^2\lvert f_{e\tau}^* f_{\mu\tau}\rvert^2 + 16\lvert g_{ee}^* g_{e\mu} + g_{e\mu}^* g_{\mu\mu} + g_{e\tau}^* g_{\mu\tau}\rvert^2 < 1.6 \times 10^{-6}\,(m_k/\text{TeV})^4$
$BR(\tau \to e\gamma) < 3.3 \times 10^{-8}$	$r^2\lvert f_{e\mu}^* f_{\mu\tau}\rvert^2 + 16\lvert g_{ee}^* g_{e\tau} + g_{e\mu}^* g_{\mu\tau} + g_{e\tau}^* g_{\tau\tau}\rvert^2 < 0.52\,(m_k/\text{TeV})^4$
$BR(\tau \to \mu\gamma) < 4.4 \times 10^{-8}$	$r^2\lvert f_{e\mu}^* f_{e\tau}\rvert^2 + 16\lvert g_{e\mu}^* g_{e\tau} + g_{\mu\mu}^* g_{\mu\tau} + g_{\mu\tau}^* g_{\tau\tau}\rvert^2 < 0.7\,(m_k/\text{TeV})^4$

Table III: Constraints from loop-level lepton flavour violating interactions and anomalous magnetic moments [3, 17].

IH spectrum, however, $f_{\mu\tau} \sim 0.2 f_{e\mu}$ ($f_{\mu\tau} \sim (0.15 - 0.3)\, f_{e\mu}$ if we vary the angles in their 3σ range), and therefore, if this measurement is confirmed, the IH scheme in the ZB model would be disfavoured.

Finally, one-loop level lepton flavour violating constraints coming from $\ell_a^- \to \ell_b^- \gamma$ decays[3] and anomalous magnetic moments of electron and muon are collected in table III, including the recent limit on BR($\mu \to e\gamma$) from the MEG Collaboration [17].

Given that lepton number is not conserved, another interesting low energy process that could arise in the ZB model is neutrinoless double beta decay ($0\nu2\beta$). However, since the singly and doubly charged scalars do not couple to hadrons and are singlet under the weak SU(2) (therefore, do not couple to W gauge bosons), the $0\nu2\beta$ rate is dominated by the Majorana neutrino exchange [34] and it is proportional to the $\lvert(\mathcal{M}_\nu)_{ee}\rvert^2$ matrix element. In

[3] As was shown in [30], doubly charged scalars can give logarithmic enhanced contributions to muon-electron conversion in nuclei. Moreover, planned experiments will improve current limits by four orders of magnitude [31–33]; however, at present, limits are still not competitive with $\mu \to e\gamma$.

the NH case,

$$(\mathcal{M}_\nu^{NH})_{ee} = \sqrt{\Delta_S} c_{13}^2 s_{12}^2 e^{i\phi} + \sqrt{\Delta_A} s_{13}^2 \,. \tag{16}$$

Using neutrino oscillation data, one obtains $0.001 \lesssim$ eV$|(\mathcal{M}_\nu^{NH})_{ee}| \lesssim 0.004\,$eV and therefore it is outside the reach of present and near future $0\nu2\beta$ decay experiments.

In the IH case,

$$(\mathcal{M}_\nu^{IH})_{ee} = \sqrt{\Delta_A + \Delta_S} c_{13}^2 s_{12}^2 e^{i\phi} + \sqrt{\Delta_A} c_{13}^2 c_{12}^2 \,. \tag{17}$$

Then, $0.01\,\text{eV} \lesssim |(\mathcal{M}_\nu^{NH})_{ee}| \lesssim 0.05\,$eV and, therefore, it is observable in planned $0\nu2\beta$ decay experiments.

C. Non-standard interactions.

The heavy scalars of the ZB model induce non-standard lepton interactions at tree level, which have been thoroughly analyzed in [13]. In particular, by integrating out the singly charged scalar h^+, the following dimension-6 operators are generated:

$$\mathcal{L}_{d=6}^{NSI} = 2\sqrt{2} G_F \epsilon_{\alpha\beta}^{\rho\sigma} (\overline{\nu_\alpha} \gamma^\mu P_L \nu_\beta)(\overline{\ell_\rho} \gamma_\mu P_L \ell_\sigma), \tag{18}$$

where ℓ refer to the charged leptons and the standard NSI parameters $\epsilon_{\alpha\beta}^{\rho\sigma}$ are given by

$$\epsilon_{\alpha\beta}^{\rho\sigma} = \frac{f_{\sigma\beta} f_{\rho\alpha}^*}{\sqrt{2} G_F m_h^2}. \tag{19}$$

Regarding neutrino propagation in matter, the relevant NSI parameters are $\epsilon_{\alpha\beta}^m = \epsilon_{\alpha\beta}^{ee}$. Since the couplings $f_{\sigma\beta}$ are antisymmetric, in the ZB model only $\epsilon_{\mu\tau}^m, \epsilon_{\mu\mu}^m$ and $\epsilon_{\tau\tau}^m$ are non zero. NSI can also affect the neutrino production in a neutrino factory, via the processes $\mu \to e\overline{\nu_\beta}\nu_\alpha$. Source effects in the $\nu_\mu \to \nu_\tau$ and $\nu_e \to \nu_\tau$ channels are produced by the NSI parameters

$$\epsilon_{\mu\tau}^s = \epsilon_{\tau e}^{e\mu} = \frac{f_{\mu e} f_{e\tau}^*}{\sqrt{2} G_F m_h^2}, \tag{20}$$

$$\epsilon_{e\tau}^s = \epsilon_{\mu\tau}^{e\mu} = \frac{f_{\mu\tau} f_{e\mu}^*}{\sqrt{2} G_F m_h^2}, \tag{21}$$

respectively. Notice that $\epsilon_{\mu\tau}^m = -\epsilon_{\mu\tau}^{s*}$, since both NSI parameters are related to the couplings $f_{e\mu}$ and $f_{e\tau}$.

As we discuss in section V, the ratios of Yukawa couplings $f_{e\mu}/f_{\mu\tau}$ and $f_{e\tau}/f_{\mu\tau}$ are entirely determined by the neutrino mixing angles and Dirac phase of the PMNS matrix U – see

eqs. (37) and (38) –, so the impact of the improved bounds on BR($\mu \to e\gamma$) can be easily estimated: given that the limit is now ~ 0.05 times smaller than in the study of [13], and the contribution of the singly charged scalar h^+ to BR($\mu \to e\gamma$) depends on $|f^*_{e\tau} f_{\mu\tau}|^2$, the current constraints on $|f_{\alpha\beta}|$ are roughly a factor 2 tighter than before. Therefore, since the strength of the NSI depends on $\epsilon^{\rho\sigma}_{\alpha\beta} \propto f_{\sigma\beta} f^*_{\rho\alpha}$, generically we expect that the allowed size of the NSI is reduced by a factor $\sim 1/4$. According to [13][4], this implies that in the most favorable case of IH neutrino mass spectrum, $\epsilon^s_{e\tau}$ and $\epsilon^s_{\mu\tau}$ are in the range $3 \times (10^{-5} - 10^{-4})$, which is in a range difficult to probe, but it might be in a future neutrino factory with a ν_τ near detector [35].

D. Bounds on the masses of the charged scalars.

Regarding limits on singly-charged bosons decaying to leptons, the best limit still comes from LEP II, $m_h > 100$ GeV.

ATLAS and CMS have placed limits on doubly-charged boson masses from searches of dilepton final states, using data samples corresponding to $\sqrt{s} = 7$ TeV with an integrated luminosity of 4.7 fb^{-1} and 4.9 fb^{-1}, respectively [18, 19]. The authors of [36] show that, with current data at 8 TeV and 20 fb^{-1}, all the bounds are expected to become about ~ 100 GeV more stringent if no significant signal is seen. Further tests on the nature of the doubly charged scalar (i.e., singlet or triplet of $SU(2)_L$) can be obtained by analysing tau lepton decay distributions which are sensitive to the chiral structure of the couplings [37]. The main production mechanisms of doubly-charged bosons at hadron colliders are pair production via an s-channel exchange of a photon or a Z-boson, and associated production with a charged boson via the exchange of a W-boson (see [38, 39] for a general analysis of the production and detection at LHC of doubly charged scalars belonging to different electroweak representations). In the Zee-Babu model, the associated production is absent, because the new scalars are $SU(2)_L$ singlets.

The ATLAS analysis [18] focuses on the $ee, \mu\mu, e\mu$ channels and assumes that the rest of

[4] Notice that although the analysis of [13] has been done for $\kappa = 1$, the impact on NSI of the new bounds from BR($\mu \to e\gamma$) (and in general from any LFV decay $\ell_\alpha \to \ell_\beta \gamma$) is independent of the value of κ chosen, because they constraint directly $|f^*_{\alpha\sigma} f_{\sigma\beta}|/m_h^2$, which is the same combination that appears in the NSI parameters, eq. (19). The only effect of increasing κ may be that a given point $(f_{\alpha\sigma}, f_{\sigma\beta}, m_h)$ is able to fit neutrino masses with smaller g_{ab} and therefore possibly lighter m_k.

the channels can make up to 90% of the total decays. Then, the limits for the Zee-Babu model are, at the 95% C.L., 322, 306, 310 GeV (151, 176, 151 GeV) for branching ratios of 100% (10%) to the $ee, \mu\mu, e\mu$ channels. Notice that in [18] the limits on doubly-charged bosons coupling to left-handed leptons are applied, in addition to the seesaw type II case, to the Zee-Babu model. However, this is not so, as the doubly-charged singlets in the Zee-Babu model are $SU(2)_L$ singlets and thus couple only to right-handed leptons, at variance with the seesaw type II models, where the doubly-charged bosons are $SU(2)_L$ triplets and do couple only to left-handed leptons. Therefore, in the Zee-Babu case they have a reduced production cross section, due to their different couplings to the Z-boson, around 2.5 times smaller than for the case of the triplet [40], and less stringent limits apply: for the Zee-Babu model one should look at the second part of table I of [18], the one for $H_R^{\pm\pm} \equiv k^{\pm\pm}$.

The CMS Collaboration has searched for doubly-charged bosons which are $SU(2)_L$ triplets, both assuming that they decay to the different dilepton final states $\ell\ell$ ($\ell = e, \mu, \tau$) 100% of the times, i.e., BR$(k^{++} \to \ell\ell) = 1$, and also considering several benchmark points with different branching ratios.

The CMS 95% C.L. limits for pair production of $SU(2)_L$ singlets, which is the one relevant for the Zee-Babu Model, are around $60 - 80$ GeV less stringent [39, 40]:

- $ee, \mu\mu, e\mu$: 310 GeV,
- $e\tau, \mu\tau$: 220 GeV,
- $\tau\tau$: 100 GeV.

Note that whenever the branching ratio to $\tau\tau$ is less than 30% (see table I and VI of [19]), the bounds are ~ 280 GeV, provided that there is a significant fraction of decays into light leptons ($ee, \mu\mu, e\mu$).

In the Zee-Babu model the decay width of $k^{\pm\pm}$ into same sign leptons is given by

$$\Gamma(k \to \ell_a \ell_b) = \frac{|g_{ab}|^2}{4\pi(1+\delta_{ab})} m_k \ . \tag{22}$$

Since the g_{ab} couplings are free parameters, the BRs of the different decay modes are a priori unknown, so we can not apply directly these bounds. As we will see in the numerical analysis, section V, once neutrino oscillation data and low energy constraints are taken into

account, the branching ratio to $\tau\tau$ is very small in the Zee-Babu model, less than about 1%. Then, a conservative limit is $m_k > 220$ GeV.

Moreover, in the ZB model for $m_k > 2\,m_h > 200$ GeV, it can happen that the doubly charged scalar decays predominantly into hh, which can easily escape detection. This way the constraints from dilepton searches could be evaded. The relevant decay width is given by

$$\Gamma(k \to hh) = \frac{1}{8\pi}\left[\frac{\mu}{m_k}\right]^2 m_k \sqrt{1 - \frac{4m_h^2}{m_k^2}}\,. \tag{23}$$

Then, even for $g_{ab} \sim 1$, for $m_h = 100$ GeV and $m_k = 200$ GeV, we have that $\frac{\Gamma(k\to hh)}{\Gamma(k\to \ell\ell)} \geq 1$ for $\mu \geq m_k$, which is still natural as long it is not very large. Thus, we take $m_k \geq 200$ GeV in the numerical analysis.

E. Stability of the potential.

In this section we consider further constraints on the ZB model parameter space coming from vacuum stability conditions. The Hamiltonian in quantum mechanics has to be bounded from below, this requires that the quartic part of the scalar potential in eq. (2) should be positive for all values of the fields and for all scales. Then, if two of the fields H, k or h vanish one immediately finds[5]:

$$\lambda_H > 0, \qquad \lambda_h > 0, \qquad \lambda_k > 0\,. \tag{24}$$

Moreover the positivity of the potential whenever one of the scalar fields H, h, k is zero implies

$$\alpha, \beta, \gamma > -1\,, \tag{25}$$

where we have defined

$$\alpha = \lambda_{hH}/(2\sqrt{\lambda_H\lambda_h})\,,\ \beta = \lambda_{kH}/(2\sqrt{\lambda_H\lambda_k})\,,\ \gamma = \lambda_{hk}/(2\sqrt{\lambda_h\lambda_k})\,. \tag{26}$$

Eq. (25) constrains only negative mixed couplings, $\lambda_{xH}, \lambda_{hk}$ $(x = h, k)$, since for positive ones the potential is definite positive and only the perturbativity limit, $\lambda_{xH}, \lambda_{hk} \lesssim 4\pi$ applies.

[5] We do not consider the possibility of zero couplings, which can only appear at very specific scales.

Finally, if at least two of the mixed couplings are negative, there is an extra constraint, which can be written as:

$$1-\alpha^2-\beta^2-\gamma^2+2\alpha\beta\gamma>0 \qquad \vee \qquad \alpha+\beta+\gamma>-1\,. \tag{27}$$

We have checked that the above conditions, eqs. (24, 25, 27), are equivalent to the ones derived in [41] for the Zee model, but they differ from the ones used in [22] for the ZB model, which seem not to be symmetric under the exchange of α, β, γ, as they should. Our constraints also agree with the results obtained by using copositive criteria (see for instance [42]).

The discovery of the Higgs boson with mass $m_H \sim 125$ GeV at the LHC has raised the interest on the vacuum stability of the SM potential: for the current central values of the strong coupling constant and the Higgs and top quark masses, the Higgs self-coupling λ_H would turn negative at a scale $\Lambda \sim 10^{10} - 10^{13}$ GeV [43], indicating the existence of new physics beyond the SM below that scale. In fact, by using state of the art radiative corrections, the authors of [43] find that absolute stability of the SM Higgs potential up to the Planck scale is excluded at 98% C.L. for $m_H < 126$ GeV.

The one-loop renormalization group equations (RGEs) in the ZB model are written in Appendix A. For a given set of parameters defined at the electroweak scale, and satisfying the stability conditions discussed above, we calculate the running couplings numerically by using one-loop RGEs. From eqs. (A1), we see that the new scalar couplings $\lambda_{hH}, \lambda_{kH}$ always contribute positively to the running of the Higgs quartic coupling λ_H, compensating for the large and negative contribution of the top quark Yukawa coupling. Therefore, the vacuum stability problem can be alleviated in the ZB model with λ_H remaining positive up to the Planck scale for the present central values of m_t and m_H if λ_{xH} are not extremely small ($\lambda_{xH} \sim \pm 0.2$ are enough to stabilize λ_H maintaining stability/perturbativity of all couplings up to the Planck scale (see fig. 2)).

On the other hand, as we discuss in section III, the slight excess in the Higgs diphoton decay channel found at LHC can be accommodated in the ZB model with relatively light singlet scalars and large, negative, mixed couplings $\lambda_{hH}, \lambda_{kH}$. However for such values of the scalar couplings at the electroweak scale, the RGEs lead to vacuum instability ($2\sqrt{\lambda_H \lambda_x} + \lambda_{xH} < 0$, $x = h, k$) and/or non-perturbativity ($\lambda_x > 4\pi$) well below the Planck scale. This can be seen in fig. 2 where we have performed a complete scan of the quartic couplings

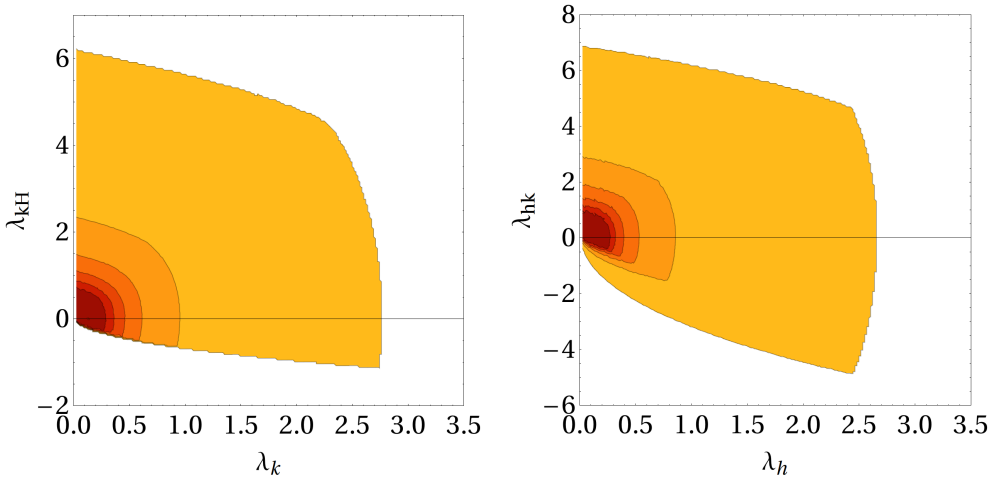

Figure 2: Allowed regions in λ_{kH} vs λ_k (left) and λ_{hk} vs λ_h (right), taken at the m_Z scale, if perturbativity/stability is required to be valid up to $10^3, 10^6, 10^9, 10^{12}, 10^{15}, 10^{18}$ GeV (from light to dark colours). The rest of the parameters entering the RGE are taken at their measured value or varied in the range allowed by the perturbativity/stability requirement up to the given scale.

of the scalar potential, run all of them from m_Z up to a given scale ($\mu = 10^{3n}$ GeV with $n = 1, 2, \cdots, 6$), and check that stability (as explained before) and perturbativity ($\lambda_i < 4\pi$) are satisfied at all scales below μ. On the left we represent the region allowed in the λ_{kH}–λ_k plane, with λ's taken at the m_Z scale, when stability/perturbativity is imposed up to the different scales μ. Lighter regions correspond to small scales and obviously include the regions of larger scales. A similar plot is obtained for λ_{hH} vs λ_h. On the right we present the equivalent results for the couplings λ_{hk} vs λ_h.

III. $H \to \gamma\gamma$ AND $H \to Z\gamma$

It remains an open question whether the 125 GeV Higgs boson discovered by ATLAS [20] and CMS [21] is the SM one or has some extra features coming from new physics. While all the present measurements of the Higgs properties are consistent with the SM values, the uncertainties are still large, so there is plenty of room for non-standard signals to show up in the upcoming 13-14 TeV run data. Moreover, the present experimental situation of the $H \to \gamma\gamma$ decay channel is far from clear: although the last reported analysis of the CMS

and ATLAS Collaborations on the diphoton signal strength are barely consistent with each other within 2σ, ATLAS still observes a $\sim 2\sigma$ excess over the SM prediction [44], while the CMS measurement has become consistent with the SM at 1σ [45]:

$$\begin{aligned} \text{ATLAS}: \; & R_{\gamma\gamma} = 1.55^{+0.33}_{-0.28}\,, \\ \text{CMS}: \; & R_{\gamma\gamma} = 0.78^{+0.28}_{-0.26}\,, \;\; \text{MVA analysis} \\ \text{CMS}: \; & R_{\gamma\gamma} = 1.11^{+0.32}_{-0.31}\,. \;\; \text{cut based analysis} \end{aligned} \tag{28}$$

It is thus worthwhile to explore whether an eventually confirmed deviation from the SM prediction in the $H \to \gamma\gamma$ channel can be accommodated within the ZB model.

In the SM the $H \to \gamma\gamma$ channel is dominated by the W boson loop contribution, which interferes destructively with the top quark one. Since the Higgs coupling to photons is induced at the loop-level, extra charged fermions or scalars with significant couplings to the Higgs can change drastically the $H \to \gamma\gamma$ channel with respect to the Standard Model expectations, either enhancing it or reducing it [46]. Moreover, in the absence of direct signatures of new particles at LHC, the enhanced Higgs diphoton decay rate might provide an indirect hint of physics beyond the SM.

The value of the $H \to \gamma\gamma$ decay width in the ZB model with respect to the SM one is given by [46–48]:

$$R_{\gamma\gamma} = \frac{\Gamma(H \to \gamma\gamma)_{ZB}}{\Gamma(H \to \gamma\gamma)_{SM}} = \left|1 + \delta R(m_h, \lambda_{hH}) + 4\,\delta R(m_k, \lambda_{kH})\right|^2 , \tag{29}$$

where we have defined $\delta R(m_x, \lambda_{xH})$ for the scalar x with mass m_x and coupling to the Higgs λ_{xH} as:

$$\delta R(m_x, \lambda_{xH}) \equiv \frac{\lambda_{xH}\, v^2}{2m_x^2} \frac{A_0(\tau_x)}{A_1(\tau_W) + \frac{4}{3} A_{1/2}(\tau_t)}\,, \tag{30}$$

with $\tau_i \equiv \frac{4m_i^2}{m_H^2}$ and the loop functions $A_i(x)$ $(i = 0, 1/2, 1)$ are defined in Appendix B. Notice that the dominant W contribution is $A_1(\tau_W) = -8.32$ for a Higgs mass of 125 GeV, while $A_0(\tau_{h,k}) > 0$, therefore in order to obtain a constructive interference we need to consider negative couplings $\lambda_{hH}, \lambda_{kH}$.

As discussed in sec. II E, stability of the potential imposes that $2\sqrt{\lambda_H \lambda_x} + \lambda_{xH} > 0$, for $x = h, k$. Since $M_H \sim 125$ GeV fixes the value of the Higgs self-coupling to $\lambda_H \sim 0.13$, it is immediately apparent that large and negative λ_{xH} couplings are going to be in conflict with stability of the potential, unless we push λ_x close to the naive perturbative limit $(\lambda_x < 4\pi)$,

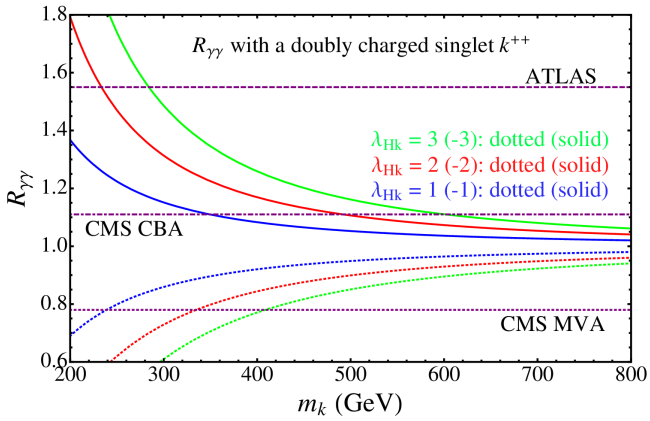

Figure 3: $R_{\gamma\gamma}$ in the presence of a doubly charged particle. Both an enhancement (as seen by ATLAS [44]) or a suppression (as seen by CMS [45]), can be accommodated. For the same masses and couplings, the singly-charged produces a smaller enhancement/suppression than the doubly-charged, due to its smaller charge.

for which $-3 \lesssim \lambda_{hH}, \lambda_{kH}$. Notice that this fact is not a special feature of the ZB model, but a generic problem of any scenario in which the enhancement of the Higgs diphoton decay rate is due to a virtual charged scalar.

We can consider three different cases:

- If $m_h \ll m_k$,
$$R^h_{\gamma\gamma} \approx |1 + \delta R(m_h, \lambda_{hH})|^2 \ ; \tag{31}$$
- If $m_k \ll m_h$,
$$R^k_{\gamma\gamma} \approx |1 + 4\delta R(m_k, \lambda_{kH})|^2 \ ; \tag{32}$$
- If $m_h \approx m_k \equiv m_S$, with
$$R^S_{\gamma\gamma} \approx |1 + \delta R(m_S, \lambda_{hH}) + 4\,\delta R(m_S, \lambda_{kH})|^2 \ . \tag{33}$$

For the same masses and couplings of both singlets, the doubly charged produces a larger enhancement/suppression than the singly-charged, due to its greater charge.

The largest enhancement can happen when both charged scalars are about the same mass and these masses are low enough. We show in fig. 3 the prediction of the ratio $R_{\gamma\gamma}$ when the doubly charged scalar k dominates, for different values of the coupling with the Higgs,

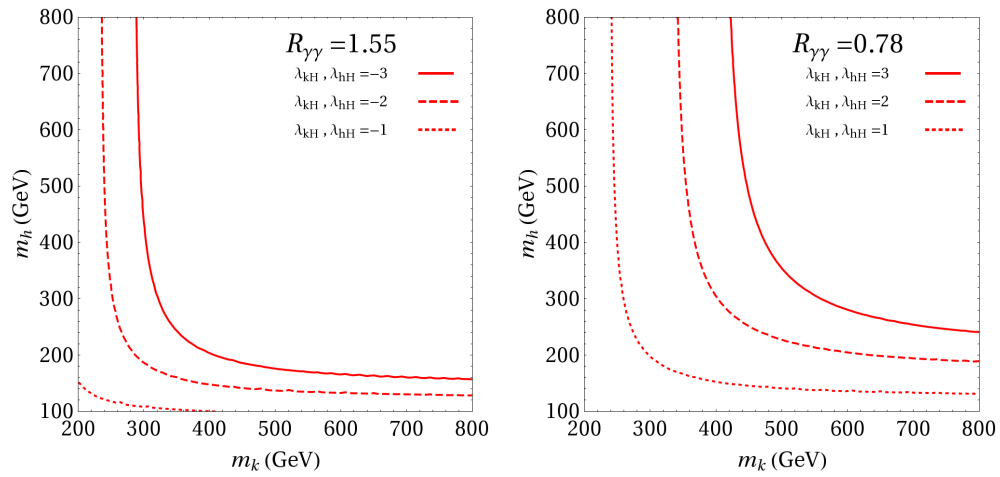

Figure 4: Contour of $R_{\gamma\gamma} = 1.55$ (left) [44] and $R_{\gamma\gamma} = 0.78$ (right) [45] in the presence of a singly charged and doubly charged particle with the same couplings.

λ_{kH}. Both an enhancement (as seen by ATLAS [44]) or a suppression (as seen by CMS [45]), can be accommodated. In fact, deviations from the SM value are expected, i.e., $R_{\gamma\gamma} \neq 1$, in particular for below the TeV scale singlets and sizeable scalar couplings. Of course, even for light singlets it is possible that $R_{\gamma\gamma} \approx 1$, either because the relevant scalar couplings are tiny or due to a cancellation between the contributions of the singly charged and the doubly charged scalars.

In principle, the enhancement $R_{\gamma\gamma}$ induced by a singly charged scalar h of similar mass and coupling to the Higgs $\lambda_{hH} \sim \lambda_{kH}$ is smaller; however since the lower limit on m_h from LEP II direct searches is weaker $m_h > 100$ GeV, as discussed in the previous section, and the largest contribution occurs for lower masses, the resulting values of $R_{\gamma\gamma}$ for the allowed range of m_h are comparable to the doubly charged case.

We show in fig. 4 the contours of $R_{\gamma\gamma} = 1.55$ (0.78), motivated by the experimental results of ATLAS and CMS [44, 45], in the plane of the singly and doubly charged masses, for various negative (positive) couplings. In summary, to obtain $R_{\gamma\gamma} \sim 1.5$ we need $m_h \lesssim 200\,\text{GeV}$ and/or $m_k \lesssim 300\,\text{GeV}$. As it will be shown in the numerical analysis section, these scalar masses are in tension with describing neutrino oscillation data and being compatible with current low-energy bounds in the ZB model if naturality is required at the level of $\kappa = 1$, especially for the NH spectrum. Moreover, the large negative values of the couplings

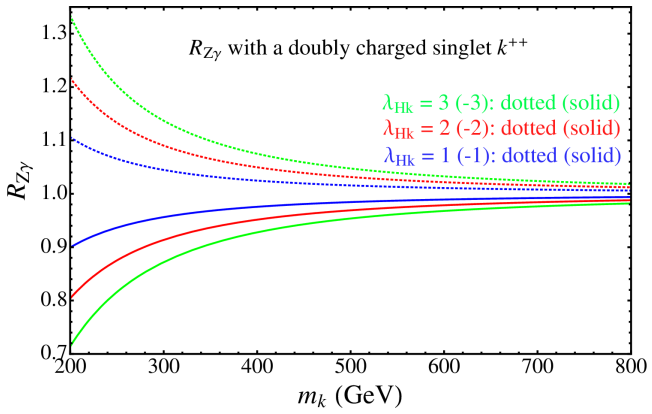

Figure 5: $R_{\gamma Z}$ in the presence of a doubly charged particle. As can be seen, $H \to Z\gamma$ is anticorrelated with respect to $H \to \gamma\gamma$.

$\lambda_{xH} \sim -2$ required to obtain such enhancement also induce vacuum instability of the ZB scalar potential, unless the corresponding coupling λ_x is close to the perturbative limit, $\lambda_x \sim 8$.

There is a correlation between $H \to \gamma\gamma$ and $H \to Z\gamma$ [46, 49, 50]. The ratio of the $H \to Z\gamma$ decay rate in the ZB model with respect to the SM one is:

$$R_{Z\gamma} = \frac{\Gamma(H \to Z\gamma)_{ZB}}{\Gamma(H \to Z\gamma)_{SM}} = \left| 1 - g_{Zhh} \frac{\lambda_{hH}\, v^2}{m_h^2} \frac{A_0(\tau_h, \lambda_h)}{\mathcal{A}_{SM}^{Z\gamma}} - g_{Zkk} \frac{2\lambda_{kH}\, v^2}{m_k^2} \frac{A_0(\tau_k, \lambda_k)}{\mathcal{A}_{SM}^{Z\gamma}} , \right|^2 \tag{34}$$

where $\mathcal{A}_{SM}^{Z\gamma}$ is the SM $H \to Z\gamma$ decay amplitude,

$$\mathcal{A}_{SM}^{Z\gamma} = \cot\theta_W A_1(\tau_W, \lambda_W) + 6Q_t \frac{T_3^t - 2Q_t s_W^2}{s_W c_W} A_{1/2}(\tau_t, \lambda_t) \,, \tag{35}$$

with $\lambda_i \equiv \frac{4m_i^2}{m_Z^2}$, and the Z boson couplings to the new charged scalars are $g_{Zxx} = -Q_x \cot\theta_W$, $x = h, k$. The loop functions $A_i(x, y)$ $(i = 0, 1/2, 1)$ can be found in Appendix B.

In fact, to have an enhancement in the $H \to \gamma\gamma$ channel, we need negative couplings of the singlets with the Higgs, which in turn implies that the $H \to Z\gamma$ channel is reduced with respect to SM prediction, as can be seen in fig. 5.

IV. ANALYTICAL ESTIMATES

In this section we give some order of magnitude estimates of the free parameters in the ZB model, which complement and help to understand our full numerical analysis. In

particular, we want to estimate to which extent light charged scalar masses, for instance like those required to fit an enhanced Higgs diphoton decay rate or to have a chance of being discovered at the LHC, are consistent with neutrino oscillation data and low-energy constraints.

As discussed in sec. II, with respect to the SM the ZB model has 17 extra parameters relevant for neutrino masses (9 moduli and 5 phases from the Yukawa couplings f, g, and 3 mass parameters from the charged scalar sector, m_h, m_k and μ), plus 5 quartic couplings in the scalar potential. However, some of the free parameters can be traded by the measured neutrino masses and mixings, ensuring in this way that the experimental data is reproduced and reducing the number of free variables as follows.

Since $\det f = 0$, there is an eigenvector $\mathbf{a} = (f_{\mu\tau}, -f_{e\tau}, f_{e\mu})$ which corresponds to the zero eigenvalue, $f\mathbf{a} = 0$ [10]. Then, by exploiting the fact that $\mathbf{a}$ is also an eigenvector of $\mathcal{M}_\nu$, we have

$$D_\nu U^T \mathbf{a} = 0, \tag{36}$$

which leads to three equations, one of which is trivially satisfied because one element of D_ν is zero. The other two equations allow to write the ratios of Yukawa couplings f_{ij} in terms of the neutrino mixing angles and Dirac phase as follows:

$$\begin{aligned} \frac{f_{e\tau}}{f_{\mu\tau}} &= \tan\theta_{12}\frac{\cos\theta_{23}}{\cos\theta_{13}} + \tan\theta_{13}\sin\theta_{23}e^{-i\delta}\,, \\ \frac{f_{e\mu}}{f_{\mu\tau}} &= \tan\theta_{12}\frac{\sin\theta_{23}}{\cos\theta_{13}} - \tan\theta_{13}\cos\theta_{23}e^{-i\delta}\,, \end{aligned} \tag{37}$$

in the NH case, and

$$\begin{aligned} \frac{f_{e\tau}}{f_{\mu\tau}} &= -\frac{\sin\theta_{23}}{\tan\theta_{13}}e^{-i\delta}\,, \\ \frac{f_{e\mu}}{f_{\mu\tau}} &= \frac{\cos\theta_{23}}{\tan\theta_{13}}e^{-i\delta}\,, \end{aligned} \tag{38}$$

for IH spectrum. Therefore, we choose $f_{\mu\tau}$ as a free, real, parameter and obtain (complex) $f_{e\mu}$ and $f_{e\tau}$ from the above equations. Notice that the measured values, $s^2_{12} \sim 0.3$, $s^2_{23} \sim 0.4$ and $s^2_{13} \sim 0.02$ imply that, for NH, the first term on the right-hand side of eqs. (37) dominates and leads to $f_{e\mu} \sim f_{\mu\tau}/2 \sim f_{e\tau}$. Conversely, for IH it is clear that $f_{e\tau}/f_{e\mu} = -\tan\theta_{23} \sim -1$ and $|f_{e\mu}/f_{\mu\tau}| \sim |f_{e\tau}/f_{\mu\tau}| \sim 4$. Of course, to explain such fine-tuned relations of Yukawa couplings a complete theory of flavour would be needed, which is beyond the scope of this work.

Regarding the Yukawa couplings g, we keep $g_{ee}, g_{e\mu}$ and $g_{e\tau}$ as free complex parameters and fix the remaining ones $(g_{\mu\mu}, g_{\mu\tau}, g_{\tau\tau})$ by imposing the equality of the three elements m_{22}, m_{23} and m_{33} of the neutrino mass matrix $\mathcal{M}_\nu$, written in terms of the parameters of the ZB model in eq. (13), and in terms of the masses and mixings measured in neutrino oscillation experiments in eq. (14), i.e.,

$$m_{ij} = (U D_\nu U^T)_{ij} = \zeta f_{ia} \omega_{ab} f_{jb}, \tag{39}$$

where we have defined $\omega_{ab} \equiv m_a g^*_{ab} m_b$, and $\zeta = \frac{\mu}{48\pi^2 M^2} \tilde{I}(r)$, being r the ratio of the scalar masses, $r \equiv m_k^2/m_h^2$.

Because of the hierarchy among the charged lepton masses, $m_e \ll m_\mu, m_\tau$, it is natural to assume that $\omega_{ee}, \omega_{e\mu}, \omega_{e\tau} \ll \omega_{\mu\mu}, \omega_{\mu\tau}, \omega_{\tau\tau}$. Within the approximation $\omega_{ea} = 0$, the equation (39) for neutrino masses is simplified, and we can easily estimate the ranges of parameters consistent with neutrino oscillation data. Thus in this section we neglect them, although we keep all ω_{ab} in the full numerical analysis[6] We then have

$$m_{22} \simeq \zeta f_{\mu\tau}^2 \omega_{\tau\tau}, \;\; m_{23} \simeq -\zeta f_{\mu\tau}^2 \omega_{\mu\tau}, \;\; m_{33} \simeq \zeta f_{\mu\tau}^2 \omega_{\mu\mu}. \tag{40}$$

From the large atmospheric angle we expect

$$|\omega_{\tau\tau}| \simeq |\omega_{\mu\tau}| \simeq |\omega_{\mu\mu}|, \tag{41}$$

which leads to a definite hierarchy among the corresponding g_{ab} couplings:

$$g_{\tau\tau} : g_{\mu\tau} : g_{\mu\mu} \sim m_\mu^2/m_\tau^2 : m_\mu/m_\tau : 1. \tag{42}$$

It is now convenient to write the mass matrix elements m_{ij} in terms of the neutrino masses and mixings. In the normal hierarchy case this gives

$$\begin{aligned}
\zeta f_{\mu\tau}^2 \omega_{\tau\tau} &\simeq m_3 c_{13}^2 s_{23}^2 + m_2 e^{i\phi} (c_{12} c_{23} - e^{i\delta} s_{12} s_{13} s_{23})^2 \,, \\
\zeta f_{\mu\tau}^2 \omega_{\mu\tau} &\simeq -m_3 c_{13}^2 c_{23} s_{23} + m_2 e^{i\phi} (c_{12} s_{23} + e^{i\delta} c_{23} s_{12} s_{13})(c_{12} c_{23} - e^{i\delta} s_{12} s_{13} s_{23}) \,, \\
\zeta f_{\mu\tau}^2 \omega_{\mu\mu} &\simeq m_3 c_{13}^2 c_{23}^2 + m_2 e^{i\phi} (c_{12} s_{23} + e^{i\delta} c_{23} s_{12} s_{13})^2 \,,
\end{aligned} \tag{43}$$

which for $m_3 \simeq 0.05$ eV and $m_2 \simeq 0.009$ eV, leads to

$$\zeta f_{\mu\tau}^2 |\omega_{ab}| \simeq 0.025 \text{ eV} \,, \qquad a, b = \mu, \tau, \tag{44}$$

[6] We find that, in general, this is a very good approximation.

in agreement with the expectations of eq. (41).

In the inverted hierarchy case, eqs. (40) read

$$\begin{aligned}
\zeta f_{\mu\tau}^2 \omega_{\tau\tau} &\simeq m_1(c_{23}s_{12} + e^{i\delta}c_{12}s_{13}s_{23})^2 + m_2 e^{i\phi}(c_{12}c_{23} - e^{i\delta}s_{12}s_{13}s_{23})^2\,, \\
\zeta f_{\mu\tau}^2 \omega_{\mu\tau} &\simeq m_1(s_{12}s_{23} - e^{i\delta}c_{12}c_{23}s_{13})(c_{23}s_{12} + e^{i\delta}c_{12}s_{13}s_{23}) \\
&+ m_2 e^{i\phi}(c_{12}s_{23} + e^{i\delta}c_{23}s_{12}s_{13})(c_{12}c_{23} - e^{i\delta}s_{12}s_{13}s_{23})\,, \\
\zeta f_{\mu\tau}^2 \omega_{\mu\mu} &\simeq m_1(s_{12}s_{23} - e^{i\delta}c_{12}c_{23}s_{13})^2 + m_2 e^{i\phi}(c_{12}s_{23} + e^{i\delta}c_{23}s_{12}s_{13})^2,
\end{aligned} \tag{45}$$

where $m_1 \simeq m_2 \simeq 0.05$ eV. It is important to notice that for $e^{i\phi} \sim e^{i\delta} \sim 1$ the matrix elements m_{ij} are of the same order as in the NH spectrum, i.e.,

$$\zeta f_{\mu\tau}^2 |\omega_{ab}| \simeq 0.025\,\text{eV}\,, \qquad a, b = \mu, \tau. \tag{46}$$

and therefore the hierarchy of couplings in eq. (42) is also obtained. However, in the IH case there is a strong cancellation for Majorana phases close to π, so we can obtain smaller values of ω_{ab}. In particular, for $\phi = \delta = \pi$ and the best fit values of the masses and mixing angles we find

$$\zeta f_{\mu\tau}^2 |\omega_{\mu\mu}| \simeq 0.003\,\text{eV}, \tag{47}$$

which allows for a smaller $g_{\mu\mu}$ and, as a consequence, a lighter m_k still consistent with the experimental limits. On the contrary, if $\phi \sim \pi$ and $\delta \sim 0$, $|\omega_{\tau\tau}|$ can be very small and therefore $g_{\tau\tau} \ll (m_\mu^2/m_\tau)^2\, g_{\mu\mu}$, although this cancellation has no phenomenological impact. Therefore, although in the following analytic approximations we assume the hierarchy of couplings in eq. (42), one has to keep in mind that a larger parameter space is expected to be allowed when $\phi \simeq \delta \simeq \pi$. Indeed we will confirm in the full numerical analysis of section V that this region is specially favoured for light m_k.

Now we can estimate the lowest scalar masses able to reproduce current neutrino data. Using the neutrino mass equation we can write[7]

$$\frac{m_{33}}{0.05\,\text{eV}} \simeq 500 |g_{\mu\mu}||f_{\mu\tau}|^2 \frac{\mu}{M}\frac{\text{TeV}}{M}\tilde{I}(r). \tag{48}$$

The upper bound on $\tau \to 3\mu$ decay implies that $|g_{\mu\mu}| \lesssim 0.4(m_k/\text{TeV})$, while the new MEG limits on $\mu \to e\gamma$ lead to $\epsilon|f_{\mu\tau}|^2 \lesssim 1.3 \cdot 10^{-3}(m_h/\text{TeV})^2$, where $\epsilon \equiv |f_{e\tau}/f_{\mu\tau}| \sim 1/2$ (4) for

[7] Notice that similar limits are derived from any of the 23 block elements of $\mathcal{M}_\nu$ when assuming the hierarchy of the g couplings given in eq. (42).

NH (IH). Substituting these constraints in eq. (48) we obtain

$$\frac{m_{33}}{0.05\,\text{eV}} \lesssim 0.26\,\frac{\mu\, m_k}{\epsilon\, M^2}\left(\frac{m_h}{\text{TeV}}\right)^2 \tilde{I}(r), \tag{49}$$

which can be translated into a lower bound on the scalar masses. Using that $m_{33} \sim 0.025$ eV from neutrino oscillation data, if $m_h > m_k$ then $\mu \leq \kappa\, m_k$ and $\tilde{I}(r) \sim 1$, so eq. (49) implies that

$$m_h > m_k \gtrsim \frac{1\,\text{TeV}}{\sqrt{\kappa}} \qquad \text{NH}, \tag{50}$$

$$m_h > m_k \gtrsim \frac{3\,\text{TeV}}{\sqrt{\kappa}} \qquad \text{IH}. \tag{51}$$

On the contrary, if $m_h < m_k$, we find

$$m_k > m_h \gtrsim \sqrt{\frac{m_k}{m_h\,\kappa\,\tilde{I}(r)}}\,1\,\text{TeV} \qquad \text{NH}, \tag{52}$$

$$m_k > m_h \gtrsim \sqrt{\frac{m_k}{m_h\,\kappa\,\tilde{I}(r)}}\,3\,\text{TeV} \qquad \text{IH}. \tag{53}$$

From the above results[8], we conclude that:

1. It is easier to reconcile an enhanced Higgs diphoton decay rate with neutrino oscillation data if the former is due to the doubly charged scalar loop contribution, since the lower bounds from neutrino masses are similar, while the BR($H \to \gamma\gamma$) can be accounted for by a heavier m_k. Moreover, if the enhancement is due to a light m_h, then m_k can not be very heavy, because otherwise neutrino masses are too small.

2. For a NH neutrino mass spectrum, it is possible to fit simultaneously neutrino oscillation data, lepton flavour violation constraints and an enhanced BR($H \to \gamma\gamma$) only if the trilinear coupling μ is large, namely $\kappa \gtrsim 4(10)$ for $\min(m_h, m_k) = 500$ (300) GeV, respectively.

3. In general, the case of IH neutrino masses is in conflict with an enhanced Higgs diphoton rate unless $\kappa \sim \mathcal{O}(30)$. However if we take into account the strong cancellations in $\omega_{\mu\mu}$ when $\phi \simeq \delta \simeq \pi$, and allow for a smaller $m_{33} \sim 0.003$ eV, it is also possible to fit all data with $\kappa \sim 4$.

[8] Our limits in the IH case differ from those in [11]. We traced this difference to the fact that in the estimates of [11] the perturbativity bound $|g_{\mu\mu}| < 1$ is imposed, but for low masses, $m_k < 2$ TeV, such bound is always satisfied, and the relevant bound is $|g_{\mu\mu}| \lesssim 0.4(m_k/\text{TeV})$, which depends on m_k and changes the scaling with ϵ, leading to a weaker lower bound on the charged scalar masses in our case. We thank Martin Hirsch for discussions about this point.

V. NUMERICAL ANALYSIS

In order to explore exhaustively the highly multi-dimensional parameter space of the ZB model, naive grid scans are completely inappropriate, the method of choice is resorting to Monte Carlo driven Markov Chains (MCMC) that incorporate all the current experimental information described in precedence. As parameters we will use $\{s^2_{ij}, \Delta_A, \Delta_S, \delta, \phi, f_{\mu\tau}, m_h, m_k, \mu, g_{ee}, g_{e\mu}, g_{e\tau}\}$, and we allow them to vary within the ranges showed in table IV.

Had we tried to use our MCMC to obtain a posteriori probability distribution functions with a canonical Bayesian meaning, the choice of priors would have had a significant role. Nevertheless, since our aim is to explore where in parameter space could the ZB model adequately reproduce experimental data without weighting in the available parameter space volume (that is, the "metric" in parameter space given by the priors), we will represent instead profiles of highest likelihood (equivalently profiles of minimal $\chi^2 \equiv -2\ln\mathcal{L}$ with $\mathcal{L}$ the likelihood) which, on the contrary, can be interpreted on a frequentist basis. This is not a choice that we make because of the merits or demerits of either statistical school: our goal remains to understand if and where the ZB "works well", i.e. could fit experimental data. The interpretation of the results/plots will be clear: they show the regions where the model is in agreement with data without regard to their size when the remaining information (parameters and observables) is marginalized over[9]. In this case, exploring the parameter space in a uniform, logarithmic or other manner, in some given parameter will not affect our results (only the computational efficiency required to reach them will be, of course, affected).

For the modelling of experimental data we typically resort to individual Gaussian likelihoods for measured quantities. Bounds are implemented through smooth likelihood functions that include, piecewise, a constant and a Gaussian-like behaviour. For the sake of clarity: if the experimental bound for a given observable $\mathcal{O}$ is $B^{\mathcal{O}}_{[90\%\mathrm{CL}]}$ at 90% CL (1.64σ in one dimension), the χ^2 contribution associated to the model prediction $\mathcal{O}_{\mathrm{th}}$ for this observ-

[9] Typically both approaches should converge to similar results when (experimental) information abounds; in a study such as this one, if they differ, rather than sticking to one or the other, from the physical point of view we would only conclude that the current experimental data is not yet sufficient to pin down or exclude the model.

able is

$$\chi^2(\mathcal{O}_{\rm th}) = \begin{cases} 0, \ \mathcal{O}_{\rm th} < B^{\mathcal{O}}_{[90\%\rm CL]}/1.64, \\ \left(\frac{1.64\mathcal{O}_{\rm th}}{B^{\mathcal{O}}_{[90\%\rm CL]}} - 1\right)^2 \left(\frac{1.64}{0.64}\right)^2, \ \mathcal{O}_{\rm th} \geq B^{\mathcal{O}}_{[90\%\rm CL]}/1.64. \end{cases}$$

In this way we avoid imposing sharp stepwise bounds or half-Gaussian with best value at zero that may penalize deviating from null predictions when this might not be supported by experimental evidence (in particular when the number of bounds included in the analysis is significant).

Simulations are done for both normal and inverted hierarchy. In each point of the parameter space we compute the full χ^2, including all measurements and bounds. In the plots we show the regions with the total $\Delta\chi^2 \leq 6$, which corresponds to 95% confidence levels with two variables.

Parameter	Allowed range
Δ_S	$(7.50 \pm 0.19) \times 10^{-5}\,\text{eV}^2$
Δ_A	$(2.45 \pm 0.07) \times 10^{-3}\text{eV}^2$
$\sin^2\theta_{12}$	0.30 ± 0.13
$\sin^2\theta_{23}$	$(0.42 \pm 0.04) \cup (0.60 \pm 0.04)$
$\sin^2\theta_{13}$	0.023 ± 0.002
δ, ϕ	$[0, 2\pi]$
$\arg(g_{ee}), \arg(g_{e\mu}), \arg(g_{e\tau})$	$[0, 2\pi]$
$f_{\mu\tau}, \lvert g_{ee}\rvert, \lvert g_{e\mu}\rvert, \lvert g_{e\tau}\rvert$	$[10^{-7}, 5]$
m_h	$[100, 2 \times 10^3]\,\text{GeV}$
m_k	$[200, 2 \times 10^3]\,\text{GeV}$
μ	$[1, 2\kappa \times 10^3]\,\text{GeV}$

Table IV: Allowed ranges for the parameter scan (Neutrino oscillation parameters are obtained from [51–53]).

To compare our results with the analysis presented a few years ago by some of us [12] some remarks are in order: first, here we have updated the experimental input on LFV and neutrino oscillation parameters, as well as LHC direct searches. The new limits, in particular on $\mu \to e\gamma$, tend to reduce the allowed regions but not dramatically. Especially important is the determination of $\sin\theta_{13}$: as shown in [12], already before its measurement the ZB

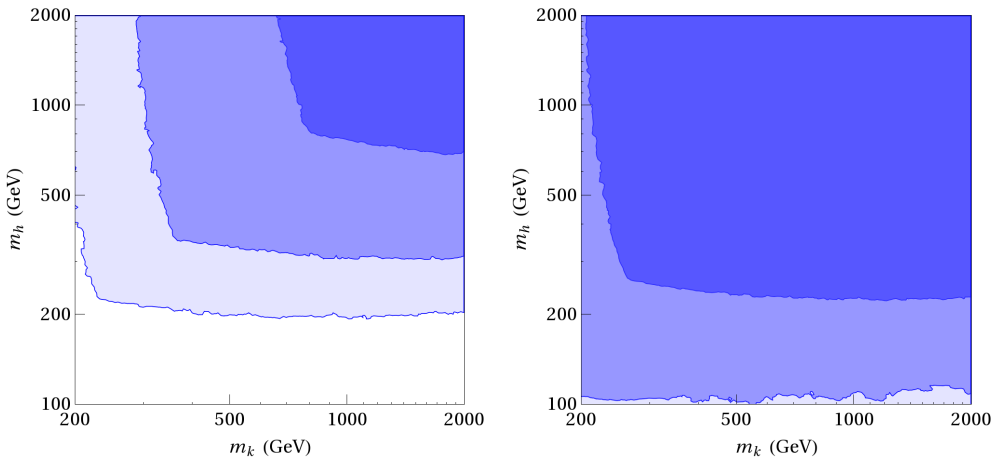

Figure 6: m_h vs m_k for NH (left) and IH (right) for different values of the perturbative parameter $\kappa = 1, 5, 4\pi$ (dark to light colours).

model predicted a large mixing angle θ_{13} in the case of IH spectrum, close to the previous experimental upper limit, while for NH any value of θ_{13} below the bound was allowed. In fact, a very small value of θ_{13} would have ruled out the IH possibility within the ZB model. Second, although the scanning of parameters is performed like in [12], we have chosen here to present results in terms of profiles of highest likelihood, which are insensitive to the volume of the parameter space and the priors used to scan it. This allows us to explore regions where parameters are fine tuned (after all, Yukawa couplings always require a certain degree of fine tuning). This is important since, as we have seen, the model is highly constrained at present and less conservative assumptions could exclude it before time, at least in the region of low masses. Moreover, we focus only on the region of masses with phenomenological interest ($m_{h,k} < 2$ TeV) precisely to explore better the region of low masses.

In fig. 6 we depict the points allowed by neutrino oscillation data and all low energy constraints in the plane (m_h, m_k) for the two mass orderings (NH and IH) and different values of the fine-tuning parameter in eq. (9) ($\kappa = 1$ darker, $\kappa = 5$ dark, $\kappa = 4\pi$ light). The results of the numerical analysis imply that in general the indirect lower bounds on m_h and m_k from neutrino oscillation data and low energy constraints are stronger than the current limits from direct searches, except when cancellations occur for $\delta, \phi \sim \pi$, especially in the IH case, and/or when naturality assumptions on μ are relaxed, allowing for $\kappa = 4\pi$. In table V we summarize the lower bounds on the scalar masses obtained for the three values

	NH			IH		
κ	1	5	4π	1	5	4π
m_h (GeV)	700 (1000)	300 (400)	200 (250)	220 ($>$ 2000)	100 (1000)	100 (650)
m_k (GeV)	700 (1100)	300 (450)	200 (250)	200 ($>$ 2000)	200 (1000)	200 (550)

Table V: Lower bounds for the scalar masses for NH and IH and the naturality constraints parametrized by the three values of κ. We present results for $\delta = \pi$ ($\delta = 0$) (see figs. 6 and 7).

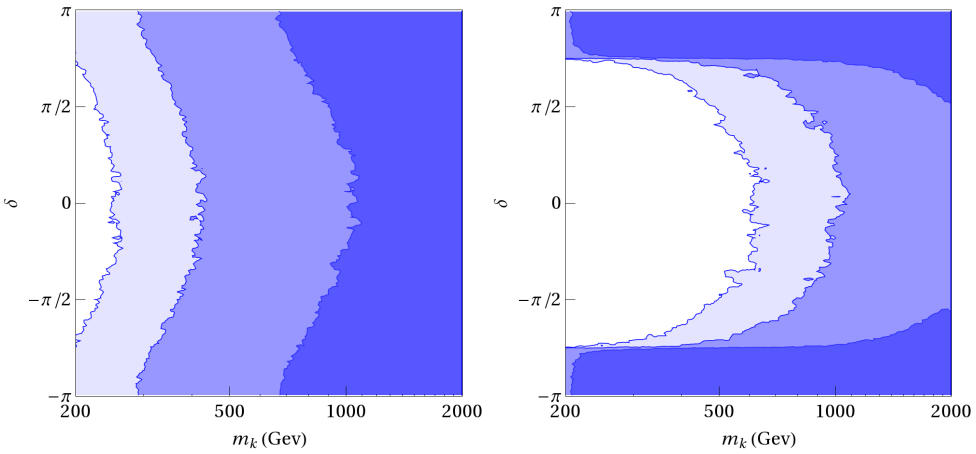

Figure 7: δ vs m_k in NH (left) and IH (right).

of the naturality parameter κ, and two illustrative values of the Dirac phase, $\delta = 0, \pi$. For $\delta \sim -\pi/2$, as might be suggested by a recent analysis [51], the bounds are slightly weaker than in the $\delta = 0$ case (see fig. 7).

The correlation between the CP phase δ of the neutrino mixing matrix and the scalar masses is illustrated in fig. 7, where we plot δ versus the doubly charged scalar mass, m_k.[10] Such correlation is especially relevant in the IH case, where scalar masses lower than ~ 1 TeV are only allowed if $\delta \sim \pi$. A similar correlation with the phase ϕ was already found in [12] for IH spectrum, so we do not show it here.

Regarding the singly charged scalar $h^\pm$, the width of its decay modes ($e\nu, \mu\nu, \tau\nu$) is fixed by the f_{ia} couplings to leptons (see for instance [11, 12] for the relevant formulae). Therefore,

[10] The correlation of δ with m_h is entirely analogous.

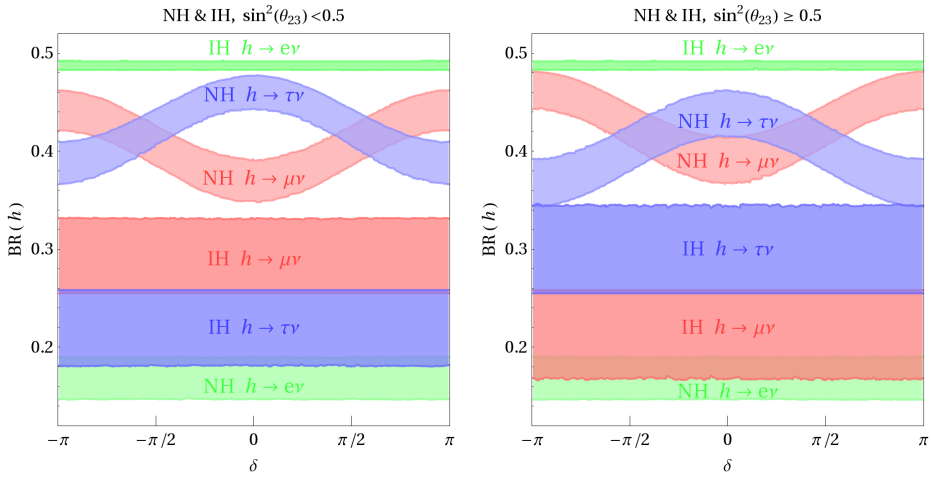

Figure 8: Branching ratios of the charged singlet h to $e\nu, \mu\nu, \tau\nu$ splitting the two currently allowed octants of θ_{23}, $\theta_{23} < 45°$ ($\theta_{23} > 45°$) left (right). One can see the dependence on δ for the NH spectrum in the $\mu\nu$ and $\tau\nu$ channels. The most significant change between octants is the interchange of the $\mu\nu$ and $\tau\nu$ for the IH case. The bands are 95% C.L. regions.

after the measurement of θ_{13}, present neutrino oscillation data determine completely the BRs of h from eqs. (37) and (38), up to a residual dependence on the CP phase δ in the case of NH spectrum. In this case, a very precise measurement of the branching ratios in the $\mu\nu$ or $\tau\nu$ channels (probably in a next generation collider) will predict the CP phase δ, and viceversa. We show the ranges attainable by the different BRs in fig. 8, as a function of δ, splitting the two currently allowed octants of θ_{23}. The most significant change between octants is the interchange of the $\mu\nu$ and $\tau\nu$ for the IH case. Clearly, the best option to discriminate between hierarchies is the $e\nu$ channel.

An important point of the ZB model is that the doubly charged scalar can decay to two singly charged scalars, which are difficult to detect at the LHC. However, in fig. 6 we see that for a NH neutrino mass spectrum $m_h > 200$ GeV, and the channel $k \to hh$ is closed for $m_k < 400$ GeV. Therefore, present bounds on m_k from dilepton searches at LHC discussed in II D apply. For the IH case, the $k \to hh$ channel is always open and can be dominant, unless $\kappa = 1$, for which we obtain that it is closed in the region $m_k < 440$ GeV. Thus in general current direct bounds from LHC are weaker.

Let us now turn to the g_{ab} couplings. We find always $g_{\tau\tau} \ll g_{\mu\tau}$, both for the NH

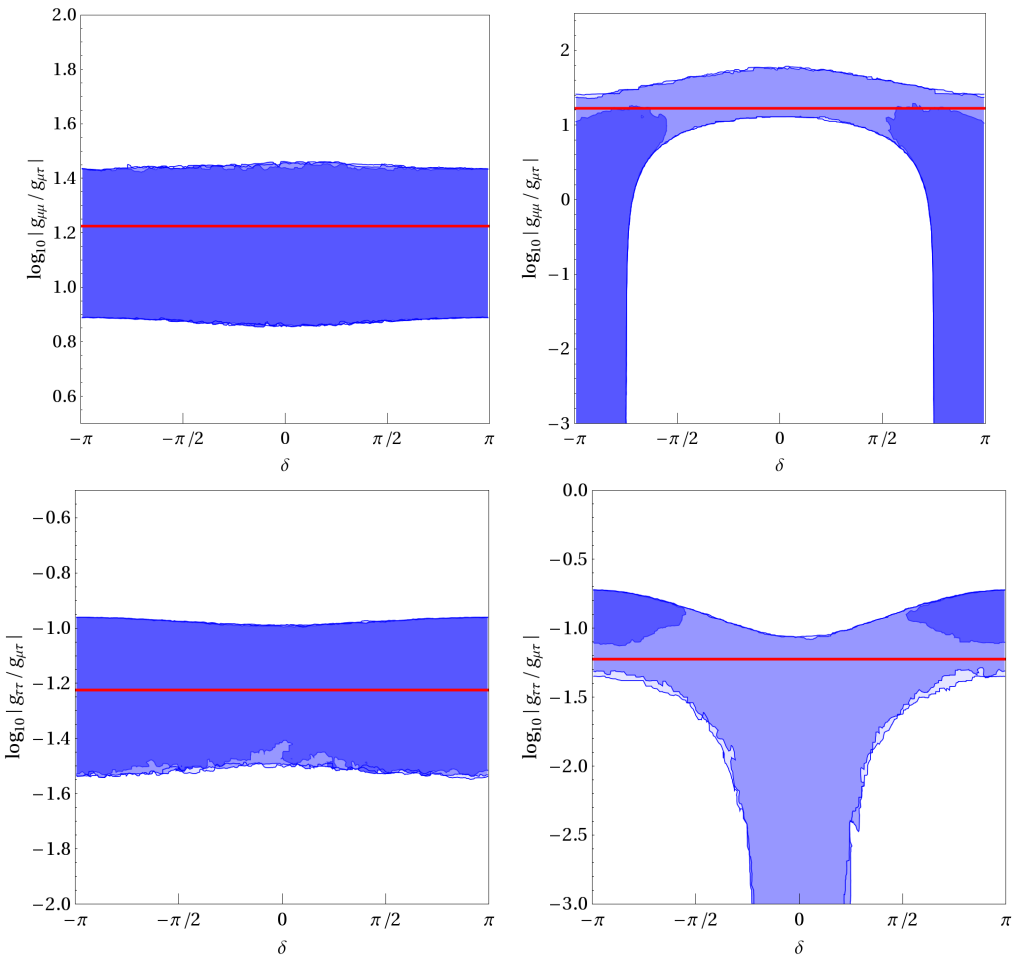

Figure 9: $\log|g_{\mu\mu}/g_{\mu\tau}|$ and $\log|g_{\tau\tau}/g_{\mu\tau}|$ vs δ for NH (left) and IH (right). The horizontal red lines represent the naive approximation in eq. (42).

and IH cases, in agreement with the analytic estimates in eq. (42); however the expected ratio $g_{\mu\mu}/g_{\mu\tau} \sim m_\tau/m_\mu$ is only fulfilled for the NH spectrum, since in the IH case large cancellations when the phases of the PMNS matrix U are $\delta \sim \phi \sim \pi$ lead to smaller $g_{\mu\mu} \ll g_{\mu\tau}$. This can be seen in fig. 9, where we show the ratios $g_{\tau\tau}/g_{\mu\tau}$ and $g_{\mu\mu}/g_{\mu\tau}$ obtained in the numerical simulation as a function of δ, together with the expectation based on the analytic approximations, which is just a constant fixed by the charged lepton masses

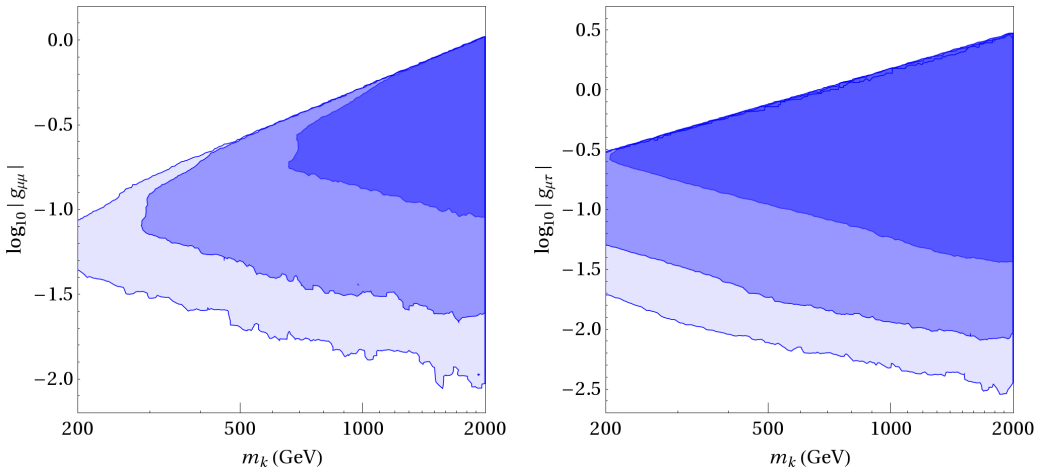

Figure 10: $\log|g_{\mu\mu}|$ vs m_k for NH (left) and $\log|g_{\mu\tau}|$ vs m_k for IH (right).

(red horizontal line)[11].

To set the absolute scale of the couplings we present in fig. 10 the value of the largest couplings against m_k, namely $g_{\mu\mu}$ in the NH case, and $g_{\mu\tau}$ in the IH case. We see that in both cases the couplings are always in the range from 10^{-2} to 1 and therefore they tend to dominate the decays of the k^{++}.

Regarding the couplings g_{ea}, which are not determined by the neutrino mass matrix, bounds from LFV charged lepton decays strongly constrain $g_{e\tau}$ and $g_{e\mu}$ to be less than $\mathcal{O}(0.01)$, while g_{ee} can be larger, $\mathcal{O}(1)$. The constraint on $|g_{ee}g_{e\mu}|$ from $\mu \to 3e$ implies that $|g_{ee}g_{e\mu}| < 2.3 \times 10^{-5}\,(m_k/\text{TeV})^2$ and it is illustrated in fig. 11.

Since the widths of the $k^{\pm\pm}$ leptonic decay modes are directly related to these couplings, from the above results we can readily infer the corresponding BRs. We find that the probability of $k \to e\mu, e\tau, \tau\tau$ is always negligible (even in the IH case, $g_{e\mu}$ can be at most 0.1 and only when $\delta \sim \pi$). For $m_k \lesssim 400$ GeV, and NH neutrino spectrum, $\text{BR}(k \to ee) + \text{BR}(k \to \mu\mu) \sim 1$, since the $k \to hh$ decay channel is closed; therefore $k^{\pm\pm}$ can not evade current LHC bounds on doubly-charged scalar searches and the limit $m_k > 310$ GeV applies (400 GeV if no signal is found at 8 TeV with 20 fb^{-1} [36]). In the same m_k range, for IH

[11] In the NH case there can also be cancellations with the $g_{e\tau}$ terms, which have been neglected in eq. (43), that would allow much smaller values of $g_{\tau\tau}$ and $g_{\mu\tau}$, but those only occur for $\kappa = 4\pi$ and in a tiny region of the parameter space.

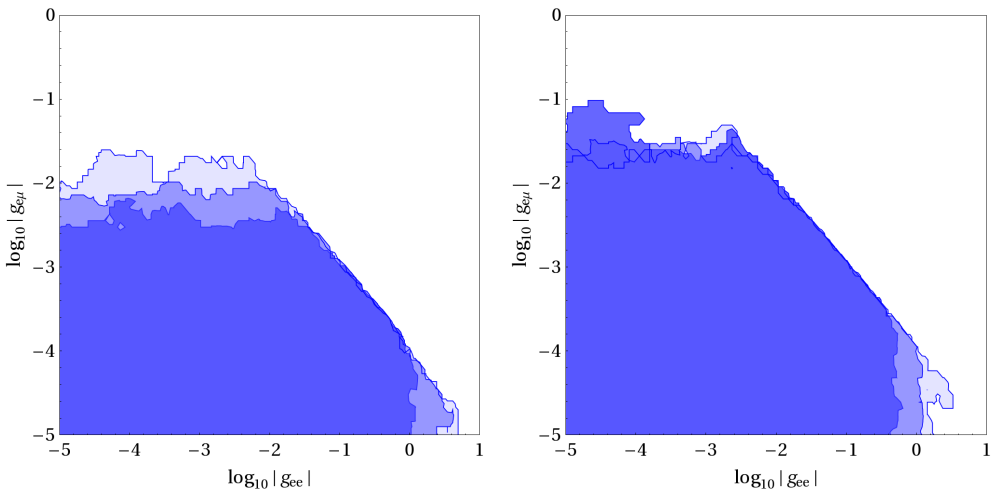

Figure 11: $\log|g_{e\mu}|$ vs $\log|g_{ee}|$ for NH (left) and IH (right).

neutrino spectrum the BR($k \to \mu\tau$) can also be significant and the channel $k \to hh$ is open (unless $\kappa = 1$, for which it is only open for $m_k > 440$ GeV), thus the present bound is weaker.

When the upcoming LHC 13-14 TeV data is available, it is important to take into account that the decay channel $k \to hh$ is open for $m_k \gtrsim 400$ GeV, and can be dominant, so in this mass range limits on doubly-charged scalars from dilepton searches will not apply to the ZB model. On the contrary, if a doubly charged scalar were detected at LHC in any mass range, neutrino oscillation data and low energy constraints are powerful enough to falsify the ZB model to a large extent. For instance, we know that BR($k \to e\mu, e\tau, \tau\tau$) are negligible for any neutrino mass spectrum, while a sizeable BR($k \to \mu\tau$) is only compatible with an IH spectrum.

VI. CONCLUSIONS

We have analyzed the ZB model in the light of recent data: the measured neutrino mixing angle θ_{13}, limits from the rare decay $\mu \to e\gamma$ and LHC results. Although the model contains many free parameters, neutrino oscillation data and low energy constraints are powerful enough to rule out sizeable regions of the parameter space. A large source of uncertainty comes from the mass scale of the new physics, which is unknown. Since we are interested

on possible signatures at the LHC, we present results for the masses of the extra scalar fields below 2 TeV. Previous analyses [11, 12] have shown that larger mass scales are always allowed, given the absence of significant deviations from the SM besides neutrino masses.

Even within this reduced scenario, there is still a free mass parameter, the trilinear coupling between the charged scalars, μ, which remains mainly unconstrained. Naturality arguments together with perturbativity and vacuum stability bounds, indicate that μ can not be much larger than the physical scalar masses, m_k, m_h, but it is not possible to determine a precise theoretical limit. Because the neutrino masses depend linearly on the parameter μ, the ability of the model to accommodate all present data is quite sensitive to the upper limit allowed for it, so we have considered three limiting values, $\mu < \kappa \min(m_k, m_h)$, with $\kappa = 1, 5, 4\pi$. Within the above ranges for the mass parameters of the ZB model, we have performed an exhaustive numerical analysis using Monte Carlo Markov Chains (MCMC), incorporating all the current experimental information available, both for NH and IH neutrino masses. The results of the analysis are presented in sec. V and summarized in figs. 6 – 11.

We have addressed the possibility that the slight excess in the Higgs diphoton decay observed by the ATLAS collaboration is due to virtual loops of the extra charged scalars of the ZB model, $h^{\pm}$ and $k^{\pm\pm}$. Note that in the Zee-Babu model, as the new particles are singlets, there is a negative correlation between $H \to \gamma\gamma$ and $H \to \gamma Z$. Although a similar study has been performed in [22], it was limited to the scalar sector parameters of the model, and neutrino data, which we find crucial to determine the allowed charged scalar masses, was not included in the analysis. In agreement with [22], we find that in order to accommodate an enhanced $H \to \gamma\gamma$ decay rate, large and negative $\lambda_{hH}, \lambda_{kH}$ couplings are needed, together with light scalar masses $m_h < 200$ GeV, $m_k < 300$ GeV. Such couplings are in conflict with the stability of the potential, unless the self-couplings $\lambda_{h,k}$ are pushed close to the naive perturbative limit, $\sim 4\pi$. As a consequence, even if vacuum stability and perturbativity constraints are satisfied at the electroweak scale, RGE running leads to non-perturbative couplings at scales not far from the electroweak scale, as shown in fig. 2.

When neutrino data and low energy constraints are taken into account, we still find regions of the parameter space in which such enhancement is compatible with all current experimental data; in particular, it seems easier if the enhancement is due to the doubly-charged scalar loop contribution. As can be seen in fig. 6, in the NH case, the trilinear

coupling μ should be near its upper limit, while in the IH case lower masses can be achieved in the region $\delta \sim \phi \sim \pi$ due to cancellations.

Regarding LHC bounds on the doubly-charged scalar mass, they are largely dependent on the BRs of the $k^{\pm\pm}$ decay modes, namely same sign leptons $\ell_a^\pm \ell_b^\pm$ and $h^\pm h^\pm$. The leptonic decay widths are controlled by the g_{ab} couplings to the right-handed leptons, which are in principle unknown. By imposing that the measured neutrino mass matrix is reproduced, within the approximation $m_e = 0$ one obtains analytically that $g_{\tau\tau} : g_{\mu\tau} : g_{\mu\mu} \sim m_\mu^2/m_\tau^2 : m_\mu/m_\tau : 1$, while there is no information on the g_{ea} couplings. Our numerical analysis confirms the above ratio of couplings in the case of NH, but for the IH spectrum there can be large cancellations if the PMNS matrix phases δ, ϕ are close to π, leading to $g_{\tau\tau} \ll g_{\mu\tau} \sim g_{\mu\mu}$. In both cases, $g_{e\mu}, g_{e\tau} \lesssim 0.1$.

Moreover, in NH, if $m_k < 400$ GeV for $\kappa = 4\pi$ ($m_k < 600$ GeV if $\kappa = 5$), $m_h < m_k/2$ is ruled out, therefore the decay channel $k \to hh$ is kinematically closed and the LHC bounds from doubly-charged scalar searches can not be evaded. In IH, however, for $\delta \sim \phi \sim \pi$ the $k \to hh$ channel is open unless $\kappa = 1$, while if δ is very different from π, indirect bounds on m_k set a much stronger constraint than direct LHC searches.

As a consequence, if the light neutrino spectrum is NH, k decays mainly to $ee, \mu\mu$, and the current bound from LHC is $m_k > 310$ GeV, while if the spectrum is IH, k may also decay to $\mu\tau$ and hh, so the present bound is weaker, about 200 GeV. Were a doubly-charged boson discovered at LHC, the measurement of its leptonic BRs could rule out the ZB model, or predict a definite neutrino mass spectrum. Conversely, if a CP phase δ is measured in future neutrino oscillation experiments to be quite different from π together with an IH spectrum, the mass of the charged scalars of the ZB model will be pushed up well outside the LHC reach.

Note: During the final stages of this work we became aware of [54], where an analysis of the Zee-Babu model was performed. Our bounds on the scalar masses are comparable to theirs taking into account the slightly different procedures, in particular that they fix the neutrino oscillation parameters to their best fit values and we allow them to vary in their two sigma range. While in our work we focus on prospects for the LHC, in [54] the possibility of detecting the doubly charged singlet in a future linear collider is studied.

Acknowledgments

We are thankful to the authors of [54] for sharing with us their work and for useful discussions. We also thank Marcela Carena, Ian Low and Carlos Wagner for discussions. This work has been partially supported by the European Union FP7 ITN INVISIBLES (Marie Curie Actions, PITN- GA-2011- 289442), by the Spanish MINECO under grants FPA2011-23897, FPA2011-29678, Consolider-Ingenio PAU (CSD2007-00060) and CPAN (CSD2007- 00042) and by Generalitat Valenciana grants PROMETEO/2009/116 and PROMETEO/2009/128. M.N. is supported by a postdoctoral fellowship of project CERN/FP/123580/2011 at CFTP (PEst-OE/FIS/UI0777/2013), projects granted by *Fundação para a Ciència e a Tecnologia* (Portugal), and partially funded by POCTI (FEDER). J.H.-G. is supported by the MINECO under the FPU program. He would also like to acknowledge NORDITA for their hospitality during the revision of the final version of this work, carried out during the "News in Neutrino Physics" program.

Appendix A: RGES IN THE ZB MODEL

$$
\begin{aligned}
16\pi^2\beta_H &= \frac{3}{8}\left[(g^2+g'^2)^2+2g^4\right]-(3g'^2+9g^2)\lambda_H+24\lambda_H^2+\lambda_{hH}^2+\lambda_{kH}^2-6y_t^4+12\lambda_H y_t^2\\
16\pi^2\beta_h &= 6g'^4-12g'^2\lambda_h+20\lambda_h^2+2\lambda_{hH}^2+\lambda_{hk}^2\\
16\pi^2\beta_k &= 96g'^4-48g'^2\lambda_k+20\lambda_k^2+2\lambda_{kH}^2+\lambda_{hk}^2\\
16\pi^2\beta_{hH} &= 3g'^4-(\frac{15}{2}g'^2+\frac{9}{2}g^2)\lambda_{hH}+12\lambda_H\lambda_{hH}+8\lambda_h\lambda_{hH}+2\lambda_{kH}\lambda_{hk}+4\lambda_{hH}^2+6\lambda_{hH}y_t^2\\
16\pi^2\beta_{kH} &= 12g'^4-(\frac{51}{2}g'^2+\frac{9}{2}g^2)\lambda_{kH}+12\lambda_H\lambda_{kH}+8\lambda_k\lambda_{kH}+2\lambda_{hH}\lambda_{hk}+4\lambda_{kH}^2+6\lambda_{kH}y_t^2\\
16\pi^2\beta_{hk} &= 48g'^4-30g'^2\lambda_{hk}+4\lambda_{kH}\lambda_{hH}+8\lambda_h\lambda_{hk}+8\lambda_k\lambda_{hk}+4\lambda_{hk}^2\ ,
\end{aligned}
\tag{A1}
$$

$$
\begin{aligned}
16\pi^2\beta_{g'} &= \frac{5}{3}\left(\frac{41}{10}+1\right)g'^3\\
16\pi^2\beta_g &= -\frac{19}{6}g^3\\
16\pi^2\beta_{g_3} &= -7g_3^3\ ,
\end{aligned}
\tag{A2}
$$

$$
16\pi^2\beta_t = y_t\left\{\frac{9}{2}y_t^2-\left(\frac{17}{12}g'^2+\frac{9}{4}g^2+8g_3^2\right)\right\}\ . \tag{A3}
$$

Here g_3, g, g' are the SM $SU(3)_C$, $SU(2)_L$ and $U(1)_Y$ gauge couplings, respectively, and we have neglected all the Yukawa couplings but the top quark Yukawa, y_t. We have also neglected the f_{ab}, g_{ab} couplings because for the range of singlet scalar masses that we consider (≤ 2 TeV), they are are severely constrained by LFV and are much smaller than 1 except for some corners of the parameter space where some of them could be order one. For the analysis of the vacuum stability of the scalar potential f_{ab}, g_{ab} are subdominant, specially in the region of large and negative mixed scalar couplings required to accommodate the diphoton excess in Higgs decays. For smaller mixed scalar couplings, however, a more detailed analysis including all Yukawa couplings and taking also into account leading two-loop effects (as well as top quark mass uncertainties for the Higgs quartic coupling) should be carried out, which is beyond the scope of this work.

Appendix B: LOOP FUNCTIONS FOR $H \to \gamma\gamma$ AND $H \to Z\gamma$

- Functions relevant for $H \to \gamma\gamma$:

$$A_0(x) = -x + x^2 f\left(\frac{1}{x}\right) \tag{B1}$$

$$A_{1/2}(x) = 2x + 2x(1-x) f\left(\frac{1}{x}\right) \tag{B2}$$

$$A_1(x) = -2 - 3x - 3x(2-x) f\left(\frac{1}{x}\right) \tag{B3}$$

- Functions relevant for $H \to Z\gamma$:

$$A_0(x,y) = I_1(x,y) \tag{B4}$$

$$A_{1/2}(x,y) = I_1(x,y) - I_2(x,y) \tag{B5}$$

$$A_1(x,y) = 4(3 - \tan^2\theta_w) I_2(x,y) + \left[(1 + 2x^{-1})\tan^2\theta_w - (5 + 2x^{-1})\right] I_1(x,y) \tag{B6}$$

where

$$I_1(x,y) = \frac{xy}{2(x-y)} + \frac{x^2y^2}{2(x-y)^2}\left[f(x^{-1}) - f(y^{-1})\right] + \frac{x^2y}{(x-y)^2}\left[g(x^{-1}) - g(y^{-1})\right] \tag{B7}$$

$$I_2(x,y) = -\frac{xy}{2(x-y)}\left[f(x^{-1}) - f(y^{-1})\right] \tag{B8}$$

and, for a Higgs mass below the kinematic threshold of the loop particle, $m_H < 2m_i$,

$$f(x) = \arcsin^2\sqrt{x}\,, \tag{B9}$$

$$g(x) = \sqrt{x^{-1} - 1}\arcsin\sqrt{x}\,. \tag{B10}$$

[1] R. Mohapatra, S. Antusch, K. Babu, G. Barenboim, M.-C. Chen, *et al.*, *Theory of neutrinos: A White paper*, *Rept.Prog.Phys.* **70** (2007) 1757–1867, [arXiv:hep-ph/0510213] [InSPIRE].

[2] M. Gonzalez-Garcia and M. Maltoni, *Phenomenology with Massive Neutrinos*, *Phys.Rept.* **460** (2008) 1–129, [arXiv:0704.1800] [InSPIRE].

[3] **Particle Data Group**, J. Beringer *et al.*, *Review of Particle Physics (RPP)*, *Phys.Rev.* **D86** (2012) 010001 [InSPIRE].

[4] **Intensity Frontier Neutrino Working Group**, A. de Gouvea *et al.*, *Neutrinos*, [arXiv:1310.4340] [InSPIRE].

[5] A. Zee, *Quantum Numbers of Majorana Neutrino Masses*, *Nucl.Phys.* **B264** (1986) 99 [InSPIRE].

[6] K. Babu, *Model of 'Calculable' Majorana Neutrino Masses*, *Phys.Lett.* **B203** (1988) 132 [InSPIRE].

[7] T. Cheng and L.-F. Li, *Neutrino Masses, Mixings and Oscillations in SU(2) x U(1) Models of Electroweak Interactions*, *Phys.Rev.* **D22** (1980) 2860 [InSPIRE].

[8] F. del Aguila, A. Aparici, S. Bhattacharya, A. Santamaria, and J. Wudka, *A realistic model of neutrino masses with a large neutrinoless double beta decay rate*, *JHEP* **1205** (2012) 133, [arXiv:1111.6960] [InSPIRE].

[9] F. del Aguila, A. Aparici, S. Bhattacharya, A. Santamaria, and J. Wudka, *Neutrinoless double β decay with small neutrino masses*, *PoS* **Corfu2012** (2013) 028, [arXiv:1305.4900] [InSPIRE].

[10] K. Babu and C. Macesanu, *Two loop neutrino mass generation and its experimental consequences*, *Phys.Rev.* **D67** (2003) 073010, [arXiv:hep-ph/0212058] [InSPIRE].

[11] D. Aristizabal Sierra and M. Hirsch, *Experimental tests for the Babu-Zee two-loop model of Majorana neutrino masses*, *JHEP* **0612** (2006) 052, [arXiv:hep-ph/0609307] [InSPIRE].

[12] M. Nebot, J. F. Oliver, D. Palao, and A. Santamaria, *Prospects for the Zee-Babu Model at the CERN LHC and low energy experiments*, *Phys.Rev.* **D77** (2008) 093013, [arXiv:0711.0483] [InSPIRE].

[13] T. Ohlsson, T. Schwetz, and H. Zhang, *Non-standard neutrino interactions in the Zee-Babu model*, *Phys.Lett.* **B681** (2009) 269–275, [arXiv:0909.0455] [InSPIRE].

[14] **DOUBLE-CHOOZ Collaboration**, Y. Abe *et al.*, *Indication for the disappearance of reactor electron antineutrinos in the Double Chooz experiment*, *Phys.Rev.Lett.* **108** (2012) 131801, [arXiv:1112.6353] [InSPIRE].

[15] **DAYA-BAY Collaboration**, F. An *et al.*, *Observation of electron-antineutrino disappearance at Daya Bay*, *Phys.Rev.Lett.* **108** (2012) 171803, [arXiv:1203.1669] [InSPIRE].

[16] **RENO collaboration**, J. Ahn *et al.*, *Observation of Reactor Electron Antineutrino Disappearance in the RENO Experiment*, *Phys.Rev.Lett.* **108** (2012) 191802, [arXiv:1204.0626] [InSPIRE].

[17] **MEG Collaboration**, J. Adam *et al.*, *New constraint on the existence of the $\mu \to e\gamma$ decay*, *Phys.Rev.Lett.* **110** (2013) 201801, [arXiv:1303.0754] [InSPIRE].

[18] **ATLAS Collaboration**, G. Aad *et al.*, *Search for doubly-charged Higgs bosons in like-sign dilepton final states at $\sqrt{s} = 7$ TeV with the ATLAS detector*, *Eur.Phys.J.* **C72** (2012) 2244, [arXiv:1210.5070] [InSPIRE].

[19] **CMS Collaboration**, S. Chatrchyan *et al.*, *A search for a doubly-charged Higgs boson in pp collisions at $\sqrt{s} = 7$ TeV*, *Eur.Phys.J.* **C72** (2012) 2189, [arXiv:1207.2666] [InSPIRE].

[20] **ATLAS Collaboration**, G. Aad *et al.*, *Observation of a new particle in the search for the Standard Model Higgs boson with the ATLAS detector at the LHC*, *Phys.Lett.* **B716** (2012) 1–29, [arXiv:1207.7214] [InSPIRE].

[21] **CMS Collaboration**, S. Chatrchyan *et al.*, *Observation of a new boson at a mass of 125 GeV with the CMS experiment at the LHC*, *Phys.Lett.* **B716** (2012) 30–61, [arXiv:1207.7235] [InSPIRE].

[22] W. Chao, J.-H. Zhang, and Y. Zhang, *Vacuum Stability and Higgs Diphoton Decay Rate in the Zee-Babu Model*, *JHEP* **1306** (2013) 039, [arXiv:1212.6272] [InSPIRE].

[23] D. Dicus and V. Mathur, *Upper bounds on the values of masses in unified gauge theories*, *Phys.Rev.* **D7** (1973) 3111–3114 [InSPIRE].

[24] B. W. Lee, C. Quigg, and H. Thacker, *Weak Interactions at Very High-Energies: The Role of the Higgs Boson Mass*, *Phys.Rev.* **D16** (1977) 1519 [InSPIRE].

[25] J. Frere, D. Jones, and S. Raby, *Fermion Masses and Induction of the Weak Scale by Supergravity*, *Nucl.Phys.* **B222** (1983) 11 [InSPIRE].

[26] L. Alvarez-Gaume, J. Polchinski, and M. B. Wise, *Minimal Low-Energy Supergravity*,

Nucl.Phys. **B221** (1983) 495 [InSPIRE].

[27] J. Casas and S. Dimopoulos, *Stability bounds on flavor violating trilinear soft terms in the MSSM*, *Phys.Lett.* **B387** (1996) 107–112, [arXiv:hep-ph/9606237] [InSPIRE].

[28] K. L. McDonald and B. McKellar, *Evaluating the two loop diagram responsible for neutrino mass in Babu's model*, [arXiv:hep-ph/0309270] [InSPIRE].

[29] A. Pich, *Precision Tau Physics*, [arXiv:1310.7922] [InSPIRE].

[30] M. Raidal and A. Santamaria, *Muon electron conversion in nuclei versus mu $\to e\gamma$: an effective field theory point of view*, *Phys.Lett.* **B421** (1998) 250–258, [arXiv:hep-ph/9710389] [InSPIRE].

[31] H. Witte, B. Muratori, K. Hock, R. Appleby, H. Owen, *et al.*, *Status of the PRISM FFAG Design for the Next Generation Muon-to-Electron Conversion Experiment*, *Conf.Proc.* **C1205201** (2012) 79–81 [InSPIRE].

[32] **COMET Collaboration**, Y. Kuno, *A search for muon-to-electron conversion at J-PARC: The COMET experiment*, *PTEP* **2013** (2013) 022C01 [InSPIRE].

[33] **mu2e Collaboration**, G. Onorato, *The Mu2e experiment at Fermilab: $\mu^- N \to e^- N$*, *Nucl.Instrum.Meth.* **A718** (2013) 102–103 [InSPIRE].

[34] F. del Aguila, A. Aparici, S. Bhattacharya, A. Santamaria, and J. Wudka, *Effective Lagrangian approach to neutrinoless double beta decay and neutrino masses*, *JHEP* **1206** (2012) 146, [arXiv:1204.5986] [InSPIRE].

[35] J. Tang and W. Winter, *Physics with near detectors at a neutrino factory*, *Phys.Rev.* **D80** (2009) 053001, [arXiv:0903.3039] [InSPIRE].

[36] F. del Aguila and M. Chala, *LHC bounds on Lepton Number Violation mediated by doubly and singly-charged scalars*, [arXiv:1311.1510] [InSPIRE].

[37] H. Sugiyama, K. Tsumura, and H. Yokoya, *Discrimination of models including doubly charged scalar bosons by using tau lepton decay distributions*, *Phys.Lett.* **B717** (2012) 229–234, [arXiv:1207.0179] [InSPIRE].

[38] F. del Aguila, M. Chala, A. Santamaria, and J. Wudka, *Discriminating between lepton number violating scalars using events with four and three charged leptons at the LHC*, *Phys.Lett.* **B725** (2013) 310–315, [arXiv:1305.3904] [InSPIRE].

[39] F. del Aguila, M. Chala, A. Santamaria, and J. Wudka, *Distinguishing between lepton number violating scalars at the LHC*, [arXiv:1307.0510] [InSPIRE].

[40] M. Muhlleitner and M. Spira, *A Note on doubly charged Higgs pair production at hadron colliders*, *Phys.Rev.* **D68** (2003) 117701, [arXiv:hep-ph/0305288] [InSPIRE].

[41] S. Kanemura, T. Kasai, G.-L. Lin, Y. Okada, J.-J. Tseng, *et al.*, *Phenomenology of Higgs bosons in the Zee model*, *Phys.Rev.* **D64** (2001) 053007, [arXiv:hep-ph/0011357] [InSPIRE].

[42] K. Kannike, *Vacuum Stability Conditions From Copositivity Criteria*, *Eur.Phys.J.* **C72** (2012) 2093, [arXiv:1205.3781] [InSPIRE].

[43] G. Degrassi, S. Di Vita, J. Elias-Miro, J. R. Espinosa, G. F. Giudice, *et al.*, *Higgs mass and vacuum stability in the Standard Model at NNLO*, *JHEP* **1208** (2012) 098, [arXiv:1205.6497] [InSPIRE].

[44] **ATLAS Collaboration**, *Measurements of the properties of the Higgs-like boson in the two photon decay channel with the ATLAS detector using 25* fb^{-1} *of proton-proton collision data*, [InSPIRE].

[45] **CMS Collaboration**, *Updated measurements of the Higgs boson at 125 GeV in the two photon decay channel*, [InSPIRE].

[46] M. Carena, I. Low, and C. E. Wagner, *Implications of a Modified Higgs to Diphoton Decay Width*, *JHEP* **1208** (2012) 060, [arXiv:1206.1082] [InSPIRE].

[47] J. R. Ellis, M. K. Gaillard, and D. V. Nanopoulos, *A Phenomenological Profile of the Higgs Boson*, *Nucl.Phys.* **B106** (1976) 292 [InSPIRE].

[48] M. A. Shifman, A. Vainshtein, M. Voloshin, and V. I. Zakharov, *Low-Energy Theorems for Higgs Boson Couplings to Photons*, *Sov.J.Nucl.Phys.* **30** (1979) 711–716 [InSPIRE].

[49] J. F. Gunion, H. E. Haber, G. L. Kane, and S. Dawson, *The Higgs Hunter's Guide*, *Front.Phys.* **80** (2000) 1–448 [InSPIRE].

[50] C.-S. Chen, C.-Q. Geng, D. Huang, and L.-H. Tsai, *New Scalar Contributions to* $h \to Z\gamma$, *Phys.Rev.* **D87** (2013) 075019, [arXiv:1301.4694] [InSPIRE].

[51] M. Gonzalez-Garcia, M. Maltoni, J. Salvado, and T. Schwetz, *Global fit to three neutrino mixing: critical look at present precision*, *JHEP* **1212** (2012) 123, [arXiv:1209.3023] [InSPIRE].

[52] D. Forero, M. Tortola, and J. Valle, *Global status of neutrino oscillation parameters after Neutrino-2012*, *Phys.Rev.* **D86** (2012) 073012, [arXiv:1205.4018] [InSPIRE].

[53] G. Fogli, E. Lisi, A. Marrone, D. Montanino, A. Palazzo, *et al.*, *Global analysis of neutrino masses, mixings and phases: entering the era of leptonic CP violation searches*, *Phys.Rev.*

D86 (2012) 013012, [arXiv:1205.5254] [InSPIRE].

[54] D. Schmidt, T. Schwetz, and H. Zhang, *Status of the Zee-Babu model for neutrino mass and possible tests at a like-sign linear collider*, [arXiv:1402.2251] [InSPIRE].

Published for SISSA by Springer

Received: *April 4, 2012*
Accepted: *June 15, 2012*
Published: *July 5, 2012*

On the nature of the fourth generation neutrino and its implications

Alberto Aparici, Juan Herrero-García, Nuria Rius and Arcadi Santamaria

Departament de Física Teórica, and IFIC, Universidad de Valencia-CSIC
Edificio de Institutos de Paterna, Apt. 22085, 46071 Valencia, Spain

E-mail: alberto.aparici@uv.es, juan.a.herrero@uv.es, nuria@ific.uv.es, arcadi.santamaria@uv.es

Abstract: We consider the neutrino sector of a Standard Model with four generations. While the three light neutrinos can obtain their masses from a variety of mechanisms with or without new neutral fermions, fourth-generation neutrinos need at least one new relatively light right-handed neutrino. If lepton number is not conserved this neutrino must have a Majorana mass term whose size depends on the underlying mechanism for lepton number violation. Majorana masses for the fourth-generation neutrinos induce relative large two-loop contributions to the light neutrino masses which could be even larger than the cosmological bounds. This sets strong limits on the mass parameters and mixings of the fourth-generation neutrinos.

Keywords: Beyond Standard Model, Neutrino Physics

ArXiv ePrint: 1204.1021

doi:10.1007/JHEP07(2012)030

JHEP07(2012)030

Contents

JHEP07(2012)030

1 Introduction

In the framework of the Standard Model (SM), fermions are grouped into three families, each containing a doublet of quarks and a doublet of leptons. The number of families is not a constructive parameter of the theory, and it could well be four or more; for this reason, the enlargement of the SM with new generations has been commonly considered [1], and it has proven to help in dealing with several problems, such as the lack of CP violation in the SM to explain the baryon asymmetry of the universe [2] or the structure of the leptonic mass matrices [3]. The currently available SM observables, however, constrain quite tightly the properties of such new families [4], and the global electroweak fits seem to disfavour a scenario with more than five generations [5, 6]; maybe the most striking result against the existence of additional families is the LEP measurement of the number of neutrinos

at the Z peak, which forbids more than three light neutrinos [4], but even this can be dodged if the neutrinos of the new generations are too heavy to be produced in Z decays. All in all, the existence of new generations is not actually excluded, and it seems worth being considered [1], even more now that the LHC is working and exploring the relevant mass range.

On the other hand, right-handed neutrinos constitute a common new physics proposal, usually linked to the generation of neutrino masses. This is particularly interesting nowadays, ever since we gathered compelling evidence that neutrinos do have masses, that they lie well below the other fermions' ones, and that their mixing patterns differ extraordinarily from those of the quark sector (for a review on the matter of neutrino masses see, for example, [7]). The most straightforward way to construct a mass term for the neutrinos within the SM is just to rely on the Higgs mechanism, and so to write the corresponding Yukawa couplings; for that aim, one needs some fermionic fields which carry no SM charge: right-handed neutrinos. However, we do not know whether neutrinos are Dirac or Majorana. If they are Dirac, the smallness of the neutrino mass scale remains unexplained, for it would be just a product of the smallness of the corresponding Yukawa couplings. In order to provide such an explanation, many models and mechanisms have been proposed: in the so-called see-saw models, the lightness of the neutrino mass scale is a consequence of the heaviness of another scale. For instance, this scale is the lepton-number-violating (LNV) Majorana mass of the extra right-handed neutrinos in type I see-saw [8–11]. On the other hand, radiative models propose that neutrino masses are originated via suppressed, high-order processes [12–15]. Although some of these proposals do not require right-handed neutrinos, for the sake of generality it is a good idea to consider their possible involvement in the generation of neutrino masses.

In this work we aim to discuss the naturality of the various scenarios arising when new generations and right-handed neutrinos are brought together. Several previous works have considered such association, either explicitly, in order to provide a mechanism for mass generation, or implicitly, when assuming Dirac neutrinos in their analyses [16–25]. We argue that unless a symmetry is invoked which separates the new family from the first three, the coexistence of both Dirac and Majorana neutrinos is not stable under radiative corrections and doesn't seem natural [25, 26]. Furthermore, the presence of a fourth family plus a right-handed Majorana neutrino triggers the generation of Majorana masses for the light species through a well-known mechanism [16, 17, 23, 25, 27–29]; the upper bounds on the light neutrino masses can thus be translated into bounds on the mixings with the new, heavy generations.

This paper is structured as follows. In section 2 we start by reviewing the different mechanisms which can provide light neutrino masses. In section 3 we discuss the naturalness of those mechanisms to generate the fourth-family neutrino mass and conclude that at least one right-handed neutrino is needed. Assuming that light neutrinos are Majorana, we use naturalness arguments to provide a lower bound on the Majorana mass of the right-handed neutrino. In section 4 we consider a minimal four generation SM with only one relatively light right-handed neutrino and Majorana masses for light neutrinos parametrized by the Weinberg operator [30, 31]. We describe the radiative, two-loop contribution of the

JHEP07(2012)030

heavy fourth-family neutrinos to the light neutrino mass matrix. In section 5 we discuss the phenomenological consequences of this minimal four-generation scenario with heavy Majorana neutrinos (lepton flavour violation, universality bounds, light neutrino masses, neutrinoless double beta decay,...), and we conclude in section 6. Appendix A is devoted to describe an explicit example in which a finite Majorana mass for the fourth-generation right-handed neutrino is radiatively generated.

2 Light neutrino masses

The huge hierarchy between neutrino masses and those of all other fermions has triggered the appearance of many different mechanisms to explain the lightness of neutrinos. Here we briefly review some of these mechanisms, with special emphasis on the frameworks that are able to explain neutrino masses including a fourth generation, which will be discussed in the next section.

2.1 Dirac masses

If there are right-handed neutrinos and a conserved global symmetry (for instance $B-L$) prevents them from having a Majorana mass, neutrinos are Dirac particles, as all other fermions in the SM. However, in this scenario there is no explanation for the smallness of neutrino masses, having to impose by hand extremely tiny Yukawa couplings, approximately 6 (11) orders of magnitude smaller than the electron (top) one. Therefore, although in principle it is possible, a Dirac nature does not seem the most natural option for neutrinos (but see, for example, [3], for a proposal in this direction which avoids tiny Yukawas).

2.2 Seesaw

Seesaw models are minimal extensions of the SM which can naturally lead to tiny (Majorana) neutrino masses, keeping the SM gauge symmetry, $\mathrm{SU(3)_C} \otimes \mathrm{SU(2)_L} \otimes \mathrm{U(1)_Y}$ and renormalizability, but giving up the (accidental) lepton number conservation of the SM. Let's explain briefly the different types to fix notation.

2.2.1 Type I: fermionic singlets

In type I see-saw [8–11, 32], n SM fermionic singlets with zero hypercharge are added to the SM; these have the quantum numbers of right-handed neutrinos, and can be denoted by $\nu_{\mathrm{R}i}$. Note that to explain neutrino data, which requires al least two massive neutrinos, a minimum of two extra singlets are needed. Having no charges under the SM, Majorana masses for right-handed neutrinos are allowed by gauge invariance, so the new terms in the Lagrangian are:

$$\mathcal{L}_{\nu_{\mathrm{R}}} = i\,\overline{\nu_{\mathrm{R}}}\gamma^{\mu}\partial_{\mu}\nu_{\mathrm{R}} - \left(\frac{1}{2}\overline{\nu_{\mathrm{R}}^{c}}M\nu_{\mathrm{R}} + \bar{\ell}\,\tilde{\phi}\,Y\,\nu_{\mathrm{R}} + \mathrm{H.c.}\right), \tag{2.1}$$

where ℓ and ϕ are respectively the lepton and Higgs SM doublets, $\tilde{\phi} = i\,\tau_2\,\phi^*$ with τ_2, the second Pauli matrix, acting on the $SU(2)_{\mathrm{L}}$ indices, M is a $n \times n$ symmetric matrix, Y is a general $3 \times n$ matrix and we have omitted flavour indices for simplicity. After spontaneous

JHEP07(2012)030

symmetry breaking (SSB), $\langle\phi\rangle = v_\phi$ with $v_\phi = 174\,\text{GeV}$, the neutrino mass terms are given by

$$\mathcal{L}_{\nu\,\text{mass}} = -\frac{1}{2}\left(\overline{\nu_\text{L}}\ \overline{\nu_\text{R}^\text{c}}\right)\begin{pmatrix} 0 & m_\text{D} \\ m_\text{D}^\text{T} & M \end{pmatrix}\begin{pmatrix} \nu_\text{L}^\text{c} \\ \nu_\text{R} \end{pmatrix} + \text{H.c.}\,, \tag{2.2}$$

where $m_D = Y v_\phi$. The mass scale for right-handed neutrinos is in principle free, however if $M \gg m_\text{D}$, upon block-diagonalization one obtains n heavy leptons which are mainly SM singlets, with masses $\sim M$, and the well-known see-saw formula for the effective light neutrino Majorana mass matrix,

$$m_\nu \simeq -m_\text{D}\, M^{-1}\, m_\text{D}^\text{T}\,, \tag{2.3}$$

which naturally explains the smallness of light neutrino masses as a consequence of the presence of heavy SM singlet leptons.

2.2.2 Type II: scalar triplet

The type II see-saw [33–37] only adds to the SM field content one scalar triplet with hypercharge $Y = 1$ (we adopt the convention that $Q = Y + T_3$) and assigns to it lepton number $L = -2$. In the doublet representation of $\text{SU}(2)_\text{L}$ the triplet can be written as a 2×2 matrix, whose components are

$$\chi = \begin{pmatrix} \chi^+/\sqrt{2} & \chi^{++} \\ \chi_0 & -\chi^+/\sqrt{2} \end{pmatrix}. \tag{2.4}$$

Gauge invariance allows a Yukawa coupling of the scalar triplet to two lepton doublets,

$$\mathcal{L}_\chi = \left((Y_\chi^\dagger)_{\alpha\beta}\,\bar{\tilde{\ell}}_\alpha \chi \ell_\beta + \text{H.c.}\right) - V(\phi, \chi) \tag{2.5}$$

where Y_χ is a symmetric matrix in flavour space, and $\tilde{\ell} = i\tau_2\,\ell^\text{c}$. The scalar potential has, among others, the following terms:

$$V(\phi, \chi) = m_\chi^2\,\text{Tr}[\chi\chi^\dagger] - \left(\mu\,\tilde{\phi}^\dagger \chi^\dagger \phi + \text{H.c.}\right) + \ldots \tag{2.6}$$

The μ coupling violates lepton number explicitly, and it induces a vacuum expectation value (VEV) for the triplet via the VEV of the doublet, even if $m_\chi > 0$. In the limit $m_\chi \gg v_\phi$ this VEV can be approximated by:

$$\langle\chi\rangle \equiv v_\chi \simeq \frac{\mu v_\phi^2}{m_\chi^2}; \tag{2.7}$$

then, the Yukawa couplings in equation (2.5) lead to a Majorana mass matrix for the left-handed neutrinos

$$m_\nu = 2 Y_\chi v_\chi = 2 Y_\chi \frac{\mu v_\phi^2}{m_\chi^2}. \tag{2.8}$$

Neutrino masses are thus proportional to both Y_χ and μ. Such dependence can be understood from the Lagrangian, since the breaking of lepton number L results from the

JHEP07(2012)030

simultaneous presence of the Yukawa and μ couplings. As long as m_χ^2 is positive and large, v_χ will be small, in agreement with the constraints from the ρ parameter, $v_\chi \lesssim 6$ GeV [38].[1] Moreover, the parameter μ, which has dimensions of mass, can be naturally small, because in its absence lepton number is recovered, increasing the symmetry of the model.

2.2.3 Type III: fermionic triplets

In the type III see-saw model [40, 41], the SM is extended by fermion $\mathrm{SU}(2)_\mathrm{L}$ triplets Σ_α with zero hypercharge. As in type I, at least two fermion triplets are needed to have two non-vanishing light neutrino masses. We choose the spinors Σ_α to be right-handed under Lorentz transformations and write them in SU(2) Cartesian components $\vec{\Sigma}_\alpha = (\Sigma_\alpha^1, \Sigma_\alpha^2, \Sigma_\alpha^3)$. The Cartesian components can be written in terms of charge eigenstates as usual

$$\Sigma_\alpha^+ = \frac{1}{\sqrt{2}}(\Sigma_\alpha^1 - i\Sigma_\alpha^2)\,, \qquad \Sigma_\alpha^0 = \Sigma_\alpha^3\,, \qquad \Sigma_\alpha^- = \frac{1}{\sqrt{2}}(\Sigma_\alpha^1 + i\Sigma_\alpha^2)\,, \tag{2.9}$$

and the charged components can be further combined into negatively charged Dirac fermions $E_\alpha = \Sigma_\alpha^- + \Sigma_\alpha^{+\mathrm{c}}$. Using standard four-component notation the new terms in the Lagrangian are given by

$$\mathcal{L}_\Sigma = i\,\overline{\vec{\Sigma}_\alpha}\gamma^\mu D_\mu \cdot \vec{\Sigma}_\alpha - \left(\frac{1}{2}M_{\alpha\beta}\overline{\vec{\Sigma}_\alpha^{\mathrm{c}}}\cdot\vec{\Sigma}_\beta + Y_{\alpha\beta}\,\overline{\ell_\alpha}\,\left(\vec{\tau}\cdot\vec{\Sigma}_\beta\right)\tilde{\phi} + \mathrm{H.c.}\right)\,, \tag{2.10}$$

where Y is the Yukawa coupling of the fermion triplets to the SM lepton doublets and the Higgs, and M their Majorana mass matrix, which can be chosen to be diagonal and real in flavour space.

After SSB the neutrino mass matrix can be written as

$$\mathcal{L}_{\nu\,\mathrm{mass}} = -\frac{1}{2}\left(\overline{\nu_\mathrm{L}}\;\;\overline{\Sigma^{0\mathrm{c}}}\right)\begin{pmatrix} 0 & m_\mathrm{D} \\ m_\mathrm{D}^\mathrm{T} & M \end{pmatrix}\begin{pmatrix} \nu_\mathrm{L}^\mathrm{c} \\ \Sigma^0 \end{pmatrix} + \mathrm{H.c.}\,, \tag{2.11}$$

which is the same as in the type I see-saw just replacing the singlet right-handed neutrinos by the neutral component of the triplets, Σ_α^0, and therefore leads to a light neutrino Majorana mass matrix

$$m_\nu \simeq -m_\mathrm{D}\,M^{-1}\,m_\mathrm{D}^\mathrm{T}\,. \tag{2.12}$$

However, since the triplet has also charged components with the same Majorana mass, in this case there are stringent lower bounds on the new mass scale, $M \gtrsim 100$ GeV.

2.3 Others

Here we briefly summarize non minimal mechanisms which also lead to Majorana light neutrino masses. Most of these models do not include right-handed neutrinos and are designed to obtain tiny Majorana masses for the left-handed SM neutrinos, so we can anticipate that they will not be appropriate for the fourth generation.

[1] This bound is calculated after the inclusion of the one-loop corrections to the ρ parameter, and is slightly looser than other previously obtained from electroweak global fits (see, for example, [39]). Note also that the authors of [38] use a different normalisation for the VEV, and hence the difference between their value and the one we present here.

JHEP07(2012)030

a) Radiative mechanisms. Small Majorana neutrino masses may also be induced by radiative corrections [12–15]. Typically, on top of loop factors of at least $1/(4\pi)^2$, there are additional suppressions due to couplings or ratios of masses, leading to the observed light neutrino masses with a new physics scale not far above the electroweak one.

b) Supersymmetry. There is an intrinsically supersymmetric way of breaking lepton number by breaking the so-called R parity [42–51] (for a review see [52]). In this scenario, the SM doublet neutrinos mix with the neutralinos, i.e., the supersymmetric (fermionic) partners of the neutral gauge and Higgs bosons. As a consequence, Majorana masses for neutrinos (generated at tree level and at one loop) are naturally small because they are proportional to the small R-parity-breaking parameters.

2.4 Weinberg operator

As we have mentioned, it does not seem very natural that neutrinos are Dirac particles; assuming that they are Majorana, we will be often interested in abstracting from the actual mechanism of mass generation. In such case, if the light degrees of freedom are those of the SM we can parametrise the Majorana masses in terms of the well-known dimension 5 Weinberg operator[2] [30, 31]:

$$\mathcal{L}_5 = \frac{1}{2}\frac{c_{\alpha\beta}}{\Lambda_W}(\overline{\ell_\alpha}\tilde{\phi})\,(\phi^\dagger\tilde{\ell_\beta}) + \text{H.c.}\,, \tag{2.13}$$

where $\Lambda_W \gg v_\phi$ is the scale of new physics and $c_{\alpha\beta}$ are model-dependent coefficients with flavour structure, which in some models can carry additional suppression due to loop factors (as is the case in radiative mechanisms) and/or ratios of mass parameters (for instance in type II see-saw $c \propto \mu/m_\chi$). In those cases we will assume that Λ_W is directly related to the masses of the new particles and absorb all suppression factors in $c_{\alpha\beta}$.

Upon electroweak symmetry breaking, the Weinberg operator leads to a Majorana mass matrix for the light neutrinos of the form

$$m_\nu = c\,\frac{v_\phi^2}{\Lambda_W}\,. \tag{2.14}$$

Notice that if $c_{\alpha\beta}$ is suppressed, the scale Λ_W does not need to be extremely large in order to fit light neutrino masses and, thus, the Weinberg operator can parametrize a variety of Majorana neutrino mass models, including those with masses generated radiatively.

3 Fourth-generation neutrino masses

If there exists a fourth generation, the fourth-generation neutrinos must be massive (with masses $\gtrsim m_Z/2$ in order to avoid the strong limits for the number of active neutrinos found at LEP). In principle all mass mechanisms available for the light neutrinos are also available to the fourth-generation neutrinos, however, the fact that they must be quite

[2] In supersymmetric models, $\tilde{\phi} = H_u$, since there are two Higgs doublets.

JHEP07(2012)030

massive changes completely the discussion of the naturalness of the different mechanisms. Let us discuss them:

a) Dirac masses.

Since the fourth generation must be at the electroweak scale, this mechanism of mass generation is quite natural for the fourth-generation neutrinos as long as lepton number is conserved.

b) Fermionic singlets with Majorana mass.

If lepton number is not conserved there is no reason to forbid a Majorana mass term for right-handed neutrinos (see the discussion below). However if $m_R \gg m_D$ the see-saw formula applies and the spectrum contains a relatively light, almost-active neutrino with mass $m_4 \sim m_D^2/m_R$, which must be heavier than $m_Z/2$. Therefore $m_R < m_D^2/m_Z$ and the mass of the right-handed neutrino cannot be much larger than the electroweak scale. On the other hand, if $m_R \ll m_D$ there are two almost degenerate neutrinos and we are in the pseudo-Dirac limit, which does not pose any problem.

c) Scalar triplet.

In principle, as in the case of light neutrinos, scalar triplets could also be used to obtain Majorana masses for the fourth-generation neutrinos. However, the strong limits on the triplet's VEV coming from the ρ parameter $v_\chi \lesssim 6$ GeV will yield fourth-generation neutrino masses too small. This limit could be relaxed a bit if radiative corrections to the ρ parameter coming from triplet masses are large and such that cancel in part the deviations induced by the triplet's VEV, but this will require quite a high degree of fine tuning among rather different quantities. Therefore, this mechanism alone is not a natural mechanism for the fourth-generation neutrino masses.

d) Fermionic triplets.

This is similar to b), but together with the right-handed neutrinos there come new charged fermions degenerate with the neutral component. Since production limits tell us that the charged fermions must be heavier than about 100 GeV, in this case the pseudo-Dirac limit is not possible. Moreover these new fermions cannot be extremely heavy, because otherwise the active neutrino will be too light. We conclude that this mechanism is viable but much more constrained than b).

e) Radiative mechanisms and SUSY with broken R parity.

Neutrino masses in these models are strongly suppressed with respect to the electroweak scale by either loop factors, couplings and/or ratios of masses. Therefore they are not viable for the fourth generation.

f) Weinberg operator.

In principle the Weinberg operator could also be used to give Majorana masses to the fourth-generation neutrinos. However, it will provide masses $\mathcal{O}(v_\phi^2/\Lambda_W)$ which

JHEP07(2012)030

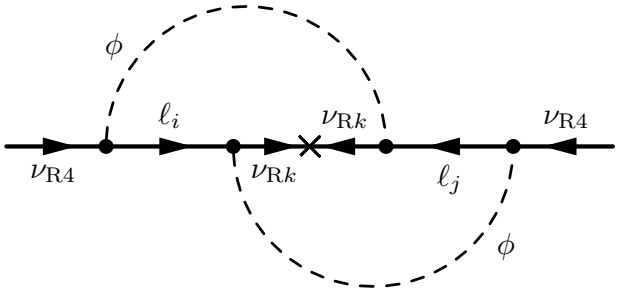

Figure 1. The two-loop process that provides a Majorana mass for the fourth-generation right-handed neutrino in the framework of type I see-saw. The indices i and j represent any of the four families; the index k, however, represents only the right-handed neutrinos associated to the generation of masses for the light families, $k = 1, 2, 3$.

should be $\gtrsim m_Z/2$, so the scale of new physics Λ_W can not be much larger than the electroweak scale v_ϕ and the effective theory does not make sense. Therefore the Weinberg operator does not provide a useful parametrization of the fourth-generation neutrino mass.

We can therefore conclude that only a), b) (which includes a) in some limit) and possibly d) are good mechanisms for the fourth-generation neutrino masses. It seems then that to describe correctly the fourth-generation neutrino one needs at least one right-handed neutrino (either SM singlet or triplet) which has standard Dirac couplings to the doublets. If this RH neutrino is a SM triplet, we have seen that its Majorana mass is in the range $100\,\mathrm{GeV} \lesssim m_R \lesssim$ few TeV.

However, if the right-handed neutrino is a SM singlet it could have a very small or even vanishing Majorana mass term. Is it natural to have Dirac neutrinos for the fourth generation? The answer is simple: yes, provided there is a symmetry that protects them from acquiring a Majorana mass term. This is not the situation if the light neutrinos are Majorana, as most of the SM extensions that we considered in section 2, and they can mix freely with the heavy fourth family. We argue that in such a case a Majorana mass term for the fourth right-handed neutrino should be allowed just on symmetry grounds, and in fact, based on naturality arguments, a lower bound for this Majorana mass can be given.

Let us consider first the case in which the three light neutrinos obtain their masses via a type-I see-saw containing heavy right-handed neutrinos with masses $m_{\mathrm{R}k}$ (with $k = 1, 2, 3$) of the order of 10^{12}–$10^{15}\,\mathrm{GeV}$. Since lepton number is not conserved it is natural to consider a Majorana mass term for the fourth right-handed neutrino, ν_{R4}. However, in order to satisfy the LEP bounds on the number of light active neutrinos, m_{R4} should be, at most, of the order of a few TeV and, therefore, much smaller than $m_{\mathrm{R}k}$. Thus, one might think that perhaps it is more natural to set directly $m_{\mathrm{R4}} = 0$ and consider only Dirac neutrinos for the fourth generation. The question that arises then is whether this choice is stable or not under radiative corrections and what is the natural size one might expect for m_{R4}, since setting $m_{\mathrm{R4}} = 0$ does not increase the symmetries of the Lagrangian. The

JHEP07(2012)030

answer can be obtained from the diagram in figure 1 which gives a logarithmically divergent contribution to $m_{\mathrm{R}4}$ induced by the presence of the three heavy Majorana neutrino masses, $m_{\mathrm{R}k}$ [25, 26]. Thus, above the $m_{\mathrm{R}k}$ scale, $m_{\mathrm{R}4}$ and $m_{\mathrm{R}k}$ mix under renormalization and do not run independently. Therefore, even if one finds a model in which $m_{\mathrm{R}4} = 0$ at some scale $\Lambda_C > m_{\mathrm{R}k}$, $m_{\mathrm{R}4}$ will be generated by running from Λ_C to $m_{\mathrm{R}k}$. This running can easily be estimated from the diagram in figure 1 and, barring accidental cancellations, one should require

$$m_{\mathrm{R}4} \gtrsim \frac{1}{(4\pi)^4} \sum_{ijk} Y_{i4} Y_{ik}^* m_{\mathrm{R}k} Y_{jk}^* Y_{j4} \ln(\Lambda_C/m_{\mathrm{R}k}) \gtrsim \frac{1}{(4\pi)^4} \sum_{ijk} Y_{i4} Y_{ik}^* m_{\mathrm{R}k} Y_{jk}^* Y_{j4} \,, \tag{3.1}$$

where $i, j = 1, 2, 3, 4$, $k = 1, 2, 3$ and in the last step we have taken $\ln(\Lambda_C/m_{\mathrm{R}k}) \gtrsim 1$. Of course, given a particular renormalizable model yielding $m_{\mathrm{R}4} = 0$ at tree level (see appendix A for an explicit example) one should be able to compute the full two-loop mass $m_{\mathrm{R}4}$, which will be finite and will contain the logarithmic contributions we have just discussed.

Eq. (3.1) sets the lower bound that we had announced. Let us now estimate its value; bearing in mind that in type I see-saw the light neutrino masses are given by[3] $(m_\nu)_{ij} \sim \sum_k Y_{ik} Y_{jk} v_\phi^2 / m_{\mathrm{R}k}$. Then, by taking all $m_{\mathrm{R}k}$ of the same order we can rewrite the bound as

$$m_{\mathrm{R}4} \gtrsim \sum_{ij} \frac{Y_{i4} (m_\nu^*)_{ij} Y_{j4}}{(4\pi)^4} \frac{m_{\mathrm{R}k}^2}{v_\phi^2} \,. \tag{3.2}$$

To give a conservative estimate we consider only the contribution of the first three generations because we expect their Yukawa couplings to the fourth right-handed neutrino to be somewhat suppressed due to universality and LFV constraints [16, 17, 23, 53] (say, $Y_{k4} \sim 10^{-2}$). Once we fix the neutrino masses and the Yukawa couplings between the fourth-generation neutrino and the first three, $m_{\mathrm{R}4}$ grows quadratically with $m_{\mathrm{R}k}$. For $m_\nu = 0.01$ eV and $Y_{k4} = 0.01$ we obtain that $m_{\mathrm{R}4}$ is of order keV, GeV, PeV for $m_{\mathrm{R}k} = 10^9, 10^{12}, 10^{15}$ GeV, respectively. The contribution of the fourth active neutrino is not necessarily suppressed by the Yuwawa couplings and, in principle, by using it, even more restrictive bounds on $m_{\mathrm{R}4}$ could be set. However, as $(m_\nu)_{44}$ is model-dependent,[4] we keep the most conservative bound.

Let us consider now the case in which the three light neutrinos obtain their masses through the type II see-saw mechanism (see section 2.2.2), i.e., through their coupling to a scalar triplet, χ, which develops a VEV. As discussed in section 3, this triplet cannot be the only source Majorana masses for the fourth-generation neutrinos and, at least, one right-handed neutrino is needed. We will assume then that there is a right-handed neutrino which has Yukawa couplings to the four SM doublets. In this scenario one can easily see that the right-handed neutrino will acquire, at two loops (as seen in figure 2), a Majorana

[3] Notice that by integrating out the three heavy right-handed neutrinos we obtain a Majorana neutrino mass matrix for the four active neutrinos which is of the order of the light neutrino masses.

[4] In this case, $(m_\nu)_{44}$ is the see-saw mass induced by only the three heavy right-handed neutrinos, thus, it could even be zero if the Yukawas between the fourth lepton doublet and the three right-handed neutrinos vanish for some reason.

JHEP07(2012)030

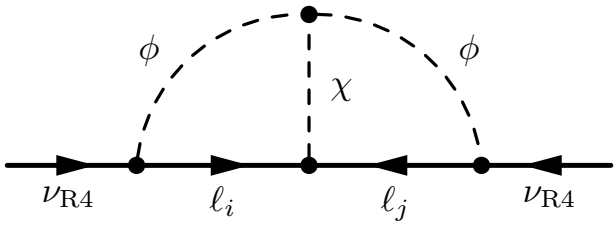

Figure 2. The process that provides a Majorana mass for the right-handed neutrino associated to the fourth generation in the framework of type II see-saw.

mass. This just reflects the fact that the right-handed neutrino mass $m_{\mathrm{R}4}$ and the trilinear coupling of the triplet, μ, mix under renormalization. Applying the same arguments used in the case of see-saw type I for light neutrino masses and the estimate of the diagram in figure 2 we can write

$$m_{\mathrm{R}4} \gtrsim \frac{\mu}{(4\pi)^4} \sum_{ij} Y_{i4} (Y_\chi^*)_{ij} Y_{j4} \,, \tag{3.3}$$

where Y_χ are the Yukawa couplings of the triplet to the lepton doublets and, as before, we have taken $\ln(\Lambda_C/m_\chi) \gtrsim 1$. As in the type I see-saw case the result can also be expressed in terms of the light neutrino masses $(m_\nu)_{ij} \sim (Y_\chi)_{ij} \mu v_\phi^2/m_\chi^2$; thus

$$m_{\mathrm{R}4} \gtrsim \sum_{ij} \frac{Y_{i4} (m_\nu^*)_{ij} Y_{j4}}{(4\pi)^4} \frac{m_\chi^2}{v_\phi^2} \,, \tag{3.4}$$

which shows a similar structure to that obtained for type I see-saw, eq. (3.2). The same result is obtained for type III see-saw, whose couplings are analogous to those of type I.

The similarity of the two results suggests that bounds of this type are quite general and should appear in all kinds of four-generation models with light Majorana neutrinos. In fact, as discussed in section 2.4, light Majorana neutrino masses can be parametrized in many models by means of the Weinberg operator, eq. (2.13), which yields neutrino masses given by eq. (2.14). Then, one could draw a two-loop diagram analogous to the diagrams in figures 1 and 2 but with the propagators of heavy particles pinched and substituted by one insertion of the Weinberg operator. This diagram is quadratically divergent and, therefore, its contribution to $m_{\mathrm{R}4}$ can not be reliably computed in the effective field theory because it depends on the details of the matching with the full theory from which the effective one originates (in fact it vanishes in dimensional regularization or in any other regularization scheme allowing symmetric integration), but one can use naive dimensional analysis to estimate contributions of order

$$m_{\mathrm{R}4} \sim \frac{\Lambda_W}{(4\pi)^4} \sum_{ij} Y_{i4} c_{ij}^* Y_{j4} \sim \frac{Y_{i4} (m_\nu^*)_{ij} Y_{j4}}{(4\pi)^4} \frac{\Lambda_W^2}{v_\phi^2} \tag{3.5}$$

which is precisely the result obtained in the see-saw models discussed above if one identifies $\Lambda_W \sim m_{\mathrm{R}k}, m_\chi$. However, it is important to remark that in the low energy effective theory $m_{\mathrm{R}4}$ is a free parameter, and eq. (3.5) is only a naive dimensional analysis estimate of what one would expect in a more complete theory.

JHEP07(2012)030

4 Light neutrino masses induced by new generations

After the discussion above, to describe correctly the neutrino sector of models with four generations we need just one relatively light right-handed neutrino, $\nu_{\rm R}$, to give Dirac mass terms to the fourth-generation neutrinos, while Majorana masses for light neutrinos can be parametrized by the Weinberg operator. We will work in this minimal four-generation scenario, thus, the relevant part of the Lagrangian for our discussion is

$$\mathcal{L}_Y = -\bar{\ell} Y_e e_{\rm R} \phi - \bar{\ell} y \nu_{\rm R} \tilde{\phi} - \frac{1}{2} \overline{\nu_{\rm R}^{\rm c}} m_{\rm R} \nu_{\rm R} + \frac{1}{2v_\phi^2} (\bar{\ell}\tilde{\phi}) m_{\rm L} (\phi^\dagger \tilde{\ell}) + \text{H.c.}\,, \tag{4.1}$$

where ℓ and $e_{\rm R}$ contain the four generation components while $\nu_{\rm R}$ is the only right-handed neutrino. Thus Y_e is a completely general 4×4 complex matrix, y is a 4 component column vector, $m_{\rm R}$ is just a number and $m_{\rm L}$ is a general complex symmetric 4×4 matrix. The Dirac limit is recovered when $m_{\rm R}=0$ and $m_{\rm L}=0$. Since light neutrino masses are very small, we will assume $m_{\rm L} \ll v_\phi$ while $m_{\rm R}$, as we immediately see, cannot be very large to ensure there are only three light active neutrinos. Moreover, as shown in the previous section, we do not expect it to be zero if $m_{\rm L}$ is not zero.

Above we have taken for $m_{\rm L}$ a general complex symmetric 4×4 matrix in spite of the fact that to describe the light neutrino sector we just need a 3×3 matrix. This is because in most of the neutrino mass models one also obtains contributions to the fourth-generation Weinberg operator. For instance, we give below the values of $m_{\rm L}$ one obtains for the different types of seesaw.

If the three light neutrino masses are generated by the seesaw mechanism type I or type III, we need three of the right-handed neutrinos much heavier than the fourth. We can always choose a basis in which the Majorana mass matrix of right-handed neutrinos is diagonal and integrate out the three heavy right-handed neutrinos. The result can be writen in terms of the Weinberg operator in (4.1) with

$$(m_{\rm L})_{\alpha\beta} = -\sum_{k=1,2,3} \frac{(Y_\nu)_{\alpha k}\,(Y_\nu)_{\beta k}}{m_{{\rm R}k}} v_\phi^2\,, \tag{4.2}$$

where $m_{{\rm R}k}$ are the eigenvalues of the diagonal Majorana mass matrix of the three heavy right-handed neutrinos, while $(Y_\nu)_{\alpha k}$ are the Yukawa couplings of the three heavy right-handed neutrinos with the four lepton doublets. Then, the 4×4 mass matrix (4.2) is projective and has at most rank 3.

If the three light neutrino masses are generated by the VEV of a triplet (type II see-saw), we will have

$$(m_{\rm L})_{\alpha\beta} = 2(Y_\chi)_{\alpha\beta} v_\chi \tag{4.3}$$

being $(Y_\chi)_{\alpha\beta}$ the Yukawa couplings of the 4 lepton doublets to the triplet and $v_\chi \sim \mu v_\phi^2/m_\chi^2$ its VEV. In this case, $m_{\rm L}$ is a completely general 4×4 symmetric complex matrix.

After SSB the neutrino mass matrix (in the basis $(\nu_{{\rm L}\alpha}^{\rm c}, \nu_{\rm R})$) is

$$M = \begin{pmatrix} m_{\rm L} & y v_\phi \\ y^{\rm T} v_\phi & m_{\rm R} \end{pmatrix}. \tag{4.4}$$

JHEP07(2012)030

To diagonalize this mass matrix we perform first a 4×4 rotation in order to separate heavy from light degrees of freedom, so we change from the flavour basis $(\nu_e,\nu_\mu,\nu_\tau,\nu_E)$ to a new basis $\nu'_1,\nu'_2,\nu'_3,\nu'_4$ in which the first three states are light (with masses given by $m_{\rm L}$) and only ν'_4 mixes with $\nu_{\rm R}$. Then, we have $\nu_\alpha=\sum_i V_{\alpha i}\nu'_i$ $(i=1,\cdots,4,\ \alpha=e,\mu,\tau,E)$, where V is a orthogonal matrix, and we define

$$N_\alpha\equiv V_{\alpha4}=\frac{y_\alpha}{\sqrt{\sum_\beta y_\beta^2}}\,. \tag{4.5}$$

Now, we are free to choose ν'_1,ν'_2,ν'_3 in any combination of $\nu_e,\nu_\mu,\nu_\tau,\nu_E$ as long as they are orthogonal to ν'_4, i.e., $\sum_\alpha V_{\alpha k}N_\alpha=0$ for k=1,2,3. The orthogonality of V almost fixes all its elements in terms of N_α, but still leaves us some freedom to set three of them to zero. Following [16, 17] we choose $V_{\tau1}=V_{E1}=V_{E2}=0$ for convenience. The transpose of the matrix V is:

$$V^{\rm T}=\begin{pmatrix} \frac{N_\mu}{\sqrt{N_e^2+N_\mu^2}} & \frac{-N_e}{\sqrt{N_e^2+N_\mu^2}} & 0 & 0\\ \frac{N_eN_\tau}{\sqrt{(N_e^2+N_\mu^2)(1-N_E^2)}} & \frac{N_\mu N_\tau}{\sqrt{(N_e^2+N_\mu^2)(1-N_E^2)}} & \frac{-N_e^2-N_\mu^2}{\sqrt{(N_e^2+N_\mu^2)(1-N_E^2)}} & 0\\ \frac{N_eN_E}{\sqrt{(1-N_E^2)}} & \frac{N_\mu N_E}{\sqrt{(1-N_E^2)}} & \frac{N_\tau N_E}{\sqrt{(1-N_E^2)}} & -\sqrt{(1-N_E^2)}\\ N_e & N_\mu & N_\tau & N_E\,. \end{pmatrix} \tag{4.6}$$

After this rotation the neutrino mass matrix is

$$\tilde M=\begin{pmatrix} & & & \omega_1 & 0\\ & \tilde m_{\rm L} & & \omega_2 & 0\\ & & & \omega_3 & 0\\ \omega_1 & \omega_2 & \omega_3 & \omega_4 & m_{\rm D}\\ 0 & 0 & 0 & m_{\rm D} & m_{\rm R} \end{pmatrix}, \tag{4.7}$$

where $(\tilde m_{\rm L})_{kk'}=(Vm_{\rm L}V^{\rm T})_{kk'}$ is a 3×3 matrix with $k,k'=1,2,3$, $\omega_k=(Vm_{\rm L}V^{\rm T})_{4k}$, $\omega_4=(Vm_{\rm L}V^{\rm T})_{44}$ and $m_{\rm D}=v_\phi\sqrt{\sum_\alpha y_\alpha^2}$. Since $\tilde m_{\rm L},\omega_k,\omega_4\ll m_{\rm R},m_{\rm D}$, the matrix $\tilde M$ can be block-diagonalized using the see-saw formula. Then, the mass matrix of the light neutrinos (at tree level) will be

$$m_\nu^{(0)}=\tilde m_{\rm L}-\frac{m_{\rm R}}{m_{\rm R}\omega_4-m_{\rm D}^2}\vec\omega\cdot\vec\omega^{\rm T}\,, \tag{4.8}$$

while the heavy sector will be obtained after diagonalizing the 2×2 matrix

$$M_H=\begin{pmatrix}\omega_4 & m_{\rm D}\\ m_{\rm D} & m_{\rm R}\end{pmatrix}\,. \tag{4.9}$$

Neglecting ω_4, this diagonalization leads to two Majorana neutrinos

$$\nu_4=i\cos\theta(-\nu'_4+\nu'^{\rm c}_4)+i\sin\theta(\nu_{\rm R}-\nu^{\rm c}_{\rm R}) \tag{4.10}$$

$$\nu_4=-\sin\theta(\nu'_4+\nu'^{\rm c}_4)+\cos\theta(\nu_{\rm R}+\nu^{\rm c}_{\rm R}) \tag{4.11}$$

JHEP07(2012)030

with masses

$$m_{4,\bar{4}} = \frac{1}{2}\left(\sqrt{{m_{\rm R}}^2 + 4m_{\rm D}^2} \mp m_{\rm R}\right) , \tag{4.12}$$

and mixing angle $\tan^2\theta = m_4/m_{\bar{4}}$. The imaginary unit factor i and the relative signs in ν_4 are necessary to keep the mass terms positive and preserve the canonical Majorana condition $\nu_4 = \nu_4^c$. If $m_{\rm R} \ll m_{\rm D}$, we have $m_4 \approx m_{\bar{4}}$, $\tan\theta \approx 1$, and we say we are in the pseudo-Dirac limit while when $m_{\rm R} \gg m_{\rm D}$, $m_4 \approx m_{\rm D}^2/m_{\rm R}$ and $m_{\bar{4}} \approx m_{\rm R}$, $\tan\theta \approx m_{\rm D}/m_{\rm R}$ and we say we are in the see-saw limit.

Eq. (4.8) can be used as long as $m_{\rm R}\omega_4 - m_{\rm D}^2$ is different from zero. However, we expect $m_{\rm R}$ to be below few TeV and ω_4 below 1 eV. Therefore $m_{\rm R}\omega_4 \ll m_{\rm D}^2$ unless $m_{\rm D}$ is very small but, in that case, the fourth-generation neutrinos will be too light. Thus, the correction to the 3×3 neutrino mass matrix is projective (only one eigenvalue different from zero) and it is naturally order $m_{\rm L}^2$ and, therefore, negligible.

Summarizing, there are two heavy neutrinos 4 and $\bar{4}$ (with a small pollution from $m_{\rm L}$ which can be neglected) and a tree-level mass matrix for the light neutrinos $m_\nu^{(0)} \simeq \tilde{m}_{\rm L}$. Therefore, neglecting the small ω_i's in eq. (4.7), the 5×5 unitary matrix which relates the flavour with the mass eigenstate basis can be written as $U = U_H \cdot U_L$, being U_H the rotation in the heavy sector which diagonalizes the mass matrix M_H in eq. (4.9) and U_L given by

$$U_L = \begin{pmatrix} & & 0 \\ & V & 0 \\ & & 0 \\ & & 0 \\ 0\,0\,0\,0 & & 1 \end{pmatrix} \begin{pmatrix} & & 0\,0 \\ & W & 0\,0 \\ & & 0\,0 \\ 0\,0\,0 & & 1\,0 \\ 0\,0\,0 & & 0\,1 \end{pmatrix} , \tag{4.13}$$

where V rotates from the ν_i' basis to the flavour basis (see eq. (4.6)) and W is the matrix which diagonalizes $\tilde{m}_{\rm L}$. Within this approximation, the mixing among the light and the heavy sector, which we wish to constrain, depends on $(U_L)_{\alpha 4} = V_{\alpha 4} = N_\alpha$.

Having fixed the tree-level neutrino mass spectrum and given the huge hierarchies present we should consider the stability of the results against radiative corrections. One can check that there are no rank-changing one-loop corrections to the neutrino mass matrices. This result can be easily understood in the ν_i' basis that we defined before, since the light neutrinos (ν_1', ν_2', ν_3') are decoupled from the heavy sector, $\nu_4, \nu_{\bar{4}}$, so there are not one-loop diagrams involving the fourth-generation neutrinos with light ones as external legs.

However it has been shown [16, 17, 23, 27] that two-loop corrections induced by the fourth-generation fermions can generate neutrino masses for the light neutrinos even if they were not present at tree level, see figure 3. In the ν_i' basis the result reads (see [23] for details)

$$(m_\nu)_{ij}^{(2)} = -\frac{g^4}{m_W^4} m_{\rm R} m_{\rm D}^2 \sum_\alpha V_{\alpha i} V_{\alpha 4} m_\alpha^2 \sum_\beta V_{\beta j} V_{\beta 4} m_\beta^2 I_{\alpha\beta} , \tag{4.14}$$

where the sums run over the charged leptons $\alpha, \beta = e, \mu, \tau, E$ while $i, j = 1, 2, 3$, and $I_{\alpha\beta}$ is a loop integral which was discussed in [23]. When $m_{\rm R} = 0$, $(m_\nu)_{ij}^{(2)} = 0$, as it should, because

JHEP07(2012)030

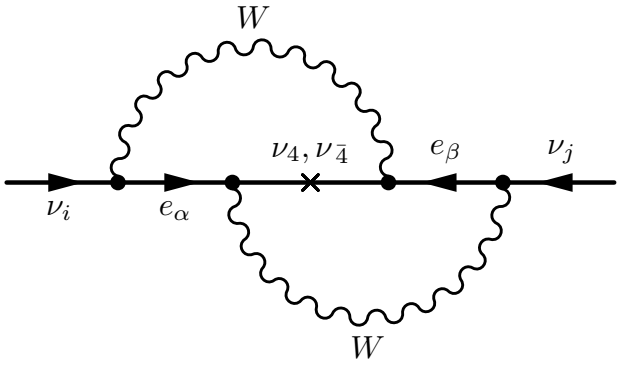

Figure 3. Two-loop diagram generating light neutrino masses in the presence of a Majorana fourth generation.

in that case lepton number is conserved. Also when $m_{\rm D} = 0$ we obtain $(m_\nu)^{(2)}_{ij} = 0$, since then the right-handed neutrino decouples completely and lepton number is again conserved.

To see more clearly the structure of this mass matrix we can approximate $m_e = m_\mu = m_\tau = 0$; then, since we have chosen $V_{\tau 1} = V_{E1} = V_{E2} = 0$, the only non-vanishing element in $(m_\nu)^{(2)}_{ij}$ is $(m_\nu)^{(2)}_{33}$ and it is proportional to $V^2_{E3} N^2_E m^4_E I_{EE}$. Therefore, the largest contribution to $(m_\nu)^{(2)}$ is given by:

$$\begin{aligned}(m_\nu)^{(2)}_{33} &= -\frac{g^4}{m^4_W} N^2_E (N^2_e + N^2_\mu + N^2_\tau) m_{\rm R} m^2_{\rm D} m^4_E I_{EE} \\ &\approx \frac{g^4}{2(4\pi)^4} (N^2_e + N^2_\mu + N^2_\tau) m_{\rm R} \frac{m^2_{\rm D} m^2_E}{m^4_W} \ln \frac{m_E}{m_{\bar{4}}}\,, \end{aligned} \tag{4.15}$$

where in the last line we have used the approximated expression of the loop integral I_{EE} in the case $m_E \gg m_{4,\bar{4}} \gg m_W$ for definiteness, but other mass relations lead to analogous conclusions. Keeping all the charged lepton masses one can easily show that the eigenvalues of the light neutrino mass matrix are proportional to m^4_μ, m^4_τ, m^4_E which gives a huge hierarchy between neutrino masses. Therefore, as discussed in [23, 26], these radiative corrections cannot explain by themselves the observed spectrum of masses and mixings, although they lead to a strong constraint for this kind of SM extensions which we will analyze in the next section.

5 Phenomenological constraints

5.1 Direct searches

Let us now discuss the constraints that several phenomenological tests impose on the parameters of this minimal four-generation (4G) model. Direct searches for the new heavy leptons can be used to set limits on the Yukawa couplings and the Majorana mass of the $\nu_{\rm R}$. In the case of the heavy charged lepton, searches at LEP [4] yield $m_E > 100.8$ GeV (assuming it decays rapidly to νW; a slightly poorer bound is obtained if the lepton is

JHEP07(2012)030

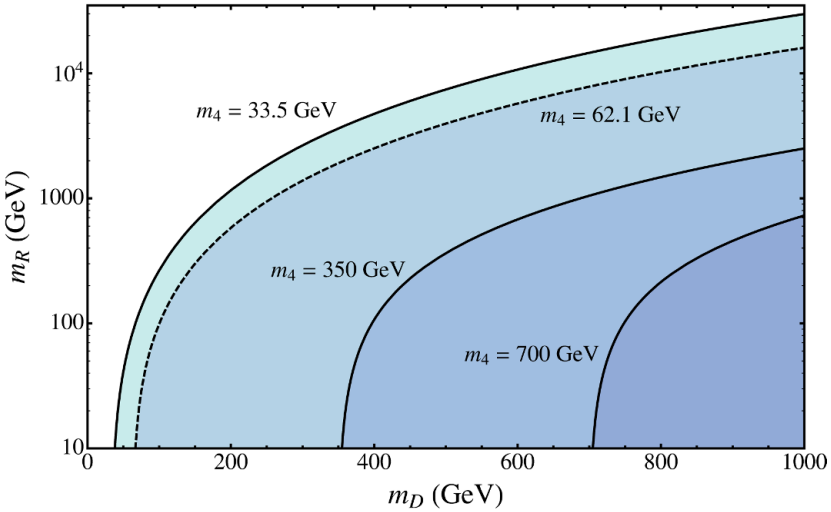

Figure 4. The shaded region shows the allowed values for the Majorana and Dirac masses of the heavy neutrinos given the LEP bound $m_N > 33.5$ GeV on stable neutrinos with both Dirac and Majorana masses. We also display a dashed line in the 62.1 GeV limit for unstable neutrinos. Two more lines are drawn for completeness, giving an idea of the combination of parameters that produces two possible, allowed masses for the lightest heavy neutrino.

long-lived and can be tracked inside the detectors), which can be immediately translated into a bound on the corresponding Yukawa. For the heavy neutrinos, we can have different bounds depending on their stability and the Dirac or Majorana character of their masses [4]: stable neutrinos, for example (understood here as 'stable enough to get out of the detectors after production'), are only constrained by the requirement that they don't show up in the invisible decays of the Z boson. Unstable (visible) neutrinos get tighter bounds due to the non-observation of their decay products. As we are not making any *a priori* assumption about the neutrino mass structure, we will select here the most conservative from this set of bounds; that corresponds to a stable neutrino with both Dirac and Majorana mass terms, for which we demand $m_N > 33.5$ GeV [54]. The weakest bound for an unstable neutrino, which applies if it has again both Dirac and Majorana mass terms, will also be of use; we need in that case $m_N > 62.1$ GeV [20]. As these bounds apply to the physical masses of the neutrinos, which as seen in eqs. (4.10)–(4.12) are nonlinear combinations of the Dirac and Majorana components, we display in figure 4 the translation of the 33.5 and 62.1 GeV bounds into the $m_{\rm D} - m_{\rm R}$ plane, together with several other lines to give an idea of the relations between physical masses and Lagrangian parameters.

As explained in section 4, the neutrino Yukawas y_α encode the mixings between the flavour-eigenstate neutrinos ν_α and the mass eigenstates $\nu_{4,\bar{4}}$. Thus, we can use mixing-mediated LFV processes to constrain the values of the light neutrino Yukawas y_e, y_μ, y_τ. It is important to note, however, that the situation is not the same for 'stable' and unstable neutrinos; so-called stable neutral leptons are constrained to decay outside the detectors, which implies that the mean free path must go beyond $\mathcal{O}$(m). The lightest of our heavy

JHEP07(2012)030

Experimental bounds at 90% C.L. [4, 56]	Constraints on the mixings
$B(\mu \to e\gamma) < 2.4 \times 10^{-12}$	$N_e N_\mu < 2.85 \times 10^{-4}$
$B(\tau \to e\gamma) < 1.85 \times 10^{-7}$	$N_e N_\tau < 0.079$
$B(\tau \to \mu\gamma) < 2.5 \times 10^{-7}$	$N_\mu N_\tau < 0.093$

Table 1. Summary of the constraints derived from low-energy radiative decays.

neutrinos can only decay through mixing (the main channel being $\nu_4 \to \ell_\alpha W$, $\alpha = e, \mu, \tau$, with a possibly virtual W depending on the mass of the ν_4), so this statement is actually a constraint on the Yukawas, implying $y_\alpha \sim N_\alpha \lesssim 10^{-6}$. This constraint is much stronger than any other phenomenolgical bound, and so it ends the discussion for stable neutrinos, which must have very small mixings that won't be observable in low-energy experiments in the near future (see below). For the rest of this section we will consider the case of unstable neutrinos, which present a richer variety of constraints.

5.2 Lepton flavour violation

Let us now discuss the bounds on violation of lepton family number that can shed light on the relevant mixings of our model; the most stringent limits are derived from the non-observation of radiative decays of the form $\ell_\alpha \to \ell_\beta \gamma$.[5] In our model, the ratios for such processes are given by

$$B(\ell_\alpha \to \ell_\beta \gamma) \equiv \frac{\Gamma(\ell_\alpha \to \ell_\beta \gamma)}{\Gamma(\ell_\alpha \to \ell_\beta \nu \bar{\nu})} = \frac{3\alpha}{2\pi} \left| \sum_{a=4,\bar{4}} U_{\beta a} U^*_{\alpha a} \, H\left(m_a^2/m_W^2\right) \right|^2 , \tag{5.1}$$

where $H(x)$ is a loop function that can be found in [53], and the sum proceeds over all the heavy neutrinos[6] (one in the Dirac case, two if they are Majorana). The weakest bounds are obtained if only one neutrino with light mass runs inside the loop; this corresponds either to the Dirac limit with a low mass or to a hard see-saw limit, with the heavy neutrino almost decoupled due to its small mixing. We will assume this scenario in our calculations in order to produce conservative bounds. Table 1 summarises the experimental limits and the constraints that can be extracted from these processes.

5.3 Universality tests

A second class of constraints upon family mixing arises from the tests of universality in weak interactions. For our purposes, these are either direct comparison of decay rates of one particle into two different weak-mediated channels, or comparison of the decay rates of two different particles into the same channel.[7] If the weak couplings are to be the

[5] Bounds obtained from present data on μ–e conversion in nuclei [4] are of the same order. However, there are plans to improve the sensitivity in μ–e conversion in 4 and even 6 orders of magnitude [55], therefore we expect from this process much stronger bounds in the future.

[6] Note this expression contains the contributions from the light neutrinos; by using unitarity of the mixing matrix, they are included in the definition of $H(x)$.

[7] Data from neutrino oscillations can also be used to constrain the elements of the leptonic mixing matrix [57], however, they lead to weaker bounds than the ones obtained here.

JHEP07(2012)030

Experimental bounds at 90% C.L. [4]	Constraints on the mixings
$\frac{R_{\pi\to e/\pi\to\mu}}{R^{\rm SM}_{\pi\to e/\pi\to\mu}} = 0.996 \pm 0.005$	$N_e^2 - N_\mu^2 = 0.004 \pm 0.005$
$\frac{R_{\tau\to e/\tau\to\mu}}{R^{\rm SM}_{\tau\to e/\tau\to\mu}} = 1.000 \pm 0.007$	$N_e^2 - N_\mu^2 = 0.000 \pm 0.007$
$\frac{R_{\tau\to e/\mu\to e}}{R^{\rm SM}_{\tau\to e/\mu\to e}} = 1.003 \pm 0.007$	$N_\mu^2 - N_\tau^2 = 0.003 \pm 0.007$
$\frac{R_{\tau\to\mu/\mu\to e}}{R^{\rm SM}_{\tau\to\mu/\mu\to e}} = 1.001 \pm 0.007$	$N_e^2 - N_\tau^2 = 0.001 \pm 0.007$

Table 2. Summary of the constraints derived from universality tests in weak decays. The ratios marked as "SM" represent the theoretical predictions of a 3G Standard Model.

same for all families these rates should differ only in known kinematic factors or calculable higher-order corrections. The relevant ratios are:

$$R_{\pi\to e/\pi\to\mu} \equiv \frac{\Gamma(\pi\to e\nu)}{\Gamma(\pi\to\mu\nu)}\,, \qquad R_{\tau\to\mu/\tau\to e} \equiv \frac{\Gamma(\tau\to\mu\nu\bar{\nu})}{\Gamma(\tau\to e\nu\bar{\nu})}\,,$$
$$R_{\tau\to e/\mu\to e} \equiv \frac{\Gamma(\tau\to e\nu\bar{\nu})}{\Gamma(\mu\to e\nu\bar{\nu})}\,, \qquad R_{\tau\to\mu/\mu\to e} \equiv \frac{\Gamma(\tau\to\mu\nu\bar{\nu})}{\Gamma(\mu\to e\nu\bar{\nu})}\,,$$

and their theoretical values in a 3G SM can be consulted, for example, in [58]. Comparison of the experimental values and the 3G predictions yields values very close to 1, as can be seen in table 2; in our 4G model, family mixing induces deviations from this behaviour that must be kept under control. Essentially, these deviations result from the fact that the flavour-eigenstate neutrinos ν_e, ν_μ, ν_τ have a small component of the heavy neutrinos $\nu_4, \nu_{\bar{4}}$, which cannot be produced in the decays of pions, taus or muons; the corresponding mixings N_e, N_μ, N_τ are then forced to be small. In table 2 we also show the constraints that this processes impose on the mixing parameters.

In figure 5 we collect all the relevant LFV constraints from tables 1 and 2. As can be read from the graphs, the final bounds we can set on the mixings of the light families are

$$\begin{aligned} N_e &< 0.08 \\ N_\mu &< 0.03 \\ N_\tau &< 0.3 \end{aligned} \tag{5.2}$$

5.4 Light neutrino masses

Finally, there is a further constraint that can be set upon the mixings of the model: as explained in section 4, the two-loop mechanism which gives small Majorana masses for the light neutrinos cannot explain by itself the observed pattern of masses in this simple model; it, nevertheless, still has the potential to generate *too large* masses, which would exclude the model. Of course, one could always invoke cancellations between these two-loop masses and other contributions (for example, the Weinberg operator), but we think

JHEP07(2012)030

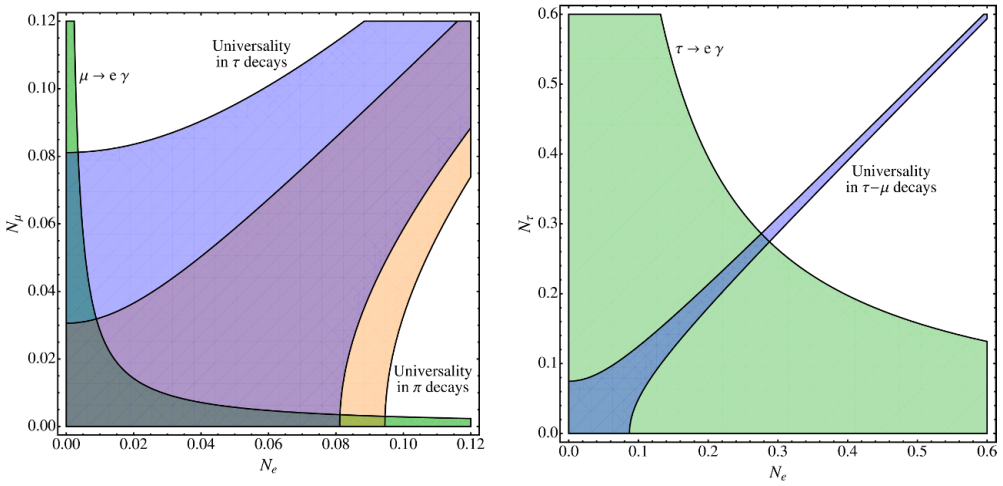

Figure 5. These two graphs present the allowed regions for the mixing parameters in our model at 90% confidence level, according to several LFV tests. The left plot displays the constraints in the $N_e - N_\mu$ plane, which are much more stringent and suffice to bound both N_e and N_μ. The right plot displays the $N_e - N_\tau$ plane; the $N_\mu - N_\tau$ plane offers slighly poorer constraints and is not displayed.

that this wouldn't be a natural situation and choose not to consider it. If we bar such cancellations we need to impose that the two-loop masses don't go above some limit, and thus a bound can be set upon the parameters that participate in the two-loop mechanism, essentially the mixings and the Majorana mass, as seen in equation (4.14). Figure 6 shows the allowed regions for this constraint; the curves are constructed using the lowest possible values of the fourth-generation Dirac masses, in order to provide conservative limits (this implies using a different value of m_{D} for each m_{R}, as we must also impose that m_4 is above 62.1 GeV). We show two possible limits: $m_\nu^{(2)} < 0.05$ eV ensures that the largest two-loop mass is below the atmospheric mass scale; this, of course, does not guarantee that it doesn't distort the neutrino spectrum, which may contain smaller masses, so this bound can be contemplated as rather conservative (particular models may need to impose a stronger bound to be phenomenologically viable). An even more conservative constraint is obtained if we impose $m_\nu^{(2)} < 0.3$ eV, meaning that the largest of the two-loop masses is not above the bound imposed by cosmology to each mass of the degenerate spectrum, $\sum_k m_k \lesssim 1\,\mathrm{eV}$ [59, 60]. Two-loop masses as large as 0.3 eV will in most cases spoil the structure of neutrino masses, but there may be pathological cases in which such situation is allowed (for example, if the Weinberg operator generates a massless neutrino and two massive ones near the 0.3 eV limit; then the two-loop diagram might provide the third mass to fit the mass splittings). Even with these conservative assumptions, the two-loop bound proves to be much stronger than those derived from universality and LFV for most of the parameter space. It is, therefore, a limit to be kept in mind when considering 4G models with Majorana neutrinos.

JHEP07(2012)030

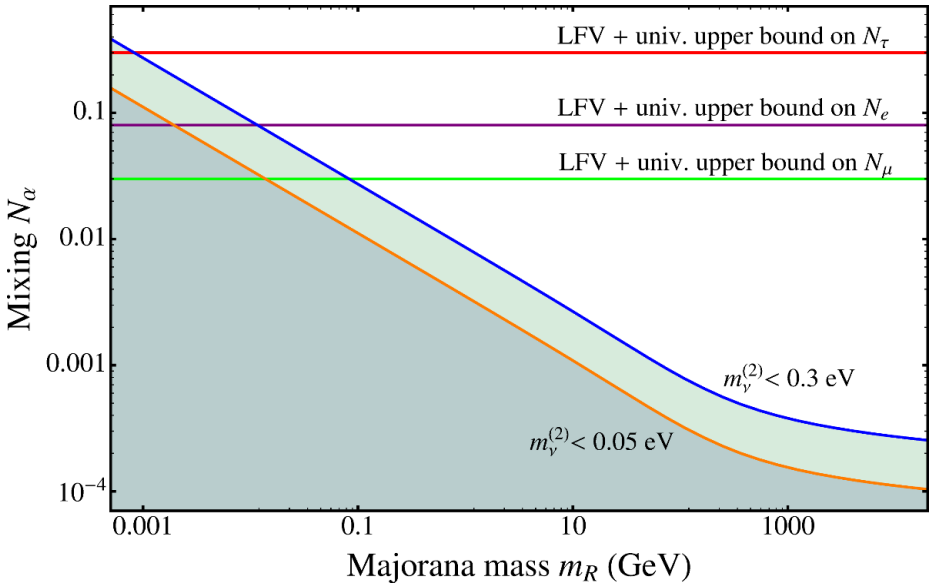

Figure 6. Summary of the constraints on the mixings of the model, as defined in equation (4.5). The three horizontal lines present the upper bounds in equation (5.2), derived from universality tests and limits on LFV processes. The two shaded areas display the allowed region derived from the fact that the two-loop diagram does not disturb the correct structure for the light neutrino masses, assumed to arise from any other mechanism. This last bound applies to any of the mixings.

5.5 Neutrinoless double beta decay ($0\nu2\beta$)

In our framework, the contributions to the amplitude of neutrinoless double beta decay ($0\nu2\beta$) can be written as:

$$A = A_L + A_{\rm md} + A_4\,, \tag{5.3}$$

where A_L stands for the light neutrino contribution (i.e., neutrino masses $m_k \ll p_{\rm eff} \sim 100$ MeV), given by

$$A_L \propto \sum_k^{\rm light} m_k U_{ek}^2 M^{0\nu2\beta}(m_k) \simeq m_{ee} M^{0\nu2\beta}(0)\,, \tag{5.4}$$

with $M^{0\nu2\beta}(0) \propto 1/p_{\rm eff}^2$ the nuclear matrix element. The cosmology upper bound on the sum of neutrino masses, $\sum_k m_k \lesssim 1\,$eV [59, 60], combined with neutrino oscillation data, leads to an upper limit on each neutrino mass $m_k \lesssim 0.3\,$eV and on the element of the neutrino mass matrix relevant to $0\nu2\beta$ decay, $m_{ee} \lesssim 0.3\,$eV.

$A_{\rm md}$ represents the additional, model dependent contribution due to the unknown physics which generates the three light neutrino masses parametrized by the Weinberg operator. We assume that this last term is negligible compared to A_L, as it is the case if the underlying mechanism for neutrino masses is any of the standard three see-saw types [61].

JHEP07(2012)030

We focus then on the contribution from the fourth-generation neutrinos $(\nu_4, \nu_{\bar{4}})$, given by

$$\begin{aligned} A_4 &\propto N_e^2 \left(m_4 \cos^2\theta M^{0\nu2\beta}(m_4) - m_{\bar{4}} \sin^2\theta M^{0\nu2\beta}(m_{\bar{4}}) \right) \\ &\propto N_e^2 \left(\frac{\cos^2\theta}{m_4} - \frac{\sin^2\theta}{m_{\bar{4}}} \right) = N_e^2 \frac{m_{\bar{4}}^2 - m_4^2}{m_4 m_{\bar{4}} (m_4 + m_{\bar{4}})} = N_e^2 \frac{m_{\rm R}}{m_{\rm D}^2} \,, \end{aligned} \tag{5.5}$$

where we have used that $M^{0\nu2\beta}(m_a) \propto 1/m_a^2$ for $a = 4, \bar{4}$, $\tan^2\theta = m_4/m_{\bar{4}}$, $m_4 m_{\bar{4}} = m_{\rm D}^2$ and $m_{\bar{4}} - m_4 = m_{\rm R}$. From eqs. (5.4) and (5.5) we see that the fourth-generation neutrino contribution to the $0\nu2\beta$ amplitude can be dominant provided $N_e^2 m_{\rm R}/m_{\rm D}^2 > m_{ee}/(100\,{\rm MeV})^2$. Notice, in fact, that the value of m_{ee} could be zero if normal hierarchy is realised and the neutrino phases have the appropriate values; in this extreme case the only contribution would be that of the fourth generation, which would dominate $0\nu2\beta$.

Now we can exploit the dependence on $N_e^2 m_{\rm R}$ of both A_4 and $(m_\nu)_{33}^{(2)}$ in eq. (4.15) to constrain the fourth-generation neutrino contribution to the $0\nu2\beta$ decay amplitude,[8] namely

$$A_4 \leq \left(\frac{4\pi m_W}{g m_{\rm D}} \right)^4 \frac{2(m_\nu)_{33}^{(2)}}{m_E^2 \ln \frac{m_E}{m_{\bar{4}}}} \lesssim 190 (m_\nu)_{33}^{(2)} \left(\frac{50\,{\rm GeV}}{m_{\rm D}} \right)^4 {\rm GeV}^{-1} \,, \tag{5.6}$$

where we have taken into account the LEP limit, $m_E \gtrsim 100\,{\rm GeV}$ and set $\ln(m_E/m_{\bar{4}}) \simeq 1$. From this equation, it is clear that the largest fourth-generation contributions to the amplitude A_4 correspond to a small Dirac neutrino mass, $m_{\rm D}$. Imposing that the two-loop mass matrix element $(m_\nu)_{33}^{(2)}$ is below the cosmology upper bound, 0.3 eV, we obtain $A_4 < 6 \times 10^{-8} (50\,{\rm GeV}/m_{\rm D})^4\,{\rm GeV}^{-1}$, while if we require that the two-loop contribution is at most the atmospheric mass scale, 0.05 eV, we find $A_4 < 10^{-8} (50\,{\rm GeV}/m_{\rm D})^4\,{\rm GeV}^{-1}$. On the other hand, the non-observation of $0\nu2\beta$ implies that $A_4 < 10^{-8}\,{\rm GeV}^{-1}$ [62], while future sensitivity is expected to improve this limit one order of magnitude. Bringing these two results together, we see that, once the constraint from light neutrino masses is taken into account, the contribution of the fourth-generation neutrinos to the $0\nu2\beta$ decay amplitude can reach observable values only in the small region of parameter space $m_{\rm D} \lesssim 100$ GeV (see figure 4), even though it is the dominant one for a larger set of allowed masses and mixings.

5.6 Four generations and the Higgs boson

It is well known that due to the presence of a new generation there is an enhancement of the Higgs-gluon-gluon vertex, which arises from a triangle diagram with all quarks running in the loop. This vertex is enhanced approximately by a factor 3 in the presence of a heavy fourth generation, therefore the Higgs production cross section through gluon fusion at the LHC is enhanced by a factor of 9. However, Higgs decay channels are also strongly modified, in particular the Higgs to gluon decays are equally enhanced, while the $\gamma\gamma$ channel is reduced because of a cancellation between the quark and W contributions. Moreover some of these channels, $\gamma\gamma$ for instance, suffer from important electroweak radiative corrections [63].

[8] Note that $(m_\nu)_{33}^{(2)}$ receives contributions from N_e, N_μ and N_τ, while $0\nu2\beta$ only involves N_e.

JHEP07(2012)030

With the first LHC data, ATLAS and CMS ruled out at 95% C.L the range $120 - 600\,\text{GeV}$ for a SM4 Higgs boson, assuming very large masses for the fourth-generation particles [64]. However, different authors have noticed that if fourth-generation neutrinos are light enough ($m_W/2 \lesssim m_{\nu_4} \lesssim m_W$), the decay mode of the Higgs into fourth-generation neutrinos can be dominant for $m_H \lesssim 2m_W$ [65–68]. Moreover, if the lightest fourth-generation neutrino is long-lived this decay channel is invisible and the excluded range for the SM4 Higgs boson is reduced to $160 - 500\,\text{GeV}$ [67, 68]. In general, if the fourth-generation neutrinos have both Dirac (m_D) and Majorana (m_R) masses, the Higgs can decay to more channels: $\nu_4\nu_4$, $\nu_{\bar{4}}\nu_{\bar{4}}$ and $\nu_4\nu_{\bar{4}}$.

Recently, ATLAS and CMS have analysed new data, including more Higgs decay channels [69, 70], and they have a preliminary low-mass ($\sim 125\,\text{GeV}$) hint of the Higgs boson in several channels.[9] In particular there is an excess in the $\gamma\gamma$ channel with respect to the SM3 prediction. For such a light Higgs, the expected ratio of number of events into $\gamma\gamma$ for SM4 over SM3 is about $1.5 - 2.5$ at leading order [72, 73]. However, a global fit to all relevant observables (Higgs searches and electroweak precision data), assuming Dirac neutrinos and a Higgs mass of 125 GeV, shows that data are better described by the SM3 [74]. On the other hand, as commented above, within the SM4 the cancellations in the $\gamma\gamma$ channel at leading order render next-to-leading order radiative corrections important. These corrections tend to decrease even further the two-photon production rate $\sigma(gg \to H) \times BR(H \to \gamma\gamma)|_{SM4}$. Therefore, were the 125 GeV Higgs hint confirmed, by combining the $\gamma\gamma$, ZZ^*, WW^* and the $f\bar{f}$ channels a perturbative SM4 *with just one SM Higgs doublet* would be excluded, even in the case $m_{\nu_4} < m_W$ [75, 76]. Otherwise, in principle it seems possible that if $m_{\nu_4} \lesssim m_W$ and ν_4 is long-lived, some portion of the low Higgs mass parameter space, previously allowed to be between $114 - 160\,\text{GeV}$, is still allowed by the new data. Moreover, if one does not trust the convergence of perturbation theory in the $\gamma\gamma$ channel and drops it from the global analysis, including Higgs searches, R_b and oblique parameters, the SM4 with Dirac neutrinos is strongly constrained but still viable [77]. Considering neutrino Majorana masses will presumably open up even more the allowed parameter space of the model.

The previous bounds from LEP on the masses of unstable (in collider sense) fourth-generation neutrinos were $m_{\nu_4} > 62.1\,\text{GeV}$. Using CDF inclusive like-sign dilepton analysis, ν_4 masses below m_W can be excluded for Higgs masses up to $2m_W$ [67], therefore in this case the ATLAS and CMS analysis for the Higgs boson still apply, and at least the range $120 - 600\,\text{GeV}$ for a SM4 Higgs boson is excluded.

To know definitely whether the SM4 Higgs boson is excluded or not, we will have to wait for new data and a combined analysis of the different channels, $\gamma\gamma$, ZZ^*, WW^* and $f\bar{f}$, including correctly all radiative corrections. However, even if the SM-like four-generation Higgs is excluded, many possibilities may arise in extensions of a four-generation scenario, for instance, with an extra Higgs doublet (see [78, 79] where the observed signatures of LHC are explained in the framework of 4G two-Higgs-doublet models).

[9] Also Fermilab CDF and D0 have presented some preliminary results pointing to some excess around this mass which can be assigned mainly to $H \to b\bar{b}$ decays in HW and HZ associated production [71].

JHEP07(2012)030

6 Conclusions

We have addressed the question of the generation and nature of neutrino masses in the context of the SM with four families of quarks and leptons.

The three light neutrinos can obtain their masses from a variety of mechanisms with or without new neutral fermions, but the huge hierarchy among such masses and those of the remaining fermions is more naturally explained assuming that they have Majorana nature.

On the other hand, current bounds on fourth-generation neutrino masses imply that, although in principle the same mechanisms are also available, most of them are not natural or provide too small fourth-generation neutrino masses; therefore, we have argued that at least one right-handed neutrino is needed. This would suggest that, contrary to the light neutrinos, fourth-generation ones are naturally Dirac.

However, we have shown that if lepton number is not conserved in the light neutrino sector, the right-handed neutrino must have a Majorana mass term whose size depends on the underlying mechanism for LNV, unless Yukawa couplings of the light leptons to the right-handed neutrino are forbidden. We have estimated the natural size of such Majorana mass term within two frameworks for the light neutrino masses, namely see-saw type I and type II. We have seen that, even if we set it to zero by hand in the Lagrangian at tree level, it is generated at two-loops , and although it depends on the Yukawa couplings and the LNV scale responsible for light neutrino masses, it can be up to the TeV scale. We have developed a model where this Majorana mass is forbidden at tree level by a global symmetry, and it is generated radiatively and finite once this symmetry is broken spontaneously (see appendix A).

We have then considered a minimal four-generation scenario, with neutrino Majorana masses parametrized by the Weinberg operator and one right-handed neutrino $\nu_{\rm R}$, which has Yukawa couplings to the four lepton doublets and non-zero Majorana mass. We have analyzed the phenomenological constraints on the parameter space of such a model, derived from direct searches for four-generation leptons, universality tests, charged lepton flavour-violating processes and neutrinoless double beta decay. We have pointed out that the Majorana mass for the fourth-generation neutrino induces relatively large two-loop contributions to the light neutrino masses, which can easily exceed the atmospheric scale and the cosmological bounds. Indeed, this sets the strongest limits on the masses and mixings of fourth-generation neutrinos, collected in figure 6.

To summarize, in the context of a SM with four generations, we have shown that if light neutrinos are Majorana particles, it is natural that also the fourth-generation neutrino has the Majorana character. We did so by calculating the fourth-neutrino Majorana masses induced by the three light neutrino ones. This has important implications for the neutrino and Higgs sectors of these models, which are being actively tested at the LHC.

JHEP07(2012)030

Acknowledgments

We thank Enrique Fernández-Martínez and Jacobo López-Pavón for fruitful discussions on the matter of neutrinoless double beta decay. This work has been partially supported by the Spanish MICINN under grants FPA-2007-60323, FPA-2008-03373, FPA2011-23897, FPA2011-29678-C02-01, Consolider-Ingenio PAU (CSD2007-00060) and CPAN (CSD2007- 00042) and by Generalitat Valenciana grants PROMETEO/2009/116 and PROMETEO/2009/128. A.A. and J.H.-G. are supported by the MICINN under the FPU program.

A A model for calculable right-handed neutrino masses

In this appendix we present a model which gives a realistic pattern of neutrino masses in the context of the SM with four-generations and in which the right-handed neutrino mass of the fourth generation is generated radiatively and finite. This is an illustration of the general (model-independent) mechanism discussed in section 3 which allowed us to estimate the size of Majorana neutrino masses for the fourth-generation right-handed neutrinos if the three light active neutrinos are Majorana particles.

Let us consider the SM with four generations and four right-handed neutrinos $\nu_{\mathrm{R}i}$ ($i = 1, \cdots, 4$). To implement the ordinary see-saw, we need three of them very heavy while one of them should be much lighter in order to avoid a too light fourth-generation active neutrino. Then, it is natural to require that one of the fourth right-handed neutrino is massless at tree level and let its mass be generated by radiative corrections. For that purpose we add three extra chiral singlets $s_{\mathrm{L}a}$ ($a = 1, \cdots, 3$). In order to break lepton number we will also include a complex scalar singlet σ

We assign lepton number in the following way

$$\ell_j \to e^{i\alpha}\ell_j\,, \quad e_{\mathrm{R}j} \to e^{i\alpha}e_{\mathrm{R}j}\,, \quad \nu_{\mathrm{R}j} \to e^{i\alpha}\nu_{\mathrm{R}j}\,, \quad \sigma \to e^{i\alpha}\sigma\,; \tag{A.1}$$

the $s_{\mathrm{L}a}$ do not carry lepton number. With these assignments and the requirement that lepton number is conserved we have the following Yukawa Lagrangian

$$\mathcal{L}_Y = -\overline{\ell}\, Y_e e_{\mathrm{R}}\phi - \overline{\ell}\, Y_\nu \nu_{\mathrm{R}}\tilde{\phi} - \sigma\, \overline{\nu_{\mathrm{R}}}\, y^*\, s_{\mathrm{L}} - \frac{1}{2}\,\overline{s_{\mathrm{L}}^c} M^* s_{\mathrm{L}} + \mathrm{H.c.}\,, \tag{A.2}$$

where Y_e and Y_ν are the ordinary four-generation Yukawa couplings, y_{ia}, along this appendix, is a general 4×3 matrix while M is a symmetric 3×3 matrix, which without loss of generality can be taken diagonal and positive. We choose the scalar potential in such a way that lepton number is conserved and subsequently spontaneously broken by the VEV of σ, $v_\sigma = \langle\sigma\rangle$. Thus, the model will contain a singlet Majoron. Alternatively, we could also choose to softly break lepton number in the potential to avoid the Majoron without changing the point we would like to illustrate. Before spontaneous symmetry breaking only $s_{\mathrm{L}a}$ are massive. We will take M very large (around GUT scale). After σ gets a VEV (which is somewhat free, but we can take it just a bit below M), we will have a mass

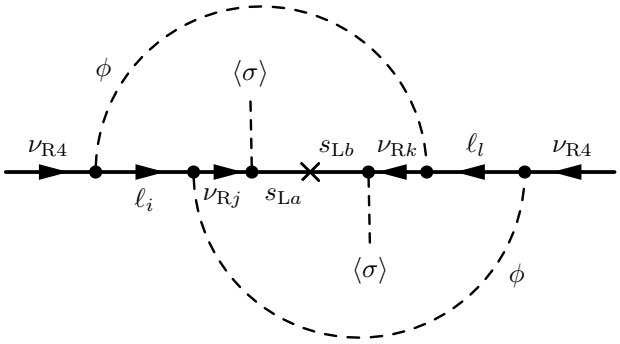

Figure 7. The process which generates masses for the right-handed neutrinos at two loops.

matrix for the combined system $\nu_{\mathrm{R}} - s_{\mathrm{L}}$ of see-saw type. Therefore, if $y\, v_\sigma \ll M$ the four right-handed neutrinos will get a 4×4 Majorana mass matrix

$$M_{\mathrm{R}}^{(0)} \simeq v_\sigma^2\, y M^{-1} y^{\mathrm{T}}\,; \tag{A.3}$$

this is basically the see-saw formula but applied to the right-handed neutrinos and changing the VEV of the Higgs doublet for that of the singlet σ. This matrix has rank 3 and, therefore, only three of the right-handed neutrinos will obtain a tree-level mass. The other neutrino will remain massless at tree level. However, at two loops, due to the mechanism described in section 3, also the fourth right-handed neutrino will acquire a Majorana mass. We depict the diagram giving rise to this mass in figure 7; the diagram is obviously finite by power counting and the generated mass matrix can be estimated as

$$M_{\mathrm{R}}^{(2)} \sim \frac{v_\sigma^2}{(4\pi)^4} \left(Y_\nu^\dagger Y_\nu\right)^{\mathrm{T}} y M^{-1} y^{\mathrm{T}}\, Y_\nu^\dagger Y_\nu \ln\left(\frac{M}{y v_\sigma}\right) \tag{A.4}$$

Since Y_e does not enter in these calculations we can choose a basis in which Y_e is arbitrary but Y_ν is diagonal and real. If we take the logarithm order 1, $\ln\left(\frac{M}{y v_\sigma}\right) \sim 1$, we see that $M_{\mathrm{R}}^{(2)}$ is also projective but in a different direction, given by $y' = \left(Y_\nu^\dagger Y_\nu\right)^{\mathrm{T}} y$; then we can write the full right-handed neutrino mass matrix as

$$M_{\mathrm{R}} \sim v_\sigma^2 \left(y M^{-1} y^{\mathrm{T}} + \frac{1}{(4\pi)^4}\, y' M^{-1} y'^{\mathrm{T}}\right)\,, \tag{A.5}$$

which, in general, has rank 4 and gives a Majorana mass to the fourth right-handed neutrino. To see how it works, let us discuss a simplified example, with the following structure for the s_{L} Yukawas:

$$y = \begin{pmatrix} y_1 & 0 & 0 \\ 0 & y_2 & 0 \\ 0 & 0 & y_3 \\ 0 & 0 & y_4 \end{pmatrix}\,. \tag{A.6}$$

JHEP07(2012)030

Let us also choose M diagonal and with elements M_i; then, at tree level we obtain an almost diagonal mass matrix,

$$M_{\rm R}^{(0)} = v_\sigma^2 \begin{pmatrix} \frac{y_1^2}{M_1} & 0 & 0 & 0 \\ 0 & \frac{y_2^2}{M_2} & 0 & 0 \\ 0 & 0 & \frac{y_3^2}{M_3} & \frac{y_3 y_4}{M_3} \\ 0 & 0 & \frac{y_3 y_4}{M_3} & \frac{y_4^2}{M_3} \end{pmatrix} , \tag{A.7}$$

which has a zero eigenvalue. At two loops we will have

$$M_{\rm R}^{(2)} = \frac{v_\sigma^2}{(4\pi)^4} \begin{pmatrix} \frac{y_1'^2}{M_1} & 0 & 0 & 0 \\ 0 & \frac{y_2'^2}{M_2} & 0 & 0 \\ 0 & 0 & \frac{y_3'^2}{M_3} & \frac{y_3' y_4'}{M_3} \\ 0 & 0 & \frac{y_3' y_4'}{M_3} & \frac{y_4'^2}{M_3} \end{pmatrix} , \tag{A.8}$$

with $y_i' = y_i {(Y_\nu)_i}^2$, and $(Y_\nu)_i$ the diagonal elements of Y_ν. $M_{\rm R}^{(2)}$ has also rank 3. However, the sum of $M_{\rm R}^{(0)}$ and $M_{\rm R}^{(2)}$ has rank 4, and the fourth $\nu_{\rm R}$ acquires a mass. We can estimate it by considering $M_{\rm R}^{(2)}$ a small perturbation to $M_{\rm R}^{(0)}$ and find that

$$m_{\rm R4} \sim \frac{v_\sigma^2}{(4\pi)^4 M_3} \frac{y_4^2\, y_3^2}{y_3^2 + y_4^2} \left((Y_\nu)_4^2 - (Y_\nu)_3^2 \right)^2 , \tag{A.9}$$

while the mass of the third right-handed neutrino is of order (the other two are also order $y^2 v_\sigma^2/M$ as can be seen from the mass matrix)

$$m_{\rm R3} \sim (y_3^2 + y_4^2)\, \frac{v_\sigma^2}{M_3} . \tag{A.10}$$

Therefore, if we rewrite the fourth-generation right-handed neutrino mass $m_{\rm R4}$ in terms of $m_{\rm R3}$ we have

$$m_{\rm R4} \sim \frac{m_{\rm R3}}{(4\pi)^4} \frac{y_4^2\, y_3^2}{(y_3^2 + y_4^2)^2} \left((Y_\nu)_4^2 - (Y_\nu)_3^2 \right)^2 , \tag{A.11}$$

which is roughly the structure that one would expect from the effective theory obtained by integrating the new fermions $s_{{\rm L}a}$, *i.e*, $m_{\rm R4}$ obtains a contribution proportional to the heavy right-handed Majorana masses $m_{\rm R3}$ suppressed by a two-loop factor and Yukawa couplings. After all, the diagram in figure 7 reduces to the diagram in figure 1 when the fermion lines of $s_{{\rm L}a}$ are contracted to a point. The result also shows that, as expected, the exact coefficient depends on the details of the model. These expressions could be generalized to a more general structure of Yukawa couplings, leading to similar, although more complicated expressions.

As for other features of this model, we will just mention that as lepton number is broken spontaneously, a Majoron will appear. Since the Majoron is a singlet and v_σ is large their couplings to standard model particles are suppressed and, therefore, this Majoron should not create any problem. On the other hand, it could have some advantages in cosmological contexts; if lepton number is also broken softly (for instance with a mass term σ^2) the

JHEP07(2012)030

Majoron will become a massive pseudo-Majoron, which could constitute a good dark matter candidate.

In any case, this simple example illustrates how the general mechanism discussed in section 3 works in a complete renormalizable model; if m_{R4} is zero at tree level and light neutrinos are Majorana (therefore lepton number is not conserved), in general m_{R4} will be generated at two-loops with the behaviour discussed in section 3.

References

[1] B. Holdom et al., *Four Statements about the Fourth Generation*, *PMC Phys.* **A 3** (2009) 4 [arXiv:0904.4698] [INSPIRE].

[2] W.-S. Hou, *Source of CP-violation for the Baryon Asymmetry of the Universe*, *Chin. J. Phys.* **47** (2009) 134 [arXiv:0803.1234] [INSPIRE].

[3] J.I. Silva-Marcos, *Symmetries, large leptonic mixing and a fourth generation*, *JHEP* **12** (2002) 036 [hep-ph/0204217] [INSPIRE].

[4] Particle Data Group collaboration, K. Nakamura et al., *Review of particle physics*, *J. Phys.* **G 37** (2010) 075021 [INSPIRE].

[5] H.-J. He, N. Polonsky and S.-f. Su, *Extra families, Higgs spectrum and oblique corrections*, *Phys. Rev.* **D 64** (2001) 053004 [hep-ph/0102144] [INSPIRE].

[6] V. Novikov, A. Rozanov and M. Vysotsky, *Once more on extra quark-lepton generations and precision measurements*, *Phys. Atom. Nucl.* **73** (2010) 636 [arXiv:0904.4570] [INSPIRE].

[7] M. Gonzalez-Garcia and M. Maltoni, *Phenomenology with Massive Neutrinos*, *Phys. Rept.* **460** (2008) 1 [arXiv:0704.1800] [INSPIRE].

[8] P. Minkowski, $\mu \to e\gamma$ *at a Rate of One Out of 1-Billion Muon Decays?*, *Phys. Lett.* **B 67** (1977) 421 [INSPIRE].

[9] M. Gell-Mann, P. Ramond and R. Slansky, *Complex Spinors and Unified Theories*, *Conf. Proc.* **C790927** (1979) 315 [INSPIRE].

[10] T. Yanagida, *Horizontal Symmetry and Masses of Neutrinos*, *Conf. Proc.* **C7902131** (1979) 95 [INSPIRE].

[11] R.N. Mohapatra and G. Senjanović, *Neutrino Mass and Spontaneous Parity Violation*, *Phys. Rev. Lett.* **44** (1980) 912 [INSPIRE].

[12] A. Zee, *A Theory of Lepton Number Violation, Neutrino Majorana Mass and Oscillation*, *Phys. Lett.* **B 93** (1980) 389 [*Erratum ibid.* **B 95** (1980) 461] [INSPIRE].

[13] A. Zee, *Quantum numbers of Majorana neutrino masses*, *Nucl. Phys.* **B 264** (1986) 99 [INSPIRE].

[14] K. Babu, *Model of 'Calculable' Majorana Neutrino Masses*, *Phys. Lett.* **B 203** (1988) 132 [INSPIRE].

[15] E. Ma, *Verifiable radiative seesaw mechanism of neutrino mass and dark matter*, *Phys. Rev.* **D 73** (2006) 077301 [hep-ph/0601225] [INSPIRE].

[16] K. Babu and E. Ma, *Natural Hierarchy of Radiatively Induced Majorana Neutrino Masses*, *Phys. Rev. Lett.* **61** (1988) 674 [INSPIRE].

JHEP07(2012)030

[17] K. Babu, E. Ma and J.T. Pantaleone, *Model of Radiative Neutrino Masses: Mixing and a Possible Fourth Generation*, *Phys. Lett.* **B 218** (1989) 233 [INSPIRE].

[18] C. Hill and E. Paschos, *A Naturally Heavy Fourth Generation Neutrino*, *Phys. Lett.* **B 241** (1990) 96 [INSPIRE].

[19] R. Mohapatra and X. Zhang, *Restrictions on B-L symmetry breaking implied by a fourth generation neutrino*, *Phys. Lett.* **B 305** (1993) 106 [hep-ph/9301286] [INSPIRE].

[20] L.M. Carpenter and A. Rajaraman, *Revisiting Constraints on Fourth Generation Neutrino Masses*, *Phys. Rev.* **D 82** (2010) 114019 [arXiv:1005.0628] [INSPIRE].

[21] A. Rajaraman and D. Whiteson, *Tevatron Discovery Potential for Fourth Generation Neutrinos: Dirac, Majorana and Everything in Between*, *Phys. Rev.* **D 82** (2010) 051702 [arXiv:1005.4407] [INSPIRE].

[22] A. Lenz, H. Pas and D. Schalla, *Constraints on fourth generation Majorana neutrinos*, *J. Phys. Conf. Ser.* **259** (2010) 012096 [arXiv:1010.3883] [INSPIRE].

[23] A. Aparici, J. Herrero-Garcia, N. Rius and A. Santamaria, *Neutrino masses from new generations*, *JHEP* **07** (2011) 122 [arXiv:1104.4068] [INSPIRE].

[24] A. Lenz, H. Pas and D. Schalla, *Fourth Generation Majorana Neutrinos*, *Phys. Rev.* **D 85** (2012) 075025 [arXiv:1104.2465] [INSPIRE].

[25] M.A. Schmidt and A.Y. Smirnov, *Neutrino Masses and a Fourth Generation of Fermions*, *Nucl. Phys.* **B 857** (2012) 1 [arXiv:1110.0874] [INSPIRE].

[26] A. Aparici, J. Herrero-Garcia, N. Rius and A. Santamaria, *Implications of new generations on neutrino masses*, arXiv:1110.0663 [INSPIRE].

[27] S. Petcov and S. Toshev, *Conservation of lepton charges, massive Majorana and massless neutrinos*, *Phys. Lett.* **B 143** (1984) 175 [INSPIRE].

[28] G. Branco, W. Grimus and L. Lavoura, *The seesaw mechanism in the presence of a conserved lepton number*, *Nucl. Phys.* **B 312** (1989) 492 [INSPIRE].

[29] W. Grimus and H. Neufeld, *Radiative neutrino masses in an* SU(2) × U(1) *model*, *Nucl. Phys.* **B 325** (1989) 18 [INSPIRE].

[30] S. Weinberg, *Baryon and Lepton Nonconserving Processes*, *Phys. Rev. Lett.* **43** (1979) 1566 [INSPIRE].

[31] H. Weldon and A. Zee, *Operator analysis of new physics*, *Nucl. Phys.* **B 173** (1980) 269 [INSPIRE].

[32] P. Ramond, *The Family Group in Grand Unified Theories*, hep-ph/9809459 [INSPIRE].

[33] W. Konetschny and W. Kummer, *Nonconservation of Total Lepton Number with Scalar Bosons*, *Phys. Lett.* **B 70** (1977) 433 [INSPIRE].

[34] T. Cheng and L.-F. Li, *Neutrino Masses, Mixings and Oscillations in* SU(2) × U(1) *Models of Electroweak Interactions*, *Phys. Rev.* **D 22** (1980) 2860 [INSPIRE].

[35] G. Lazarides, Q. Shafi and C. Wetterich, *Proton Lifetime and Fermion Masses in an* SO(10) *Model*, *Nucl. Phys.* **B 181** (1981) 287 [INSPIRE].

[36] M. Magg and C. Wetterich, *Neutrino mass problem and gauge hierarchy*, *Phys. Lett.* **B 94** (1980) 61 [INSPIRE].

JHEP07(2012)030

[37] J. Schechter and J. Valle, *Neutrino Masses in* SU(2) × U(1) *Theories*, *Phys. Rev.* **D 22** (1980) 2227 [INSPIRE].

[38] S. Kanemura and K. Yagyu, *Radiative corrections to electroweak parameters in the Higgs triplet model and implication with the recent Higgs boson searches*, arXiv:1201.6287 [INSPIRE].

[39] F. del Aguila, J. Aguilar-Saavedra, J. de Blas and M. Pérez-Victoria, *Electroweak constraints on see-saw messengers and their implications for LHC*, arXiv:0806.1023 [INSPIRE].

[40] R. Foot, H. Lew, X. He and G.C. Joshi, *Seesaw neutrino masses induced by a triplet of leptons*, *Z. Phys.* **C 44** (1989) 441 [INSPIRE].

[41] E. Ma and D. Roy, *Heavy triplet leptons and new gauge boson*, *Nucl. Phys.* **B 644** (2002) 290 [hep-ph/0206150] [INSPIRE].

[42] C. Aulakh and R.N. Mohapatra, *Neutrino as the Supersymmetric Partner of the Majoron*, *Phys. Lett.* **B 119** (1982) 136 [INSPIRE].

[43] L.J. Hall and M. Suzuki, *Explicit R-Parity Breaking in Supersymmetric Models*, *Nucl. Phys.* **B 231** (1984) 419 [INSPIRE].

[44] I.-H. Lee, *Lepton Number Violation in Softly Broken Supersymmetry*, *Phys. Lett.* **B 138** (1984) 121 [INSPIRE].

[45] I.-H. Lee, *Lepton Number Violation in Softly Broken Supersymmetry. 2.*, *Nucl. Phys.* **B 246** (1984) 120 [INSPIRE].

[46] J.R. Ellis, G. Gelmini, C. Jarlskog, G.G. Ross and J. Valle, *Phenomenology of Supersymmetry with Broken R-Parity*, *Phys. Lett.* **B 150** (1985) 142 [INSPIRE].

[47] G.G. Ross and J. Valle, *Supersymmetric Models Without R-Parity*, *Phys. Lett.* **B 151** (1985) 375 [INSPIRE].

[48] S. Dawson, *R-Parity Breaking in Supersymmetric Theories*, *Nucl. Phys.* **B 261** (1985) 297 [INSPIRE].

[49] A. Santamaria and J. Valle, *Spontaneous R-Parity Violation in Supersymmetry: A Model for Solar Neutrino Oscillations*, *Phys. Lett.* **B 195** (1987) 423 [INSPIRE].

[50] A. Masiero and J. Valle, *A model for spontaneous R parity breaking*, *Phys. Lett.* **B 251** (1990) 273 [INSPIRE].

[51] M. Hirsch, M. Diaz, W. Porod, J. Romao and J. Valle, *Neutrino masses and mixings from supersymmetry with bilinear R parity violation: A Theory for solar and atmospheric neutrino oscillations*, *Phys. Rev.* **D 62** (2000) 113008 [*Erratum ibid.* **D 65** (2002) 119901] [hep-ph/0004115] [INSPIRE].

[52] R. Barbier et al., *R-parity violating supersymmetry*, *Phys. Rept.* **420** (2005) 1 [hep-ph/0406039] [INSPIRE].

[53] A.J. Buras, B. Duling, T. Feldmann, T. Heidsieck and C. Promberger, *Lepton Flavour Violation in the Presence of a Fourth Generation of Quarks and Leptons*, *JHEP* **09** (2010) 104 [arXiv:1006.5356] [INSPIRE].

[54] L.M. Carpenter, *Fourth Generation Lepton Sectors with Stable Majorana Neutrinos: From LEP to LHC*, arXiv:1010.5502 [INSPIRE].

[55] COMET collaboration, E.V. Hungerford, *COMET/PRISM muon to electron conversion at J-PARC*, *AIP Conf. Proc.* **1182** (2009) 694 [INSPIRE].

JHEP07(2012)030

[56] MEG collaboration, J. Adam et al., *New limit on the lepton-flavour violating decay $\mu^+ \to e^+\gamma$*, *Phys. Rev. Lett.* **107** (2011) 171801 [arXiv:1107.5547] [INSPIRE].

[57] S. Antusch, C. Biggio, E. Fernandez-Martinez, M. Gavela and J. Lopez-Pavon, *Unitarity of the Leptonic Mixing Matrix*, *JHEP* **10** (2006) 084 [hep-ph/0607020] [INSPIRE].

[58] A. Pich, *Lepton universality*, *NATO Adv. Study Inst. Ser. B Phys.* **363** (1997) 173 [hep-ph/9701263] [INSPIRE].

[59] S. Hannestad, A. Mirizzi, G.G. Raffelt and Y.Y. Wong, *Neutrino and axion hot dark matter bounds after WMAP-7*, *JCAP* **08** (2010) 001 [arXiv:1004.0695] [INSPIRE].

[60] M. Gonzalez-Garcia, M. Maltoni and J. Salvado, *Robust Cosmological Bounds on Neutrinos and their Combination with Oscillation Results*, *JHEP* **08** (2010) 117 [arXiv:1006.3795] [INSPIRE].

[61] M. Blennow, E. Fernandez-Martinez, J. Lopez-Pavon and J. Menendez, *Neutrinoless double beta decay in seesaw models*, *JHEP* **07** (2010) 096 [arXiv:1005.3240] [INSPIRE].

[62] H. Pas, M. Hirsch, H. Klapdor-Kleingrothaus and S. Kovalenko, *A Superformula for neutrinoless double beta decay. 2. The Short range part*, *Phys. Lett.* **B 498** (2001) 35 [hep-ph/0008182] [INSPIRE].

[63] A. Denner et al., *Higgs production and decay with a fourth Standard-Model-like fermion generation*, *Eur. Phys. J.* **C 72** (2012) 1992 [arXiv:1111.6395] [INSPIRE].

[64] ATLAS collaboration, *Combined Standard Model Higgs boson searches with up to* 2.3fb^{-1} *of pp collisions at* $\sqrt{s} = 7$ *TeV at the LHC*, ATLAS-CONF-2011-157 (2011).

[65] K. Belotsky, D. Fargion, M. Khlopov, R. Konoplich and K. Shibaev, *Invisible Higgs boson decay into massive neutrinos of fourth generation*, *Phys. Rev.* **D 68** (2003) 054027 [hep-ph/0210153] [INSPIRE].

[66] W.-Y. Keung and P. Schwaller, *Long Lived Fourth Generation and the Higgs*, *JHEP* **06** (2011) 054 [arXiv:1103.3765] [INSPIRE].

[67] L.M. Carpenter and D. Whiteson, *Higgs Decays to Unstable Neutrinos: Collider Constraints from Inclusive Like-Sign Dilepton Searches*, arXiv:1107.2123 [INSPIRE].

[68] S. Cetin, T. Cuhadar-Donszelmann, M. Sahin, S. Sultansoy and G. Unel, *Impact of the relatively light fourth family neutrino on the Higgs boson search*, *Phys. Lett.* **B 710** (2012) 328 [arXiv:1108.4071] [INSPIRE].

[69] ATLAS collaboration, G. Aad et al., *Combined search for the Standard Model Higgs boson using up to* 4.9fb^{-1} *of pp collision data at* $\sqrt{s} = 7$ *TeV with the ATLAS detector at the LHC*, *Phys. Lett.* **B 710** (2012) 49 [arXiv:1202.1408] [INSPIRE].

[70] CMS collaboration, S. Chatrchyan et al., *Combined results of searches for the standard model Higgs boson in pp collisions at* $\sqrt{s} = 7$ *TeV*, *Phys. Lett.* **B 710** (2012) 26 [arXiv:1202.1488] [INSPIRE].

[71] TEVNPH (Tevatron New Phenomina and Higgs Working Group), CDF, D0 collaborations, *Combined CDF and D0 measurement of WZ and ZZ production in final states with b-tagged jets*, arXiv:1203.3782 [INSPIRE].

[72] G. Guo, B. Ren and X.-G. He, *LHC Evidence Of A 126 GeV Higgs Boson From* $H \to \gamma\gamma$ *With Three And Four Generations*, arXiv:1112.3188 [INSPIRE].

JHEP07(2012)030

[73] X. Ruan and Z. Zhang, *Impact on the Higgs Production Cross Section and Decay Branching Fractions of Heavy Quarks and Leptons in a Fourth Generation Model*, arXiv:1105.1634 [INSPIRE].

[74] O. Eberhardt et al., *Joint analysis of Higgs decays and electroweak precision observables in the Standard Model with a sequential fourth generation*, arXiv:1204.3872 [INSPIRE].

[75] A. Djouadi and A. Lenz, *Sealing the fate of a fourth generation of fermions*, arXiv:1204.1252 [INSPIRE].

[76] E. Kuflik, Y. Nir and T. Volansky, *Implications of Higgs Searches on the Four Generation Standard Model*, arXiv:1204.1975 [INSPIRE].

[77] M. Buchkremer, J.-M. Gerard and F. Maltoni, *Closing in on a perturbative fourth generation*, arXiv:1204.5403 [INSPIRE].

[78] N. Chen and H.-J. He, *LHC Signatures of Two-Higgs-Doublets with Fourth Family*, *JHEP* **04** (2012) 062 [arXiv:1202.3072] [INSPIRE].

[79] L. Bellantoni, J. Erler, J.J. Heckman and E. Ramirez-Homs, *Masses of a Fourth Generation with Two Higgs Doublets*, arXiv:1205.5580 [INSPIRE].

JHEP07(2012)030

Published for SISSA by Springer

Received: *April 26, 2011*
Revised: *May 30, 2011*
Accepted: *June 27, 2011*
Published: *July 28, 2011*

JHEP07(2011)122

Neutrino masses from new generations

Alberto Aparici, Juan Herrero-García, Nuria Rius and Arcadi Santamaria

Depto. de Física Teòrica, and IFIC, Universidad de Valencia-CSIC,
Edificio de Institutos de Paterna, Apt. 22085, 46071 Valencia, Spain

E-mail: alberto.aparici@uv.es, juan.a.herrero@uv.es, nuria@ific.uv.es, arcadi.santamaria@uv.es

Abstract: We reconsider the possibility that Majorana masses for the three known neutrinos are generated radiatively by the presence of a fourth generation and one right-handed neutrino with Yukawa couplings and a Majorana mass term. We find that the observed light neutrino mass hierarchy is not compatible with low energy universality bounds in this minimal scenario, but all present data can be accommodated with five generations and two right-handed neutrinos. Within this framework, we explore the parameter space regions which are currently allowed and could lead to observable effects in neutrinoless double beta decay, μ–e conversion in nuclei and $\mu \to e\gamma$ experiments. We also discuss the detection prospects at LHC.

Keywords: Beyond Standard Model, Neutrino Physics

ArXiv ePrint: 1104.4068

doi:10.1007/JHEP07(2011)122

Contents

JHEP07(2011)122

1 Introduction

Neutrino oscillation data [1–14] require at least two massive neutrinos with large mixing, providing one of the strongest evidences of physics beyond the Standard Model (SM). However, the new physics scale responsible for neutrino masses is largely unknown. With the starting of the LHC, new physics scales of order TeV will become testable through direct production of new particles, so it is very interesting to explore low-energy scenarios for neutrino masses. Moreover, typically, these scenarios also lead to observable signatures in precision experiments, such as violations of universality, charged lepton flavour violating (LFV) rare decays such as $\ell_i \to \ell_j\gamma$ or μ–e conversion in nuclei, which, being complementary to the LHC measurements, may help to discriminate among different models. Regarding the fundamental question of the neutrino mass nature, Dirac or Majorana, lepton-number-violating low-scale models may give additional contributions to neutrinoless double beta ($0\nu2\beta$) decay process, shedding new light on this issue.

On the other hand, one of the most natural extensions of the SM that has been extensively explored in the last years is the addition of one (or more) sequential generations of quarks and leptons [15]. This extension is very natural and has a rich phenomenology

both at LHC as well as in LFV processes. Moreover, new generations address some of the open questions in the SM and can accommodate emerging hints on new physics (see for instance [16] for a recent review).

Theoretically, apart from simplicity, there are no compelling arguments in favour of only three families. In theories with extra dimensions one can relate the number of families to the topology of the compact extra dimensions or set constraints on the number of chiral families and allowed gauge groups by requiring anomaly cancellation. Then, one can build models to justify only three generations at low energies. However, one could also build other models in order to justify four or more generations. In the SM in four dimensions anomalies cancel within each generation and, therefore, the number of families is in principle free.

From the phenomenological point of view it seems that the most striking argument against new generations is the measurement of the invisible Z-boson decay width, $\Gamma_{\rm inv}$, which effectively counts the number of light degrees of freedom coupled to the Z-boson (lighter than $m_Z/2$) which is very close to 3 [17]. However, if neutrinos from new families are heavy they do not contribute to $\Gamma_{\rm inv}$ and, then, additional generations are allowed. Still, pairs of virtual heavy fermions from new generations contribute to the electroweak parameters and spoil the agreement of the SM with experiment. Global fits of models with additional generations to the electroweak data have been performed [18, 19] and the conclusion is that they favour no more that five generations with appropriate masses for the new particles. Although some controversy exists on the interpretation of the data (see for instance [20]) most of the fits make some simplifying assumptions on the mass spectrum of the new generations and do not consider Majorana neutrino masses for the new generations or the possibility of breaking dynamically the gauge symmetry via the condensation of the new generations' fermions; all these will give additional contributions to the oblique parameters and will modify the fits. Therefore, in view that soon we will see or exclude new generations thanks to the LHC, it is wise to approach this possibility with an open mind.

From the discussion above, it seems that neutrinos from new generations are very different from the ones discovered up to now, since they should have a mass 10^{11} times larger. However, this apparent difference is naturally explained within the framework that we are going to explore. In the SM neutrinos are massless because there are no right-handed neutrinos and because, with the minimal Higgs sector, lepton number is automatically conserved. We now know that neutrinos have masses, therefore the SM has to be modified to accommodate them; the simplest possibility is to add three right-handed neutrinos with Dirac mass terms, like for the rest of the fermions in the SM. If one then considers the SM with four generations (and four right-handed neutrinos), it is very difficult to justify why the neutrino from the fourth generation is 10^{11} times heavier than the three observed ones. This difficulty is alleviated if right-handed neutrinos have Majorana masses at the electroweak scale and the Dirac masses of the neutrinos are of the order of magnitude of their corresponding charged leptons [21]. Then, the see-saw mechanism is operative and gives neutrino masses $m_1 \sim m_e^2/M$, $m_2 \sim m_\mu^2/M$, $m_3 \sim m_\tau^2/M$, $m_4 \sim m_E^2/M \sim m_E$ (we denote by E the fourth generation charged lepton). Although with a common Majorana mass M at the electroweak scale it is not possible to obtain m_3 light enough to fit the

JHEP07(2011)122

observed neutrino masses, this could be solved by allowing different Majorana masses for the different generations; but then one should explain why $M_2, M_3 \gg M_4$.

Right-handed neutrinos, however, do not have gauge charges and are not needed to cancel anomalies, therefore their number is not linked to the number of generations. In fact, an extension of the SM with four generations and just one right-handed neutrino with both Dirac and a Majorana masses at the electroweak scale leads, at tree level, to three massless and two heavy Majorana neutrinos. Since lepton number is broken in the model, the three massless neutrinos acquire Majorana masses at two loops therefore providing a natural explanation for the tiny masses of the three known neutrinos [22].[1] More generally, it has been shown that in the SM with n_L lepton doublets, n_H Higgs doublets and $n_R < n_L$ right-handed neutrino singlets with Yukawa and Majorana mass terms there are $n_L - n_R$ massless Majorana neutrinos at tree level, of which $n_L - n_R - \max(0, n_L - n_H n_R)$ states acquire mass by neutral Higgs exchange at one loop [24–26]. The remaining $\max(0, n_L - n_H n_R)$ states get masses at two loops. Similar extensions could be built with additional hyperchargeless fermion triplets, like in type III see-saw.

In this work we reconsider the model of ref. [22], without enlarging the scalar sector of the SM but allowing for extra generations. The paper is organised as follows. In section 2 we summarize current neutrino data and searches for new generations. In section 3 we review the radiative neutrino mass generation at two loops, and show that the observed light neutrino mass hierarchy can not be accommodated in the minimal scenario with four generations. In section 4 we present a five generation example which leads to the observed neutrino masses and (close to tribimaximal) mixing. We introduce a simple parametrization of the model and explore the parameter space allowed by current neutrino data, universality, charged lepton flavour violating rare decays $\ell_i \to \ell_j \gamma$ and $0\nu2\beta$ decay, as well as the regions that will be probed in near future experiments (MEG, μ–e conversion in nuclei). Section 5 is devoted to collider phenomenology and we summarize our results in section 6.

2 Framework and review

It has been well established in the last decade that neutrinos are massive, thanks to the results obtained with solar [1–4, 11], and atmospheric [6, 7, 10] neutrinos, confirmed in experiments using man-made beams: neutrinos from nuclear reactors [5] and accelerators [8, 12].

The minimum description of all neutrino data requires mixing among the three neutrino states with definite flavour $(\nu_e, \nu_\mu, \nu_\tau)$, which can be expressed as quantum superpositions of three massive states ν_i $(i = 1, 2, 3)$ with masses m_i. The standard parametrization of the leptonic mixing matrix, $U_{\rm PMNS}$, is:

$$U_{\rm PMNS} = \begin{pmatrix} c_{13}c_{12} & c_{13}s_{12} & s_{13}e^{-i\delta} \\ -c_{23}s_{12} - s_{23}s_{13}c_{12}e^{i\delta} & c_{23}c_{12} - s_{23}s_{13}s_{12}e^{i\delta} & s_{23}c_{13} \\ s_{23}s_{12} - c_{23}s_{13}c_{12}e^{i\delta} & -s_{23}c_{12} - c_{23}s_{13}s_{12}e^{i\delta} & c_{23}c_{13} \end{pmatrix} \begin{pmatrix} e^{i\phi_1} & & \\ & e^{i\phi_2} & \\ & & 1 \end{pmatrix}, \quad (2.1)$$

[1] Two-loop quantum corrections within the SM with only two massive Majorana neutrinos also lead to a (tiny) mass for the third one [23].

JHEP07(2011)122

Light neutrino best fit values
$\Delta m^2_{21} = (7.64^{+0.19}_{-0.18}) \times 10^{-5}\,\mathrm{eV}^2$
$\Delta m^2_{31} = \begin{cases} (2.45 \pm 0.09) \times 10^{-3}\,\mathrm{eV}^2 & \mathrm{NH} \\ -(2.34^{+0.10}_{-0.09}) \times 10^{-3}\,\mathrm{eV}^2 & \mathrm{IH} \end{cases}$
$\sin^2\theta_{12} = 0.316 \pm 0.016$
$\sin^2\theta_{23} = \begin{cases} 0.51 \pm 0.06 & \mathrm{NH} \\ 0.52 \pm 0.06 & \mathrm{IH} \end{cases}$
$\sin^2\theta_{13} = \begin{cases} 0.017^{+0.007}_{-0.009} & \mathrm{NH} \\ 0.020^{+0.008}_{-0.009} & \mathrm{IH} \end{cases}$

Table 1. The best fit values of the light neutrino parameters and their 1σ errors from [27].

where $c_{ij} \equiv \cos\theta_{ij}$ and $s_{ij} \equiv \sin\theta_{ij}$. In addition to the Dirac-type phase δ, analogous to that of the quark sector, there are two physical phases ϕ_i if neutrinos are Majorana particles. The measurement of these parameters is by now restricted to oscillation experiments which are only sensitive to mass-squared splittings ($\Delta m^2_{ij} \equiv m^2_i - m^2_j$). Moreover, oscillations in vacuum cannot determine the sign of the splittings. As a consequence, an uncertainty in the ordering of the masses remains; the two possibilities are:

$$m_1 < m_2 < m_3\,, \tag{2.2}$$

$$m_3 < m_1 < m_2\,. \tag{2.3}$$

The first option is the so-called normal hierarchy spectrum while the second one is the inverted hierarchy scheme; in this form they correspond to the two possible choices of the sign of $\Delta m^2_{31} \equiv \Delta m^2_{\mathrm{atm}}$, which is still undetermined, while $\Delta m^2_{21} \equiv \Delta m^2_{\mathrm{sol}}$ is known to be positive. Within this minimal context, two mixing angles and two mass-squared splittings are relatively well determined from oscillation experiments (see table 1), there is a slight hint of $\theta_{13} > 0$ and nothing is known about the phases.

Regarding the absolute neutrino mass scale, it is constrained by laboratory experiments searching for its kinematic effects in Tritium β-decay, which are sensitive to the so-called effective electron neutrino mass,

$$m^2_{\nu_e} \equiv \sum_i m^2_i |U_{ei}|^2. \tag{2.4}$$

The present upper limit is $m_{\nu_e} < 2.2\,\mathrm{eV}$ at 95% confidence level (CL) [28, 29], while a new experimental project, KATRIN [30], is underway, with an estimated sensitivity limit $m_{\nu_e} \sim 0.2\,\mathrm{eV}$. However, cosmological observations provide the tightest constraints on the absolute scale of neutrino masses, via their contribution to the energy density of the Universe and the growth of structure. In general these bounds depend on the assumptions made about the expansion history as well as on the cosmological data included in the

JHEP07(2011)122

analysis [31]. Combining CMB and large scale structure data quite robust bounds have been obtained: $\sum_i m_i < 0.4\,\text{eV}$ at 95% CL within the ΛCDM model [32] and $\sum_i m_i < 1.5\,\text{eV}$ at 95% CL when allowing for several departures from ΛCDM [33].

Finally, if neutrinos are Majorana particles complementary information on neutrino masses can be obtained from $0\nu2\beta$ decay. The contribution of the known light neutrinos to the $0\nu2\beta$ decay amplitude is proportional to the effective Majorana mass of ν_e, $m_{ee} = |\sum_i m_i U_{ei}^2|$, which depends not only on the masses and mixing angles of the U_{PMNS} matrix but also on the phases. The present bound from the Heidelberg-Moscow group is $m_{ee} < 0.34\,\text{eV}$ at 90% CL [34], but future experiments can reach sensitivities of up to $m_{ee} \sim 0.01\,\text{eV}$ [35].

We now briefly review the current status of searches for new sequential generations. Direct production of the 4$^{\text{th}}$ generation quarks t' and b', assuming $t' \to Wq$ and $b' \to Wt$ has been searched in CDF, leading to the lower mass bounds $m_{t'} > 335\,\text{GeV}$ and $m_{b'} > 385\,\text{GeV}$ [36, 37]. Limits on new generation leptons, from LEP II, are weaker: $m_{\ell'} > 100.8\,\text{GeV}$ and $m_{\nu'} > 80.5\,(90.3)\,\text{GeV}$ for pure Majorana (Dirac) particles, assuming that the 4$^{\text{th}}$ generation leptons are unstable, i.e., their mixing with the known leptons is large enough so that they decay inside the detector [17]. When neutrinos have both Dirac and Majorana masses, their coupling to the Z boson may be reduced by the neutrino mixing angle and the bound on the lightest neutrino mass may be relaxed to 63 GeV [38]. While the bound on a charged lepton stable on collider lifetimes is still about 100 GeV, in the case of stable neutrinos the only limit comes from the LEP I measurement of the invisible Z width, $m_{\nu'} > 39.5\,(45)\,\text{GeV}$ for pure Majorana (Dirac) particles [17].

Even if new generation fermions are very heavy and cannot de directly produced, they affect electroweak observables through radiative corrections. Recent works have shown that a fourth generation is consistent with electroweak precision observables [20, 39, 40], provided there is a heavy Higgs and the mass splittings of the new SU(2) doublets satisfy [40][2]

$$|m_{t'} - m_{b'}| < 80\,\text{GeV}, \tag{2.5}$$

$$|m_{\ell'} - m_{\nu'}| < 140\,\text{GeV}. \tag{2.6}$$

Notice, however, that a long-lived fourth generation can reopen a large portion of the parameter space [41].

In addition to these phenomenological bounds one can place some upper limits by using perturbative unitarity, triviality and by imposing the stability of the Higgs potential at one loop. Typically one obtains limits of the order of the TeV [42] for degenerate lepton doublets and about 600 GeV for degenerate quark doublets.

A very striking effect of new generations is the enhancement of the Higgs-gluon-gluon vertex which arises from a triangle diagram with all quarks running in the loop. This vertex is enhanced approximately by a factor 3 (5) in the presence of a heavy fourth (fifth) generation [39, 43]. Therefore, the Higgs production cross section through gluon fusion at the Tevatron and the LHC is enhanced by a factor of 9 (25) in the presence of a fourth (fifth)

[2]The allowed quark mass splittings depend on the Higgs mass, according to the approximate formula $m_{t'} - m_{b'} \simeq \left(1 + \frac{1}{5}\log(\frac{m_H}{115\,\text{GeV}})\right) \times 50\,\text{GeV}$ from ref. [39].

JHEP07(2011)122

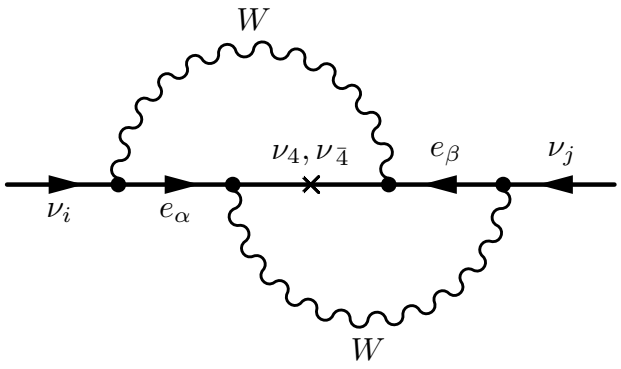

Figure 1. Two-loop diagram contributing to neutrino masses in the four-generation model.

generation. Thus, a combined analysis from CDF and D0 for four generations has excluded a SM-like Higgs boson with mass between 131 GeV and 204 GeV at 95% CL [44], while LHC data already excludes 144 GeV $< m_H <$ 207 GeV at 95% CL [45]. From these results, we estimate roughly that $m_H > 300$ GeV in the case of five generations. However, these limits may be softened if the fourth generation neutrinos are long-lived and the branching ratio of the decay channel $H \to \nu_4 \bar{\nu}_4$ is significant [46].

Putting all together, a general analysis seems to suggest that at most only two extra generations are allowed [19] unless new additional physics is invoked. If extra generations exist, the Higgs should be heavy. Extra generation quarks should also be quite heavy and be almost degenerate within a generation. The constraints on new generation leptons are milder; charged lepton and Dirac neutrino masses should be in the range 100–1000 GeV and, as we will see in section 4.3, this range will increase if neutrinos have both Dirac and Majorana mass terms.

3 Four generations

If we add one right-handed neutrino ν_R to the SM with three generations and we do not impose lepton number conservation, so that there is a Majorana mass term for the right-handed neutrino, a particular linear combination of ν_e, ν_μ, ν_τ, call it ν'_3, will couple to ν_R and get a Majorana mass at tree level. The other two linear combinations are massless at tree level but, since lepton number is broken, no symmetry protects them from acquiring a Majorana mass at the quantum level. In fact, they obtain a mass at two loops by the exchange of two W bosons (same diagram as in figure 1, but with $\nu_3, \nu_{\bar{3}}$ running in the loop). This leads to two extremely small neutrino masses, as desired, but there is a huge hierarchy between the tree-level mass, for ν_3, and the two-loop-level masses, for ν_1 and ν_2, therefore this possibility cannot accommodate the observed neutrino masses.[3]

Analogously, we can extend the SM by adding a complete fourth generation and one right handed neutrino ν_R with a Majorana mass term [22, 26, 48, 49]. We denote the new

[3]See however [47] for a model with three generations, one right-handed neutrino singlet and two Higgs doublets which can accommodate neutrino masses and mixings.

JHEP07(2011)122

charged lepton E and the new neutrino ν_E. The relevant part of the Lagrangian is

$$\mathcal{L}_Y = -\bar{\ell} Y_e e_R \phi - \bar{\ell} Y_\nu \nu_R \tilde{\phi} - \frac{1}{2} \overline{\nu_R^c} m_R \nu_R + \text{H.c.}\,, \tag{3.1}$$

where ℓ represents the left-handed lepton SU(2) doublets, e_R the right-handed charged leptons, ν_R the right-handed singlet and flavour indices are omitted. In generation space ℓ and e_R are organized as column vectors with four components. Thus, Y_e is a general, 4×4 matrix, Y_ν is a general four-component column vector whose elements we denote by y_α with $\alpha = e, \mu, \tau, E$, and m_R is a Majorana mass term. The standard kinetic terms, not shown in eq. (3.1), are invariant under general unitary transformations $\ell \to V_\ell \ell$, $e_R \to V_e e_R$ and $\nu_R \to e^{i\alpha} \nu_R$. One can use those transformations, V_ℓ and V_e, to choose Y_e diagonal and positive and also m_R can be taken positive by absorbing its phase in ν_R. Y_ν is in general arbitrary; however, there is still a rephasing invariance in ℓ and e_R that will allow us to remove all phases in Y_ν.

After spontaneous symmetry breaking (SSB) the mass matrix for the neutral leptons is a 5×5 Majorana symmetric matrix which has the standard see-saw structure with only one right-handed neutrino Majorana mass term. Therefore, it leads to two massive Majorana and three massless Weyl neutrinos. From the Lagrangian it is clear that only the linear combination of left-handed neutrinos $\nu_4' \propto y_e \nu_e + y_\mu \nu_\mu + y_\tau \nu_\tau + y_E \nu_E$ will pair up with ν_R to acquire a Dirac mass term. Thus, it is convenient to pass from the flavour basis $(\nu_e, \nu_\mu, \nu_\tau, \nu_E)$ to a new one $\nu_1', \nu_2', \nu_3', \nu_4'$ where the first three states will be massless at tree level and only ν_4' will mix with ν_R. If V is the orthogonal matrix that passes from one basis to the other we will have $\nu_\alpha = \sum_i V_{\alpha i} \nu_i'$ $(i = 1, \cdots, 4,\ \alpha = e, \mu, \tau, E)$ with $V_{\alpha 4} \equiv N_\alpha = y_\alpha / \sqrt{\sum_\beta y_\beta^2}$. Since ν_1', ν_2', ν_3' are massless, we are free to choose them in any combination of $\nu_e, \nu_\mu, \nu_\tau, \nu_E$ as long as they are orthogonal to ν_4', i.e., $\sum_\alpha V_{\alpha i} N_\alpha = 0$ for $i = 1, 2, 3$. The orthogonality of V almost fixes all its elements in terms of N_α, but still leaves us some freedom to set three of them to zero. Following [22, 48] we choose $V_{\tau 1} = V_{E1} = V_{E2} = 0$ for convenience.

After this change of basis, we are left with a non-trivial 2×2 mass matrix for ν_4' and ν_R which can easily be diagonalized and leads to two Majorana neutrinos

$$\begin{aligned} \nu_4 &= i \cos\theta(-\nu_4' + \nu_4'^c) + i \sin\theta(\nu_R - \nu_R^c)\,, \\ \nu_{\bar{4}} &= -\sin\theta(\nu_4' + \nu_4'^c) + \cos\theta(\nu_R + \nu_R^c)\,, \\ m_{4,\bar{4}} &= \frac{1}{2}\Big(\sqrt{{m_R}^2 + 4 m_D^2} \mp m_R\Big)\,, \end{aligned} \tag{3.2}$$

where $m_D = v\sqrt{\sum_i y_i^2}$, with $v = \langle \phi^{(0)} \rangle$, and $\tan^2\theta = m_4 / m_{\bar{4}}$. The factor i and the relative signs in ν_4 are necessary to keep the mass terms positive and preserve the canonical Majorana condition $\nu_4 = \nu_4^c$. If $m_R \ll m_D$, we have $m_4 \approx m_{\bar{4}}$, $\tan\theta \approx 1$, and we say we are in the pseudo-Dirac limit while when $m_R \gg m_D$, $m_4 \approx m_D^2 / m_R$ and $m_{\bar{4}} \approx m_R$, $\tan\theta \approx m_D / m_R$ and we say we are in the see-saw limit.

Since lepton number is broken by the ν_R Majorana mass term, there is no symmetry which prevents the tree-level massless neutrinos from gaining Majorana masses at higher

JHEP07(2011)122

order. In fact, Majorana masses for the light neutrinos, ν'_1, ν'_2, ν'_3, are generated at two loops by the diagram of figure 1, and are given by

$$M_{ij} = -\frac{g^4}{m_W^4} m_R m_D^2 \sum_\alpha V_{\alpha i} V_{\alpha 4} m_\alpha^2 \sum_\beta V_{\beta j} V_{\beta 4} m_\beta^2 I_{\alpha\beta}\,, \tag{3.3}$$

where the sums run over the charged leptons $\alpha, \beta = e, \mu, \tau, E$ while $i, j = 1, 2, 3$, and

$$I_{\alpha\beta} = J(m_4, m_{\bar{4}}, m_\alpha, m_\beta, 0) - \frac{3}{4} J(m_4, m_{\bar{4}}, m_\alpha, m_\beta, m_W)\,, \tag{3.4}$$

with $J(m_4, m_{\bar{4}}, m_\alpha, m_\beta, m_W)$ the two-loop integral defined and computed in appendix A.

When $m_R = 0$, $M_{ij} = 0$, as it should, because in that case lepton number is conserved. Also when $m_D = 0$ we obtain $M_{ij} = 0$, since then the right-handed neutrino decouples completely and lepton number is again conserved.

To see more clearly the structure of this mass matrix we can take, for the moment, the limit $m_e = m_\mu = m_\tau = 0$; then, since we have chosen $V_{\tau 1} = V_{E1} = V_{E2} = 0$, the only non-vanishing element in M_{ij} is M_{33} and it is proportional to $V_{E3}^2 N_E^2 m_E^4 I_{EE}$. Keeping all the masses one can easily show that the eigenvalues of the light neutrino mass matrix are proportional to m_μ^4, m_τ^4, m_E^4 which gives a huge hierarchy between neutrino masses. Moreover, for $m_E \gg m_{4,\bar{4}} \gg m_W$, the loop integrals in eq. (3.4) can be well approximated by (see appendix A):

$$I_{EE} \approx \frac{-1}{(4\pi)^4 2 m_E^2} \ln \frac{m_E}{m_{\bar{4}}} \tag{3.5}$$

and

$$I_{\mu\mu} \approx I_{\tau\tau} \approx \frac{-1}{(4\pi)^4 2 m_{\bar{4}}^2} \ln \frac{m_{\bar{4}}}{m_4}\,, \tag{3.6}$$

leading to only two light neutrino masses, since the mass matrix in eq. (3.3) has rank 2 if the three light charged lepton masses are neglected in $I_{\alpha\beta}$. The third light neutrino mass is generated when at least m_τ is taken into account in the loop integral, leading to a further suppression. Within the above approximation, the following ratio of ν_2 and ν_3 masses is obtained [50]:

$$\frac{m_2}{m_3} \lesssim \frac{1}{4N_E^2} \left(\frac{m_\tau}{m_E}\right)^2 \left(\frac{m_\tau}{m_{\bar{4}}}\right)^2 \lesssim \frac{10^{-7}}{N_E^2}\,, \tag{3.7}$$

where we have taken $\ln(m_{\bar{4}}/m_4) \approx \ln(m_E/m_{\bar{4}}) \approx 1$ and in the last step we used that $m_E, m_{\bar{4}} \gtrsim 100\,\text{GeV}$. To overcome this huge hierarchy one would need very small values of N_E which would imply that the heavy neutrinos are not mainly ν_E but some combination of the three known neutrinos ν_e, ν_μ, ν_τ; but this is not possible since it would yield observable effects in a variety of processes, like $\pi \to \mu\nu$, $\pi \to e\nu$, $\tau \to e\nu\nu$, $\tau \to \mu\nu\nu$. This requires that $y_{e,\mu,\tau} \lesssim 10^{-2} y_E$ [51, 52] and then $N_E \approx 1$.

Therefore, although the idea is very attractive, the simplest version is unable to accommodate the observed spectrum of neutrino masses and mixings. However, notice that whenever a new generation and a right-handed neutrino with Majorana mass at (or below) the TeV scale are added to the SM, the two-loop contribution to neutrino masses is always present and provides an important constraint for this kind of SM extensions.

JHEP07(2011)122

In the following we modify the original idea by adding one additional generation and one additional fermion singlet. We will see that this minimal modification is able to accommodate all current data.

4 Five generation working example

4.1 The five generations model

We add two generations to the SM and two right-handed neutrinos. We denote the two charged leptons by E and F and the two right-handed singlets by ν_{4R} and ν_{5R}. The Lagrangian is exactly the same we used for four generations (3.1) but now ℓ and e are organized as five-component column vectors while ν_R is a two-component column vector containing ν_{4R} and ν_{5R}. Thus, Y_e is a general, 5×5 matrix, Y_ν is a general 5×2 matrix and m_R is now a general symmetric 2×2 matrix. The kinetic terms are invariant under general unitary transformations $\ell \to V_\ell \ell$, $e_R \to V_e e_R$ and $\nu \to V_\nu \nu$, which can be used to choose Y_e diagonal and positive and m_R diagonal with positive elements m_{4R} and m_{5R}. After this choice, there is still some rephasing invariance $\ell_i \to e^{i\alpha_i}\ell_i$, $e_{iR} \to e^{i\alpha_i} e_{iR}$ broken only by Y_ν, which can be used to remove five phases in Y_ν. Therefore

$$Y_\nu = \left(y,\, y' \right), \tag{4.1}$$

where y and y' are five-component column vectors with components y_α and y'_α respectively ($\alpha = e, \mu, \tau, E, F$), one of which can be taken real while the other, in general, will contain phases. The model, contrary to the four-generation case, has additional sources of CP violation in the leptonic sector. However, since at the moment we are not interested in CP violation, for simplicity we will take all y_α and y'_α real.

Much as in the four-generation case, the linear combination $\nu'_4 \propto \sum_\alpha y_\alpha \nu_\alpha$ only couples to ν_{4R} and the combination $\nu'_5 \propto \sum_\alpha y'_\alpha \nu_\alpha$ only couples to ν_{5R}. Therefore, the tree-level spectrum will contain three massless neutrinos (the linear combinations orthogonal to ν'_4 and ν'_5) and four heavy Majorana neutrinos. Unfortunately, since in the general case ν'_4 and ν'_5 may not be orthogonal to each other, the diagonalization becomes much more cumbersome than in the four-generation case. Since we just want to provide a working example, we choose ν'_4 and ν'_5 orthogonal to each other, i.e., $\sum_\alpha y_\alpha y'_\alpha = 0$. This simplifies enormously the analysis of the model and allows us to adopt a diagonalization procedure analogous to the one followed in the four-generation case.

We change from the flavour fields $\nu_e, \nu_\mu, \nu_\tau, \nu_E, \nu_F$ to a new basis $\nu'_1, \nu'_2, \nu'_3, \nu'_4, \nu'_5$ where ν'_1, ν'_2, ν'_3 are massless at tree level, so we are free to choose them in any combination of the flavour states as long as they are orthogonal to ν'_4 and ν'_5. Thus, if V is the orthogonal matrix that passes from one basis to the other $\nu_\alpha = \sum_i V_{\alpha i} \nu'_i$ ($i = 1, \cdots, 5$, $\alpha = e, \mu, \tau, E, F$) we have $V_{\alpha 4} = N_\alpha = y_\alpha / \sqrt{\sum_\beta y_\beta^2}$, $V_{\alpha 5} = N'_\alpha = y'_\alpha / \sqrt{\sum_\beta y'^2_\beta}$, and $\sum_\beta N_\beta N'_\beta = 0$. The rest of the elements in $V_{\alpha i}$ can be found by using the orthogonality of V, which gives us 12 equations (9 orthogonality and 3 normalization conditions, because N_α and N'_α are already normalized and orthogonal), therefore we still can choose at will three elements of $V_{\alpha i}$; for

JHEP07(2011)122

instance we could choose $V_{F1} = V_{F2} = V_{E1} = 0$. In this case

$$V = \begin{pmatrix} V_{e1} & V_{e2} & V_{e3} & N_e & N'_e \\ V_{\mu 1} & V_{\mu 2} & V_{\mu 3} & N_\mu & N'_\mu \\ V_{\tau 1} & V_{\tau 2} & V_{\tau 3} & N_\tau & N'_\tau \\ 0 & V_{E2} & V_{E3} & N_E & N'_E \\ 0 & 0 & V_{F3} & N_F & N'_F \end{pmatrix} . \tag{4.2}$$

Moreover, since $\sum_\alpha N_\alpha N'_\alpha = 0$, the 4×4 mass matrix of ν'_4, ν_{4R}, ν'_5 and ν_{5R} is block-diagonal and can be separated in two 2×2 matrices (for ν'_4 and ν_{4R} and ν'_5 and ν_{5R} respectively) with the same form found in the four-generation case. Its diagonalization leads to four Majorana massive fields:

$$\begin{aligned} \nu_a &= i\cos\theta_a(-\nu'_a + \nu'^c_a) + i\sin\theta_a(\nu_{aR} - \nu^c_{aR}) , \\ \nu_{\bar{a}} &= -\sin\theta_a(\nu'_a + \nu'^c_a) + \cos\theta_a(\nu_{aR} + \nu^c_{aR}) , \\ m_{a,\bar{a}} &= \frac{1}{2}\Big(\sqrt{m^2_{aR} + 4m^2_{aD}} \mp m_{aR}\Big) , \end{aligned} \tag{4.3}$$

with $a = 4, 5$, $\tan^2\theta_a = m_a/m_{\bar{a}}$, $m_{4D} = v\sqrt{\sum_\alpha y^2_\alpha}$ and $m_{5D} = v\sqrt{\sum_\alpha y'^2_\alpha}$.

4.2 Two-loop neutrino masses

As in the case of four generations, the diagrams of figure 1 (now with the four massive neutrinos running in the loop) will generate a non-vanishing mass matrix for the three neutrinos ν'_1, ν'_2, ν'_3 given by

$$M_{ij} = -\frac{g^4}{m^4_W} \sum_{a=4,5} m_{aR} m^2_{aD} \sum_\alpha V_{\alpha i} V_{\alpha a} m^2_\alpha \sum_\beta V_{\beta j} V_{\beta a} m^2_\beta I^{(a)}_{\alpha\beta} , \tag{4.4}$$

with $I^{(a)}_{\alpha\beta}$ given by (3.4) with a labeling the contribution of the 4^{th} and 5^{th} generations.

To analyze this mass matrix first we will impose several phenomenological constraints:

a) The model should be compatible with the observed universality of fermion couplings and have small rates of lepton flavour violation in the charged sector. This requires $y_e, y_\mu, y_\tau, y'_e, y'_\mu, y'_\tau \ll y_E, y_F, y'_E, y'_F$.

b) The model should fit the observed pattern of masses and mixings. A good starting point would be to have expressions able to reproduce the tribimaximal (TBM) mixing structure.

The constraint **a)** together with the orthogonality condition implies that $y_E y'_E + y_F y'_F \approx 0$, which can be satisfied, for instance, if $y_F = y'_E = 0$, that is, ν_E only couples to ν_{4R} and ν_F only couples to ν_{5R}. Then, one can define $y_\alpha = y_E(\epsilon_e, \epsilon_\mu, \epsilon_\tau, 1, 0)$, $y'_\alpha = y'_F(\epsilon'_e, \epsilon'_\mu, \epsilon'_\tau, 0, 1)$, where ϵ_i and ϵ'_i are at least $\mathcal{O}(10^{-2})$ in order to satisfy universality constraints[4] (see section 4.3.2 for more details). Thus, to order ϵ, $N_\alpha \approx (\epsilon_e, \epsilon_\mu, \epsilon_\tau, 1, 0)$, $N'_\alpha \approx (\epsilon'_e, \epsilon'_\mu, \epsilon'_\tau, 0, 1)$,

[4]This pattern of couplings can easily be enforced by using a discrete symmetry which is subsequently broken at order ϵ.

JHEP07(2011)122

and since for $i \neq 4,5$ $\sum_\alpha V_{\alpha i} N_\alpha = \sum_\alpha V_{\alpha i} N'_\alpha = 0$, all the entries $V_{\alpha i}$ with $\alpha = e, \mu, \tau$, $i = 1, 2, 3$ can be order one. Now if we choose $V_{F1} = V_{F2} = V_{E1} = 0$ one can see that V_{E2}, V_{E3} are $\mathcal{O}(\epsilon)$ while V_{F3} is $\mathcal{O}(\epsilon')$.

A further simplification occurs if we assume that $V_{E3} = 0$, since in that case E only couples to ν'_2 and and F only couples to ν'_3. Then, in the limit $m_e = m_\mu = m_\tau = 0$ the neutrino mass matrix M_{ij} in eq. (4.4) is already diagonal and we can easily estimate the size of the two larger eigenvalues by neglecting the masses of the known charged leptons in front of m_E and m_F. We find[5]

$$M_{22} \sim \epsilon^2 m_{4R} \frac{g^4 m_{4D}^2 m_E^2}{m_W^4 (4\pi)^4 2} \ln \frac{m_E}{m_{\bar{4}}}\,, \qquad M_{33} \sim \epsilon'^2 m_{5R} \frac{g^4 m_{5D}^2 m_F^2}{m_W^4 (4\pi)^4 2} \ln \frac{m_F}{m_{\bar{5}}}\,. \tag{4.5}$$

Taking $m_F \sim m_{5D} \sim m_W/g$ and $\epsilon' \sim 10^{-2}$ we find $M_{33} \sim 2 \times 10^{-9} m_{5R}$, therefore, to obtain $M_{33} \sim 0.05\,\text{eV}$ we need $m_{5R} \sim 20\,\text{MeV}$ (or $\epsilon' \lesssim 10^{-3}$ for $m_{5R} \sim 1\,\text{GeV}$). Since m_{5R} and m_{4R} control the splitting between the two heavy Majorana neutrinos we are naturally in the pseudo-Dirac regime unless the ϵ's are below 10^{-4}. We also see that the higher $m_{4D(5D)}$ or $m_{E(F)}$, the lower the ϵ (ϵ') that is needed for a given $m_{4R(5R)}$. On the other hand, it is clear that the required hierarchy between M_{33} and M_{22} can be easily achieved both in the normal and the inverted hierarchy cases, while the degenerate case cannot be fitted within this scheme since the third neutrino mass is proportional to m_τ^4. After discussing the phenomenology of the model with more detail in section 4.3, we present the allowed regions of the parameter space in figure 4.

Now let us turn to constraint **b)**, that is, the light neutrino mixings. With our simplifying choices the diagonal entries of the light neutrino mass matrix are proportional to m_τ^4, m_E^4, m_F^4, whereas the off-diagonal ones are proportional to $m_\tau^2 m_E^2$ and $m_\tau^2 m_F^2$. Therefore the neutrino states ν'_1, ν'_2, ν'_3 are very close to being the true mass eigenstates and the first 3×3 elements of V, $V_{\alpha i}$, with $\alpha = e, \mu, \tau$, $i = 1, 2, 3$ give us directly the PMNS mixing matrix (up to permutations). Then, by using the orthogonality conditions it is easy to find the structure of Yukawas that reproduce a given pattern for the PMNS matrix. Let us study separately the two phenomenologically viable cases, normal hierarchy (NH) and inverted hierarchy (IH).

4.2.1 Normal hierarchy

In the normal hierarchy case ($m_1 < m_2 < m_3$), the experimental data tell us that $m_3 \approx \sqrt{|\triangle m_{31}^2|} \approx 0.05\,\text{eV}$, $m_2 \approx \sqrt{\triangle m_{21}^2} \approx 0.01\,\text{eV}$ and allow for $m_1 \ll m_2$. The structures we have found (by choosing $V_{F1} = V_{F2} = V_{E1} = V_{E3} = 0$) automatically fall in this scheme, since (for $m_{E,F} \gg m_{4,\bar{4},5,\bar{5}} \gg m_W$) we obtain $(m_1, m_2, m_3) \propto (m_\tau^4/m_{\bar{4}}^2, m_E^2, m_F^2)$. Is there any choice of the Yukawa couplings y_α and y'_α that leads naturally to some phenomenologically successful structure, for instance TBM? If we impose TBM in $V_{\alpha i}$ ($\alpha = e, \mu, \tau$, $i = 1, 2, 3$), given the structure of N_α and N'_α, the orthogonality of V (at order ϵ^2) immediately tells us that $\epsilon_e = \epsilon_\mu = -\epsilon_\tau \equiv \epsilon$, $\epsilon'_e = 0, \epsilon'_\mu = \epsilon'_\tau \equiv \epsilon'$, and finally

[5] Note that the position of the eigenvalues in M_{ij} depends on the position of the zeros in $V_{\alpha i}$. The choice we made is very convenient to reproduce the normal hierarchy spectrum.

JHEP07(2011)122

$V_{E2} = -\epsilon\sqrt{3}$, $V_{F3} = -\epsilon'\sqrt{2}$. Therefore, a successful choice of the Yukawas will be

$$\begin{aligned} y_\alpha &= y_E(\epsilon, \epsilon, -\epsilon, 1, 0)\,, \\ y'_\alpha &= y'_F(0, \epsilon', \epsilon', 0, 1)\,, \end{aligned} \tag{4.6}$$

which, keeping only terms up to order ϵ^2, leads to

$$V \approx \begin{pmatrix} \sqrt{\frac{2}{3}} & \frac{1}{\sqrt{3}} - \frac{\sqrt{3}}{2}\epsilon^2 & 0 & \epsilon & 0 \\ -\frac{1}{\sqrt{6}} & \frac{1}{\sqrt{3}} - \frac{\sqrt{3}}{2}\epsilon^2 & \frac{1}{\sqrt{2}} - \frac{1}{\sqrt{2}}\epsilon'^2 & \epsilon & \epsilon' \\ \frac{1}{\sqrt{6}} & -\frac{1}{\sqrt{3}} + \frac{\sqrt{3}}{2}\epsilon^2 & \frac{1}{\sqrt{2}} - \frac{1}{\sqrt{2}}\epsilon'^2 & -\epsilon & \epsilon' \\ 0 & -\epsilon\sqrt{3} & 0 & 1 - \frac{3}{2}\epsilon^2 & 0 \\ 0 & 0 & -\epsilon'\sqrt{2} & 0 & 1 - \epsilon'^2 \end{pmatrix} + \mathcal{O}(\epsilon^3)\,. \tag{4.7}$$

Assuming that $m_{E,F} \gg m_{4,\bar{4},5,\bar{5}} \gg m_W$, we find:

$$m_2 = -\frac{3g^4}{m_W^4}\epsilon^2 m_{4D}^2 m_{4R} m_E^4 I_{EE} \approx \frac{3g^4}{2(4\pi)^4 m_W^4}\epsilon^2 m_{4D}^2 m_{4R} m_E^2 \ln\frac{m_E}{m_{\bar{4}}}\,, \tag{4.8}$$

$$m_3 = -\frac{2g^4}{m_W^4}\epsilon'^2 m_{5D}^2 m_{5R} m_F^4 I_{FF} \approx \frac{g^4}{(4\pi)^4 m_W^4}\epsilon'^2 m_{5D}^2 m_{5R} m_F^2 \ln\frac{m_F}{m_{\bar{5}}}\,, \tag{4.9}$$

and the required ratio $m_3/m_2 \approx 5$ can be easily accommodated, for instance if the fifth generation is heavier than the fourth one or $\epsilon' > \epsilon$.

4.2.2 Inverted hierarchy

In the inverted hierarchy case ($m_3 < m_1 \lesssim m_2$), we have $m_2 \approx m_1 \approx \sqrt{|\triangle m_{31}^2|} \approx 0.05\,\text{eV}$ and $m_3 \ll m_1$ is allowed. Therefore now we need $(m_1, m_2, m_3) \propto (m_E^2, m_F^2, m_\tau^4/m_{\bar{4}}^2)$, which is just a cyclic permutation of the three eigenvalues. This ordering cannot be obtained directly with our previous choice for the zeroes in $V_{\alpha i}$, so now it is convenient to choose $V_{F1} = V_{F3} = V_{E3} = V_{E2} = 0$ instead. Following the same procedure as above, we find that

$$\begin{aligned} y_\alpha &= y_E(-2\epsilon, \epsilon, -\epsilon, 1, 0)\,, \\ y'_\alpha &= y'_F(\epsilon', \epsilon', -\epsilon', 0, 1) \end{aligned} \tag{4.10}$$

will reproduce the desired TBM pattern, leading to

$$V \approx \begin{pmatrix} \sqrt{\frac{2}{3}} - \sqrt{6}\epsilon^2 & \frac{1}{\sqrt{3}} - \frac{\sqrt{3}}{2}\epsilon'^2 & 0 & -2\epsilon & \epsilon' \\ -\frac{1}{\sqrt{6}} + \sqrt{\frac{3}{2}}\,\epsilon^2 & \frac{1}{\sqrt{3}} - \frac{\sqrt{3}}{2}\epsilon'^2 & \frac{1}{\sqrt{2}} & \epsilon & \epsilon' \\ \frac{1}{\sqrt{6}} - \sqrt{\frac{3}{2}}\,\epsilon^2 & -\frac{1}{\sqrt{3}} + \frac{\sqrt{3}}{2}\epsilon'^2 & \frac{1}{\sqrt{2}} & -\epsilon & -\epsilon' \\ \epsilon\sqrt{6} & 0 & 0 & 1 - 3\,\epsilon^2 & 0 \\ 0 & -\epsilon'\sqrt{3} & 0 & 0 & 1 - \frac{3}{2}\epsilon'^2 \end{pmatrix} + \mathcal{O}(\epsilon^3)\,. \tag{4.11}$$

JHEP07(2011)122

Assuming that $m_{E,F} \gg m_{4,\bar{4},5,\bar{5}} \gg m_W$, we get:

$$m_1 \approx \frac{3g^4}{(4\pi)^4 m_W^4} \epsilon^2 m_{4D}^2 m_{4R} m_E^2 \ln \frac{m_E}{m_{\bar{4}}}\,, \tag{4.12}$$

$$m_2 \approx \frac{3g^4}{2(4\pi)^4 m_W^4} \epsilon'^2 m_{5D}^2 m_{5R} m_F^2 \ln \frac{m_F}{m_{\bar{5}}}\,, \tag{4.13}$$

while the ratio of masses between the heaviest neutrinos, $m_1/m_2 \approx 1$ can be obtained by choosing the different parameters in their natural range.

Thus, the model accommodates the light neutrino masses and mixings. In the next section we will analyse current phenomenological bounds on the mixings between the new generations and the first three, ϵ, ϵ'.

4.3 The parameters of the model

We have seen above that neutrino masses are proportional to $\epsilon^2 m_{4R}$ (or $\epsilon'^2 m_{5R}$) and a product of masses, $m_{4D}^2 m_E^2$ (or $m_{5D}^2 m_F^2$), which come from the Higgs mechanism and are proportional to Yukawa couplings. As discussed in section 2 the values of these masses cannot vary too much; perturbative unitarity requires they are smaller than about 1 TeV [42] while lower limits for charged leptons masses from colliders are about 100 GeV. Lower limits for neutral fermions are a bit less uncertain. In the case of unstable pure Dirac neutrinos ($m_{aR} = 0$, $a = 4, 5$) the neutrino masses are basically m_{aD} and the lower limits are about 90 GeV, therefore, in that case, $m_{aD} \gtrsim 90\,\text{GeV}$. If neutrinos have both Dirac and Majorana mass terms ($m_{aR} \neq 0$) the masses are given by eq. (4.3) and the lower limits are[6] $m_{\bar{a}} \geq m_a > 63\,\text{GeV}$, then the upper limits on $m_{aD} < 1\,\text{TeV}$ automatically imply $m_{aR} \lesssim 16\,\text{TeV}$ and therefore $m_{\bar{a}} \lesssim 16\,\text{TeV}$. More generally in figure 2 we present the allowed regions in the plane m_{aR} vs m_{aD} given the lower bound on $m_a > 63\,\text{GeV}$ and the upper limit on $m_{aD} < 1000\,\text{GeV}$. We also plot the lines corresponding to $m_a = 200$, 400, 600 and 800 GeV.

To be definite we will take

$$\begin{aligned} 100\,\text{GeV} &< m_{4D}, m_{5D}, m_E, m_F < 1000\,\text{GeV}, \\ 63\,\text{GeV} &\lesssim m_a \leq m_{aD} \leq m_{\bar{a}} \lesssim 16\,\text{TeV}, \end{aligned}$$

with $m_a m_{\bar{a}} = m_{aD}^2$ and $m_{\bar{a}} - m_a = m_{aR}$. In addition there are strong constrains from the electroweak oblique parameters which in the pure Dirac case require some degeneracy of masses, $m_{4D} \simeq m_E$ ($m_{5D} \simeq m_F$). However, these constraints depend on the complete spectrum of the theory (masses of quarks and leptons from new generations and the Higgs boson mass) and are less certain. In fact, contributions from the splitting of masses in the quark sector can be compensated in part by lepton contributions with large m_{aR} [53, 54], which, if we do take into account the constraints set by LEP II can vary from essentially zero (Dirac case) to 16 TeV.

[6] Notice that in our scenario there is a lower bound on the mixing ϵ, in order to obtain the correct scale of light neutrino masses, which implies that the heavy neutrinos would have decayed inside the detector at LEP.

JHEP07(2011)122

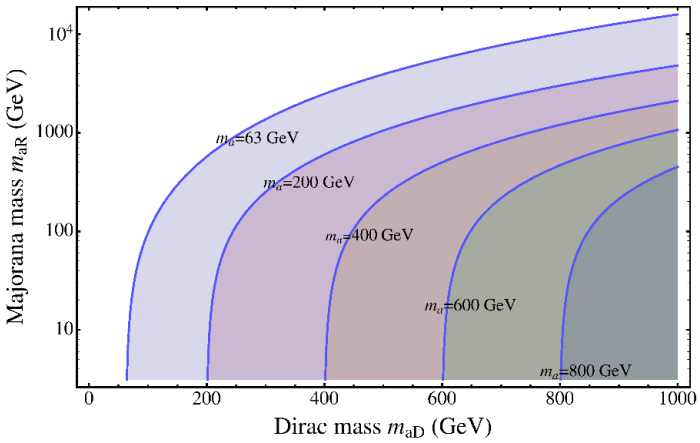

Figure 2. Allowed region in m_{aR}–m_{aD} given the present lower limit ($m_a > 63\,\text{GeV}$) on the mass of an extra generation neutrino ($a = 4, 5$ refers the 4^{th} or 5^{th} generation).

The other parameters that enter neutrino masses are the ϵ's, which characterize the mixing of light neutrinos with heavy neutrinos, and the m_R's, which characterize the amount of total lepton number breaking. The ϵ parameters will produce violations of universality and flavour lepton number conservation in low energy processes. The combination of data from these processes will allow us to constrain both ϵ and ϵ'. On the other hand, to obtain information on the m_R's we will use the light neutrino masses, which in the model are Majorana particles. We will also study the contributions of the heavy neutrinos to neutrinoless double beta decay.

4.3.1 Lepton flavour violation processes ($\mu \to e\gamma$ and μ–e conversion)

The general expression for the branching ratio of $\mu \to e\gamma$ produced through a virtual pair W-neutrino is:

$$B(\mu \to e\gamma) = \frac{3\alpha}{2\pi} |\delta_\nu|^2, \tag{4.14}$$

where

$$\delta_\nu = \sum_i U_{ei} U^*_{\mu i} H(m^2_{\chi_i}/m^2_W) \tag{4.15}$$

and H is the loop function for this process [51]

$$H(x) = \frac{x(2x^2+5x-1)}{4(x-1)^3} - \frac{3x^3 \log(x)}{2(x-1)^4},$$

with m_{χ_i} the masses of all heavy neutrinos running in the loop and U_{ei} and $U_{\mu i}$ their couplings to the electron and the muon respectively. In (4.14) we have used the unitarity of the mixing matrix and neglected the light neutrino masses to rewrite the final result only in terms of the heavy neutrino contributions. Then, as the mixings of the heavy neutrinos with the light leptons are different in normal and inverted hierarchy, so are the $\mu \to e\gamma$ amplitudes generated; one can see just by inspection of the mixing matrices, eqs. (4.7)

JHEP07(2011)122

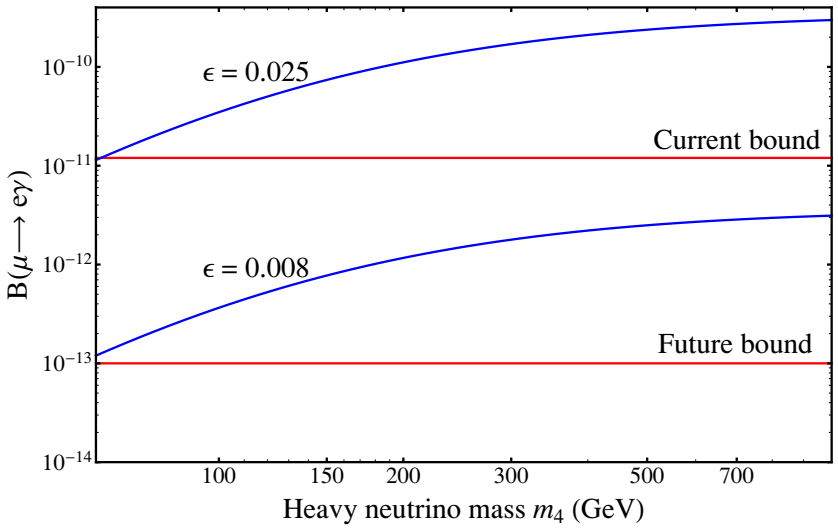

Figure 3. $B(\mu \to e\gamma)$ against m_4 for different values of ϵ in the NH case. We also display present and future limits on $B(\mu \to e\gamma)$ as horizontal lines.

and (4.11) that in NH only the pair $\nu_4, \nu_{\bar{4}}$ couples to both the electron and the muon, whereas in IH the four heavy neutrinos contribute to the process. The predicted branching ratios are

$$\text{NH:} \qquad B(\mu \to e\gamma) = \frac{3\alpha}{2\pi}\, \bar{H}_4^2\, \epsilon^4, \tag{4.16}$$

$$\text{IH:} \qquad B(\mu \to e\gamma) = \frac{3\alpha}{2\pi}\, \left[\bar{H}_5\, \epsilon'^2 - 2\, \bar{H}_4\, \epsilon^2\right]^2, \tag{4.17}$$

where

$$\bar{H}_a \equiv \cos^2\theta_a H(m_a^2/m_W^2) + \sin^2\theta_a H(m_{\bar{a}}^2/m_W^2)\,.$$

Now since $H(x)$ is a monotonically increasing function and $m_{\bar{a}} \geq m_a > 63\,\text{GeV}$ we have $\bar{H}_a \geq H(m_a^2/m_W^2) > 0.09$ which gives the less stringent constraint on ϵ and ϵ'. The experimental bound reads $B(\mu \to e\gamma) < 1.2 \times 10^{-11}$, and it is translated into

$$\text{NH:} \qquad \epsilon < 0.03\,, \tag{4.18}$$

$$\text{IH:} \qquad |\epsilon'^2 - 2\,\epsilon^2| < 7 \times 10^{-4}. \tag{4.19}$$

To see how these bounds depend on the masses of the heavy neutrinos we display in figure 3 $B(\mu \to e\gamma)$ against the mass of the heavy neutrino m_4 in the NH case. For IH we expect similar results unless there are strong cancellations. We also display as horizontal lines present limits [17] $B(\mu \to e\gamma) < 1.2 \times 10^{-11}$ and near future limits [55]. From the figure we can extract a conservative bound of the order of the one quoted above, $\epsilon < 0.03$.

Some extra information could be extracted from $\tau \to e\gamma$ and $\tau \to \mu\gamma$. Thus, from $B(\tau \to e\gamma) < 3.3 \times 10^{-8}$ we obtain $\epsilon < 0.3$ in the case of NH and $|\epsilon'^2 - 2\,\epsilon^2| < 0.08$, limits that show exactly the same dependence on ϵ and ϵ' as the one obtained in $\mu \to e\gamma$, but

JHEP07(2011)122

which are roughly one order of magnitude worse. From $B(\tau \to \mu\gamma) < 4.4 \times 10^{-8}$, although the bounds are of the same order of magnitude as for $B(\tau \to e\gamma)$, we obtain different combinations of ϵ's, $|\epsilon'^2 - \epsilon^2| < 0.09$ for NH and $\epsilon'^2 + \epsilon^2 < 0.09$ for IH.

Another very interesting process which gives information on ϵ is μ–e conversion in nuclei. From present data [17] one obtains bounds similar to the limit obtained from $\mu \to e\gamma$. However, there are plans to improve the sensitivity in μ–e conversion in 4 and even 6 orders of magnitude [56], therefore we expect much stronger bounds in the future coming from μ–e conversion. Strong correlations between both processes exist, as can be seen in [51].

4.3.2 Universality bounds

New heavy generations that couple to the observed fermions can potentially lead to violations of universality in charged currents because of the "effective" lack of unitarity in the mixings when the heavy generations cannot be produced. Data from neutrino oscillation experiments can also be used to constrain deviations from unitarity of some of the elements of the leptonic mixing matrix [57], however, in our scenario they lead to weaker bounds than the ones obtained here.

There are different types of universality bounds which constrain the mixings of light fermions with new generations:

- Lepton-hadron universality. One compares weak couplings of quarks and leptons using muon decay and nuclear β decay, which are very well tested. In our case this involves mixings both in the quark and lepton sectors and they are not useful to test individually the lepton mixings we are interested in.

- Relations between muon decay, m_Z, m_W and the weak mixing angle $\sin^2\theta_W$. These are very well-determined relations in the SM, and in our case they are modified because the heavy neutrinos cannot be produced in ordinary muon decay. Unfortunately, these relations depend strongly on the ρ parameter, which receives contributions from the Higgs and very large contributions from the heavy fermions of the new generations. Therefore, although these type of relations could be used to set bounds on the ϵ's, they would depend on other unknown parameters.

- Ratios of decay widths of similar processes. The bounds obtained from this type of processes are very robust because most of the uncertainties cancel in the ratios. We will only consider the most precise among these ratios, which are well measured and can be computed accurately [58–60]:

$$R_{\pi\to e/\pi\to\mu} \equiv \frac{\Gamma(\pi \to e\bar{\nu})}{\Gamma(\pi \to \mu\bar{\nu})}\,, \tag{4.20}$$

$$R_{\tau\to e/\tau\to\mu} \equiv \frac{\Gamma(\tau \to e\bar{\nu}\nu)}{\Gamma(\tau \to \mu\bar{\nu}\nu)}\,, \tag{4.21}$$

$$R_{\tau\to e/\mu\to e} \equiv \frac{\Gamma(\tau \to e\bar{\nu}\nu)}{\Gamma(\mu \to e\bar{\nu}\nu)} = B_{\tau\to e}\frac{\tau_\mu}{\tau_\tau}\,, \tag{4.22}$$

JHEP07(2011)122

Observable	R [17]	$R^{\rm SM}$	$R/R^{\rm SM}$
$R_{\pi\to e/\pi\to\mu}$	$(1.230 \pm 0.004) \times 10^{-4}$	$(1.2352 \pm 0.0001) \times 10^{-4}$	$0.996 \pm 0.003.$
$R_{\tau\to e/\tau\to\mu}$	1.028 ± 0.004	1.02821 ± 0.00001	1.000 ± 0.004
$R_{\tau\to\mu/\mu\to e}$	$(1.31 \pm 0.06) \times 10^{6}$	$(1.3086 \pm 0.0006) \times 10^{6}$	1.001 ± 0.004

Table 2. Relevant universality tests.

$$R_{\tau\to\mu/\mu\to e} \equiv \frac{\Gamma(\tau\to\mu\bar{\nu}\nu)}{\Gamma(\mu\to e\bar{\nu}\nu)} = B_{\tau\to\mu}\frac{\tau_\mu}{\tau_\tau}\,, \tag{4.23}$$

where $B_{\tau\to f} = \Gamma(\tau\to f\bar{\nu}\nu)/\Gamma(\tau\to \text{all})$ is the branching ratio of the tau decay to the fermion f, and $\tau_f = 1/\Gamma(f\to\text{all})$ its lifetime. In our model there are corrections to these ratios because ν_e, ν_μ and ν_τ have a small part of $\nu_{4,\bar{4}}$ and $\nu_{5,\bar{5}}$, which are heavy and cannot be produced. This leads to an additional violation of universality which depends on the mixings of ν_e, ν_μ and ν_τ with $\nu_{4,\bar{4}}$ and $\nu_{5,\bar{5}}$. For $R_{\pi\to e/\pi\to\mu}$, and using the $V_{\alpha i}$ in (4.7) and (4.11), we find that

$$\frac{R_{\pi\to e/\pi\to\mu}}{R^{\rm SM}_{\pi\to e/\pi\to\mu}} = \frac{|V_{e1}|^2+|V_{e2}|^2+|V_{e3}|^2}{|V_{\mu1}|^2+|V_{\mu2}|^2+|V_{\mu3}|^2} = \begin{cases} 1+\epsilon'^2 & \text{NH} \\ 1-3\epsilon^2 & \text{IH} \end{cases}. \tag{4.24}$$

$R_{\tau\to e/\tau\to\mu}/R^{\rm SM}_{\tau\to e/\tau\to\mu}$ tests exactly the same couplings, therefore the result is the same as in (4.24).

$R_{\tau\to e/\mu\to e}$ gives a different information because it tests τ/μ universality; however, we find that for both NH and IH $R_{\tau\to e/\mu\to e}/R^{\rm SM}_{\tau\to e/\mu\to e} = 1$, and since it is independent of the ϵ's, this process does not give any further information. This is a consequence of our choice for the Yukawa couplings,[7] which, up to signs, are equal for the τ and μ neutrinos.

Finally for $R_{\tau\to\mu/\mu\to e}$, using our mixing matrices, we find

$$\frac{R_{\tau\to\mu/\mu\to e}}{R^{\rm SM}_{\tau\to\mu/\mu\to e}} = \frac{|V_{\tau1}|^2+|V_{\tau2}|^2+|V_{\tau3}|^2}{|V_{e1}|^2+|V_{e2}|^2+|V_{e3}|^2} = \begin{cases} 1-\epsilon'^2 & \text{NH} \\ 1+3\epsilon^2 & \text{IH} \end{cases}, \tag{4.25}$$

which gives exactly the inverse combinations of those obtained from e/μ universality tests.

Therefore, if we combine the three results, $R_{\pi\to e/\pi\to\mu}/R^{\rm SM}_{\pi\to e/\pi\to\mu}$,$R_{\tau\to e/\tau\to\mu}/R^{\rm SM}_{\tau\to e/\tau\to\mu}$ and $(R_{\tau\to\mu/\mu\to e}/R^{\rm SM}_{\tau\to\mu/\mu\to e})^{-1}$ and use the data collected in table 2, we obtain

$$0.998 \pm 0.002 = \begin{cases} 1+\epsilon'^2 & \text{NH} \\ 1-3\epsilon^2 & \text{IH} \end{cases}, \tag{4.26}$$

which translates into the following upper 90% CL limits on ϵ' and ϵ

$$\text{NH:} \qquad \epsilon' < 0.04\,, \tag{4.27}$$

$$\text{IH:} \qquad \epsilon < 0.04\,. \tag{4.28}$$

[7] Which, in turn, is a consequence of the TBM structure we wanted to reproduce.

JHEP07(2011)122

Notice that although in the IH case we have more sensitivity than in the NH case because of the factor of 3 we finally obtain similar limits in the two cases. This is because in the NH case the deviation from 1 obtained in the model is always positive while the present measured value is slightly smaller than 1 (in both cases we used the Feldman & Cousins prescription [61] to set 90% CL limits).

Now we can use all data from LFV and universality and conclude that in the NH case we have $\epsilon < 0.03$, basically from $\mu \to e\gamma$, and $\epsilon' < 0.04$, basically from universality tests. In the IH case we obtain that, except in a narrow band around $\epsilon'^2 \simeq 2\epsilon^2$, $\epsilon \lesssim 0.02$ and $\epsilon' \lesssim 0.03$ basically from $\mu \to e\gamma$; if $\epsilon'^2 \simeq 2\epsilon^2$ there is a cancellation in $\mu \to e\gamma$ but still one can combine these data with the universality limits to obtain $\epsilon \lesssim 0.04$ and $\epsilon' \lesssim 0.06$.

4.3.3 Neutrinoless double beta decay ($0\nu2\beta$)

As commented above m_{4R}, m_{5R} are the relevant parameters which encapsulate the non-conservation of total lepton number and they control, together with the ϵ's, the neutrino masses. Therefore, it would be useful to have additional independent information on these parameters. The most promising experiments to test the non-conservation of total lepton number are neutrinoless double beta decay experiments. The standard contribution, produced by light neutrinos, to $0\nu2\beta$ has largely been studied (for a recent review see for instance [35]) and, given the expected future sensitivity, $m_{ee} = 0.01\,\text{eV}$, it will be very difficult to see it unless the neutrino spectrum is inverted or degenerate. However, if heavy neutrinos from new families are Majorana particles, they lead to tree-level effects in neutrinoless double beta decay [62], while, in our scenario, light neutrino masses are generated at two loops; thus, in principle, it is possible that these new contributions dominate over the standard ones.

The contribution of new generation heavy neutrinos (with mass larger than about the proton mass, m_p) to the rate of neutrinoless double beta decay can be written in terms of an effective mass,

$$\langle M_N \rangle^{-1} = \sum_a U_{ea}^2 M_a^{-1}, \tag{4.29}$$

where U_{ea} is the coupling of the electron to the left-handed component of the heavy neutrino a. The non-observation of neutrinoless double beta decay implies that [63]

$$\langle M_N \rangle > 10^8\,\text{GeV}. \tag{4.30}$$

In the case of NH the electron only couples to ν_4 and $\nu_{\bar{4}}$ (see eqs. (4.7) and (4.3)), thus

$$\langle M_N \rangle^{-1} = 2\epsilon^2 \left(\frac{\cos^2\theta}{m_4} - \frac{\sin^2\theta}{m_{\bar{4}}} \right) = \epsilon^2 \frac{m_{4R}}{m_{4D}^2}\,, \tag{4.31}$$

and using (4.30), we get:

$$m_{4R}\epsilon^2/m_{4D}^2 < 10^{-8}\,\text{GeV}^{-1}. \tag{4.32}$$

This is the same combination of the relevant parameters ($m_{4R}\epsilon^2$) that appears in (4.8) for m_2, therefore we can use neutrino data to set bounds on the heavy neutrino contribution

JHEP07(2011)122

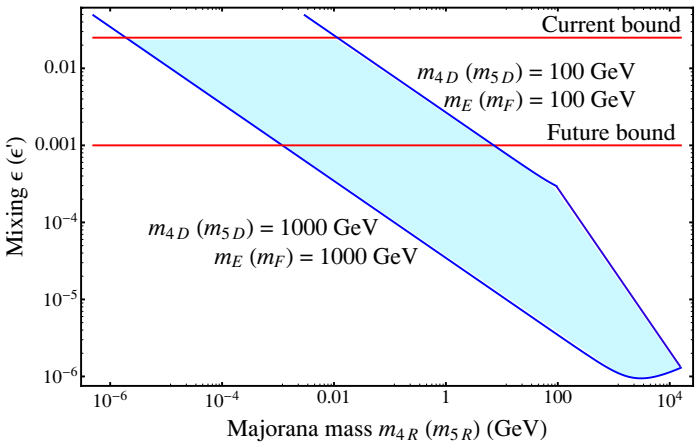

Figure 4. Parameter space that predicts the right scale for heavy and light neutrinos (blue region between the curves). As a comparison we also present the current bound from $\mu \to e\gamma$ and future limits from μ–e conversion experiments.

to neutrinoless double beta decay written in terms of the effective mass. We obtain

$$\langle M_N \rangle = \frac{3g^4 m_{4D}^4 m_E^2 \ln \dfrac{m_E}{m_{\bar{4}}}}{2m_2(4\pi)^4 m_W^4} \gtrsim 2 \times 10^{11}\,\text{GeV}, \tag{4.33}$$

where we have used $m_2 \sim 0.01\,\text{eV}$, typical values for $m_{4D} \sim m_E \sim 100\,\text{GeV}$ and $\ln(m_E/m_{\bar{4}}) \sim 1$. This is far from present, eq. (4.30), and future sensitivities.

In the case of IH, the effective mass is given by

$$\langle M_N \rangle^{-1} = 4\epsilon^2 m_{4R}/m_{4D}^2 + \epsilon'^2 m_{5R}/m_{5D}^2\,, \tag{4.34}$$

leading also to unobservable effects in $0\nu2\beta$ decay.

To summarize all phenomenological constraints on the model, in figure 4 we show in blue the allowed region in the ϵ–m_{4R} plane, which leads to $M_{33} \sim 0.05\,\text{eV}$ varying the charged lepton masses $m_E\,(m_F)$ and the Dirac neutrino masses $m_{4D}\,(m_{5D})$ between 100 GeV–1 TeV, and imposing the LEP bound on the physical neutrino mass, $m_4 > 63\,\text{GeV}$. We also plot the present bounds on the mixings $\epsilon\,(\epsilon')$ from $\mu \to e\gamma$ and future limits from μ–e conversion if expectations are attained.

5 Collider signatures

As we mentioned before, the LHC offers a unique opportunity to discover (or exclude) new sequential generations of quarks and leptons. For instance, with $1\,\text{fb}^{-1}$ at 7 TeV, the exclusion bound on b' would reach 500 GeV via $b' \to Wt$ decay channel, close to the partial wave unitarity bound. Even if the t' and b' are too heavy to be seen directly, their effects may be manifest at LHC, since they induce a large $gg \to ZZ$ signal [64]. See also [41] for

JHEP07(2011)122

prospects of detecting very long-lived fourth generation quarks, i.e., in the case of extremely small mixings with the lighter three generations.

Regarding the lepton sector, the standard searches for a fourth generation have to be restricted to the parameter space which leads to the correct light neutrino mass scale, depicted in figure 4. The expected signatures depend on the nature (Dirac or Majorana) of the neutrinos, which are generally assumed to be the lightest states.

Most theoretical analysis of fourth generation Majorana neutrino at hadron colliders have focused on the process $q\bar{q}' \to W^{\pm} \to \nu_4 \ell^{\pm}$, where the fourth generation neutrino is produced in association with a light charged lepton [65–68]. Subsequently, if neutrinos are Majorana, they will decay through $\nu_4 \to W^{\mp}\ell^{\pm}$, leading to the low-background like-sign di-lepton signature in half the events. However in our model the cross section for this process is suppressed both by the mixing of the extra generations with the first three and by the small Majorana masses $m_{4R,5R}$, much as in the neutrinoless double beta decay discussed above, so it will not be observable at LHC for the parameter range that reproduce the correct scale of light neutrino masses.

Alternatively, the lighter neutrinos can be pair-produced via an s-channel Z boson, $q\bar{q} \to Z \to \nu_I \nu_J$ $(I, J = 4, \bar{4})$ [69]. Although the W production has a higher cross section than the Z at hadron colliders, and the mass reach is enhanced when only one heavy particle is produced, if the mixing angle between the extra generations and the light ones is less than about 10^{-6} the neutrino production rates in the W channel are so suppressed that they are unobservable [65]. However the rate of heavy neutrino pair-production via a Z boson is independent of this mixing, becoming the dominant production mechanism in the small mixing regime. Moreover, if the mass difference between ν_4 and $\nu_{\bar{4}}$ is at least 1 GeV, and the mixing so small that the decay $\nu_{\bar{4}} \to \nu_4 Z$ always dominates, the above processes also lead to like-sign leptons in half of the events.[8] See ref. [69] for a detailed study of the Tevatron dataset potential to exclude (or discover) fourth generation neutrinos with both, Dirac and Majorana masses, up to 150–175 GeV, depending on the mixing. For the LHC, only the pure Majorana case has been studied in ref. [70]. According to them, the LHC at $\sqrt{s} = 10\,\text{TeV}$ with $5\,\text{fb}^{-1}$ could expect to set a 95% CL mass lower limit of $m_N > 300\,\text{GeV}$ or report 3σ evidence for the ν_4 if $m_{\nu_4} < 225\,\text{GeV}$. We expect a similar sensitivity in our model, in the region $m_4 - m_{\bar{4}} > 1\,\text{GeV}$ and small mixing $(\epsilon, \epsilon' \lesssim 10^{-4})$ i.e., somehow complementary to the one probed in LFV processes. See also [71] for an evaluation of the LHC discovery potential for both Majorana and Dirac type fourth family neutrinos in the process $pp \to Z/H \to \nu_4 \bar{\nu}_4 \to W\mu W\mu$.

Searches for fourth generation charged leptons at the LHC have been studied in [72], also in a general framework with Dirac and Majorana neutrino masses, and assuming that the neutrino ν_4 is the lightest fourth generation lepton. For charged leptons with masses under about 400 GeV, the dominant production channel is charged lepton - neutrino, through the process $q\bar{q}' \to W^{\pm} \to \nu_4 E^{\pm}$. The neutrino ν_4 can only decay to $\nu_4 \to W\ell$, and being Majorana it can decay equally to $W^-\ell^+$ and $W^+\ell^-$. Therefore when a pair of

[8] In the exact Dirac limit, $\nu_{\bar{4}}$ must decay to $W\ell$ and the different contributions to same sign di-lepton production cancel, since the Dirac neutrino conserves lepton number. However, as far as $\nu_{\bar{4}}$ always decays to $\nu_4 Z$ there is no interference amplitude, and same-sign di-lepton decays are unsuppressed.

JHEP07(2011)122

fourth generation leptons are produced, we expect the decay products to contain like-sign di-leptons half of the time. The sensitivity study for this process in events with two like-sign charged leptons and at least two associated jets shows that with $\sqrt{s} = 7\,\text{TeV}$ and $1\,\text{fb}^{-1}$ of data, the LHC can exclude fourth generation charged lepton masses up to 250 GeV. It would be interesting to study the parameter space in our model that would lead to this type of signals.

In the above searches, it was assumed that the lightest neutrino decays promptly. However, if the mixing of the lightest fourth generation neutrino with the first three generation leptons is $\epsilon \lesssim 10^{-7}$ its proper lifetime will be $\tau_4 \gtrsim 10^{-10} s$. The decay length at the LHC is given by $d = \beta c \gamma \tau_4 \sim 3\ \text{cm}(\tau_4/10^{-10}s)\beta\gamma$, thus for $\tau_4 \gtrsim 10^{-10}s$ the fourth neutrino will either show displaced vertices in its decay or decay outside the detector, if $d \gtrsim \mathcal{O}(m)$, which is a typical detector size. In our scenario, such a tiny mixing is only compatible with large Majorana masses, $m_R \sim 1\,\text{TeV}$ (see figure 4), far from the pseudo-Dirac case. Searches for Majorana neutrinos stable on collider times have been discussed in [73], where it is proposed to use a quadri-lepton signal that follows from the pair production and decay of heavy neutrinos $pp \to Z \to \nu_{\bar{4}}\nu_{\bar{4}} \to \nu_4\nu_4 ZZ$, when both Z's decay leptonically. The final state is thus 4ℓ plus missing energy. For $30\,\text{fb}^{-1}$ of LHC data at 13 TeV, ν_4 masses can be tested in the range 100 to 180 GeV, and $\nu_{\bar{4}}$ masses from 150 to 250 GeV.

Finally, if the lightest fourth generation lepton is the charged one, there is a striking signal which to our knowledge has not been studied in the literature: lepton number violating like-sign fourth generation lepton pair-production, through $q\bar{q}' \to W^\pm \to E^\pm \nu_{4,\bar{4}} \to E^\pm E^\pm W^\mp$ or via W fusion, $q\bar{q} \to W^\pm W^\pm q' q' \to E^\pm E^\pm jj$. These processes are not suppressed by the small mixing with the first three generations, so in principle they could be observable in our scenario. Depending on the charged lepton lifetime, they will decay promptly to same-sign light di-leptons, show displaced vertices or leave an anomalous track of large ionization and/or low velocity. A detailed phenomenological study would be very interesting, but it is beyond the scope of this work.

6 Summary and conclusions

We have analysed a simple extension of the SM in which light neutrino masses are linked to the presence of n extra generations with both left- and right-handed neutrinos. The Yukawa neutrino matrices are rank n, so if we do not impose lepton number conservation and allow for right-handed neutrino Majorana masses, at tree level there are $2n$ massive Majorana neutrinos and three massless ones. In order to obtain heavy neutrino masses above the experimental limits from direct searches at LEP, the Dirac neutrino masses should be at the electroweak scale, similar to those of their charged lepton partners, and the right-handed neutrino Majorana masses can not be too high (of order 10 TeV at most). The three remaining neutrinos get Majorana masses at two loops, therefore this framework provides a natural explanation for the tiny masses of the known SM neutrinos. On the other hand, it should be kept in mind that the two-loop contribution to the neutrino mass matrix is always present in this type of SM extensions, therefore the experimental upper

JHEP07(2011)122

limit on the absolute light neutrino mass scale leads to a relevant constraint which has to be taken into account.

We have shown that the minimal extension with a fourth generation can not fit simultaneously the ratio of the solar and atmospheric neutrino mass scales, $\Delta m^2_{\rm sol}/\Delta m^2_{\rm atm}$, the lower bound on the heavy neutrino mass from LEP and the limits on the mixing between the fourth generation and the first three from low energy universality tests. Then, there are two possibilities: either enlarge the Higgs sector [47] or consider a five generation extension. In this work we have analyzed the second one, while the first will be studied elsewhere [74]. Notice that five generations are still allowed by the combination of collider searches for its direct production, indirect effects in Higgs boson production at Tevatron and LHC, and precision electroweak observables [19], provided the Higgs mass is roughly $m_H > 300\,\text{GeV}$. However they will be either discovered or fully excluded at LHC, making our proposal falsifiable in the very near future.

Given the large number of free parameters in a five generation framework (10 neutrino Yukawa couplings, 2 charged lepton masses and 2 right-handed neutrino Majorana masses), we have considered a very simple working example assuming that i) the linear combinations of left-handed neutrinos that get Dirac masses at tree level are orthogonal to each other, ii) each extra generation left-handed neutrino couples only to one of the two right-handed SM singlet states and iii) each extra generation charged lepton couples only to one linear combination of the (tree-level) massless neutrinos. Then, we are left with 2 neutrino Yukawa couplings y_E, y_F, 2 charged lepton masses m_E, m_F, 2 right-handed neutrino Majorana masses m_{aR}, $a = 4, 5$, which characterize the amount of total lepton number breaking, and two small parameters ϵ, ϵ' which determine the mixing among the first three generations and the new ones. Moreover, at leading order the two-loop neutrino masses m_2, m_3 depend only on $\epsilon, m_{4R}, y_E, m_E$ and $\epsilon', m_{5R}, y_F, m_F$, respectively (see eq. (4.5)). Even in this over-simplified case we are able to accommodate all current data, including the observed pattern of neutrino masses and mixings both for normal and inverted hierarchy spectrum. A definite prediction of the model (independent of the above simplifying assumptions) is that the three light neutrinos can not be degenerate.

We have explored the parameter space regions able to generate the correct scale of neutrino masses, $\sim 0.05\,\text{eV}$. We find that for typical values of m_E, m_{4D} (m_F, m_{5D}) at the electroweak scale, we need $\epsilon^2 m_{4R}$ ($\epsilon'^2 m_{5R}$) $\lesssim 1\,\text{keV}$ to obtain the atmospheric mass scale (see figure 4).

We have also studied the current bounds on the mixing parameters ϵ and ϵ' from the non-observation of LFV rare decays $\ell_\alpha \to \ell_\beta \gamma$, as well as from universality tests. All of them are independent of the Majorana masses m_{iR}, since they conserve total lepton number. Depending on the light neutrino mass spectrum (normal or inverted), the strongest bounds come from $\mu \to e\gamma$ and from universality tests in π decays. Combining the information from both processes we can set independent limits on ϵ and ϵ' which being quite conservative are of the order of the few percent, $\epsilon \lesssim 0.03$ and $\epsilon' \lesssim 0.04$.

Finally, we have analysed the phenomenological prospects of the model. With respect to LFV signals, future MEG data will improve the limits on the ϵ's by a factor of about 3 while, if expectations from μ–e conversion are attained the limits on the ϵ's will be

JHEP07(2011)122

pushed to 10^{-3}. This region of observable LFV effects corresponds to the pseudo-Dirac limit, $m_{aR} \lesssim 1\,\text{GeV}$, i.e., two pairs of strongly degenerate heavy neutrinos. In this regime, they can only be discovered at LHC using pure Dirac neutrino signatures, which are more difficult to disentangle from the background.

On the other hand, we find that in the complementary region of very small mixing $\epsilon, \epsilon' \ll 10^{-3}$, $m_{aR} \gtrsim 1\,\text{GeV}$, the lighter Majorana neutrinos $\nu_4, \nu_{\bar{4}}$ will lead to observable same-sign di-lepton signatures at LHC. A detailed study is missing, but previous results seem to indicate that a lower bound on m_4 of order 300 GeV could be set with $5\,\text{fb}^{-1}$ of LHC data at 10 TeV [70].

Acknowledgments

We thank M. Hirsch and E. Fernández-Martínez for useful discussions. This work has been partially supported by the Spanish MICINN under grants FPA-2007-60323, FPA-2008-03373, Consolider-Ingenio PAU (CSD2007-00060) and CPAN (CSD2007-00042), by Generalitat Valenciana grants PROMETEO/2009/116 and PROMETEO/2009/128 and by the European Union within the Marie Curie Research & Training Networks, MRTN-CT-2006-035482 (FLAVIAnet). A.A. and J.H.-G. are supported by the MICINN under the FPU program.

A The neutrino mass two-loop integral

The relevant integral is

$$J \equiv J(m_4, m_{\bar{4}}, m_\alpha, m_\beta, m_W) = \\ = \int_{pq} \frac{p \cdot q}{\big((p+q)^2 - m_4^2\big)\big((p+q)^2 - m_{\bar{4}}^2\big)(p^2 - m_\alpha^2)(q^2 - m_\beta^2)(p^2 - m_W^2)(q^2 - m_W^2)}\,, \qquad \text{(A.1)}$$

where

$$\int_{pq} = \iint \frac{d^4p}{(2\pi)^4} \frac{d^4q}{(2\pi)^4}\,.$$

We combine propagators with the same momentum by using

$$\frac{1}{(p^2 - m_\alpha^2)(p^2 - m_W^2)} = \frac{1}{(m_\alpha^2 - m_W^2)} \int_{m_W^2}^{m_\alpha^2} \frac{dt_1}{(p^2 - t_1)^2}\,,$$

then

$$J = \int_t \int_{pq} \frac{(pq)}{(p^2 - t_1)^2 (q^2 - t_2)^2 ((p+q)^2 - t_3)^2}\,,$$

where

$$\int_t = \frac{1}{(m_\alpha^2 - m_W^2)} \frac{1}{(m_\beta^2 - m_W^2)} \frac{1}{(m_4^2 - m_{\bar{4}}^2)} \int_{m_W^2}^{m_\alpha^2} dt_1 \int_{m_W^2}^{m_\beta^2} dt_2 \int_{m_{\bar{4}}^2}^{m_4^2} dt_3\,.$$

Now we use the standard Feynman parametrization to combine the last two propagators and perform the integral in q, which leads to

$$J = -\frac{i}{(4\pi)^2} \int_t \int_0^1 \frac{dx}{1-x} \int_p \frac{p^2}{(p^2 - t_1)^2 \big(p^2 - t_3/(1-x) - t_2/x\big)^2}\,.$$

JHEP07(2011)122

The integral in p can be reduced by using an additional Feynman parameter and the final result can be written as

$$J = -\frac{2}{(4\pi)^4}\int_0^1 dx \int_0^1 dy \int_t \frac{y(1-y)x}{t_3 xy + t_2(1-x)y + t_1 x(1-x)(1-y)}\,. \tag{A.2}$$

The integrals in t_1, t_2, t_3 can be done analytically and reduced to logarithms. The expressions obtained are complicated but can be used to feed the final numerical integration in x and y which converges smoothly for most of the parameters. The expression in (A.2) is also very useful to obtain different approximations for small masses as compared with the largest mass in the integral. For that purpose one can use

$$\lim_{a\to 0}\lim_{b\to a}\frac{1}{b-a}\int_a^b dt f(t) = \lim_{a\to 0} f(a) = f(0)\,.$$

Thus, for instance if $m_{\bar{4}}, m_4 \gg m_\alpha, m_\beta, m_W \sim 0$ we can take $t_1, t_2 \to 0$ in the integrand and perform trivially the remaining integrals,

$$J = -\frac{1}{(4\pi)^4}\frac{1}{m_{\bar{4}}^2 - m_4^2}\ln\frac{m_{\bar{4}}^2}{m_4^2}\,, \tag{A.3}$$

in agreement with the result in [48].

If $m_\beta, m_{\bar{4}}, m_4 \gg m_\alpha, m_W \sim 0$ the integral can also be computed (take $t_1 \to 0$ in the integrand and perform the rest of the integrals). The result can be written in terms of the dilogarithm function $\mathrm{Li}_2(x)$ and it is rather compact,

$$J = -\frac{1}{(4\pi)^4 m_\beta^2}\left(\frac{\pi^2}{6} - \frac{m_{\bar{4}}^2}{m_{\bar{4}}^2 - m_4^2}\left(\mathrm{Li}_2\left(1-\frac{m_\beta^2}{m_{\bar{4}}^2}\right) - \frac{m_4^2}{m_{\bar{4}}^2}\mathrm{Li}_2\left(1-\frac{m_\beta^2}{m_4^2}\right)\right)\right).$$

When $m_\beta \to 0$ it reduces, as it should, to (A.3).

We are especially interested in the case $m_\alpha = m_\beta \equiv m_E$ with $m_E > m_W$, but $m_4, m_{\bar{4}}$ could be larger or smaller than m_E (and even smaller than m_W since we only know that $m_{\bar{4}} \geq m_4 > 63\,\mathrm{GeV}$). Some asymptotic expressions can be obtained when there are large hierarchies in masses

$$J \approx -\frac{1}{(4\pi)^4}\frac{1}{m_X^2}\ln\frac{m_X^2}{m_Y^2}\,,$$

where m_X is the heaviest of $m_E, m_{\bar{4}}, m_4, m_W$ and m_Y the next to the heaviest of these masses. This expression can be used to perform analytical estimates but, since in the allowed range of masses the hierarchies cannot be huge, we do expect large corrections to these estimates. Fortunately, as commented above, the exact value of J for all values of the masses can be obtained numerically rather easily using (A.2). For fast estimates one can use

$$J \approx \frac{1}{(4\pi)^4}\frac{1}{m_{\bar{4}}^2 - m_4^2 - m_E^2}\ln\left(\frac{m_{\bar{4}}^2 + m_E^2}{m_{\bar{4}}^2}\right), \qquad m_E, m_{\bar{4}}, m_4 \gg m_W\,,$$

which interpolates smoothly the different asymptotic expressions and reproduces the complete result with an error less than 50% in the worse case.

JHEP07(2011)122

References

[1] B.T. Cleveland et al., *Measurement of the solar electron neutrino flux with the Homestake chlorine detector*, *Astrophys. J.* **496** (1998) 505 [SPIRES].

[2] GALLEX collaboration, W. Hampel et al., *GALLEX solar neutrino observations: results for GALLEX IV*, *Phys. Lett.* **B 447** (1999) 127 [SPIRES].

[3] GNO collaboration, M. Altmann et al., *GNO solar neutrino observations: results for GNO I*, *Phys. Lett.* **B 490** (2000) 16 [hep-ex/0006034] [SPIRES].

[4] SNO collaboration, Q.R. Ahmad et al., *Direct evidence for neutrino flavor transformation from neutral-current interactions in the Sudbury Neutrino Observatory*, *Phys. Rev. Lett.* **89** (2002) 011301 [nucl-ex/0204008] [SPIRES].

[5] KamLAND collaboration, K. Eguchi et al., *First results from KamLAND: evidence for reactor anti-neutrino disappearance*, *Phys. Rev. Lett.* **90** (2003) 021802 [hep-ex/0212021] [SPIRES].

[6] Super-Kamiokande collaboration, Y. Fukuda et al., *Evidence for oscillation of atmospheric neutrinos*, *Phys. Rev. Lett.* **81** (1998) 1562 [hep-ex/9807003] [SPIRES].

[7] Soudan-2 collaboration, W.W.M. Allison et al., *The atmospheric neutrino flavor ratio from a 3.9 fiducial kiloton-year exposure of Soudan 2*, *Phys. Lett.* **B 449** (1999) 137 [hep-ex/9901024] [SPIRES].

[8] K2K collaboration, E. Aliu et al., *Evidence for muon neutrino oscillation in an accelerator-based experiment*, *Phys. Rev. Lett.* **94** (2005) 081802 [hep-ex/0411038] [SPIRES].

[9] R. Davis Jr., D.S. Harmer and K.C. Hoffman, *Search for neutrinos from the sun*, *Phys. Rev. Lett.* **20** (1968) 1205 [SPIRES].

[10] KAMIOKANDE-II collaboration, K.S. Hirata et al., *Experimental study of the atmospheric neutrino flux*, *Phys. Lett.* **B 205** (1988) 416 [SPIRES].

[11] The Borexino collaboration, G. Bellini et al., *Measurement of the solar 8B neutrino rate with a liquid scintillator target and 3 MeV energy threshold in the Borexino detector*, *Phys. Rev.* **D 82** (2010) 033006 [arXiv:0808.2868] [SPIRES].

[12] MINOS collaboration, P. Adamson et al., *Search for muon-neutrino to electron-neutrino transitions in MINOS*, *Phys. Rev. Lett.* **103** (2009) 261802 [arXiv:0909.4996] [SPIRES].

[13] T. Schwetz, M.A. Tortola and J.W.F. Valle, *Three-flavour neutrino oscillation update*, *New J. Phys.* **10** (2008) 113011 [arXiv:0808.2016] [SPIRES].

[14] M.C. Gonzalez-Garcia and M. Maltoni, *Phenomenology with massive neutrinos*, *Phys. Rept.* **460** (2008) 1 [arXiv:0704.1800] [SPIRES].

[15] P.H. Frampton, P.Q. Hung and M. Sher, *Quarks and leptons beyond the third generation*, *Phys. Rept.* **330** (2000) 263 [hep-ph/9903387] [SPIRES].

[16] B. Holdom et al., *Four statements about the fourth generation*, *PMC Phys.* **A 3** (2009) 4 [arXiv:0904.4698] [SPIRES].

[17] Particle Data Group collaboration, K. Nakamura et al., *Review of particle physics*, *J. Phys.* **G 37** (2010) 075021 [SPIRES].

[18] H.-J. He, N. Polonsky and S.-f. Su, *Extra families, Higgs spectrum and oblique corrections*, *Phys. Rev.* **D 64** (2001) 053004 [hep-ph/0102144] [SPIRES].

JHEP07(2011)122

[19] V.A. Novikov, A.N. Rozanov and M.I. Vysotsky, *Once more on extra quark-lepton generations and precision measurements*, *Phys. Atom. Nucl.* **73** (2010) 636 [arXiv:0904.4570] [SPIRES].

[20] J. Erler and P. Langacker, *Precision constraints on extra fermion generations*, *Phys. Rev. Lett.* **105** (2010) 031801 [arXiv:1003.3211] [SPIRES].

[21] C.T. Hill and E.A. Paschos, *A naturally heavy fourth generation neutrino*, *Phys. Lett.* **B 241** (1990) 96 [SPIRES].

[22] K.S. Babu and E. Ma, *Natural hierarchy of radiatively induced Majorana neutrino masses*, *Phys. Rev. Lett.* **61** (1988) 674 [SPIRES].

[23] S. Davidson, G. Isidori and A. Strumia, *The smallest neutrino mass*, *Phys. Lett.* **B 646** (2007) 100 [hep-ph/0611389] [SPIRES].

[24] W. Grimus and H. Neufeld, *Radiative neutrino masses in an* SU(2) × U(1) *model*, *Nucl. Phys.* **B 325** (1989) 18 [SPIRES].

[25] G.C. Branco, W. Grimus and L. Lavoura, *The seesaw mechanism in the presence of a conserved lepton number*, *Nucl. Phys.* **B 312** (1989) 492 [SPIRES].

[26] S.T. Petcov and S.T. Toshev, *Conservation of lepton charges, massive Majorana and massless neutrinos*, *Phys. Lett.* **B 143** (1984) 175 [SPIRES].

[27] T. Schwetz, M. Tortola and J.W.F. Valle, *Global neutrino data and recent reactor fluxes: status of three-flavour oscillation parameters*, *New J. Phys.* **13** (2011) 063004 [arXiv:1103.0734] [SPIRES].

[28] J. Bonn et al., *The Mainz neutrino mass experiment*, *Nucl. Phys. Proc. Suppl.* **91** (2001) 273 [SPIRES].

[29] V.M. Lobashev et al., *Direct search for neutrino mass and anomaly in the tritium beta-spectrum: status of 'Troitsk neutrino mass' experiment*, *Nucl. Phys. Proc. Suppl.* **91** (2001) 280 [SPIRES].

[30] KATRIN collaboration, A. Osipowicz et al., *KATRIN: a next generation tritium beta decay experiment with sub-eV sensitivity for the electron neutrino mass*, hep-ex/0109033 [SPIRES].

[31] J. Lesgourgues and S. Pastor, *Massive neutrinos and cosmology*, *Phys. Rept.* **429** (2006) 307 [astro-ph/0603494] [SPIRES].

[32] B.A. Reid, L. Verde, R. Jimenez and O. Mena, *Robust neutrino constraints by combining low redshift observations with the CMB*, *JCAP* **01** (2010) 003 [arXiv:0910.0008] [SPIRES].

[33] M.C. Gonzalez-Garcia, M. Maltoni and J. Salvado, *Robust cosmological bounds on neutrinos and their combination with oscillation results*, *JHEP* **08** (2010) 117 [arXiv:1006.3795] [SPIRES].

[34] H.V. Klapdor-Kleingrothaus et al., *Latest results from the Heidelberg-Moscow double beta decay experiment*, *Eur. Phys. J.* **A 12** (2001) 147 [hep-ph/0103062] [SPIRES].

[35] F.T. Avignone III, S.R. Elliott and J. Engel, *Double beta decay, Majorana neutrinos and neutrino mass*, *Rev. Mod. Phys.* **80** (2008) 481 [arXiv:0708.1033] [SPIRES].

[36] CDF collaboration, A. Lister, *Search for heavy top-like quarks* $t' \to Wq$ *using lepton plus jets events in 1.96 TeV* $p\bar{p}$ *collisions*, arXiv:0810.3349 [SPIRES].

JHEP07(2011)122

[37] C.J. Flacco, D. Whiteson and M. Kelly, *Fourth generation quark mass limits in CKM-element space*, arXiv:1101.4976 [SPIRES].

[38] L.M. Carpenter and A. Rajaraman, *Revisiting constraints on fourth generation neutrino masses*, *Phys. Rev.* **D 82** (2010) 114019 [arXiv:1005.0628] [SPIRES].

[39] G.D. Kribs, T. Plehn, M. Spannowsky and T.M.P. Tait, *Four generations and Higgs physics*, *Phys. Rev.* **D 76** (2007) 075016 [arXiv:0706.3718] [SPIRES].

[40] O. Eberhardt, A. Lenz and J. Rohrwild, *Less space for a new family of fermions*, *Phys. Rev.* **D 82** (2010) 095006 [arXiv:1005.3505] [SPIRES].

[41] H. Murayama, V. Rentala, J. Shu and T.T. Yanagida, *Saving fourth generation and baryon number by living long*, arXiv:1012.0338 [SPIRES].

[42] M.S. Chanowitz, M.A. Furman and I. Hinchliffe, *Weak interactions of ultraheavy fermions. 2*, *Nucl. Phys.* **B 153** (1979) 402 [SPIRES].

[43] C. Anastasiou, R. Boughezal and E. Furlan, *The NNLO gluon fusion Higgs production cross-section with many heavy quarks*, *JHEP* **06** (2010) 101 [arXiv:1003.4677] [SPIRES].

[44] CDF AND D0 collaboration, T. Aaltonen et al., *Combined Tevatron upper limit on $gg \to H \to W^+W^-$ and constraints on the Higgs boson mass in fourth-generation fermion models*, *Phys. Rev.* **D 82** (2010) 011102 [arXiv:1005.3216] [SPIRES].

[45] CMS collaboration, S. Chatrchyan et al., *Measurement of WW production and search for the Higgs boson in pp collisions at $\sqrt{s} = 7$ TeV*, *Phys. Lett.* **B 699** (2011) 25 [arXiv:1102.5429] [SPIRES].

[46] W.-Y. Keung and P. Schwaller, *Long lived fourth generation and the Higgs*, *JHEP* **06** (2011) 054 [arXiv:1103.3765] [SPIRES].

[47] W. Grimus and H. Neufeld, *3-neutrino mass spectrum from combining seesaw and radiative neutrino mass mechanisms*, *Phys. Lett.* **B 486** (2000) 385 [hep-ph/9911465] [SPIRES].

[48] K.S. Babu, E. Ma and J.T. Pantaleone, *Model of radiative neutrino masses: mixing and a possible fourth generation*, *Phys. Lett.* **B 218** (1989) 233 [SPIRES].

[49] D. Choudhury, R. Ghandi, J.A. Gracey and B. Mukhopadhyaya, *Two loop neutrino masses and the solar neutrino problem*, *Phys. Rev.* **D 50** (1994) 3468 [hep-ph/9401329] [SPIRES].

[50] K.S. Babu and E. Ma, *Radiative hierarchy of Majorana neutrino masses*, *Phys. Lett.* **B 228** (1989) 508 [SPIRES].

[51] A.J. Buras, B. Duling, T. Feldmann, T. Heidsieck and C. Promberger, *Lepton flavour violation in the presence of a fourth generation of quarks and leptons*, *JHEP* **09** (2010) 104 [arXiv:1006.5356] [SPIRES].

[52] H. Lacker and A. Menzel, *Simultaneous extraction of the Fermi constant and PMNS matrix elements in the presence of a fourth generation*, *JHEP* **07** (2010) 006 [arXiv:1003.4532] [SPIRES].

[53] S. Bertolini and A. Sirlin, *Effect of a fourth fermion generation on the m(t) upper bound*, *Phys. Lett.* **B 257** (1991) 179 [SPIRES].

[54] B.A. Kniehl and H.-G. Kohrs, *Oblique radiative corrections from Majorana neutrinos*, *Phys. Rev.* **D 48** (1993) 225 [SPIRES].

[55] MEG collaboration, F. Cei, *Lepton flavour violation experiments in LHC era*, *J. Phys. Conf. Ser.* **259** (2010) 012010 [SPIRES].

JHEP07(2011)122

[56] COMET collaboration, E.V. Hungerford, *COMET/PRISM muon to electron conversion at J-PARC*, *AIP Conf. Proc.* **1182** (2009) 694 [SPIRES].

[57] S. Antusch, C. Biggio, E. Fernandez-Martinez, M.B. Gavela and J. Lopez-Pavon, *Unitarity of the leptonic mixing matrix*, *JHEP* **10** (2006) 084 [hep-ph/0607020] [SPIRES].

[58] A. Pich, *Tau physics: theory overview*, *Nucl. Phys. Proc. Suppl.* **181-182** (2008) 300 [arXiv:0806.2793] [SPIRES].

[59] V. Cirigliano and I. Rosell, $\pi/K \to e\nu$ *branching ratios to* $O(e^2p^4)$ *in chiral perturbation theory*, *JHEP* **10** (2007) 005 [arXiv:0707.4464] [SPIRES].

[60] W.J. Marciano and A. Sirlin, *Electroweak radiative corrections to tau decay*, *Phys. Rev. Lett.* **61** (1988) 1815 [SPIRES].

[61] G.J. Feldman and R.D. Cousins, *A unified approach to the classical statistical analysis of small signals*, *Phys. Rev.* **D 57** (1998) 3873 [physics/9711021] [SPIRES].

[62] A. Lenz, H. Pas and D. Schalla, *Fourth generation Majorana neutrinos*, arXiv:1104.2465 [SPIRES].

[63] H. Pas, M. Hirsch, H.V. Klapdor-Kleingrothaus and S.G. Kovalenko, *A superformula for neutrinoless double beta decay. II: The short range part*, *Phys. Lett.* **B 498** (2001) 35 [hep-ph/0008182] [SPIRES].

[64] M.S. Chanowitz, *Probing for ultraheavy quanta at LHC*, *Phys. Lett.* **B 352** (1995) 376 [hep-ph/9503458] [SPIRES].

[65] T. Han and B. Zhang, *Signatures for Majorana neutrinos at hadron colliders*, *Phys. Rev. Lett.* **97** (2006) 171804 [hep-ph/0604064] [SPIRES].

[66] A. Atre, T. Han, S. Pascoli and B. Zhang, *The search for heavy Majorana neutrinos*, *JHEP* **05** (2009) 030 [arXiv:0901.3589] [SPIRES].

[67] F. del Aguila, J.A. Aguilar-Saavedra and R. Pittau, *Heavy neutrino signals at large hadron colliders*, *JHEP* **10** (2007) 047 [hep-ph/0703261] [SPIRES].

[68] F. del Aguila, S. Bar-Shalom, A. Soni and J. Wudka, *Heavy Majorana neutrinos in the effective Lagrangian description: application to hadron colliders*, *Phys. Lett.* **B 670** (2009) 399 [arXiv:0806.0876] [SPIRES].

[69] A. Rajaraman and D. Whiteson, *Tevatron discovery potential for fourth generation neutrinos: Dirac, Majorana and everything in between*, *Phys. Rev.* **D 82** (2010) 051702 [arXiv:1005.4407] [SPIRES].

[70] A. Rajaraman and D. Whiteson, *Discovering Majorana neutrinos produced via a Z boson at hadron colliders*, *Phys. Rev.* **D 81** (2010) 071301 [arXiv:1001.1229] [SPIRES].

[71] T. Cuhadar-Donszelmann, M. Karagoz, V.E. Ozcan, S. Sultansoy and G. Unel, *Fourth family neutrinos and the Higgs boson*, *JHEP* **10** (2008) 074 [arXiv:0806.4003] [SPIRES].

[72] L.M. Carpenter, A. Rajaraman and D. Whiteson, *Searches for fourth generation charged leptons*, arXiv:1010.1011 [SPIRES].

[73] L.M. Carpenter, *Fourth generation lepton sectors with stable Majorana neutrinos: from LEP to LHC*, arXiv:1010.5502 [SPIRES].

[74] A. Aparici, J. Herrero-García, N. Rius and A. Santamaria, *Neutrino masses in the presence of a fourth generation and an enlarged Higgs sector*, work in progress.

JHEP07(2011)122

Journal of Cosmology and Astroparticle Physics
An IOP and SISSA journal

On the annual modulation signal in dark matter direct detection

Juan Herrero-Garcia,[a,b] **Thomas Schwetz**[a] **and Jure Zupan**[c,1]

[a]Max-Planck-Institut für Kernphysik,
PO Box 103980, 69029 Heidelberg, Germany
[b]Departamento de Fisica Teorica, and IFIC, Universidad de Valencia-CSIC,
Edificio de Institutos de Paterna, Apt. 22085, 46071 Valencia, Spain
[c]Department of Physics, University of Cincinnati,
Cincinnati, Ohio 45221, U.S.A.

E-mail: juan.a.herrero@uv.es, schwetz@mpi-hd.mpg.de, jure.zupan@cern.ch

Received December 15, 2011
Revised February 8, 2012
Accepted February 13, 2012
Published March 5, 2012

Abstract. We derive constraints on the annual modulation signal in Dark Matter (DM) direct detection experiments in terms of the unmodulated event rate. A general bound independent of the details of the DM distribution follows from the assumption that the motion of the earth around the sun is the only source of time variation. The bound is valid for a very general class of particle physics models and also holds in the presence of an unknown unmodulated background. More stringent bounds are obtained, if modest assumptions on symmetry properties of the DM halo are adopted. We illustrate the bounds by applying them to the annual modulation signals reported by the DAMA and CoGeNT experiments in the framework of spin-independent elastic scattering. While the DAMA signal satisfies our bounds, severe restrictions on the DM mass can be set for CoGeNT.

Keywords: dark matter theory, dark matter experiments, dark matter detectors

ArXiv ePrint: 1112.1627

[1]On leave of absence from University of Ljubljana, Depart. of Mathematics and Physics, Jadranska 19, 1000 Ljubljana, Slovenia and Josef Stefan Institute, Jamova 39, 1000 Ljubljana, Slovenia.

doi:10.1088/1475-7516/2012/03/005

JCAP03(2012)005

Contents

JCAP03(2012)005

1 Introduction

A smoking-gun signature of the dark matter (DM) signal in DM direct detection experiments is the annual modulation of the event rate. This arises because the earth rotates around the sun, while at the same time the sun moves relative to the DM halo [1, 2]. Currently, two experiments report annual modulation of the signals, DAMA with 8.9σ significance [3], and CoGeNT with a significance of 2.8σ [4]. An important question is whether the observed modulation rates are consistent with the interpretation that the signal is due to DM. Ideally, one would like to answer this question without requiring a detailed knowledge of the DM halo. As we will show below, we come very close to this ideal.

The DM scattering rate in the detector is determined by the particle physics properties of DM and by the astrophysical properties of the DM halo. The latter carry large uncertainties. When presenting results of DM direct detection experiments, it has become customary to use a "standard" Maxwellian DM velocity distribution in order to show the constraints on DM mass and scattering cross section. This is very likely an oversimplification, with N-body simulations indicating a more complicated structure of the DM halo, see e.g., [5]. It is well known that the annual modulation signal is sensitive to such deviations from the Maxwellian halo [6–8]. DM streams are particularly relevant for the annual modulation signal and can lead to large effects. These can, for instance, be comparable in size to the modulation effect due to the whole Maxwellian halo [9–12].

In the following we will derive constraints on the amplitude of the annual modulation using measured unmodulated rates. The derivation of these bounds is made possible by

the fact that the velocity of the earth rotating around the sun, $v_e \sim 30$ km/s, is much smaller than the typical velocity of DM particles in the halo, $\langle v \rangle \sim 200$ km/s, and we can expand the velocity integral to first order in v_e. The derived constraints on the annual modulation then serve as a consistency check for the hypothesis that the annual modulation is due to the DM signal. The check that we provide is (almost) independent of DM halo properties. Previously halo independent methods to interpret DM direct detection data have been developed and applied in [13–18], with different goals than ours. In ref. [14] a method for determining the DM mass independently of the halo was developed, while refs. [13, 18] focused on extracting halo properties from the data. Compatibility studies of different experiments without adopting assumptions on the halo have been performed in [15–17]. Our goal is to obtain a consistency check between the modulation amplitude and the unmodulated signal within a given experiment.

The structure of the paper is as follows: in section 2 we set up the notation, followed in section 3 by a derivation of the general bound on the modulation signal under the very mild assumption that the properties of the DM halo in our vicinity do not change on time scales of months. In section 4 we impose further symmetry requirements on the DM velocity distribution and obtain successively more stringent bounds. In section 5 we then demonstrate the usefulness of our bounds by applying them to the modulation signals reported in CoGeNT and DAMA within elastic spin-independent scattering. We find that our method leads to non-trivial restrictions on DM interpretations of the modulation signal in CoGeNT whereas the DAMA signal satisfies our bounds for the relevant DM masses. We summarize in section 6. In appendix A we consider the Maxwellian DM halo and show that the expansion in v_e is rather accurate in this case. Furthermore, we illustrate the various bounds compared to the modulation signal expected for the Maxwellian halo. Appendix B provides technical details necessary to translate the bounds derived for the halo velocity integral into observable event rates. Supplementary material related to the treatment of an unknown background is given in appendix C.

2 Notation

The differential rate in events/keV/kg/day for DM χ to scatter off a nucleus (A, Z) and depositing the nuclear recoil energy E_{nr} in the detector is

$$R(E_{nr}, t) = \frac{\rho_\chi}{m_\chi} \frac{1}{m_A} \int_{v > v_m} d^3v \frac{d\sigma_A}{dE_{nr}} v f_{\rm det}(\mathbf{v}, t). \tag{2.1}$$

Here $\rho_\chi \simeq 0.3\,\mathrm{GeV/cm^3}$ is the local DM density, m_A and m_χ are the nucleus and DM masses, σ_A the DM-nucleus scattering cross section[1] and $\mathbf{v}$ the 3-vector relative velocity between DM and the nucleus, while $v \equiv |\mathbf{v}|$. For a DM particle to deposit recoil energy E_{nr} in the detector a minimal velocity v_m is required, restricting the integral over velocities in (2.1). For elastic scattering it is

$$v_m = \sqrt{\frac{m_A E_{nr}}{2\mu_{\chi A}^2}}, \tag{2.2}$$

where $\mu_{\chi A}$ is the reduced mass of the DM-nucleus system.

[1] Throughout this work we assume that DM is dominated by a single particle species. A generalization to multi-component DM is straightforward and will be pursued in future work.

JCAP03(2012)005

The function $f_{\rm det}(\mathbf{v},t)$ describes the distribution of DM particle velocities in the detector rest frame with $f_{\rm det}(\mathbf{v},t) \geq 0$ and $\int d^3v f_{\rm det}(\mathbf{v},t) = 1$. It is related to the velocity distribution in the rest frame of the sun by

$$f_{\rm det}(\mathbf{v},t) = f_{\rm sun}(\mathbf{v} + \mathbf{v}_e(t))\,, \tag{2.3}$$

where $\mathbf{v}_e(t)$ is the velocity vector of the earth, which we write as [9]

$$\mathbf{v}_e(t) = v_e[\mathbf{e}_1 \sin\lambda(t) - \mathbf{e}_2 \cos\lambda(t)] \tag{2.4}$$

with $v_e = 29.8$ km/s, and $\lambda(t) = 2\pi(t - 0.218)$ with t in units of 1 year and $t = 0$ at January 1st, while $\mathbf{e}_1 = (-0.0670, 0.4927, -0.8676)$ and $\mathbf{e}_2 = (-0.9931, -0.1170, 0.01032)$ are orthogonal unit vectors spanning the plane of the earth's orbit, assumed to be circular. Similarly, the DM velocity distribution in the galactic frame is connected to the one in the rest frame of the sun by $f_{\rm sun}(\mathbf{v}) = f_{\rm gal}(\mathbf{v} + \mathbf{v}_{\rm sun})$, with $\mathbf{v}_{\rm sun} \approx (0, 220, 0)\,{\rm km/s} + \mathbf{v}_{\rm pec}$ and $\mathbf{v}_{\rm pec} \approx (10, 13, 7)$ km/s the peculiar velocity of the sun. We are using galactic coordinates where x points towards the galactic center, y in the direction of the galactic rotation, and z towards the galactic north, perpendicular to the disc. As shown in [7], eq. (2.4) provides an excellent approximation to describe the annual modulation signal.

In the following we consider the typical situation, where the differential cross section is given by

$$\frac{d\sigma_A}{dE_{nr}} = \frac{m_A}{2\mu_{\chi A}^2 v^2}\sigma_A^0 F^2(E_{nr})\,, \tag{2.5}$$

where σ_A^0 is the total DM-nucleus scattering cross section at zero momentum transfer, and $F(E_{nr})$ is a form factor. The event rate is then given by

$$R(E_{nr},t) = C\,F^2(E_{nr})\,\eta(v_m,t) \qquad \text{with} \qquad C = \frac{\rho_\chi \sigma_A^0}{2m_\chi \mu_{\chi A}^2} \tag{2.6}$$

and the halo integral

$$\eta(v_m,t) \equiv \int_{v>v_m} d^3v \frac{f_{\rm det}(\mathbf{v},t)}{v}\,. \tag{2.7}$$

Here and in the following v_m and E_{nr} are related by eq. (2.2). This formalism covers a wide range of possible DM-nucleus interaction models, including the standard spin-independent and spin-dependent scattering. The results we derive below apply to all the cases where $d\sigma_A/dE_{nr} \propto 1/v^2$, in which case the halo integral (2.7) is obtained. The arguments can easily be generalized to a non-trivial q^2 dependence of the interaction, which would introduce an additional E_{nr} dependent function in (2.6) but would not change (2.7). Our results do not apply, however, to a non-standard velocity dependence of the cross section, which would modify eq. (2.7).

The rate will have a time independent component and an annually modulated component which we define as

$$R(E_{nr},t) = \overline{R}(E_{nr}) + \delta R(E_{nr},t) = C\,F^2(E_{nr})\,[\overline{\eta}(v_m) + \delta\eta(v_m,t)]\,. \tag{2.8}$$

Below we will be specifically interested in purely sinusoidal time dependence with period of one year, in which case we can write

$$\begin{aligned} \delta R(E_{nr},t) &= A_R(E_{nr}) \cos 2\pi[t - t_0(E_{nr})]\,, \\ \delta\eta(v_m,t) &= A_\eta(v_m) \cos 2\pi[t - t_0(E_{nr})]\,. \end{aligned} \tag{2.9}$$

JCAP03(2012)005

The peak of the annual modulation occurs at t_0, which in general depends on E_{nr} (or equivalently on v_m). The modulation amplitudes of the event rate, A_R, and of the halo integral, A_η, are related through $A_R(E_{nr}) = CF^2(E_{nr})A_\eta(v_m) \geq 0$. We will first derive bounds on A_η in terms of the time averaged value of the halo integral $\overline{\eta}$. In section 5 we will then translate the bounds into constraints involving the observable quantities A_R and $\overline{R}$.

3 General bound on the annual modulation amplitude

Assumption 1. We assume that the only time dependence comes from $\mathbf{v}_e(t)$ and there is no explicit time dependence in $f_{\rm sun}$.

This assumption implies that the halo is spatially constant at the scale of the sun-earth distance and also constant in time on scale of months. Under this assumption we can derive a general bound on the annual modulation by expanding eq. (2.7) in $v_e/v_m \ll 1$.[2] Using for short $f \equiv f_{\rm sun}$, we have

$$\eta(v_m, t) = \int_{|\mathbf{v}-\mathbf{v}_e|>v_m} d^3v \frac{f(\mathbf{v})}{|\mathbf{v}-\mathbf{v}_e|} \tag{3.1}$$

$$= \int_{v>v_m} d^3v \frac{f(\mathbf{v})}{v} + \int d^3v f(\mathbf{v}) \frac{\mathbf{v}\cdot\mathbf{v}_e(t)}{v^3} \left[\Theta(v-v_m) - \delta(v-v_m)v_m\right] + \mathcal{O}(v_e^2/v_m^2)\,, \tag{3.2}$$

where the first term in (3.2) gives the time independent part of the DM scattering signal. In polar coordinates the time independent halo integral is then given by

$$\overline{\eta}(v_m) = \int_{v>v_m} d^3v \frac{f(\mathbf{v})}{v} = \int_{v_m} dv\, v \int_0^{2\pi} d\varphi \int_{-1}^{1} d\cos\vartheta\, f(v,\vartheta,\varphi)\,. \tag{3.3}$$

The second term in (3.2) corresponds to the time dependent part of the DM scattering signal, with $\mathbf{v}_e(t)$ given in (2.4). Expanding to linear order in v_e thus leads to an annual modulation signal that has a sinusoidal shape. One can check experimentally for the convergence of the expansion by searching for higher order terms, $\propto v_e^2 \sin^2[2\pi(t-t_0)]$, etc. Note that the expansion is in v_e/v, where $v \gtrsim v_m$, so that the accuracy is typically better than $\mathcal{O}(v_e/v_m)$. In appendix A we demonstrate explicitly that this expansion is rather accurate in the case of a Maxwellian halo.

By expanding the velocity integral in the small quantity v_e we assume that $f(\mathbf{v})$ is smooth on scales $\lesssim v_e$. Hence, our bounds do not apply in situations where $f(\mathbf{v})$ has strong structures at scales smaller than v_e. An example would be a very cold stream with velocity $v_{\rm stream}$ and a dispersion smaller than v_e. In such a case the expansion will not be accurate for v_m in the range $|v_m - v_{\rm stream}| \lesssim v_e \sin\alpha$, though it may still work to good accuracy for v_m outside this range.

The time dependent component in (3.2) has two contributions

$$\delta\eta(v_m, t) = \int d^3v f(\mathbf{v}) \frac{\mathbf{v}\cdot\mathbf{v}_e(t)}{v^3} \left[\Theta(v-v_m) - \delta(v-v_m)v_m\right]. \tag{3.4}$$

[2] Typically v_m is sensitive to both the nucleus and the DM mass. For a 10 GeV DM mass and a recoil energy E_{nr} of a few KeV, we get for the nuclei we have analysed (Ge, Na, I) that $v_m \gtrsim 5v_e$ km/s, so the expansion is rather accurate (as we have checked explicitly for a Maxwellian halo in appendix A).

JCAP03(2012)005

The term with the Θ-function comes from expanding the denominator in eq. (3.1) and involves a volume integral over the region $v > v_m$. The term with the δ-function comes from taking into account the effect of v_e on the integration boundary, and the δ-function indicates that the argument has to be evaluated at the surface $v = v_m$. Let us treat the two terms separately and define

$$\hat{\mathbf{v}}_g(v_m) g(v_m) \equiv \int d^3v f(\mathbf{v}) \frac{\mathbf{v}}{v^3} \delta(v - v_m) \,, \tag{3.5}$$

$$\hat{\mathbf{v}}_G(v_m) G(v_m) \equiv \int d^3v f(\mathbf{v}) \frac{\mathbf{v}}{v^3} \Theta(v - v_m) \,. \tag{3.6}$$

The unit vectors $\hat{\mathbf{v}}_g(v_m)$ and $\hat{\mathbf{v}}_G(v_m)$ give the corresponding weight averaged DM wind directions in the earth's rest frame. In general they point in different directions and can depend on v_m. For the Maxwellian halo they point in the same direction and are equal to $\hat{\mathbf{v}}_g = \hat{\mathbf{v}}_G = -\mathbf{v}_{\rm sun}$. We will treat such special cases in the next section. The positive functions $g(v_m)$ and $G(v_m)$ are given by

$$g(v_m) = \int_0^{2\pi} d\varphi \int_{-1}^{1} d\cos\vartheta f(v_m, \vartheta, \varphi) \cos\vartheta \,, \tag{3.7}$$

$$G(v_m) = \int_{v_m} dv \int_0^{2\pi} d\varphi \int_{-1}^{1} d\cos\vartheta' f(v, \vartheta', \varphi) \cos\vartheta' \,, \tag{3.8}$$

where $\vartheta(\vartheta')$ is the angle between $\mathbf{v}$ and $\hat{\mathbf{v}}_g(\hat{\mathbf{v}}_G)$. The time dependent halo integral is thus given by

$$\delta\eta(v_m, t) = \mathbf{v}_e(t) \cdot \left[\hat{\mathbf{v}}_G(v_m) G(v_m) - \hat{\mathbf{v}}_g(v_m) v_m g(v_m)\right] \,. \tag{3.9}$$

As already mentioned, the form of $\mathbf{v}_e(t)$ from eq. (2.4) implies that our approximations lead to strictly sinusoidal modulations, justifying the ansatz in eq. (2.9), $\delta\eta(v_m, t) = A_\eta(v_m) \cos 2\pi(t - t_0)$. Using eq. (3.9), the modulation amplitude can be constrained in the following way:

$$A_\eta(v_m) \leq v_e \left[v_m g(v_m) + G(v_m)\right] \,. \tag{3.10}$$

Note that the two terms in eq. (3.9) will contribute to the modulation amplitude proportional to $\sin\alpha_g$ and $\sin\alpha_G$, respectively, where $\alpha_{g,G}$ is the angle between $\hat{\mathbf{v}}_{g,G}$ and the direction orthogonal to the plane of the earth orbit, i.e., $\cos\alpha_{g,G} = \hat{\mathbf{v}}_{g,G} \cdot \mathbf{e_3}$, with $\mathbf{e_3} = \mathbf{e_1} \times \mathbf{e_2}$, and $\mathbf{e}_{1,2}$ given below eq. (2.4). In general $\alpha_{g,G}$ will depend on v_m. To derive the bound we have assumed the maximal possible effect, corresponding to $\sin\alpha_g = \sin\alpha_G = 1$. Since we do not know the relative sign of the contributions from $g(v_m)$ and $G(v_m)$ we have to take the sum of the moduli.

The function $g(v_m)$ is bounded from above by

$$g(v_m) \leq \int d\varphi \, d\cos\vartheta f(v_m, \varphi, \vartheta) |\cos\vartheta| \leq \int d\varphi \, d\cos\vartheta f(v_m, \varphi, \vartheta) = -\frac{1}{v_m} \frac{d\overline{\eta}}{dv_m} \,, \tag{3.11}$$

where the last equality follows from eq. (3.3). Note that $\overline{\eta}(v_m)$ is a monotonously decreasing function and therefore, $d\overline{\eta}(v_m)/dv_m \leq 0$. Using again the last equality above, also a bound for $G(v_m)$ can be derived:

$$G(v_m) \leq -\int_{v_m} dv \frac{1}{v} \frac{d\overline{\eta}}{dv} = \frac{\overline{\eta}(v_m)}{v_m} - \int_{v_m} dv \frac{\overline{\eta}(v)}{v^2} . \tag{3.12}$$

JCAP03(2012)005

The equality in (3.12) follows from integration by parts. The inequalities (3.11) and (3.12) are saturated if $f(\mathbf{v}) \propto \delta(\vartheta)$, i.e., the hypothetical situation that all DM particles have the same direction and their velocities have no transversal component. Using eqs. (3.11) and (3.12) the bound on the modulation amplitude (3.10) becomes

$$A_\eta(v_m) \leq v_e \left[-\frac{d\overline{\eta}}{dv_m} + \frac{\overline{\eta}(v_m)}{v_m} - \int_{v_m} dv \frac{\overline{\eta}(v)}{v^2} \right] \qquad \text{(Assumption 1)}\,, \tag{3.13}$$

where the first two terms on the r.h.s. are positive and the third is negative. If the DM scattering rate $\overline{R}$ is measured, the r.h.s. is fully determined experimentally by $\overline{\eta}(v_m) = \overline{R}(E_{nr})/CF^2(E_{nr})$, and can be compared to the observed modulation through $A_\eta = A_R/CF^2(E_{nr})$, see section 5 for details. Note that the phase of the modulation (which may vary with v_m) does not appear in the bound (3.13). The bound applies on the modulation amplitude, irrespective of the phase. Eq. (3.13) is one of the main results of this paper. The bound is rather general and holds under the very mild Assumption 1 specified above. For it to be saturated the DM velocity distribution at the position of the solar system would need to be highly nontrivial. For instance, the bound in (3.10) can be saturated if there is a DM stream aligned with the ecliptic and it is strong enough so that it dominates the velocity distribution at $v = v_m$. Note that even in this case, for different v_m the bound will not be saturated. To saturate in addition eq. (3.11) or (3.12), the stream should have no transversal velocity dispersion. Any modulation signal which violates, or even just saturates, this bound is very unlikely to have a DM origin.

4 Bounds on the annual modulation for symmetric halos

Assumption 2. In addition to Assumption 1 we now assume that $\hat{\mathbf{v}}_g$ defined in eq. (3.5) is independent of v_m, i.e., we assume that there is a constant direction $\hat{\mathbf{v}}_{\rm halo} \equiv \hat{\mathbf{v}}_g$ governing the shape of the DM velocity distribution in the sun's rest frame.

From this assumption it follows immediately that $\hat{\mathbf{v}}_G$ is also constant and equal to $\hat{\mathbf{v}}_{\rm halo}$, so that

$$g(v_m) = -\frac{dG}{dv_m}\,, \tag{4.1}$$

and eq. (3.9) becomes

$$\delta\eta(v_m, t) = -\mathbf{v}_e(t) \cdot \hat{\mathbf{v}}_{\rm halo} \left[v_m g(v_m) - G(v_m) \right] . \tag{4.2}$$

The crucial difference to the general case (3.9) is that we were able to pull the velocity vector in front of the bracket. The functions $v_m g(v_m)$ and $G(v_m)$ are both positive. Their relative sizes determine whether the bracket is positive or negative. For small v_m the function $G(v_m)$ typically dominates and we get an extra half a year shift in the peak of the modulation (for the Maxwellian halo the peak would then be in December). For larger v_m the boundary term $v_m g(v_m)$ dominates and the whole bracket is positive (and thus for the Maxwellian halo the peak in this case is in June, see appendix A).

Assumption 2 is fulfilled if $f(\mathbf{v})$ obeys certain symmetry requirements that we can deduce from eq. (3.5). For a given v_m we chose a coordinate system such that $\hat{\mathbf{v}}_g = (1, 0, 0)$, and

$$\int d^3v f(\mathbf{v}) v_y \delta(v - v_m) = 0\,, \qquad \int d^3v f(\mathbf{v}) v_z \delta(v - v_m) = 0\,. \tag{4.3}$$

JCAP03(2012)005

Assumption 2 implies that these relations hold for any v_m in the same coordinate system. The distribution in v_x (i.e., in the direction of $\hat{\mathbf{v}}_{\rm halo}$) can be arbitrary, and can for instance even include several peaks, as long as $\hat{\mathbf{v}}_g$ does not flip sign. Therefore, we have to require that the integral over the half-sphere with $v_x > 0$ is larger than the one with $v_x < 0$ for all v_m:

$$\int_{v_x<0} d^3v f(\mathbf{v}) v_x \delta(v - v_m) < \int_{v_x>0} d^3v f(\mathbf{v}) |v_x| \delta(v - v_m) \,. \tag{4.4}$$

One possibility to satisfy the condition (4.3) is a symmetric velocity distribution, with $f(v_x, v_y, v_z) = f(v_x, -v_y, v_z)$ and $f(v_x, v_y, v_z) = f(v_x, v_y, -v_z)$ for all v_x. Eq. (4.3) can also be satisfied for distributions asymmetric in v_y and/or v_z, however, in this case the asymmetry has to be such that the cancellation between $v_{y,z} > 0$ and < 0 happens for all radii v_m.

Assumption 2 is fulfilled for the standard Maxwellian halo, as well as for any other isotropic velocity distribution. Up to small corrections due to the peculiar velocity of the sun it holds also for tri-axial halos, and covers also streams parallel to the motion of the sun, such as a dark disc co-rotating with the galactic stellar disc [19]. Note that for all those examples the DM direction $\hat{\mathbf{v}}_{\rm halo}$ is aligned with the motion of the sun (up to the peculiar velocity that leads to sub-leading corrections). Let us introduce this as an additional assumption:

Assumption 2a. In addition to Assumption 2 we require that the preferred direction $\hat{\mathbf{v}}_{\rm halo}$ is aligned with the motion of the sun relative to the galaxy.

As mentioned above, for many realistic cases fulfilling Assumption 2 also this additional requirement is fulfilled. An exception would be the situation when the DM density at the sun's location is dominated by a single stream from an arbitrary direction and the contribution of the static halo is negligible.

Let us now use eq. (4.2) to derive a bound on the modulation. We have $\mathbf{v}_e(t) \cdot \hat{\mathbf{v}}_{\rm halo} = -v_e \sin\alpha_{\rm halo} \cos(t - t_0)$, where t_0 is now independent of v_m. Here $\alpha_{\rm halo}$ is the angle between $\hat{\mathbf{v}}_{\rm halo}$ and $\mathbf{e}_1 \times \mathbf{e}_2$, i.e., the projection of $\hat{\mathbf{v}}_{\rm halo}$ on the ecliptic plane, with $\sin\alpha_{\rm halo} \geq 0$. Assumptions 2 and 2a thus imply that the phase of the modulation is independent of v_m (and therefore independent of E_{nr}). As discussed above this is up to a sign flip of the square bracket in eq. (4.2) that can happen due to the two competing terms. To take this into account we now define

$$\delta\eta(v_m, t) = A'_\eta(v_m) \cos(t - t_0) \,, \tag{4.5}$$

where t_0 is constant and we allow a sign change for $A'_\eta(v_m)$. This is different from A_η, which has been defined to be positive in eq. (2.9). While for Assumption 2 the phase is arbitrary but constant, Assumption 2a also gives a prediction for the phase — that the maximum (or minimum) of the event rate is around June 2nd. This can be checked in the experiment by looking at the annual modulation phase at different energy bins. Hence, from the experimental information on the phase we can conclude whether Assumptions 2 or 2a may be justified and whether it makes sense to apply the corresponding test.

A useful bound on the modulation can be obtained by first integrating eq. (4.2) over v_m,

$$\begin{aligned} \int_{v_{m1}}^{v_{m2}} dv_m A'_\eta(v_m) &= v_e \sin\alpha_{\rm halo} \int_{v_{m1}}^{v_{m2}} dv_m [v_m g(v_m) - G(v_m)] \\ &= v_e \sin\alpha_{\rm halo} \left[v_{m1} G(v_{m1}) - v_{m2} G(v_{m2}) \right] \,, \end{aligned} \tag{4.6}$$

where the second equality is obtained by integrating $v_m g(v_m)$ by parts using $g(v_m) = -dG/dv_m$, eq. (4.1). Note that the A'_η and $\alpha_{\rm halo}$ are defined in such a way that A'_η is

positive for large v_m, above the last sign flip. Experimentally, this is at present the most interesting region of the parameter space. Both putative modulation signals, at CoGeNT and DAMA, have a peak close to June, and no half year phase change is seen within the observed energy range.[3]

In general we do not know which of the two $v_m G(v_m)$ terms in (4.6) dominates. Dropping the smaller of the two and using the bound (3.12) we arrive at

$$\left|\int_{v_{m1}}^{v_{m2}} dv_m A'_\eta(v_m)\right| \leq v_e |\sin\alpha_{\rm halo}| \max\left[\overline{\eta}(v_{m1}) - v_{m1}\int_{v_{m1}} dv \frac{\overline{\eta}(v)}{v^2}, v_{m1}\to v_{m2}\right]. \tag{4.7}$$

Assumption 2 allows for arbitrary directions of the DM wind, therefore we need to use $|\sin\alpha_{\rm halo}| \to 1$ above, while for Assumption 2a one has $\sin\alpha_{\rm halo} \simeq 0.5$. Note that a sign flip of A'_η will lead to cancellations in the integral on the l.h.s. of eq. (4.7) and make the bounds weaker. An observation of such a sign flip in the modulation amplitude would be a strong experimental evidence that the modulation is due to a DM signal. If such a sign flip is observed, one might be able to obtain stronger constraints by applying the bound for the region below and above the sign flip separately, to avoid the cancellations.

At present there is no indication of such a sign flip in which case the bound (4.7) simplifies to

$$\int_{v_{m1}}^{v_{m2}} dv_m A'_\eta(v_m) \leq v_e \left[\overline{\eta}(v_{m1}) - v_{m1}\int_{v_{m1}} dv \frac{\overline{\eta}(v)}{v^2}\right] \qquad \text{(Assumption 2)}, \tag{4.8}$$

and

$$\int_{v_{m1}}^{v_{m2}} dv_m A'_\eta(v_m) \leq 0.5\, v_e \left[\overline{\eta}(v_{m1}) - v_{m1}\int_{v_{m1}} dv \frac{\overline{\eta}(v)}{v^2}\right] \qquad \text{(Assumption 2a)}. \tag{4.9}$$

The bounds (3.13), (4.8), (4.9) are the central results of this paper. In the following we will refer to them as

Eq. (3.13)	"general bound"	(Assumption 1),
Eq. (4.8)	"symmetric halo"	(Assumption 2),
Eq. (4.9)	"symmetric halo, $\sin\alpha = 0.5$"	(Assumption 2a).

The term "symmetric halo" should be understood in the sense of eqs. (4.3) and (4.4).

For completeness let us also mention an unintegrated bound, even though we will not use it for the numerical analysis. Using eq. (4.2) we have for the modulation amplitude

$$A_\eta(v_m) = v_e |\sin\alpha_{\rm halo}| |v_m g(v_m) - G(v_m)|. \tag{4.10}$$

Note that the minus sign between the two terms is conserved, while in the general case, eq. (3.10), one is forced to sum the two terms in the bound. From eqs. (3.11) and (3.12) one then obtains the following bound on the modulation

$$A_\eta(v_m) \leq v_e |\sin\alpha_{\rm halo}| \max\left[\left|\frac{d\overline{\eta}}{dv_m}\right|, \frac{\overline{\eta}(v_m)}{v_m} - \int_{v_m} dv \frac{\overline{\eta}(v)}{v^2}\right]. \tag{4.11}$$

A similar bound has been obtained recently in [18]. If eq. (B4) of [18] is expanded in u our bound (4.11) is obtained, if the derivative term dominates. However, eq. (B4) of [18] seems

[3] Note that the lowest energy bin in DAMA shows a somewhat smaller modulation amplitude, which might be an indication of a phase shift below the threshold.

JCAP03(2012)005

to neglect the possibility that the second term in eq. (4.11) dominates. This assumption is justified if data show no phase flip in the modulation and correspond to v_m above the last phase flip ($A'_\eta \geq 0$). In this case eq. (4.11) becomes

$$A'_\eta(v_m) \leq -v_e \sin\alpha_{\rm halo} \frac{d\overline{\eta}}{dv_m} \,. \tag{4.12}$$

Note that this bound is complementary to the ones from eqs. (4.8), (4.9). By taking the integral over the modulation amplitude those bounds probe global properties of the amplitude over the considered energy range, whereas eq. (4.12) bounds the local size of the modulation amplitude at a given value of v_m. Both bounds are necessary conditions which a modulation signal with a DM origin has to fulfill.

5 Applying the bound to data

In this section we show how the bounds (3.13), (4.8), (4.9) obtained in v_m space for halo integrals can be applied to observable quantities, the unmodulated rate $\overline{R}$ and the amplitude of the modulation of the rate, A_R. The halo integral and the DM scattering rate are proportional to each other, see eq. (2.6). The relation is complicated by the fact that experiments typically do not observe the recoil energy E_{nr} directly. The nuclear recoil energy is related to the observed energy through a quenching factor Q. In the case of CoGeNT and DAMA the observed energy E_{ee} is measured in electron equivalent and is related to the recoil energy by $Q = E_{ee}/E_{nr}$. In general this is a nonlinear equation, as Q also depends on the recoil energy. Finally, in an experiment data is reported in bins, and the continuous bounds derived above have to be integrated over the bin sizes. We relegate the details of the derivation to appendix B, and quote below only the final results.

5.1 Single target detector

Let us first assume that the target consists of a single material, as is for instance the case for CoGeNT. We denote the modulation amplitude and the unmodulated rate in bin i as A_i and R_i, respectively, both in units of counts/day/kg/keV$_{ee}$. The general bound (3.13) then becomes

$$A_i \leq v_e \left[R_i(\alpha_i + \beta_i) - R_{i+1}\alpha'_{i+1} - \langle\kappa\rangle_i \sum_{j=i}^{N} R_j\gamma_j \right] \qquad \text{(Assumption 1)}\,, \tag{5.1}$$

and the bounds for the symmetric halo are

$$\sum_{j=i}^{N} A_j x_j \leq v_e \sin\alpha \left[R_i y_i - \langle v_m\rangle_i \sum_{j=i+1}^{N} R_j\gamma_j \right] \qquad \text{(Assumptions 2, 2a)}\,, \tag{5.2}$$

where the bounds (4.8) (Assumption 2) and (4.9) (Assumption 2a) are obtained for $\sin\alpha = 1$ and 0.5, respectively. The bin index i runs from 1 to N, while the rates R_i are zero for $i > N$. The coefficients $\alpha_i, \alpha'_i, \beta_i, \langle\kappa\rangle_i, \gamma_i, x_i, y_i, \langle v_m\rangle_i$ are given in eqs. (B.9) and (B.12). They are known quantities calculable in terms of the form factor $F(E_{nr})$, quenching factor $Q(E_{nr})$, and Jacobians needed for changing the variable from v_m to E_{ee}. They depend on the DM mass m_χ via the reduced mass $\mu_{\chi A}$, eq. (2.2), needed to convert v_m into E_{nr}. The dependence

JCAP03(2012)005

on the scattering cross section and the local DM density is encoded in the constant factor C, eq. (2.6). This factor cancels completely, as expected, since it is a common factor for the modulation as well as for the rate.

The rates R_i in the bounds (5.1) and (5.2) are the unmodulated scattering rate induced by DM without including any backgrounds. In a "background free" experiment, where the full observed event rate is due to DM, the bounds can be applied as they are. Here we want to be more conservative, and consider also the situation where an unknown background may contribute to the unmodulated rate. The remaining assumption is then just that the background itself is not modulated, only the DM signal. In each bin a fraction ω_i of the observed count rate $\mathcal{R}_i$ is due to DM, i.e.,

$$R_i = \mathcal{R}_i \omega_i \,, \qquad 0 \leq \omega_i \leq 1 \,, \tag{5.3}$$

so that we can replace $R_i \to \mathcal{R}_i \omega_i$ in eqs. (5.1) and (5.2) to obtain,

$$A_i \leq v_e \left[\mathcal{R}_i \omega_i (\alpha_i + \beta_i) - \mathcal{R}_{i+1} \omega_{i+1} \alpha'_{i+1} - \langle \kappa \rangle_i \sum_{j=i}^{N} \mathcal{R}_j \omega_j \gamma_j \right] \qquad \text{(Assumption 1)} \,, \tag{5.4}$$

$$\sum_{j=i}^{N} A_j x_j \leq v_e \sin\alpha \left[\mathcal{R}_i \omega_i y_i - \langle v_m \rangle_i \sum_{j=i+1}^{N} \mathcal{R}_j \omega_j \gamma_j \right] \qquad \text{(Assumptions 2, 2a)} \,. \tag{5.5}$$

Now we have to find a set of ω_i $(i = 1, \ldots, N)$, such that the bound becomes the "weakest". In the following we describe two different procedures for this task. Procedure 1 is easy to implement but gives slightly weaker bounds, whereas procedure 2 involves an optimization algorithm but gives somewhat more stringent bounds.

Procedure 1. We can sum eq. (5.4) from bin i to N and drop the last term in the square bracket, since $\langle \kappa \rangle_i$ and γ_i are positive:

$$\sum_{j=i}^{N} A_j \leq v_e \left[\mathcal{R}_i \omega_i \alpha_i + \sum_{j=i}^{N} \mathcal{R}_j \omega_j \beta_j \right] \leq v_e \left[\mathcal{R}_i \alpha_i + \sum_{j=i}^{N} \mathcal{R}_j \beta_j \right] \qquad \text{(Assumption 1)} \,, \tag{5.6}$$

where the last inequality was obtained by setting $\omega_i = 1$. Similarly we can drop the second term from eq. (5.5) and obtain

$$\sum_{j=i}^{N} A_j x_j \leq v_e \sin\alpha \, \mathcal{R}_i \omega_i y_i \leq v_e \sin\alpha \, \mathcal{R}_i y_i \qquad \text{(Assumptions 2, 2a)} \,, \tag{5.7}$$

where the last inequality holds for $y_i > 0$.[4] These bounds have to be satisfied for all bins i.

Procedure 2. A somewhat stronger bound can be obtained by searching for the optimal choice for the ω_i, without dropping the last terms in eqs. (5.4) and (5.5). We present here a method based on a least-square minimization (an alternative procedure is outlined in appendix C). Let us denote the r.h.s. of eqs. (5.4) and (5.5) as B_i which are functions of ω_j. Then we can construct from eq. (5.4) the following least-square function

$$X^2 = \sum_{i=1}^{N} \left(\frac{A_i - B_i}{\sigma_i^A} \right)^2 \Theta(A_i - B_i) \qquad \text{(Assumption 1)} \,, \tag{5.8}$$

[4] According to eq. (B.12) y_i can also become negative. In that case the bound (5.7) is always violated for any $\omega_i \geq 0$.

where σ_i^A is the 1σ error on A_i (errors on B_i are typically much smaller and we neglect them here). This X^2 can now be minimized with respect to ω_j under the condition $0 \leq \omega_j \leq 1$. The Θ function takes into account that there is only a contribution to X^2 if the bound is violated. Hence, X^2 will be zero if the bound is satisfied for all bins. A non-zero value of X^2 indicates that the bound is violated for some bin(s), weighted by the corresponding error in the usual way. In the case of eq. (5.5) one has to take into account that the modulation amplitude in each bin is used several times, leading to correlated errors for the l.h.s.:

$$X^2 = \sum_{i,j=1}^{N} (\mathcal{A}_i - B_i) S_{ij}^{-1} (\mathcal{A}_j - B_j) \Theta(\mathcal{A}_i - B_i) \Theta(\mathcal{A}_j - B_j) \qquad \text{(Assumption 2,2a)}\,, \tag{5.9}$$

where

$$\mathcal{A}_i \equiv \sum_{k=i}^{N} A_k x_k \qquad \text{and} \qquad S_{ij} = \sum_{k=1}^{N} \frac{d\mathcal{A}_i}{dA_k} \frac{d\mathcal{A}_j}{dA_k} \left(\sigma_k^A\right)^2 = \sum_{k=\max(i,j)}^{N} \left(x_k \sigma_k^A\right)^2 . \tag{5.10}$$

While non-zero values of the X^2 functions (5.8) and (5.9) can be considered as a qualitative measure for the violation of the bound, the precise distribution of them should be determined by Monte Carlo studies. From the definition one can expect, however, that they will be approximately χ^2 distributed if the bound is violated.

5.1.1 CoGeNT

Let us consider now the modulation signal reported by the CoGeNT experiment at 2.8σ [4]. It has been pointed out that for specific assumptions on the halo (standard Maxwellian) there is a tension between the modulated and unmodulated rate in CoGeNT [20, 22, 23]. Recent analyses on the CoGeNT modulation signal can be found in refs. [24, 25], see also [18]. Here we use the CoGeNT data for a case study and apply the above bounds assuming spin-independent elastic scattering. For the germanium quenching factor we use $E_{ee}[\text{keV}] = 0.199(E_{nr}[\text{keV}])^{1.12}$ [26]. We adopt the Helm parameterization of the spin-independent form factor, $F(E_{nr}) = 3e^{-q^2 s^2/2}[\sin(qr) - qr\cos(qr)]/(qr)^3$, with $q^2 = 2m_A E_{nr}$ and $s = 1\,\text{fm}$, $r = \sqrt{R^2 - 5s^2}$, $R = 1.2A^{1/3}\,\text{fm}$. We use the data from figure 6 of ref. [20] where the total rate $\mathcal{R}$ and the modulation amplitude A_R are given in four bins of E_{ee} between 0.5 and 3.1 keV. We reproduce the data in table 1.[5]

The modulation amplitude has been extracted in three different ways in [20]. First, by fitting independently the modulation phase for each energy bin, second, by assuming a constant phase for all bins, and third, by fixing the phase such that the modulation maximum is on June 2nd. These are precisely the requirements corresponding to our Assumptions 1, 2, 2a, respectively. We can thus use the appropriate data on the modulation for each of the three assumptions. The modulation amplitudes in the first and the second case are very similar, while in the third case (forcing the phase to equal June 2nd) the amplitudes are lower and error bars are larger.

Choosing three values of the DM mass as examples, we show in figure 1 the bound on the integrated modulation amplitude for Assumption 1, and using procedure 1. The bin labels on the horizontal axis give the ith energy bin, which is the lower limit of summation in eq. (5.6). The data on amplitudes are shown as red dots, while the bounds are shown in

[5]We thank Mariangela Lisanti for providing us the data from figure 6 of ref. [20].

JCAP03(2012)005

E_{ee} bins [keV]	Mod. (Ass. 1, 2)	Mod. (Ass. 2a)	Unmod. rate	Corrected rate
0.5–0.9	1.41 ± 0.79	0.90 ± 0.72	12.33 ± 0.52	5.29 ± 0.52
0.9–1.5	0.84 ± 0.59	0.37 ± 0.55	4.33 ± 0.39	3.36 ± 0.39
1.5–2.3	0.46 ± 0.24	0.48 ± 0.22	2.76 ± 0.16	2.76 ± 0.16
2.3–3.1	0.66 ± 0.24	0.27 ± 0.23	2.83 ± 0.17	2.83 ± 0.17

Table 1. CoGeNT data on modulation amplitude and unmodulated rate [4] in cnts/day/kg/keV, as reported in . 6 of ref. [20]. The modulation has been extracted allowing for indpendent phases in each bin (Ass. 1) and for a constant but arbitrary phase (Ass. 2) (which lead to very similar amplitudes), and by requiring the maximum at June 2nd (Ass. 2a). In the last column we show the preliminary surface events corrected unmodulated rate [21].

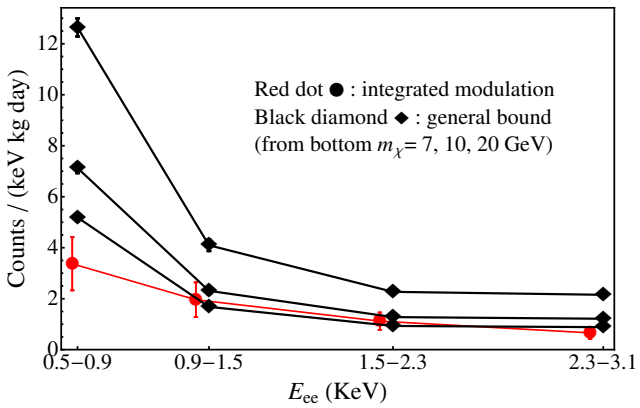

Figure 1. Procedure 1 upper bound compared to the integrated modulation amplitude from the CoGeNT data, from figure 6 of [20]. The red dots correspond to the l.h.s. of eq. (5.6). The black diamonds correspond to the upper bound obtained under Assumption 1, r.h.s. of eq. (5.6), for DM masses of $m_\chi = 7, 10, 20\,\text{GeV}$ (from bottom to top) . The bins on the horizontal axis indicate the bin i from which we start to sum the data. Error bars correspond to 1σ.

black. Whenever a red dot lies above one of the bounds (within errors), the DM hypothesis is disfavoured. In figure 1 this happens for the case of DM mass $m_\chi = 7\,\text{GeV}$. Such light DM thus cannot be the source of the modulation, even under the very general assumption on the DM halo adopted here.

We see from figure 1 that the strongest restriction comes from the bins $i = 2$ or 3. In figure 2 we show the constraints on DM mass that follow from the bounds on the modulation amplitudes in these two bins. The bounds are obtained from procedure 1 for the three Assumptions 1, 2, 2a. We observe that the bound becomes stronger for smaller DM masses. This behaviour can be understood from how the coefficients defined in appendix B depend on the reduced mass $\mu_{\chi A}$. The bounds on amplitudes are violated for DM masses below 10, 27, 33 GeV, respectively, for the three assumptions. The lower bounds on m_χ are summarized in table 2 (left part), where we also give the bounds at 1σ and 2σ. Notice that due to the smaller modulation amplitudes and larger errors when extracted from the data under Assumption 2a, at 95% CL the corresponding bound becomes weaker than the one from Assumption 2 and equal to the one from Assumption 1, although naively one would expect the opposite. This can be traced back to the fact that, under Assumption 2a, the modulation phase is forced

JCAP03(2012)005

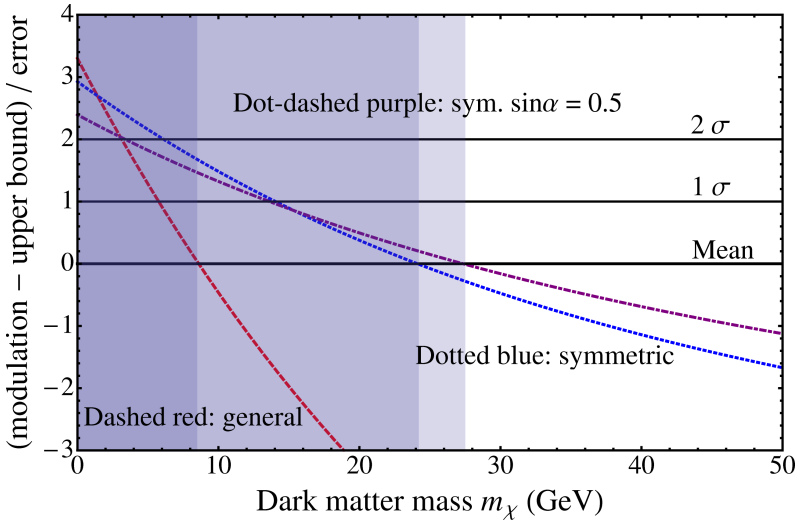

Figure 2. Bounds on the CoGeNT modulation amplitude for the three assumptions about the DM halo (1, 2, 2a), and using eqs. (5.6) and (5.7) (procedure 1). We show the l.h.s. (integrated modulation amplitude) minus the r.h.s. (upper bound) divided by the error on the l.h.s., as a function of DM mass. We sum the data starting from bin $i = 3, 2$ and 3 for Assumptions 1, 2 and 2a, respectively. The bounds are violated in the regions where the curves are above zero, which are shaded in the plot.

	unmodulated rate from [4]				corrected unmod. rate [21]			
	Mean	68%	95%	$X^2 \leq 1$	Mean	68%	95%	$X^2 \leq 1$
Ass. 1: general bound	8.5	6	3	7.3	10	6.5	3	10
Ass. 2: symmetric halo	24	14	6	18	43	25	12.5	37
Ass. 2a: sym. halo, $\sin\alpha = 0.5$	27.5	13.5	3.5	16	59.5	23	3	35

Table 2. Lower bounds on the DM mass in GeV, from the requirement that the modulation amplitude in CoGeNT is consistent with the upper bound from the unmodulated rate, according to the Assumptions 1, 2, 2a on the DM distribution. The bounds are obtained from procedure 1, requiring that eqs. (5.6) or (5.7) are satisfied for the mean value, or the 68% and 95% CL limits. The bounds labeled "$X^2 \leq 1$" are obtained from procedure 2 by requiring that X^2 defined in eqs. (5.8) or (5.9) is less than 1. In the left part of the table we use the published unmodulated event rates from [4], whereas for the right part of the table we adopt the preliminary results on surface events contamination at low energies from [21].

to take the value of June 2nd which is not the one preferred by the data. The extracted modulation signal then gets weaker and consequently the bounds are more easily satisfied. We have also checked that bounds for Assumptions 2, 2a derived from eq. (4.12) give always weaker limits than the ones discussed here, which are based on eq. (4.8) and eq. (4.9).

In figure 3 we show the X^2 functions according to procedure 2 as a function of the DM mass. For a given value of m_χ we minimize X^2 numerically with respect to the ω_j. The conclusion is similar to procedure 1, leading to similar lower bounds on the DM mass. Requiring that $X^2 \leq 1$ one finds $m_\chi \geq 7.3, 18, 16\,\text{GeV}$ for Assumptions 1, 2, 2a, respectively. We observe again the unusual situation that Assumption 2a leads to a weaker constraint, due

JCAP03(2012)005

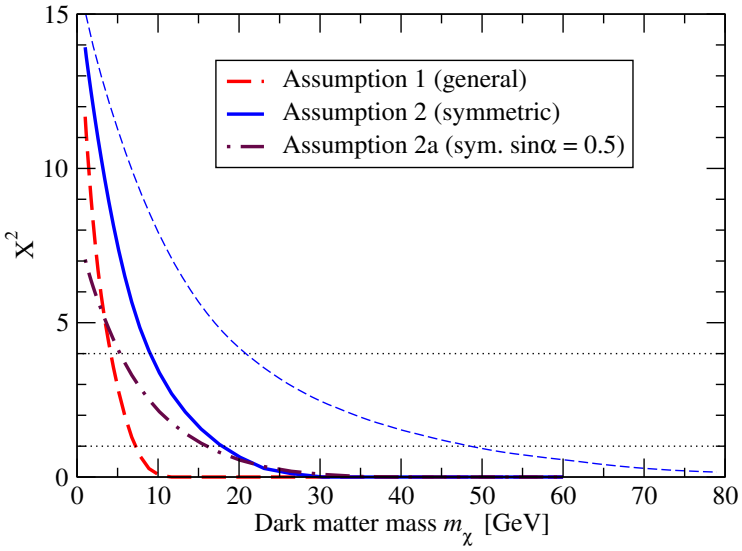

Figure 3. Bounds on the CoGeNT modulation amplitude for the three assumptions about the DM halo (1, 2, 2a), always using procedure 2. We show X^2 defined in eqs. (5.8) and (5.9) as a function of DM mass. The thin dashed curve is for illustrative purpose only; it corresponds to the data and errors on the modulation amplitude extracted with a free phase (Assumption 2) but using the bound for Assumption 2a, see text for details. If we assume that X^2 is distributed as a χ^2 with 1 d.o.f. (see below) $X^2 = 1\,(4)$ corresponds to 68% (95%) CL.

to the less significant signal for the modulation. To illustrate this effect we show in figure 3 with a thin-dashed curve also X^2 that would follow from the hypothetical situation where the modulation amplitude would be as strong as in the case of Assumption 2. That is, we allow for an arbitrary energy independent phase, but assume that this phase turned out to be June 2nd (in contrast to the real CoGeNT data), so that we could apply the bound from Assumption 2a to these data. We see that in this case one would obtain a much stronger bound, disfavoring DM masses up to 60 GeV. This example shows the potential of our method in cases of a strong modulation signal in the data. If the signal for the modulation itself is weak, the bounds we derived will also give only weak constraints.

A recent re-analysis of CoGeNT data indicates that a significant fraction of the event excess at low energies could be due to surface events [21]. Assuming that surface events are not modulated, the unmodulated rate will be reduced after subtructing the surface events, while the modulation signal will remain, leading to a strengthening of our bounds. Here we estimate this effect by using the preliminary result for a surface events rejection efficiency shown on slide 19 of the presentation in [21] (red curve). Averaging this curve for the bins used in our analysis we find that the unmodulated rate in the first and second bins are reduced by a factor 0.43 and 0.78, respectively, while the other two bins are not effected. This leads to the reduced event rates shown in the last column of table 1. Figure 4 shows the plots equivalent to figures 2 and 3 but using the surface events corrected unmodulated rate. The general bound remains essentially the same. In this case the strongest limit (from procedure 1) for the uncorrected rate comes from summing data starting from bin 3, whereas in the surface events corrected case it comes from bin 2, with only a minor reduction (79%)

JCAP03(2012)005

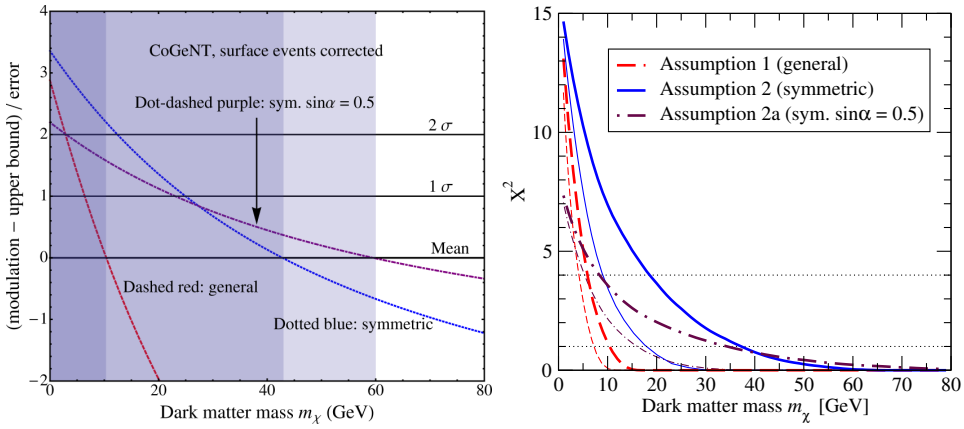

Figure 4. Bounds on the CoGeNT modulation amplitude for the preliminary surface events corrected unmodulated rate [21] for the three assumptions about the DM halo (1, 2, 2a). The left plot shows the bounds according to procedure 1, whereas the right plot shows X^2 defined in eqs. (5.8) and (5.9) (procedure 2). The thin curves in the right panel are the bounds without surface event subtruction reproduced from figure 3 for the purpose of comparison with the thick curves obtain with the surface event corrected rates.

of the rate, leading to a very similar limit. In contrast, for Assumptions 2 and 2a significantly stronger bounds are obtained, with the limit coming now from summing from bin 1, with a 43% reduced rate. The surface events corrected bounds are summarized in the right part of table. 2.

Due to the non-standard definition of the X^2 functions (5.8) and (5.9), involving the Θ-function, the actual distribution of them is not clear a priori. Therefore we have performed a Monte Carlo study in order to determine the distribution. For a given DM mass we first determine the optimal set of ω_i by minimizing the X^2. For those ω_i we assume that the bound is saturated and we simulate a large number of pseudo-data taking the r.h.s. of eqs. (5.4), (5.5) as mean value for a Gaussian with standard deviation given by the actual error on the modulation amplitude.[6] For each random data set we calculate the X^2 value and obtain therefore the distribution of X^2 assuming that the bound is saturated. Then we can compare the X^2 of the actual data and calculate the probability of obtaining a X^2 larger than the observed one. Note that this procedure is conservative, since we assume that the mean value of the random data is the bound itself. If the "true" mean values are smaller than the bound, the distribution of X^2 would be shifted towards smaller values, leading to more stringent bounds.

We show the results of this calculation in figure 5. The probabilities obtained in this way are in qualitative agreement with the numbers reported in table 2. Under assumptions 2 and 2a, surface event corrected data is inconsistent with the DM hypothesis for any DM mass at the 97% and 90% CL, respectively. We find that if the bound is violated (i.e., for small DM masses) the X^2 distribution is close to a χ^2-distribution with 1 d.o.f.. Large deviations from a χ^2-distribution occur if X^2 is close to zero (i.e., for larger DM masses). In

[6] In the case of Assumptions 2 and 2a we proceed iteratively. Starting from eq. (5.5) for $i = N$ we generate A_N, and then simulate successively A_{i-1}. This is necessary to obtain the correct random properties of the l.h.s. of eq. (5.5).

JCAP03(2012)005

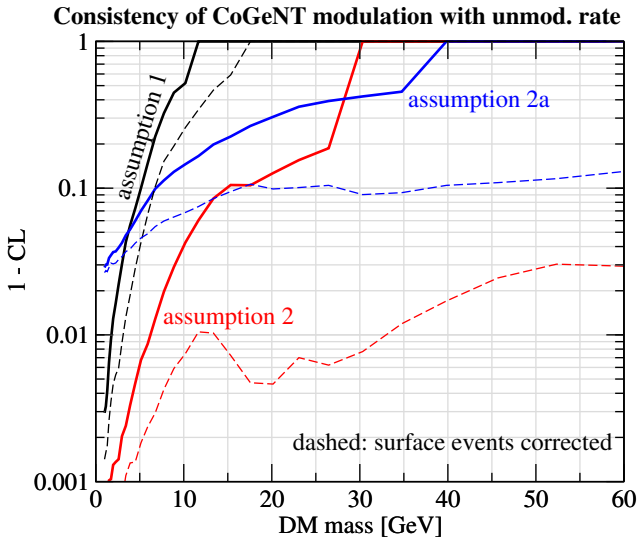

Figure 5. The probability to obtain a X^2 larger than the one obtained from CoGeNT data, as determined by Monte Carlo simulation. Dashed curves correspond to surface event corrected data.

this case the X^2 distribution is strongly peaked at small values close to zero. This indicates that in such situations it is in most cases possible to find a set of ω_i such that X^2 becomes zero. This is the reason why non-trivial constraints are obtained under assumptions 2, 2a for surface events corrected data at large masses, although the values of X^2 are relatively small, compare figure 4.

5.2 Bounds for multi-target experiments

So far we have restricted the discussion to the situation where only one target nucleus is present, as for example Ge in CoGeNT. Let us now generalize our bounds to experiments where several elements are used as DM target. In this case both the modulation amplitude as well as the unmodulated rate will receive contributions from each element: $A_i = \sum_n A_i^n$ and $R_i = \sum_n R_i^n$, where n labels the different target elements and i energy bins. The bounds from procedure 1 hold for each of the elements separately, where in general all the coefficients appearing in the equations will depend on the nucleus type. Summing eqs. (5.6) and (5.7) over n and using the fact that for positive a_i and b_i, the following inequality holds, $\sum_i a_i b_i \leq (\sum_i a_i)(\sum_j b_j)$, we derive:

$$\sum_{j=i}^{N} A_j \leq v_e \left[\mathcal{R}_i \sum_n \alpha_i^n + \sum_{j=i}^{N} \mathcal{R}_j \sum_n |\beta_j^n| \right] \qquad \text{(Assumption 1)}\,, \tag{5.11}$$

$$\sum_{j=i}^{N} A_j \min_n \left(x_j^n\right) \leq v_e \sin\alpha\, \mathcal{R}_i \sum_n |y_i^n| \qquad \text{(Assumptions 2, 2a)}\,. \tag{5.12}$$

On the l.h.s. of the last inequality it is necessary to take the minimum of x_j^n between all the nuclei present in the target, for each bin. We used that α_i and x_j are positive, see appendix B.

It is possible to generalize also the X^2 method to the case of multiple targets. For each nucleus the bounds (5.4) and (5.5) apply separately. We define the amplitude from element n

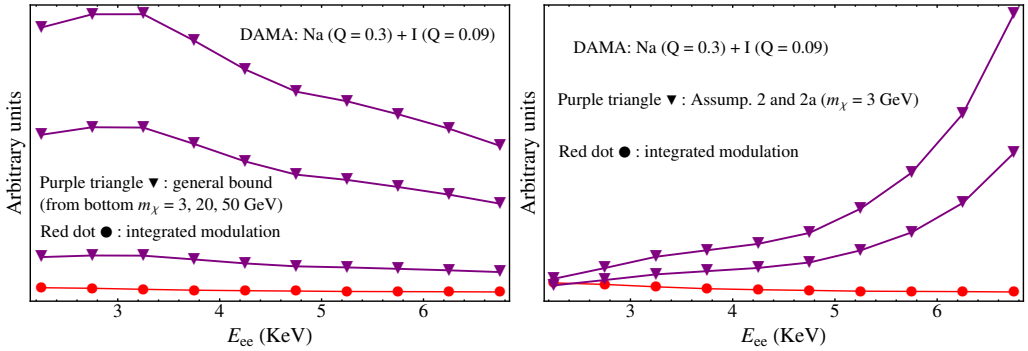

Figure 6. Upper bound compared to the integrated modulation amplitude for DAMA data for Assumption 1 (left) and Assumptions 2 and 2a (right). We assume quenching factors $q = 0.3$ and $q = 0.09$ for Na and I, respectively. The red dots correspond to the l.h.s. of eqs. (5.11) and (5.12), and the purple triangles to the r.h.s.. In the left panel we show the bounds for DM masses of $m_\chi = 3, 20, 50\,\text{GeV}$ (from bottom), in the right panel for $m_\chi = 3\,\text{GeV}$. Bins are 0.5 keV wide and we sum all bins starting from bin i shown on the horizontal axis up to 7 keVee. Error bars are negligible and are not shown for clarity. All dark matter masses are compatible with the modulation.

in the bin i as $A_i^n = \epsilon_i^n A_i$, and similarly for the rate $R_i^n = \omega_i^n \mathcal{R}_i$. Then one can construct a X^2 similar to the one in the previous section, from l.h.s. minus r.h.s. of the following inequality:

$$\epsilon_i^n A_i \leq v_e \left[\mathcal{R}_i \omega_i^n (\alpha_i^n + \beta_i^n) - \mathcal{R}_{i+1} \omega_{i+1}^n \alpha_{i+1}^n - \langle \kappa^n \rangle_i \sum_{j=i}^{N} \mathcal{R}_j \omega_j^n \gamma_j^n \right] \qquad \text{(Assumption 1)}\,. \tag{5.13}$$

This X^2 is minimized over $\omega_i^n \geq 0$, $\epsilon_i^n \geq 0$ given the constraints $\sum_n \omega_i^n \leq 1$ and $\sum_n \epsilon_i^n = 1$ for each i. A similar relation can be set up for Assumption 2.

5.2.1 DAMA

Let us now apply above bounds to the DAMA result, based on data from a NaI detector. DAMA observes a relatively large unmodulated count rate of about 1 cnt/kg/day/keV compared to the modulation amplitude of about 0.02 cnt/kg/day/keV. In contrast, CoGeNT reports a modulation amplitude in the range of 0.5 to 1 cnt/kg/day/keV, compared to an unmodulated rate of 3 to 4 cnt/kg/day/keV. Because of this much smaller modulation amplitude compared to the unmodulated rate for DAMA we expect the signal to be consistent with our bounds. It is also well known that a consistent fit of the DAMA modulated and unmodulated data is possible e.g., for a Maxwellian halo, although in certain parameter regions the unmodulated rate does provide a non-trivial constraint, see e.g. [8, 11]. In figure 6 we show the bounds for DAMA, assuming quenching factors of 0.3 for Na and 0.09 for I (constant in energy) using the spectral data on the modulated and unmodulated rates from [3]. We find that both the general bound, eq. (5.11), as well as the bounds for a symmetric halo, eq. (5.12), are consistent with the modulation even for a DM mass as small as 3 GeV. As noted above the bounds get weaker for larger DM masses, hence they do not place any relevant constraint on the dark matter interpretation of the DAMA modulation signal.

In deriving the multi-target bounds eqs. (5.11) and (5.12) we had to use inequalities related to the presence of several contributions to the rates, which makes the bounds some-

JCAP03(2012)005

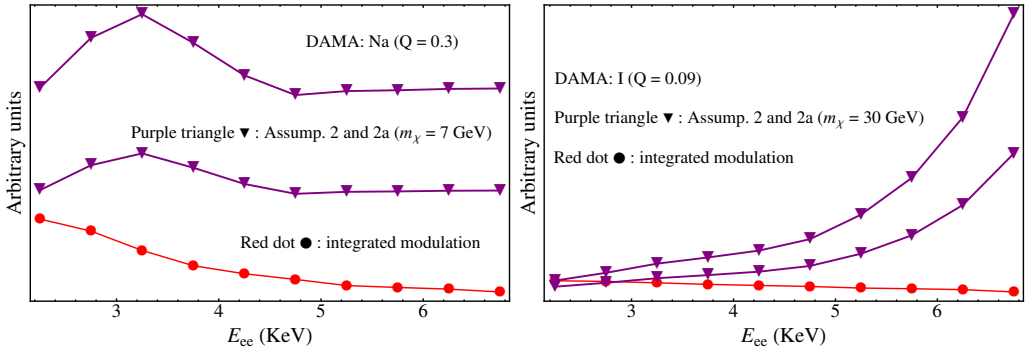

Figure 7. Upper bound compared to the integrated modulation amplitude from DAMA data for Assumptions 2 and 2a, assuming that DM scatters only on sodium (left) or iodine (right). The red dots correspond to the l.h.s. of eq. (5.7) and the purple triangles to the r.h.s., for a DM mass of $m_\chi = 7\,\text{GeV}$ (left) and 30 GeV (right). Bins are 0.5 keV wide and we sum all bins starting from bin i shown on the horizontal axis up to 7 keVee. Error bars are negligible and are not shown for clarity.

what weaker than single target bounds. In case of NaI we have a relatively large hierarchy between the two targets since $A = 23$ for Na and $A = 127$ for I. Therefore, one may consider also the situation that only one of them dominates the signal. If scattering on both targets is kinematically allowed, iodine will dominate because of the A^2 enhancement of the spin-independent scattering cross section (which we will assume here). For low DM masses, scattering on iodine may be kinematically forbidden since v_m is larger than the escape velocity of the halo and in that case the signal is provided only by scattering off Na (this requires additional assumptions on the escape velocity, which in general are not necessary for our bounds). We show the bounds for Assumptions 2 and 2a assuming that scattering on either Na or I dominates in figure 7 for some representative DM masses. In both cases only very weak constraints are obtained. While scattering on Na is consistent down to $m_\chi \approx 3\,\text{GeV}$ for Assumption 2a, scattering on iodine is consistent for $m_\chi \gtrsim 30\,\text{GeV}$ under Assumption 2. (Note that below around 30 GeV typically scattering on Na dominates.)

As expected, we conclude that based solely on our bounds the DAMA signal is compatible with assuming dark matter scattering being its origin. We do not expect that this conclusion will change significantly if bounds from procedure 2 according to eq. (5.13) were applied. Therefore, we limited ourselves to the discussion based on procedure 1 for DAMA.

6 Summary and discussion

The annual modulation is probably the most distinctive signature of dark matter and is playing (and will certainly play) a central role in revealing its existence and nature. However, it is not always clear that the modulation detected by a DM direct detection experiment is caused by the dark matter particles and not by any other unknown background source. In this work we have presented a consistency check for the amplitude of the modulation and the unmodulated count rate, which is a necessary (but not sufficient) condition for DM being the origin of an observed annual modulation.

We have derived upper bounds on the energy integrated modulation amplitude in terms of the unmodulated rate by expanding the DM velocity integral to first order in the earth's velocity $v_e \approx 30$ km/s. It holds for a wide class of particle physics models where the dif-

JCAP03(2012)005

ferential scattering cross section $d\sigma/dE_{nr}$ is proportional to $1/v^2$. Although we have only focused on elastic scattering the method can also be generalized to the inelastic case. The important aspect of our work is that our bounds hold for very general assumptions about the DM velocity distribution $f(\mathbf{v})$ in the sun's vicinity. We have presented bounds under the hypothesis of a single DM species and the following assumptions on the DM halo:

- **Assumption 1, bound in eq. (3.13):** We assume that the only time dependence is induced by the rotation of the earth around the sun. The halo itself is static on the time scale of months to years and spatially constant at the scale of the sun-earth distance. Otherwise the DM velocity distribution can have an arbitrary structure, including, for example, several streams coming from various directions. In order to saturate this bound the halo has to be very peculiar, with rather unrealistic properties.

- **Assumption 2, bound in eq. (4.8):** In addition to Assumption 1 we assume that there is just one preferred direction of the DM velocity distribution in the rest frame of the sun (independent of the minimal velocity v_m in the halo integral). This requires certain symmetries of the velocity distribution, which are specified in eqs. (4.3) and (4.4). It covers typically situations where the DM distribution is dominated by one single component, which may come from an arbitrary (but constant) direction. Assumption 2 requires that the phase of the modulation is independent of the recoil energy (up to a phase flip of half a year).

- **Assumption 2a, bound in eq. (4.9):** We require that the preferred direction from Assumption 2 is aligned with the motion of the sun. This is fulfilled for any isotropic halo, and also for tri-axial halos up to corrections due to the peculiar velocity of the sun. Furthermore, it includes the possibility of streams parallel to the motion of the sun, such as a possible dark disk. Assumption 2a requires that the maximum (or minimum) of the event rate is around June 2nd.

The theoretical bounds are obtained in terms of the minimal velocity v_m and have to be related to observable quantities by translating into recoil energy. We have outlined two possible procedures for this task in section 5 for the case of elastic scattering, taking into account statistical errors and the possibility that an unknown background may contribute to the unmodulated rate, but that it has no time-dependence. As an example we have applied the proposed consistency checks to the annual modulation signals reported by the CoGeNT and DAMA experiments. While DAMA data are compatible with a dark matter origin for its modulation, severe restrictions on the dark matter mass can be set for the case of CoGeNT. Applying our bounds we find that the CoGeNT modulation amplitude can be consistent with the unmodulated rate at the 68% CL only for DM masses $m_\chi \gtrsim 7.3, 18, 16\,\mathrm{GeV}$ for the Assumptions 1, 2, 2a, respectively. If preliminary results on a possible surface events contamination of the unmodulated rate at low energies in CoGeNT are confirmed, those bounds would become even more restrictive. In this case, CoGeNT modulation data would be inconsistent with the DM hypothesis under assumptions 2 and 2a at about 97% and 90% CL, respectively. DAMA has a relatively large unmodulated count rate of about 1 cnt/kg/day/keV compared to the modulation amplitude of about 0.02 cnt/kg/day/keV. Therefore, our bounds are not very stringent and the modulation amplitude is consistent with the unmodulated rate. In contrast, CoGeNT reports a modulation amplitude in the range of 0.5 to 1 cnt/kg/day/keV, compared to an unmodulated rate of 3 to 4 cnt/kg/day/keV. Because of this relatively large

JCAP03(2012)005

ratio between modulated and unmodulated rate our method provides stringent constraints in the case of CoGeNT. Several comments are in order:

(i) In deriving the bounds we assume a certain smoothness of the halo, since we are expanding in v_e. Spikes in the velocity distribution much narrower than 30 km/s are not covered by our procedure.

(ii) Our bounds assume that a modulation signal is present in the data. If the significance of the modulation is weak, the bounds are more easily satisfied. This effect is explicitly illustrated in section 5 by using CoGeNT data under different assumptions regarding the modulation signal. The method discussed here cannot be used to establish the presence of a modulation, it can only test whether a given modulation signal is consistent with the unmodulated rate.

(iii) In this work we have used the relation between the minimal velocity v_m and nuclear recoil energy E_{nr} implied by elastic scattering, see eq. (2.2) and appendix B. The bounds can be generalised in a straightforward way also to inelastic scattering. However, in that case $v_m = (m_A E_{nr}/\mu_{\chi A} + \delta)/\sqrt{2 m_A E_{nr}}$ has a minimum in E_{nr}, and therefore there is no one-to-one correspondence between v_m and E_{nr}. When translating from v_m to E_{nr} one has to take into account that different disconnected regions in E_{nr} can contribute to a given interval in v_m.

(iv) The type of DM-nucleus interaction (i.e., the particle physics) has to be specified before applying our bounds. Apart from the $1/v^2$ dependence of the differential cross section $d\sigma/dE_{nr}$, the E_{nr} dependence of the interaction is encoded in the form factor $F(E_{nr})$. It can describe conventional spin-independent or spin-dependent interactions, but also a possible non-trivial q^2-dependence of the DM-nucleus interaction, all of which can be absorbed into $F(E_{nr})$.

To conclude, we have presented a consistency check for the amplitude of a DM induced annual modulation compared to the unmodulated event rate in a given DM direct detection experiment. Our bounds rely only on very mild and realistic assumptions about the DM halo. We believe that the proposed method is a useful check which any annual modulation signal should pass. A violation of our bounds suggests a non-DM origin of the annual modulation, or requires rather exotic properties of the DM distribution, for example very sharp spikes and edges. Such extreme features of the halo should have other observable consequences, such as surprising spectral features or strong energy dependence of the modulation phase. Such features could be used as additional diagnostics, beyond the signatures explored here, which are restricted to the energy integrated modulation amplitude, irrespective of the phase.

Acknowledgments

We thank Felix Kahlhöfer for useful comments on the manuscript. T.S. and J.Z. are grateful for support from CERN for attending the CERN-TH institute DMUH'11, 18–29 July 2011, where this work was initiated. The work of T.S. was partly supported by the Transregio Sonderforschungsbereich TR27 "Neutrinos and Beyond" der Deutschen Forschungsgemeinschaft. J.H.-G. is supported by the MICINN under the FPU program and would like to thank the division of M. Lindner at MPIK for very kind hospitality.

JCAP03(2012)005

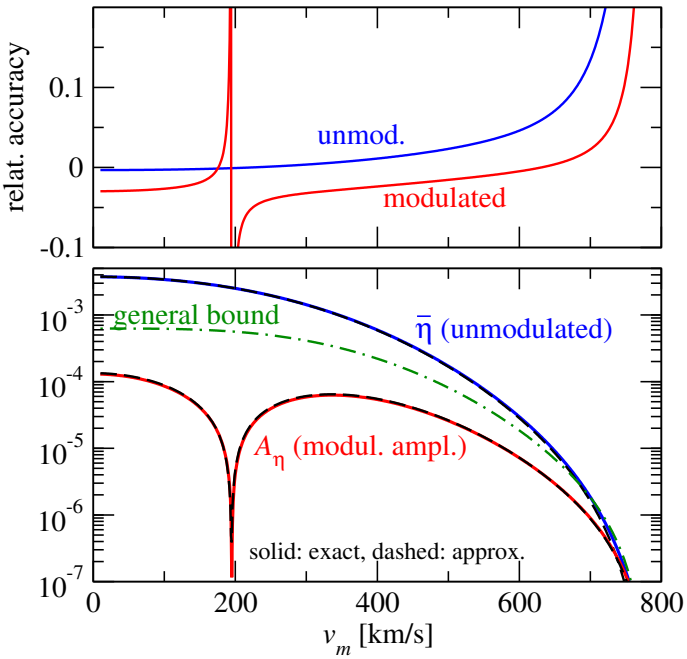

Figure 8. Comparison for the Maxwellian halo of the exact (solid line) and v_e expanded (dashed) modulated and unmodulated halo integrals A_η and $\bar{\eta}$, respectively. The modulation flips the phase by half a year below the zero of the amplitude. In the lower panel the general bound (3.13) is also shown (dashed-dotted curve). The upper panel shows the relative accuracy defined as (exact — approx)/exact.

A Maxwellian halo

As a cross check we apply our formalism to the commonly used Maxwellian velocity distribution, with a cut off at an escape velocity $v_{\rm esc}$. In the galactic rest frame it is given by

$$f_{\rm gal}(\mathbf{v}) \propto [\exp(-\mathbf{v}^2/\bar{v}^2) - \exp(v_{\rm esc}^2/\bar{v}^2)]\Theta(v_{\rm esc} - v)\,, \tag{A.1}$$

where we use $\bar{v} = 220\,{\rm km\,s^{-1}}$ and $v_{\rm esc} = 550\,{\rm km\,s^{-1}}$. This distribution is boosted to the sun's and earth's rest frames as described in section 2. For the above velocity distribution the halo integral $\eta(v_m, t)$ is known analytically. We define the "exact" modulated and unmodulated halo integrals as

$$\begin{aligned} \bar{\eta}^{\rm exact}(v_m) &\equiv \frac{1}{2}\left[\eta(v_m, t_*) + \eta(v_m, t_* + 0.5)\right]\,, \\ A'^{\,\rm exact}_\eta(v_m) &\equiv \frac{1}{2}\left[\eta(v_m, t_*) - \eta(v_m, t_* + 0.5)\right]\,, \end{aligned} \tag{A.2}$$

where for the (exact) analytic expressions $\eta(v_m, t)$ we are are using the results given in the appendix of [27]. Above, t_* is June 2nd and $A^{\rm exact}_\eta(v_m) = |A'^{\,\rm exact}_\eta(v_m)|$.

We first check the accuracy of the v_e expansion. Expanding to zeroth order in v_e gives the approximate unmodulated rate (3.3), while the modulation amplitude is given by expanding to linear order in v_e, (4.10), with $\sin\alpha_{\rm halo} = 0.5$. The comparison with the "exact"

JCAP03(2012)005

expressions is shown in figure 8. Both for the modulation amplitude and the unmodulated rate we find excellent agreement, with the differences hardly visible on logarithmic scale. As seen from the upper panel, for large regions of v_m the agreement is within few %, apart from the zero of the modulation amplitude. Minor deviations appear for large v_m values, where non-linear effects due to the cut-off at the escape velocity become important. We see that our expression for A_η captures accurately the phase flip of the modulation. At low v_m the $G(v_m)$ term in eq. (4.10) dominates, leading to the maximum of the count rate in December, the modulation amplitude becomes zero when the two terms cancel, and the maximum in June at large v_m is obtained from the $g(v_m)$ term.

We compare next the bounds with the actual modulation amplitude. The dash-dotted (green) curve in figure 8 shows the general bound, eq. (3.13), which follows from Assumption 1. Clearly, the Maxwellian halo is far from saturating this bound. Much tighter constraints are obtained from Assumptions 2 and 2a. Figure 9 shows the bounds (4.8) and (4.9) on integrals of modulation amplitudes. The shaded region shows the l.h.s. of the bounds, $\int_{v_{m1}} dv A'_\eta$, where the upper boundary of the integration is chosen so high that the DM signal vanishes. Note that A'_η flips the sign at $v_m \sim 200$ km/s, which explains the maximum of the integral around 200 km/s. The curve labeled "partial bound" corresponds to the bound following from Assumption 2, eq. (4.8), but without the second term in the square bracket. We find that it is only slightly more stringent than the general bound that follows from Assumption 1, (3.13), especially for large v_m. Although it does not capture the behaviour at low v_m it is rather similar to the full bound, eq. (4.8), (dashed curve) for $v_m \gtrsim 400$ km/s. The bound from Assumption 2a, eq. (4.9) (dash-dotted curve), which assumes $\sin\alpha_{\rm halo} = 0.5$, is roughly a factor 2 larger than the prediction for small v_{m1} and approaches the true modulation around $v_{m1} \gtrsim 400$ km/s. In the right panel we show that for a Maxwellian distribution with very small dispersion ($\overline{v} = 40$ km/s) the bound for Assumption 2a is nearly saturated. As mentioned in section 3, the inequalities used to derive the bound (4.9) become equalities if the velocity distribution $f(\mathbf{v}) \propto \delta(\vartheta)$, which is approximated by the Maxwellian with small $\overline{v}$.

B Translating bounds in v_m space to observable quantities

In sections 3 and 4 we have derived bounds involving the halo integral $\overline{\eta}(v_m)$ and the modulation amplitude $A_\eta(v_m)$. Here we give details on how to translate these bounds into bounds that involve observable rates as functions of nuclear recoil energy E_{nr}. The nuclear energy is measured in electron-equivalents, E_{ee}, which is related to E_{nr} through a quenching factor Q. We also define a differential quenching factor q,

$$q \equiv \frac{dE_{ee}}{dE_{nr}} = Q + E_{nr}\frac{dQ}{dE_{nr}}\,, \quad \text{where} \quad Q \equiv \frac{E_{ee}}{E_{nr}}\,, \tag{B.1}$$

which then gives the translation between v_m and E_{ee},

$$v_m = \sqrt{\frac{m_A E_{ee}}{2\mu_{\chi A}^2 Q}}, \qquad \frac{1}{\xi(E_{ee})} \equiv \frac{dv_m}{dE_{ee}} = \frac{dv_m}{dE_{nr}}\frac{dE_{nr}}{dE_{ee}} = \frac{1}{2\mu_{\chi A}}\sqrt{\frac{m_A Q}{2E_{ee}}}\,\frac{1}{q}\,. \tag{B.2}$$

The quenching factor Q is in general energy dependent. If it is energy independent, then $q = Q$, while if data are reported directly in E_{nr} then furthermore $q = Q = 1$. Note that q, Q, v_m, ξ, are all positive.

JCAP03(2012)005

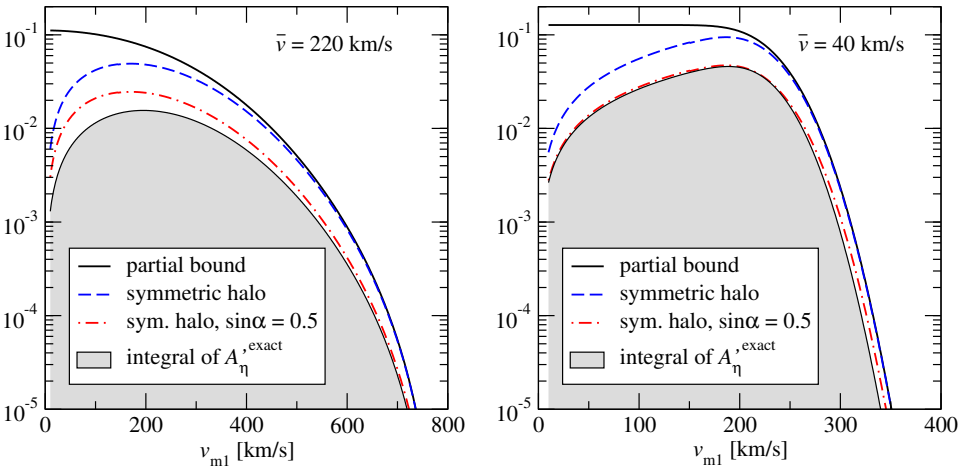

Figure 9. The bounds on the modulation amplitude for a Maxwellian velocity distribution and velocity dispersions $\overline{v} = 220$ km/s (40 km/s) in the left (right) panels. The shaded region shows the integral of $\int_{v_{m1}}^{\infty} A'^{\rm exact}_{\eta}$. We show the bound for a "symmetric halo" from eq. (4.8), and the bound from eq. (4.9) which assumes that the DM wind is parallel to the motion of the sun ("sym. halo, $\sin\alpha = 0.5$"). The solid curve ("partial bound") shows the bound eq. (4.8), but without the second term in the square bracket.

The modulation amplitude and rate in units of counts/day/kg/keV$_{ee}$ are given as

$$A_R(E_{ee}) = \kappa\, A_\eta(v_m)\,, \quad \overline{R}(E_{ee}) = \kappa\, \overline{\eta}(v_m) \quad \text{with} \quad \kappa(E_{ee}) \equiv \frac{CF^2(E_{ee}/Q)}{q(E_{ee})}\,, \tag{B.3}$$

with the constant C defined in (2.6). To keep the notation simple we use the same symbols for rate and modulation whether they depend on recoil energy in keV$_{ee}$ or keV$_{nr}$. The units are denoted in the argument (E_{ee} versus E_{nr}) and should be clear from the context.

Let us consider first the general bound following from Assumption 1. Multiplying eq. (3.13) by κ and converting the integral over v_m into E_{ee} by using eq. (B.2) one finds

$$A_R(E_{ee}) \leq v_e \left[-\frac{d(\overline{R}\xi)}{dE_{ee}} + \overline{R}\left(\frac{d\xi}{dE_{ee}} + \sqrt{\frac{2\mu_{\chi A}^2 Q}{m_A E_{ee}}} + \frac{\xi}{\kappa}\frac{d\kappa}{dE_{ee}} \right) - \kappa \int_{E_{ee}} dE_{ee} \frac{\overline{R}}{\xi\kappa} \frac{2\mu_{\chi A}^2 Q}{m_A E_{ee}} \right] \tag{B.4}$$

eq. (4.12) for Assumptions 2, 2a becomes similarly:

$$A_R(E_{ee}) \leq v_e \sin\alpha_{\rm halo} \left[-\frac{d(\overline{R}\xi)}{dE_{ee}} + \overline{R}\left(\frac{d\xi}{dE_{ee}} + \frac{\xi}{\kappa}\frac{d\kappa}{dE_{ee}} \right) \right]\,. \tag{B.5}$$

Note that the constant C containing the cross section and local DM density drops out, as expected, since it is a common pre-factor for rate as well as modulation. In practise A_R and $\overline{R}$ are given in bins in E_{ee}. Let us define the bin average of a quantity $X(E_{ee})$ as

$$\langle X \rangle_i \equiv \frac{1}{\Delta E_i} \int_{E_{i1}}^{E_{i2}} dE_{ee} X(E_{ee})\,, \tag{B.6}$$

JCAP03(2012)005

where E_{i1} and E_{i2} are the boundaries of bin i and $\Delta E_i = E_{i2} - E_{i1}$. The observed modulation and rate in bin i are then $A_i = \langle A_R \rangle_i$ and $R_i = \langle \overline{R} \rangle_i$, respectively. Now we have to perform the bin average of eq. (B.4). The first term in the square bracket gives

$$\frac{\overline{R}(E_{i1})\xi(E_{i1}) - \overline{R}(E_{i2})\xi(E_{i2})}{\Delta E_i} \approx \frac{R_i \langle \xi \rangle_i - R_{i+1} \langle \xi \rangle_{i+1}}{\Delta E_i} \,. \tag{B.7}$$

For the other two terms in the square bracket we approximate $\langle XY \rangle \approx \langle X \rangle \langle Y \rangle$ and the integral becomes a sum over bins, up to the last reported bin $i = N$. Finally we obtain

$$A_i \leq v_e \left[R_i(\alpha_i + \beta_i) - R_{i+1}\alpha'_{i+1} - \langle \kappa \rangle_i \sum_{j=i}^{N} R_j \gamma_j \right] , \tag{B.8}$$

with

$$\alpha_i \equiv \frac{\langle \xi \rangle_i}{\Delta E_i} \,, \; \alpha'_i \equiv \frac{\langle \xi \rangle_i}{\Delta E_{i-1}} \,, \; \beta_i \equiv \left\langle \frac{d\xi}{dE_{ee}} + \sqrt{\frac{2\mu_{\chi A}^2 Q}{m_A E_{ee}}} + \frac{\xi}{\kappa} \frac{d\kappa}{dE_{ee}} \right\rangle_i \,, \; \gamma_i \equiv \Delta E_i \left\langle \frac{2\mu_{\chi A}^2 Q}{m_A E_{ee} \xi \kappa} \right\rangle_i \,. \tag{B.9}$$

For eq. (B.5) we get

$$A_i \leq v_e \sin\alpha_{\rm halo} \left[R_i(\alpha_i + \beta'_i) - R_{i+1}\alpha'_{i+1} \right] \quad \text{with} \quad \beta'_i \equiv \left\langle \frac{d\xi}{dE_{ee}} + \frac{\xi}{\kappa} \frac{d\kappa}{dE_{ee}} \right\rangle_i \,. \tag{B.10}$$

Terms with indices larger than N are dropped. We see from the definitions that $\alpha_i, \alpha'_i, \gamma_i$, and $\langle \kappa \rangle_i$ are positive.

A similar calculation for the bounds (4.8) and (4.9), following from the Assumptions 2 and 2a, leads to

$$\sum_{j=i}^{N} A_j x_j \leq v_e \sin\alpha \left[R_i y_i - \langle v_m \rangle_i \sum_{j=i+1}^{N} R_j \gamma_j \right] , \tag{B.11}$$

with

$$x_i \equiv \Delta E_i \left\langle \frac{1}{\xi\kappa} \right\rangle_i \,, \qquad y_i \equiv \left\langle \frac{1}{\kappa} \right\rangle_i - \langle v_m \rangle_i \gamma_i \,, \qquad \langle v_m \rangle_i = \left\langle \sqrt{\frac{m_A E_{ee}}{2\mu_{\chi A}^2 Q}} \right\rangle_i \,, \tag{B.12}$$

and $\sin\alpha = 1$ (0.5) corresponds to Assumption 2 (2a).

Any binning procedure will lead to inaccuracies. We have estimated binning effects by slightly changing the prescription. Eq. (B.4) can be equivalently written as

$$A_R(E_{ee}) \leq v_e \left[-\xi \frac{d\overline{R}}{dE_{ee}} + \overline{R} \left(\sqrt{\frac{2\mu_{\chi A}^2 Q}{m_A E_{ee}}} + \frac{\xi}{\kappa} \frac{d\kappa}{dE_{ee}} \right) - \kappa \int_{E_{ee}} dE_{ee} \frac{\overline{R}}{\xi\kappa} \frac{2\mu_{\chi A}^2 Q}{m_A E_{ee}} \right] . \tag{B.13}$$

The first term in the square bracket can be estimated as

$$-\xi \frac{d\overline{R}}{dE_{ee}} \approx \langle \xi \rangle_i \frac{R_i - R_{i+1}}{\Delta E_i} \,, \tag{B.14}$$

and the other terms are bin-averaged similar as above. We have calculated the CoGeNT bounds also using this binning procedure and obtain similar results as with our default method. This confirms that inaccuracies due to binning are acceptable for present CoGeNT data.

JCAP03(2012)005

		unmod. rate from [4]			corrected rate [21]		
		Mean	68%	95%	Mean	68%	95%
Ass. 1:	general bound	10	5	–	12.5	5	–
Ass. 2:	symmetric halo	29.5	17	7	63	34.5	16
Ass. 2a:	sym. halo, $\sin\alpha = 0.5$	37.5	14	–	94.5	30.5	–

Table 3. Lower bounds on the DM mass in GeV, from the requirement that the CoGeNT modulation amplitude is consistent with the upper bound from the unmodulated rate, according to the Assumptions 1, 2, 2a on the DM distribution obtained as described in appendix C. In the left part of the table we use the published unmodulated event rates from [4], whereas for the right part of the table we adopt the preliminary results on surface events contamination at low energies from [21].

C Alternative procedure for optimizing the bound in presence of unknown background

In section 5 we have outlined a method based on a least-square minimization ("procedure 2") to find "optimal" values for the coefficients ω_i parameterizing the background contribution in each bin. Here we provide an alternative method for this task.

Let us consider the inequalities (5.4) and (5.5) as a system of equations for the ω_i. We observe that they have a triangular structure with respect to ω_i: the inequality for a given index i depends only on ω_j with $j \geq i$, i.e., the inequality for $i = N$ depends only on ω_N, for $i = N-1$ it depends on ω_{N-1}, ω_N, and so on. From the fact that $\alpha_i, \langle\kappa\rangle_i, \gamma_i$ are positive follows that the bound for a given i is weakest if ω_i is as large as possible and ω_j with $j > i$ are as small as possible. We can implement this requirement in an iterative way: replacing the inequality sign by an equality, we obtain a system of N linear equations in ω_i. We can solve this system by starting at $i = N$ and going up step by step to $i = 1$, in each step obtaining a value for the corresponding ω_i, to be used in the next step. If the solution for ω_i is less than one, it will be the smallest allowed value, and hence the bound for $i-1$ will be weakest. If the solution for ω_i is larger than one the bound is violated by bin i and we have to set the corresponding $\omega_i = 1$ (the largest physically allowed value). In that way we obtain a set of ω_i corresponding to the most conservative choice of background contributions to the unmodulated rate.

This method treats the inequalities as "hard bounds" and does not take into account the fact that the amplitudes are subject to experimental uncertainties. A conservative way to include uncertainties is to apply this procedure as described above but using instead of the l.h.s. of (5.4) and (5.5) its central value minus n standard deviations. In this way one aims to satisfy the inequalities within the $n\sigma$ interval for each bin. We show the results of such an analysis for CoGeNT data in table 3. Typically one finds qualitatively similar but slightly stronger bounds than for procedure 1, although if the method is considered at higher CL bounds may become weaker or even disappear, as visible in the table for the columns at 95% CL. Note, however, that subtracting $n\sigma$ from the mean value for all bins leads to very conservative limits.

References

[1] A. Drukier, K. Freese and D. Spergel, *Detecting Cold Dark Matter Candidates*, *Phys. Rev.* **D 33** (1986) 3495 [INSPIRE].

[2] K. Freese, J.A. Frieman and A. Gould, *Signal Modulation in Cold Dark Matter Detection*, *Phys. Rev.* **D 37** (1988) 3388 [INSPIRE].

[3] DAMA collaboration, R. Bernabei et al., *First results from DAMA/LIBRA and the combined results with DAMA/NaI*, *Eur. Phys. J.* **C 56** (2008) 333 [arXiv:0804.2741] [INSPIRE].

[4] C. Aalseth et al., *Search for an Annual Modulation in a P-type Point Contact Germanium Dark Matter Detector*, *Phys. Rev. Lett.* **107** (2011) 141301 [arXiv:1106.0650] [INSPIRE].

[5] M. Kuhlen et al., *Dark Matter Direct Detection with Non-Maxwellian Velocity Structure*, *JCAP* **02** (2010) 030 [arXiv:0912.2358] [INSPIRE].

[6] N. Fornengo and S. Scopel, *Temporal distortion of annual modulation at low recoil energies*, *Phys. Lett.* **B 576** (2003) 189 [hep-ph/0301132] [INSPIRE].

[7] A.M. Green, *Effect of realistic astrophysical inputs on the phase and shape of the WIMP annual modulation signal*, *Phys. Rev.* **D 68** (2003) 023004 [*Erratum ibid.* **D 69** (2004) 109902] [astro-ph/0304446] [INSPIRE].

[8] M. Fairbairn and T. Schwetz, *Spin-independent elastic WIMP scattering and the DAMA annual modulation signal*, *JCAP* **01** (2009) 037 [arXiv:0808.0704] [INSPIRE].

[9] G. Gelmini and P. Gondolo, *WIMP annual modulation with opposite phase in Late-Infall halo models*, *Phys. Rev.* **D 64** (2001) 023504 [hep-ph/0012315] [INSPIRE].

[10] C. Savage, K. Freese and P. Gondolo, *Annual Modulation of Dark Matter in the Presence of Streams*, *Phys. Rev.* **D 74** (2006) 043531 [astro-ph/0607121] [INSPIRE].

[11] S. Chang, A. Pierce and N. Weiner, *Using the Energy Spectrum at DAMA/LIBRA to Probe Light Dark Matter*, *Phys. Rev.* **D 79** (2009) 115011 [arXiv:0808.0196] [INSPIRE].

[12] A. Natarajan, C. Savage and K. Freese, *Probing dark matter streams with CoGeNT*, *Phys. Rev.* **D 84** (2011) 103005 [arXiv:1109.0014] [INSPIRE].

[13] M. Drees and C.-L. Shan, *Reconstructing the Velocity Distribution of WIMPs from Direct Dark Matter Detection Data*, *JCAP* **06** (2007) 011 [astro-ph/0703651] [INSPIRE].

[14] M. Drees and C.-L. Shan, *Model-Independent Determination of the WIMP Mass from Direct Dark Matter Detection Data*, *JCAP* **06** (2008) 012 [arXiv:0803.4477] [INSPIRE].

[15] P.J. Fox, J. Liu and N. Weiner, *Integrating Out Astrophysical Uncertainties*, *Phys. Rev.* **D 83** (2011) 103514 [arXiv:1011.1915] [INSPIRE].

[16] P.J. Fox, G.D. Kribs and T.M. Tait, *Interpreting Dark Matter Direct Detection Independently of the Local Velocity and Density Distribution*, *Phys. Rev.* **D 83** (2011) 034007 [arXiv:1011.1910] [INSPIRE].

[17] C. McCabe, *DAMA and CoGeNT without astrophysical uncertainties*, *Phys. Rev.* **D 84** (2011) 043525 [arXiv:1107.0741] [INSPIRE].

[18] M.T. Frandsen, F. Kahlhoefer, C. McCabe, S. Sarkar and K. Schmidt-Hoberg, *Resolving astrophysical uncertainties in dark matter direct detection*, *JCAP* **01** (2012) 024 [arXiv:1111.0292] [INSPIRE].

[19] J. Read, L. Mayer, A. Brooks, F. Governato and G. Lake, *A dark matter disc in three cosmological simulations of Milky Way mass galaxies*, arXiv:0902.0009 [INSPIRE].

[20] P.J. Fox, J. Kopp, M. Lisanti and N. Weiner, *A CoGeNT Modulation Analysis*, *Phys. Rev.* **D 85** (2012) 036008 [arXiv:1107.0717] [INSPIRE].

[21] J. Collar, *CoGeNT and COUPP*, talk at *TAUP 2011, 12th International Conference on Topics in Astroparticle and Underground Physics*, Munich, Germany, September 5-9 2011.

[22] M.T. Frandsen et al., *On the DAMA and CoGeNT Modulations*, *Phys. Rev.* **D 84** (2011) 041301 [arXiv:1105.3734] [INSPIRE].

JCAP03(2012)005

[23] T. Schwetz and J. Zupan, *Dark Matter attempts for CoGeNT and DAMA*, *JCAP* **08** (2011) 008 [arXiv:1106.6241] [INSPIRE].

[24] S. Chang, J. Pradler and I. Yavin, *Statistical Tests of Noise and Harmony in Dark Matter Modulation Signals*, arXiv:1111.4222 [INSPIRE].

[25] C. Arina, J. Hamann, R. Trotta and Y.Y. Wong, *Evidence for dark matter modulation in CoGeNT*, arXiv:1111.3238 [INSPIRE].

[26] P. Barbeau, J. Collar and O. Tench, *Large-Mass Ultra-Low Noise Germanium Detectors: Performance and Applications in Neutrino and Astroparticle Physics*, *JCAP* **09** (2007) 009 [nucl-ex/0701012] [INSPIRE].

[27] C. McCabe, *The Astrophysical Uncertainties Of Dark Matter Direct Detection Experiments*, *Phys. Rev.* **D 82** (2010) 023530 [arXiv:1005.0579] [INSPIRE].

JCAP03(2012)005

Astrophysics-Independent Bounds on the Annual Modulation of Dark Matter Signals

Juan Herrero-Garcia,[1,*] Thomas Schwetz,[2,†] and Jure Zupan[3,‡]

[1]*Departamento de Fisica Teorica and IFIC, Universidad de Valencia CSIC, Paterna, Apartado 22085, E-46071 Valencia, Spain*
[2]*Max-Planck-Institut für Kernphysik, Saupfercheckweg 1, 69117 Heidelberg, Germany*
[3]*Department of Physics, University of Cincinnati, Cincinnati, Ohio 45221, USA*

(Received 8 May 2012; published 4 October 2012)

We show how constraints on the time integrated event rate from a given dark matter (DM) direct detection experiment can be used to bound the amplitude of the annual modulation signal in another experiment. The method requires only mild assumptions about the properties of the local DM distribution: that it is temporally stable on the scale of months and spatially homogeneous on the ecliptic. We apply the method to the annual modulation signal in DAMA/LIBRA, which we compare to the bounds derived from XENON10, XENON100, cryogenic DM search, and SIMPLE data. Assuming a DM mass of 10 GeV, we show that under the above assumptions about the DM halo, a DM interpretation of the DAMA/LIBRA signal is excluded for several classes of models: at 6.3σ (4.6σ) for elastic isospin conserving (violating) spin-independent interactions, and at 4.9σ for elastic spin-dependent interactions on protons.

DOI: 10.1103/PhysRevLett.109.141301 PACS numbers: 95.35.+d

Dark matter (DM) constitutes a significant fraction of the energy density in the Universe, $\Omega_{\rm DM} = 0.229 \pm 0.015$ [1]. This conclusion is based entirely on gravitational effects of DM. A fundamental question is whether DM interacts also nongravitationally. Direct detection experiments, for instance, are looking for the scattering of DM particles from the galactic halo in underground detectors. A characteristic feature of the signal is an annual modulation, because Earth rotates around the Sun, while at the same time the Sun moves relative to the DM halo [2]. At present, two experiments are reporting annually modulated signals, DAMA/LIBRA [3] (DAMA for short) and CoGeNT [4], with significances of 8.9σ and 2.8σ, respectively. Assuming the standard Maxwellian DM halo and elastic spin-independent (SI) DM scattering, both claims are in tension [5,6] with bounds on time integrated rates from other experiments such as XENON10 [7], XENON100 [8], or cryogenic DM search (CDMS) [9]. The situation may change in the case of non-Maxwellian DM halos, e.g., halos with anisotropic velocity distributions or with significant substructure, for instance DM streams or DM debris flows. Recently CDMS provided a direct bound on the modulation signal, which disfavors the CoGeNT modulation without referring to any halo or particle physics model [10]. Therefore, we focus below on DAMA and CoGeNT.

In this Letter, we present a general method that avoids astrophysical uncertainties when comparing putative DM modulation signals with bounds on time averaged DM scattering rates from different experiments by combining the results from Refs. [11,12] with bounds on the modulation derived by us in Ref. [13]. We are then able to translate the bound on the DM scattering rate in one experiment into a bound on the annual modulation amplitude in a different experiment. The resulting bounds present roughly an order of magnitude improvement over Refs. [11–13].

The bounds are (almost completely) astrophysics independent. Only very mild assumptions about DM halo properties are used: (i) that it does not change on the time scales of months, (ii) that the density of DM in the halo is constant on the scales of the Earth-Sun distance, and (iii) that the DM velocity distribution does not vary strongly on scales of the Earth velocity, $v_e = 29.8$ km/s. If the modulation signal is due to DM, then the modulation amplitude has to obey the bounds. In the derivation, an expansion in v_e over the typical DM velocity $\sim$200 km/s is used. The validity of the expansion can be checked experimentally, by searching for the presence of higher harmonics in the time-stamped DM scattering data [13].

Bounds on the annual modulation.—We focus on elastic scattering of DM χ off a nucleus (A, Z), depositing the nuclear-recoil energy $E_{\rm nr}$. The differential rate in events/keV/kg/day is

$$R_A(E_{\rm nr}, t) = \frac{\rho_\chi \sigma_A^0}{2 m_\chi \mu_{\chi A}^2} F_A^2(E_{\rm nr}) \eta(v_m, t), \qquad (1)$$

with ρ_χ the local DM density, σ_A^0 the total DM-nucleus scattering cross section at zero momentum transfer, m_χ the DM mass, $\mu_{\chi A}$ the DM-nucleus reduced mass, and $F_A(E_{\rm nr})$ a nuclear form factor. For SI interactions, σ_A^0 can be written as $\sigma_A^{\rm SI} = \sigma_p [Z + (A - Z)(f_n/f_p)]^2 \mu_{\chi A}^2 / \mu_{\chi p}^2$, where σ_p is the DM-proton cross section and $f_{n,p}$ are coupling strengths to neutron and proton, respectively. Apart from ρ_χ, the astrophysics enters in Eq. (1) through the halo integral

$$\eta(v_m, t) \equiv \int_{v > v_m} d^3 v \frac{f_{\rm det}(\mathbf{v}, t)}{v}, \qquad v_m = \sqrt{\frac{m_A E_{\rm nr}}{2 \mu_{\chi A}^2}}, \qquad (2)$$

where v_m is the minimal velocity required for recoil energy $E_{\rm nr}$, and $f_{\rm det}(\mathbf{v}, t)$ describes the distribution of DM particle velocities in the detector rest frame with $f_{\rm det}(\mathbf{v}, t) \geq 0$ and $\int d^3v f_{\rm det}(\mathbf{v}, t) = 1$. The integral of the velocity distribution enters in $R_A(E_{\rm nr}, t)$ because DM scattering at different angles probes different DM velocities even for fixed $E_{\rm nr}$. The velocity distributions in the rest frames of the detector and the Sun are related by $f_{\rm det}(\mathbf{v}, t) = f_{\rm sun}[\mathbf{v} + \mathbf{v}_e(t)]$, where $\mathbf{v}_e(t)$ is the velocity vector of Earth. The rotation of the Earth around the Sun introduces a time dependence in the event rate through $\eta(v_m, t) = \bar{\eta}(v_m) + \delta\eta(v_m, t)$, where

$$\delta\eta(v_m, t) = A_\eta(v_m)\cos 2\pi[t - t_0(E_{\rm nr})], \tag{3}$$

when expanding to first order in $v_e = 29.8$ km/s $\ll v_{\rm sun} \simeq 230$ km/s, and $A_\eta(v_m) \geq 0$. The expansion can be truncated, if $f_{\rm sun}(v)$ does not show large variations on the scale of v_e, i.e., $v_e|df(v)/dv| \ll f(v)$. We are also assuming that the only time dependence comes from the rotation of Earth around the Sun and that $f_{\rm sun}(v)$ itself is constant in time and space.

Under those assumptions we schematically have $\bar{\eta} \sim \int f(v)/v$ and $A_\eta \sim v_e \int f(v)/v^2$. After some algebra, the modulation amplitude $A_\eta(v_m)$ can be shown to be bounded by the unmodulated halo integral $\bar{\eta}$ (see Ref. [13] for the derivation):

$$A_\eta(v_m) \leq v_e\left[-\frac{d\bar{\eta}}{dv_m} + \frac{\bar{\eta}(v_m)}{v_m} - \int_{v_m} dv\,\frac{\bar{\eta}(v)}{v^2}\right]. \tag{4}$$

If we further assume that the DM velocity distribution obeys certain symmetry properties such that there is only one single direction related to the DM flow, independent of v_m (see Ref. [13] for details), then one obtains a more stringent constraint:

$$\int_{v_1}^{v_2} dv_m A_\eta(v_m) \leq \sin\alpha v_e\left[\bar{\eta}(v_1) - v_1\int_{v_1} dv\,\frac{\bar{\eta}(v)}{v^2}\right]. \tag{5}$$

Here α is the angle between the DM flow and the direction orthogonal to the ecliptic. The most conservative bound is obtained for $\sin\alpha = 1$ (which would correspond to a DM stream parallel to the ecliptic). However, in many cases the DM flow will be aligned with the motion of the Sun within the Galaxy. This holds for any isotropic velocity distribution and, up to a small correction due to the peculiar velocity of the Sun, also for triaxial halos or a significant contribution from a possible dark disk. In this case, we have $\sin\alpha \simeq 0.5$.

In the following, we will use time averaged rates from various experiments to derive an upper bound on $\bar{\eta}(v_m)$. In order to be able to apply this information we integrate Eq. (4) over v_m and drop the negative terms in Eqs. (4) and (5). This gives the bounds

$$\int_{v_1}^{v_2} dv_m A_\eta(v_m) \leq v_e\left[\bar{\eta}(v_1) + \int_{v_1}^{v_2} dv\,\frac{\bar{\eta}(v)}{v}\right], \tag{6}$$

$$\int_{v_1}^{v_2} dv_m A_\eta(v_m) \leq \sin\alpha v_e\,\bar{\eta}(v_1). \tag{7}$$

In practice, the integrals on the left-hand side (LHS) are replaced by a sum over bins. Below we will refer to the relations (6) and (7) with $\sin\alpha = 0.5$ as the bounds for *general halo* and *symmetric halo*, respectively. Here *symmetric* refers to the local velocity distribution according to the sentence before Eq. (5), not the spatial distribution of DM.

Bounds on the unmodulated halo integral.—Let us first consider SI scattering with $f_n = f_p$. Generalization to isospin-violating scattering with $f_n \neq f_p$ and to spin-dependent (SD) scattering is straightforward. The predicted number of events in an interval of observed energies $[E_1, E_2]$ is

$$N^{\rm pred}_{[E_1,E_2]} = MTA^2\int_0^\infty dE_{\rm nr}F_A^2(E_{\rm nr})G_{[E_1,E_2]}(E_{\rm nr})\tilde{\eta}(v_m). \tag{8}$$

Here $G_{[E_1,E_2]}(E_{\rm nr})$ is the detector response function, which describes the contribution of events with true nuclear-recoil energy $E_{\rm nr}$ to the observed energy interval $[E_1, E_2]$. It may be nonzero outside the $E_{\rm nr} \in [E_1, E_2]$ interval due to the finite energy resolution and includes also (possibly energy dependent) efficiencies. M and T are the detector mass and exposure time, respectively, and

$$\tilde{\eta} \equiv \frac{\sigma_p\rho_\chi}{2m_\chi\mu_{\chi p}^2}\bar{\eta}, \tag{9}$$

where $\tilde{\eta}$ has units of events/kg/day/keV.

Now we can use the fact that $\tilde{\eta}$ is a monotonically decreasing function of v_m [11] (see also Refs. [14,15]). Among all possible forms for $\tilde{\eta}$ such that they pass through $\tilde{\eta}(v_m)$ at v_m, the minimal number of events is obtained for $\tilde{\eta}$ constant and equal to $\tilde{\eta}(v_m)$ until v_m and zero afterwards. Therefore, for a given v_m we have a lower bound $N^{\rm pred}_{[E_1,E_2]}(v_m) \geq \mu(v_m)$ with

$$\mu(v_m) = MTA^2\tilde{\eta}(v_m)\int_0^{E(v_m)} dE_{\rm nr}F_A^2(E_{\rm nr})G_{[E_1,E_2]}(E_{\rm nr}), \tag{10}$$

where $E(v_m)$ is given in (2). Suppose an experiment observes $N^{\rm obs}_{[E_1,E_2]}$ events in the interval $[E_1, E_2]$. Then we can obtain an upper bound on $\tilde{\eta}$ for a fixed v_m at a confidence level (C.L.) by requiring that the probability of obtaining $N^{\rm obs}_{[E_1,E_2]}$ events or less for a Poisson mean of $\mu(v_m)$ is equal to 1-C.L. Note that this is actually a lower bound on the C.L., because Eq. (10) provides only a lower bound on the true Poisson mean. For the same reason, we cannot use the commonly applied maximum-gap method to derive a

bound on $\tilde{\eta}$. If several different nuclei are present, there will be a corresponding sum in Eqs. (8) and (10).

The limit on $\tilde{\eta}$ can then be used in the right-hand side (RHS) of Eq. (6) or (7) to constrain the modulation amplitude. For concreteness we first focus on the annual modulation in DAMA. If m_χ is around 10 GeV, then DM particles do not have enough energy to produce iodine recoils above the DAMA threshold. We can thus assume that the DAMA signal is entirely due to the scattering on sodium. We define $\tilde{A}_\eta \equiv \sigma_p \rho_\chi / (2 m_\chi \mu_{\chi p}^2) A_\eta$, which is related to the observed modulation amplitude $A_i^{\rm obs}$ by

$$\tilde{A}_\eta^{\rm obs}(v_m^i) = \frac{A_i^{\rm obs} q_{\rm Na}}{A_{\rm Na}^2 \langle F_{\rm Na}^2 \rangle_i f_{\rm Na}}. \tag{11}$$

Here $q_{\rm Na} = dE_{ee}/dE_{\rm nr}$ is the sodium quenching factor, for which we take $q_{\rm Na} = 0.3$. The index i labels energy bins, with v_m^i given by the corresponding energy bin center using Eq. (2). Further, $\langle F_{\rm Na}^2 \rangle_i$ is the sodium form factor averaged over the bin width and $f_{\rm Na} = m_{\rm Na}/(m_{\rm Na} + m_{\rm I})$ is the sodium mass fraction. For the modulation amplitude in CoGeNT we proceed analogously. Note that the conversion factor from $\bar{\eta}$ to $\tilde{\eta}$ is the same as for A_η to $\tilde{A}_\eta$, and is not dependent on the nucleus. Therefore, the bounds (6) and (7) apply to $\tilde{\eta}$, $\tilde{A}_\eta$ without change, even if the LHS and RHS refer to different experiments.

Let us briefly describe the data we use to derive the upper bounds on $\tilde{\eta}$. We consider results from XENON10 [7] (XE10) and XENON100 [8] (XE100). In both cases we take into account the energy resolution due to Poisson fluctuations of single electrons. For XE100, we adopt the best-fit light-yield efficiency $L_{\rm eff}$ from Ref. [8]. The XE10 analysis is based on the so-called S2 ionization signal and we follow [7] imposing a sharp cut off of the efficiency below threshold. From CDMS, we use results from a low-threshold (LT) analysis [9] of Ge data, as well as data on Si [16]. For SIMPLE [17], we use the observed number of events and expected background events to calculate the combined Poisson probability for stages 1 and 2.

For all experiments we use the lower bound on the expected events, Eq. (10), to calculate the probability of obtaining less or equal events than observed. For XE100, CDMS Si, and SIMPLE we just use the total number of events in the entire reported energy range. For XE10 and CDMS LT, the limit can be improved if data are binned and the probabilities for each bin are multiplied. This assumes that the bins are statistically independent, which requires to make bins larger than the energy resolution. For XE10 we only use two bins. For CDMS LT, we combine the 36 bins from Fig. 1 of Ref. [9] into 9 bins of 2 keV where the energy resolution is 0.2 keV.

Results.—In Fig. 1 we show the 3σ limits on $\tilde{\eta}$ compared to the modulation amplitudes $\tilde{A}_\eta$ from DAMA and CoGeNT for a DM mass of 10 GeV. Similar results have been presented in Refs. [14,15]. The CoGeNT amplitude

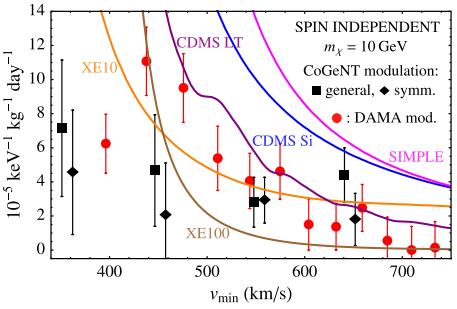

FIG. 1 (color online). 3σ upper bounds on $\tilde{\eta}$. The modulation amplitude $\tilde{A}_\eta$ is shown for DAMA (for $q_{\rm Na} = 0.3$) and CoGeNT for both free phase fit (general) and fixing the phase to June 2nd (symmetric). We assume a DM mass of 10 GeV and SI interactions.

depends on whether the phase is let to vary freely in the fit or fixed at June 2nd [6], which applies to the *general* and *symmetric* halos, respectively. Already at this level XE100 is in tension with the modulation from DAMA (and to some extent also CoGeNT).

We now apply our method. As shown in Fig. 2, the null results become significantly more constraining after applying the bound Eq. (6). DAMA and CoGeNT are strongly excluded by XE100, XE10, CDMS LT already for the general halo, and even more assuming a symmetric halo. Then also CDMS Si excludes DAMA, and there is some tension with SIMPLE (data not shown). In Fig. 3, we consider two variations of DM-nucleus interaction. The upper panel is for SD interactions with the proton, where the bound from SIMPLE is in strong disagreement with the DAMA modulation, due to the presence of fluorine in their target. (A comparable limit has been published recently by PICASSO [18].) In the lower panel of Fig. 3 we show the case of SI isospin-violating interactions with

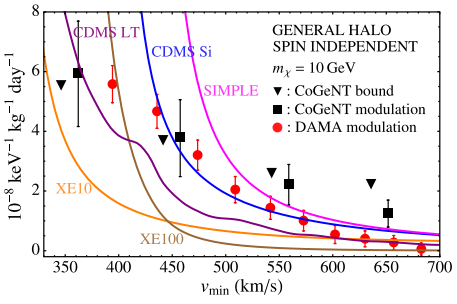

FIG. 2 (color online). Integrated modulation signals, $\int_{v_1}^{v_2} dv A_\eta$, from DAMA and CoGeNT compared to the 3σ upper bounds for the general halo, Eq. (6). We assume SI interactions and a DM mass of 10 GeV. The integral runs from $v_1 = v_{\rm min}$ to $v_2 = 743$ km/s (end of the 12th bin in DAMA).

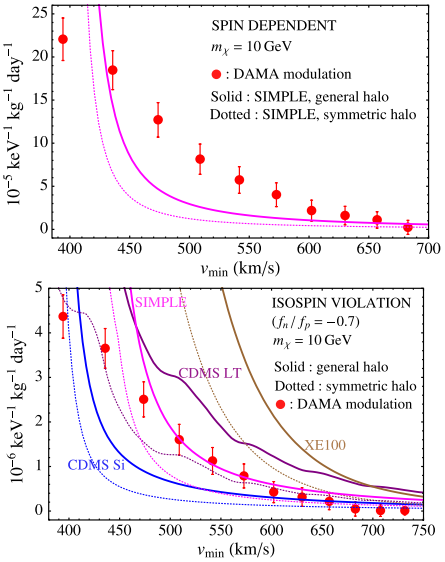

FIG. 3 (color online). Integrated modulation signal $\int_{v_{min}}^{v_2} dv A_{\tilde{\eta}}$ from DAMA compared to the 3σ upper bounds for the general halo, Eq. (6) (solid), and symmetric halo, Eq. (7) with $\sin\alpha = 0.5$ (dotted). We assume a DM mass of 10 GeV, and SD interactions on protons (upper panel) and SI interactions with $f_n/f_p = -0.7$ (lower panel).

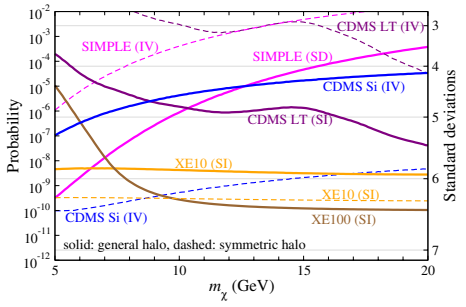

FIG. 4 (color online). The probability that the integrated modulation amplitude in DAMA (summed starting from the third bin) is compatible with the bound derived from the constraints on $\tilde{\eta}$ for various experiments as a function of the DM mass. The label SI (SD), refers to spin-independent (spin dependent) interactions with $f_n = f_p$ ($f_n = 0$), and IV refers to isospin-violating SI interactions with $f_n/f_p = -0.7$. For solid and dashed curves we use the bounds from Eqs. (6) and (7), respectively.

$f_n/f_p = -0.7$. This choice evades bounds from Xe, but now the DAMA modulation is excluded by the bounds from CDMS Si for the general halo and CDMS Si, LT, and SIMPLE for the symmetric halo.

Let us now quantify the disagreement between the observed DAMA modulation and the rate from another null-result experiment using our bounds. We first fix v_m. To each value of $\tilde{\eta}(v_m)$, Eq. (10) provides a Poisson mean $\mu(v_m)$. We can then calculate the probability p_η to obtain equal or less events than measured by the null-result experiment. Then we construct the bound on the modulation using the same value $\tilde{\eta}(v_m)$ on the RHS of Eq. (6) or (7) [the integrand $\tilde{\eta}(v)$ in Eq. (6) is calculated using the same p_η but with $v > v_m$ in Eq. (10)]. We calculate the probability p_A that the bound is not violated by assuming on the LHS of Eq. (6) or (7) a Gaussian distribution for the DAMA modulation signal with the measured standard deviations in each bin. Then $p_{\rm joint}(\tilde{\eta}) = p_\eta p_A$ is the combined probability of obtaining the experimental result for the chosen value of $\tilde{\eta}$. Then we maximize $p_{\rm joint}(\tilde{\eta})$ with respect to $\tilde{\eta}$ to obtain the highest possible joint probability.

The results of such an analysis are shown in Fig. 4. The analysis is performed at the fixed v_m corresponding to the third modulation data point in DAMA, depending on the DM mass m_χ. We find that for all considered interaction types and $m_\chi \lesssim 15$ GeV at least one experiment disfavors a DM interpretation of the DAMA modulation at more than 4σ even under the very modest assumptions of the *general halo*. In the case of SI interactions, the tension with XE100 is at more than 6σ for $m_\chi \gtrsim 8$ GeV and saturates at the significance of the modulation data point itself at about 6.4σ for $m_\chi \gtrsim 13$ GeV. The exclusion from XE10 is nearly independent of the DM mass slightly below 6σ. We show also a few examples of the joint probability in case of a *symmetric halo*.

As mentioned above, one requirement for our method to apply is that the DM velocity distribution $f(v)$ is smooth on scales $\lesssim v_e$. Results from N-body simulations [19] indicate that close to the galactic escape velocity $v_{\rm esc} \sim 550$ km/s fluctuations at such small scales can become significant due to the presence of cold unvirialized DM streams. Note however, that in all cases shown above the DAMA modulation signal is excluded already for $v_{\rm min}$ well below $v_{\rm esc}$, where $f(v)$ is expected to be sufficiently smooth [19]. Furthermore, because $\mathcal{O}(v_e^2)$ terms in the expansion of Eq. (1) lead to the appearance of a $[\cos(2\pi t)]^2$ time dependence, the validity of this approximation can be checked experimentally by searching for higher harmonics in the modulation.

While astrophysics uncertainties are avoided, the obtained bounds are still subject to nuclear, particle physics, and experimental uncertainties. For instance, the tension between the DAMA signal and the bounds depends on the value of the Na quenching factor $q_{\rm Na}$, light-yield or ionization yield efficiencies in Xe, upward fluctuations from below threshold, and so on. For example, if a value of $q_{\rm Na} = 0.45$ is adopted instead of the fiducial value of 0.3 consistency for SD and isospin-violating interactions can

be achieved in the case of the general halo at around 3σ, while for SI interactions the XE10 bound still implies tension at more than 5σ for $m_\chi \gtrsim 10$ GeV. Hence, the precise C.L. of exclusion may depend on systematic uncertainties. We also stress that the above bounds apply to elastic scattering only.

In conclusion, we have presented a powerful method to check the consistency of an annual modulation signal in a DM direct detection experiment with bounds on the total DM scattering rate from other experiments, almost completely independent of astrophysics, for a given type of DM-nucleus interaction. While our bounds strongly disfavor a DM interpretation of present annually modulated signals for several models of DM interactions (SI and SD elastic scattering), the method will be an important test that any future modulated signal will have to pass before a DM interpretation can be accepted.

J. H.-G. is supported by the MICINN under the FPU program. J. H.-G. and T. S. acknowledge support from the EU FP7 ITN INVISIBLES (MC Actions, Grant No. PITN-GA-2011-289442). J. Z. was supported in part by the U. S. National Science Foundation under Grant No. PHY1151392.

*juan.a.herrero AT uv.es
†schwetz AT mpi-hd.mpg.de
‡zupanje AT ucmail.uc.edu

[1] E. Komatsu *et al.* (WMAP Collaboration), Astrophys. J. Suppl. Ser. **192**, 18 (2011).
[2] A. K. Drukier, K. Freese, and D. N. Spergel, Phys. Rev. D **33**, 3495 (1986); K. Freese, J. A. Frieman, and A. Gould, Phys. Rev. D **37**, 3388 (1988).
[3] R. Bernabei *et al.* (DAMA Collaboration), Eur. Phys. J. C **56**, 333 (2008); , **67**, 39 (2010).
[4] C. E. Aalseth *et al.* (CoGeNT Collaboration), Phys. Rev. Lett. **107**, 141301 (2011).
[5] T. Schwetz and J. Zupan, J. Cosmol. Astropart. Phys. 08 (2011) 008; J. Kopp, T. Schwetz, and J. Zupan, J. Cosmol. Astropart. Phys. 03 (2012) 001; M. Farina, D. Pappadopulo, A. Strumia, and T. Volansky, J. Cosmol. Astropart. Phys. 11 (2011) 010.
[6] P. J. Fox, J. Kopp, M. Lisanti, and N. Weiner, Phys. Rev. D **85**, 036008 (2012).
[7] J. Angle *et al.* (XENON10 Collaboration), Phys. Rev. Lett. **107**, 051301 (2011).
[8] E. Aprile *et al.* (XENON100 Collaboration), Phys. Rev. Lett. **107**, 131302 (2011).
[9] Z. Ahmed *et al.* (CDMS-II Collaboration), Phys. Rev. Lett. **106**, 131302 (2011).
[10] Z. Ahmed *et al.* (CDMS Collaboration), arXiv:1203.1309.
[11] P. J. Fox, J. Liu, and N. Weiner, Phys. Rev. D **83**, 103514 (2011).
[12] P. J. Fox, G. D. Kribs, and T. M. P. Tait, Phys. Rev. D **83**, 034007 (2011).
[13] J. Herrero-Garcia, T. Schwetz, and J. Zupan, J. Cosmol. Astropart. Phys. 03 (2012) 005.
[14] M. T. Frandsen, F. Kahlhoefer, C. McCabe, S. Sarkar, and K. Schmidt-Hoberg, J. Cosmol. Astropart. Phys. 01 (2012) 024.
[15] P. Gondolo and G. B. Gelmini, arXiv:1202.6359.
[16] D. S. Akerib *et al.* (CDMS Collaboration), Phys. Rev. Lett. **96**, 011302 (2006).
[17] M. Felizardo *et al.* (SIMPLE Collaboration), Phys. Rev. Lett. **108**, 201302 (2012).
[18] S. Archambault *et al.* (PICASSO Collaboration), Phys. Lett. B **711**, 153 (2012).
[19] M. Kuhlen, N. Weiner, J. Diemand, P. Madau, B. Moore, D. Potter, J. Stadel, and M. Zemp, J. Cosmol. Astropart. Phys. 02 (2010) 030.

Journal of Cosmology and Astroparticle Physics
An IOP and SISSA journal

Halo-independent methods for inelastic dark matter scattering

Nassim Bozorgnia,[a] **Juan Herrero-Garcia,**[b] **Thomas Schwetz**[a] **and Jure Zupan**[c]

[a]Max-Planck-Institut für Kernphysik,
Saupfercheckweg 1, 69117 Heidelberg, Germany
[b]Departamento de Fisica Teorica, and IFIC, Universidad de Valencia-CSIC,
Edificio de Institutos de Paterna, Apt. 22085, 46071 Valencia, Spain
[c]Department of Physics, University of Cincinnati,
Cincinnati, Ohio 45221, U.S.A.

E-mail: bozorgnia@mpi-hd.mpg.de, juan.a.herrero@uv.es,
schwetz@mpi-hd.mpg.de, jure.zupan@cern.ch

Received May 21, 2013
Accepted July 6, 2013
Published July 31, 2013

Abstract. We present halo-independent methods to analyze the results of dark matter direct detection experiments assuming inelastic scattering. We focus on the annual modulation signal reported by DAMA/LIBRA and present three different halo-independent tests. First, we compare it to the upper limit on the unmodulated rate from XENON100 using (a) the trivial requirement that the amplitude of the annual modulation has to be smaller than the bound on the unmodulated rate, and (b) a bound on the annual modulation amplitude based on an expansion in the Earth's velocity. The third test uses the special predictions of the signal shape for inelastic scattering and allows for an internal consistency check of the data without referring to any astrophysics. We conclude that a strong conflict between DAMA/LIBRA and XENON100 in the framework of spin-independent inelastic scattering can be established independently of the local properties of the dark matter halo.

Keywords: dark matter theory, dark matter experiments

ArXiv ePrint: 1305.3575

doi:10.1088/1475-7516/2013/07/049

JCAP07(2013)049

Contents

JCAP07(2013)049

1 Introduction

If dark matter (DM) is a "Weakly Interacting Massive Particle" (WIMP) it may induce an observable signal in underground detectors by depositing a tiny amount of energy after scattering with a nucleus in the detector material [1]. Many experiments are currently exploring this possibility and delivering a wealth of data. Among them is the DAMA/LIBRA experiment [2] (DAMA for short) which reports the striking signature of an annual modulation of the signal in their NaI scintillator detector, with a period of one year and a maximum around June 2nd with very high statistical significance. Such an effect is expected for DM induced events because the velocity of the detector relative to the DM halo changes due to the Earth's rotation around the Sun [3, 4].

Assuming elastic spin-independent interactions the DAMA modulation signal is in strong tension with constraints on the total DM interaction rate from other experiments [5–8]. This problem can be alleviated by considering inelastic scattering [9], where the DM particle χ up-scatters to an excited state χ^* with a mass difference $\delta = m_{\chi^*} - m_\chi$ comparable to the kinetic energy of the incoming particle, which is typically $\mathcal{O}(100)\,\mathrm{keV}$. Under this hypothesis scattering off the heavy iodine nucleus is favoured compared to the relatively light sodium in the NaI crystal used in DAMA. Furthermore, the relative strength of the modulation signal compared to the unmodulated rate can be enhanced.[1] Nevertheless, under specific assumptions for the DM halo — typically a Maxwellian velocity distribution — also the inelastic scattering explanation of the DAMA signal is in tension with the bounds from XENON100 [12] and CRESST-II [10], see e.g., [13–16]. Below we show that this conclusion can be confirmed in a halo-independent way. Let us mention that any explanation of the DAMA signal based on iodine scattering is disfavoured also by KIMS results [17], since their 90% CL upper bound on the DM scattering rate on CsI is already somewhat lower than the size of the modulation amplitude observed in DAMA. This tension is completely independent of astrophysics as well as particle physics as long as scattering happens on iodine.

For typical inelastic scattering explanations of DAMA the mass splitting between the two DM states is chosen such that the minimal velocity, v_m, required to deposit the threshold energy in the detector is already close to the galactic escape velocity, $v_{\rm esc}$. Only DM particles

[1] The possibility to use inelastic scattering to reconcile the event excess observed in CRESST-II [10] with other bounds has been discussed in [11]. Here we do not follow this hypothesis and focus on the DAMA modulation signal.

with velocities in the interval, $v \in [v_{\rm esc} - \Delta v, v_{\rm esc}]$, contribute, where Δv is the range of minimal velocities probed by the experiment and is comparable to the Earth's velocity around the Sun, $v_e \approx 30\,{\rm km/s}$. In this case the DM direct detection experiment probes the tails of the DM velocity distribution, where halo-substructures such as streams or debris flows are expected. The results are thus quite sensitive to the exact history of the Milky Way halo, mergers, etc, and significantly depend on the halo properties, see e.g. [18, 19]. Therefore it is important to develop astrophysics-independent methods to evaluate whether the above conclusion on the disagreement of the DAMA signal with other bounds is robust with respect to variations of DM halo properties.

An interesting method to compare signals and/or bounds from different experiments in an astrophysics independent way has been proposed in refs. [20, 21]. This so-called v_m-method has been applied in various recent studies for elastic scattering, see e.g., [22–27]. The generalization of this method to inelastic scattering involves some complications which we are going to address in detail below.

In part of our analyses we will also use the fact that v_e is small compared to all other typical velocities in the problem. One can then derive astrophysics-independent bounds on the annual modulation signal [28] by expanding in $v_{\rm e}$ and relating the $\mathcal{O}(v_e^0)$ and $\mathcal{O}(v_e)$ terms in a halo-independent way. In [25, 28] the expansion was applied to the case of elastic DM scattering with DM masses of order 10 GeV, where the expansion is expected to be well-behaved, and it has been shown that for elastic scattering a strong tension between DAMA and constraints from other experiments can be established independent of the details of the DM halo. In the following we will generalize this type of analysis to the case of inelastic scattering, where special care has to be taken about whether the expansion in v_e remains well-behaved.

Below we will present three different tests for the consistency of the inelastic scattering interpretation of the DAMA signal, focusing on the tension with the bound from XENON100 [8]:

- the "trivial bound" obtained by the requirement that the amplitude of the annual modulation has to be smaller than the unmodulated rate,
- the bound on the annual modulation signal based on the expansion of the halo integral in v_e, and
- a test based on the predicted shape of the signal in the case of inelastic scattering which we call the "shape test" in the following.

The paper is structured as follows. We fix basic notation in section 2. In section 3 we discuss the bound on the annual modulation amplitude derived in [28]. By identifying the relevant expansion parameter we point out its limitations in the case of inelastic scattering. In section 4 we develop halo-independent methods for inelastic scattering, focusing on the tension between DAMA and XENON100, and apply the three different types of tests mentioned above. Conclusions are presented in section 5.

2 Notation

The differential rate in events/keV/kg/day for DM χ to scatter off a nucleus (A, Z) and deposit the nuclear recoil energy $E_{\rm nr}$ in the detector is

$$R(E_{\rm nr}, t) = \frac{\rho_\chi}{m_\chi} \frac{1}{m_A} \int_{v > v_m} d^3v \frac{d\sigma_A}{dE_{\rm nr}} v f_{\rm det}(\mathbf{v}, t)\,. \tag{2.1}$$

JCAP07(2013)049

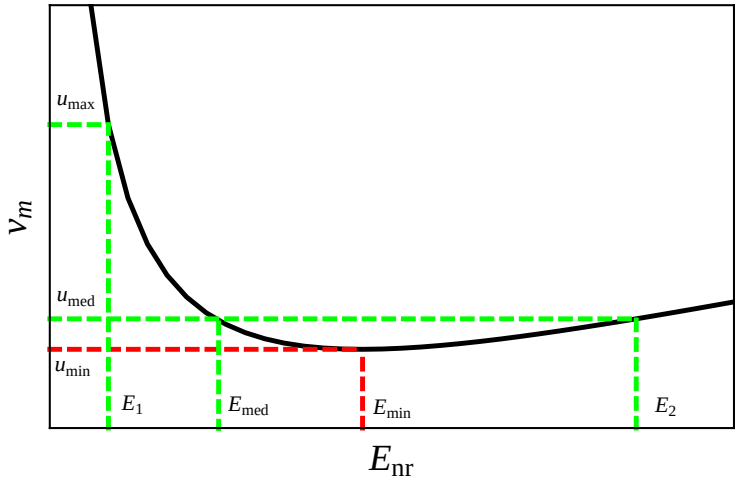

Figure 1. v_m as a function of E_{nr} for the case of inelastic scattering for some arbitrary $\delta > 0$.

Here $\rho_\chi \simeq 0.3\,\text{GeV/cm}^3$ is the local DM density, m_A and m_χ are the nucleus and DM masses, σ_A the DM-nucleus scattering cross section and $\mathbf{v}$ the 3-vector relative velocity between DM and the nucleus, while $v \equiv |\mathbf{v}|$. For a DM particle to deposit a recoil energy E_{nr} in the detector, a minimal velocity v_m is required, restricting the integral over velocities in eq. (2.1). For inelastic scattering we have

$$v_m = \sqrt{\frac{1}{2m_A E_{\text{nr}}}}\left(\frac{m_A E_{\text{nr}}}{\mu_{\chi A}} + \delta\right), \tag{2.2}$$

where $\mu_{\chi A}$ is the reduced mass of the DM-nucleus system, and δ is the mass splitting between the two dark matter states. Note that for each value of E_{nr} there is a corresponding v_m while the converse is not always true. Certain values of v_m correspond to two values of E_{nr}, others maybe to none. This is illustrated in figure 1, where we plot v_m as a function of E_{nr} for some arbitrary $\delta > 0$.

The particle physics enters in eq. (2.1) through the differential cross section. For the standard spin-independent and spin-dependent scattering the differential cross section is

$$\frac{d\sigma_A}{dE_{\text{nr}}} = \frac{m_A}{2\mu_{\chi A}^2 v^2}\sigma_A^0 F^2(E_{\text{nr}}), \tag{2.3}$$

where σ_A^0 is the total DM-nucleus scattering cross section at zero momentum transfer, and $F(E_{\text{nr}})$ is a form factor. We focus here on spin-independent inelastic scattering. We also assume that DM couples with the same strength to protons and neutrons ($f_p = f_n$). Relaxing this assumption does not change the conclusions since DM particles scattering on Xe and I have very similar dependence on f_n/f_p (cf. figure 5 of [11]). The astrophysics dependence enters in eq. (2.1) through the DM velocity distribution $f_{\text{det}}(\mathbf{v}, t)$ in the detector rest frame. Defining the halo integral

$$\eta(v_m, t) \equiv \int_{v>v_m} d^3v \frac{f_{\text{det}}(\mathbf{v}, t)}{v}, \tag{2.4}$$

JCAP07(2013)049

the event rate is given by

$$R(E_{\rm nr}, t) = C\, F^2(E_{\rm nr})\, \eta(v_m, t) \qquad \text{with} \qquad C = \frac{\rho_\chi \sigma_A^0}{2 m_\chi \mu_{\chi A}^2}\,. \tag{2.5}$$

The coefficient C contains the particle physics dependence, while $\eta(v_m, t)$ parametrizes the astrophysics dependence. The halo integral $\eta(v_m, t)$ is the basis for the astrophysics independent comparison of experiments [20, 21] and we will make extensive use of it below.

3 Bound on the annual modulation amplitude from the expansion in v_e

In ref. [28] some of us have derived an upper bound on the annual modulation amplitude in terms of the unmodulated rate. Here we briefly review the idea and generalize the bound to the case of inelastic scattering, where special care has to be taken about the validity of the expansion.

The DM velocity distribution in the rest frame of the Sun, $f(\mathbf{v})$, is related to the distribution in the detector rest frame by $f_{\rm det}(\mathbf{v}, t) = f(\mathbf{v} + \mathbf{v}_e(t))$. The basic assumption of [28] is that $f(\mathbf{v})$ is constant in time on the scale of 1 year and is constant in space on the scale of the size of the Sun-Earth distance. These are very weak requirements, called "Assumption 1" in [28], which are expected to hold for a wide range of possible DM halos. Those assumptions would be violated if a few DM substructures of $\sim 1\,$AU in size would dominate the local DM distribution. The smallest DM substructures in typical WIMP scenarios can have masses many orders of magnitude smaller than $M_\odot$, e.g. [29]. Based on numerical simulations it is estimated in [30] that Earth mass DM substructures with sizes comparable to the solar system are stable against gravitational disruption, and on average one of them will pass through the solar system every few thousand years, where such an encounter would last about 50 years. Those considerations suggest that Assumption 1 is well satisfied. Let us stress that typical DM streams or debris flows [31] which may dominate the DM halo at high velocities (especially relevant for inelastic scattering) are expected to be many orders of magnitude larger than 1 AU, and the relevant time scales are much larger than 1 yr, and hence they fulfill our assumptions, see e.g. [32] and references therein.

Under this assumption the only time dependence is due to the Earth's velocity $\mathbf{v}_e(t)$, which we write as [33]

$$\mathbf{v}_e(t) = v_e[\mathbf{e}_1 \sin\lambda(t) - \mathbf{e}_2 \cos\lambda(t)]\,, \tag{3.1}$$

with $v_e = 29.8\,$km/s, and $\lambda(t) = 2\pi(t - 0.218)$ with t in units of 1 year and $t = 0$ at January 1st, while $\mathbf{e}_1 = (-0.0670, 0.4927, -0.8676)$ and $\mathbf{e}_2 = (-0.9931, -0.1170, 0.01032)$ are orthogonal unit vectors spanning the plane of the Earth's orbit which at this order can be assumed to be circular. The DM velocity distribution in the galactic frame is connected to the one in the rest frame of the Sun by $f(\mathbf{v}) = f_{\rm gal}(\mathbf{v} + \mathbf{v}_{\rm sun})$, with $\mathbf{v}_{\rm sun} \approx (0, 220, 0)\,$km/s $+ \mathbf{v}_{\rm pec}$ and $\mathbf{v}_{\rm pec} \approx (10, 13, 7)\,$km/s the peculiar velocity of the Sun. We are using galactic coordinates where x points towards the galactic center, y in the direction of the galactic rotation, and z towards the galactic north, perpendicular to the disc. As shown in [34], eq. (3.1) provides an excellent approximation to describe the annual modulation signal.

Using the fact that v_e is small compared to other relevant velocities, one can expand the halo integral eq. (2.4) in powers of v_e. At zeroth order one obtains

$$\eta_0(v_m) = \int_{v > v_m} d^3v \frac{f(\mathbf{v})}{v}\,, \tag{3.2}$$

JCAP07(2013)049

which is responsible for the unmodulated (time averaged) rate up to terms of order v_e^2. The first order terms in v_e lead to the annual modulation signal, which due to eq. (3.1) will have a pure sinusoidal shape, such that

$$\eta(v_m, t) = \eta_0(v_m) + A_\eta(v_m) \cos 2\pi[t - t_0(v_m)] + \mathcal{O}(v_e^2)\,, \tag{3.3}$$

where the amplitude of the annual modulation, $A_\eta(v_m)$, is of first order in v_e.

In [28] it has been shown that under the above stated "Assumption 1" the modulation amplitude is bounded as

$$A_\eta(v_m) < v_e \left[-\frac{d\eta_0}{dv_m} + \frac{\eta_0}{v_m} - \int_{v_m} dv \frac{\eta_0}{v^2} \right]. \tag{3.4}$$

From eq. (3.2) it is clear that η_0 is a positive decreasing function, i.e., $d\eta_0/dv_m < 0$. As mentioned above, in the case of inelastic scattering typically only a small range in minimal velocities v_m is probed. We denote this interval by $[u_{\rm min}, u_{\rm max}]$ with $\Delta v = u_{\rm max} - u_{\rm min}$. The boundaries of this interval are determined by the threshold of the detector on one side and by the galactic escape velocity or the nuclear form factor suppression on the other side. For inelastic scattering Δv is small. It will thus be convenient to integrate the inequality (3.4) over the interval $[u_{\rm min}, u_{\rm max}]$. By changing the order of integrations of the double integral we find

$$\begin{aligned} \int_{u_{\rm min}}^{u_{\rm max}} dv A_\eta(v) &< v_e \left[\eta_0(u_{\rm min}) - \eta_0(u_{\rm max}) + u_{\rm min} \int_{u_{\rm min}}^{u_{\rm max}} dv \frac{\eta_0}{v^2} - \Delta v \int_{u_{\rm max}} dv \frac{\eta_0}{v^2} \right] \\ &< v_e \left[\eta_0(u_{\rm min}) + u_{\rm min} \int_{u_{\rm min}}^{u_{\rm max}} dv \frac{\eta_0}{v^2} \right]. \end{aligned} \tag{3.5}$$

Integrating again over $u_{\rm min}$ we obtain

$$\int_{u_{\rm min}}^{u_{\rm max}} dv A_\eta(v)(v - u_{\rm min}) < \frac{v_e}{2} \int_{u_{\rm min}}^{u_{\rm max}} dv \eta_0 \left(3 - \frac{u_{\rm min}^2}{v^2} \right) \tag{3.6}$$

$$< \frac{v_e}{2} \left(3 - \frac{u_{\rm min}^2}{u_{\rm max}^2} \right) \int_{u_{\rm min}}^{u_{\rm max}} dv \eta_0\,. \tag{3.7}$$

Hence we obtained a bound on the integral of the annual modulation in terms of an integral of the unmodulated rate at first order in v_e.[2] This bound receives no corrections at order $\mathcal{O}(v_e^2)$ and hence is valid up to (but not including) terms of order $\mathcal{O}(v_e^3)$ [35]. In applying eq. (3.7) we use only an upper bound, $\eta_{\rm bnd}$ on the unmodulated signal η_0, allowing also for the presence of background. However, we assume that A_η is background free, i.e., the background shows no annual modulation.

Let us define the average over the velocity interval by

$$\langle X \rangle = \frac{1}{\Delta v} \int_{u_{\rm min}}^{u_{\rm max}} dv X(v)\,. \tag{3.8}$$

Estimating $\int_{u_{\rm min}}^{u_{\rm max}} dv A_\eta(v)(v - u_{\rm min}) \sim \Delta v \int_{u_{\rm min}}^{u_{\rm max}} dv A_\eta(v)$ and neglecting $\mathcal{O}(1)$ coefficients we obtain from eq. (3.7)

$$\langle A_\eta \rangle \lesssim \frac{v_e}{\Delta v} \langle \eta_0 \rangle\,. \tag{3.9}$$

[2] Below we will use the bound (3.7) for the numerical analysis since this will allow for easy comparison with the "trivial bound" discussed later. The numerical difference between the bounds using (3.7) or (3.6) is small, typically less than 10%.

JCAP07(2013)049

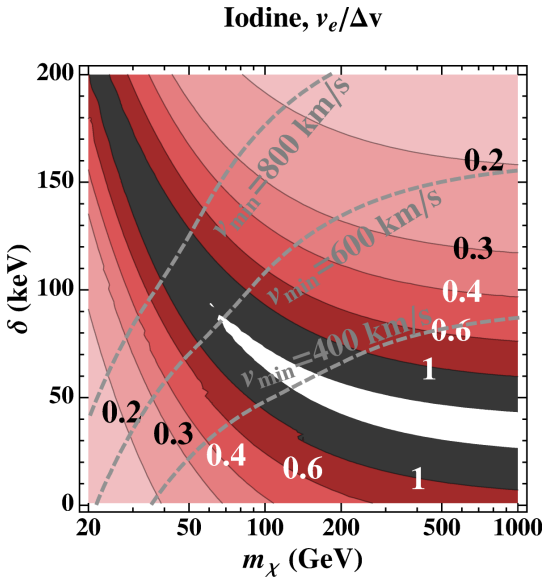

Figure 2. Contours of the ratio $v_e/\Delta v$ as a function of DM mass m_χ and mass splitting δ for scattering on iodine in DAMA, assuming that Δv is the overlap between the velocity ranges corresponding to the DAMA $[2,4]$ keVee energy range for scattering on iodine and the XENON100 $[6.61, 43.04]$ keV range. Dashed curves show contours of constant $v_m = 400, 600, 800$ km/s, with v_m being the minimal velocity corresponding to the above energy interval for the given δ and m_χ.

This shows that the expansion parameter in deriving the bound (3.7) is $v_e/\Delta v$. In contrast to expressions like $v_e/u_{\rm min}$ which are always small, the ratio $v_e/\Delta v$ can become of order one, in particular for inelastic scattering.

As an example we show in figure 2 the ratio $v_e/\Delta v$ as a function of the DM mass m_χ and the inelasticity parameter δ. Elastic scattering is recovered for $\delta = 0$. The velocity interval Δv is chosen having in mind a possible explanation for DAMA. The signal in DAMA is predominantly in the energy region $[2,4]$ keVee. As explained in section 4 below, we take for Δv the overlap between the velocity ranges corresponding to the DAMA $[2,4]$ keVee interval for scattering on iodine and the XENON100 $[6.61, 43.04]$ keV interval. From figure 2 one sees that the expansion parameter $v_e/\Delta v \gtrsim 1$ for a non-negligible part of the parameter space of DM masses m_χ and mass splittings δ. For those values of m_χ and δ the bound eq. (3.7) does not apply. Still, in a significant part of the parameter space $v_e/\Delta v$ is sufficiently small such that the expansion can be performed. In particular, we observe from the figure that for elastic scattering ($\delta = 0$) and $m_\chi \lesssim 50$ the expansion parameter is small, justifying the approach of ref. [25].

4 Halo-independent tests for inelastic scattering

In this section we present three different halo-independent tests of the tension between the DAMA annual modulation signal [2] and the bound from XENON100 [8] in the framework of inelastic scattering. The tests are presented in the following order. First, we present the shape test which is a test based on the predicted shape of the signal. Second, we present the bound on the annual modulation signal from eq. (3.7). Third, we present the trivial bound

JCAP07(2013)049

which is based on the fact that the amplitude of the annual modulation must be smaller than the unmodulated rate.

The v_m method [20, 21] to compare different experiments like DAMA and XENON100 requires to translate the physical observations in nuclear recoil energy $E_{\rm nr}$ into v_m space using eq. (2.2). Then experiments can be directly compared based on the halo integral $\eta(v_m)$ or inequalities such as eq. (3.7) [25]. However, for inelastic scattering this involves some complications. The reason is that in inelastic scattering each minimal velocity v_m can correspond to up to two values of $E_{\rm nr}$, depending on the values of m_χ and δ. This has to be taken into account when translating an observation at a given $E_{\rm nr}$ into v_m, since the relation between them is no longer unique (as it is for elastic scattering). Solving eq. (2.2) for $E_{\rm nr}$, one obtains two solutions $E_\pm$ as a function of v_m,

$$E_\pm = \left(\frac{\mu_{\chi A}}{m_A}\right)\left[(\mu_{\chi A} v_m^2 - \delta) \pm v_m \sqrt{\mu_{\chi A}(\mu_{\chi A} v_m^2 - 2\delta)}\right]. \tag{4.1}$$

There is a minimal value of v_m given by $\sqrt{2\delta/\mu_{\chi A}}$ at an energy $E_{\rm min} = \mu_{\chi A}\delta/M_A$.

Let us consider the following situation, having in mind DAMA: we have a region $[E_1, E_2]$ in nuclear recoil energy where the modulation amplitude is non-zero. We assume that E_1 is the threshold energy of the detector. When mapped into v_m space according to eq. (2.2) we obtain that the whole interval $[E_1, E_2]$ is mapped into a small region in v_m, between $u_{\rm min}$ and $u_{\rm max}$ with $u_{\rm max} - u_{\rm min} \ll u_{\rm min}$, where $u_{\rm min}$ and $u_{\rm max}$ are the minimum and maximum values of v_m in the $[E_1, E_2]$ interval, respectively. For the special case plotted in figure 1, $u_{\rm min} = v_m(E_{\rm min})$, and $u_{\rm max} = v_m(E_1)$. In general, depending on the shape of v_m as a function of $E_{\rm nr}$ in the interval $[E_1, E_2]$, $u_{\rm max}$ may either be $v_m(E_1)$ (as in the case shown in figure 1) or $v_m(E_2)$. Furthermore, in cases where $E_{\rm min}$ falls outside of the interval $[E_1, E_2]$, $u_{\rm min}$ will either be $v_m(E_1)$ or $v_m(E_2)$. We will not discuss all these cases here explicitly, but as an example focus on the case shown in figure 1.

To compute the bound in eq. (3.7) using DAMA data, we need to numerically compute integrals such as $\int_{u_{\rm min}}^{u_{\rm max}} dv h(v) A_\eta^{\rm obs}(v)$ where $h(v) = v - u_{\rm min}$ is specified in eq. (3.7) (we leave it general here to apply the same formalism also to the bound in eq. (4.7) discussed later on, where $h(v) = 1$) and $A_\eta^{\rm obs}(v)$ is the observed amplitude of the annual modulation in units of events/kg/day/keV. In order to compute those integrals we have to consider the functional relation between v_m and $E_{\rm nr}$ in the relevant interval $[E_1, E_2]$. Let us discuss for instance the situation depicted in figure 1. In this case we have

$$\begin{aligned}\int_{u_{\rm min}}^{u_{\rm max}} dv h(v) \tilde{A}_\eta^{\rm obs}(v) &= \int_{u_{\rm min}}^{u_{\rm med}} dv h(v) \tilde{A}_\eta^{\rm obs}(v) + \int_{u_{\rm med}}^{u_{\rm max}} dv h(v) \tilde{A}_\eta^{\rm obs}(v) \\ &= \int_{u_{\rm min}}^{u_{\rm med}} dv h(v) \tilde{A}_\eta^{\rm obs}(v) + \int_{E_{\rm med}}^{E_1} dE_{\rm nr} \frac{dv}{dE_{\rm nr}} h(E_{\rm nr}) \tilde{A}_\eta^{\rm obs}(v)\,. \end{aligned} \tag{4.2}$$

Here, $u_{\rm med} = v_m(E_2)$ and $E_{\rm med} = E_-(u_{\rm med})$. The integrals can be written as a sum of several integrals which are evaluated over energy bins, as given by the DAMA binning. We take four bins of equal size in the $[2, 4]$ keVee range for the DAMA data. In each bin we write [25]

$$\tilde{A}_\eta^{\rm obs}(v_i) = \frac{A_i^{\rm obs} q_I}{A_{\rm I}^2 F_{\rm I}^2(E_{\rm nr}) f_{\rm I}}\,, \tag{4.3}$$

JCAP07(2013)049

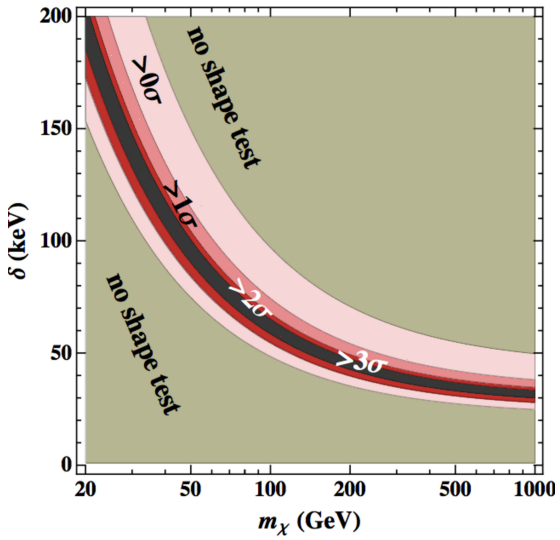

Figure 3. The DM exclusion regions (red bands, with significance as denoted) that follow from the internal consistency shape test for DAMA data, see eq. (4.4). In the gray region denoted by "no shape test" there is a one-to-one correspondence between $E_{\rm nr}$ and v_m since $E_{\rm min}$ lies outside the relevant energy interval $[E_1, E_2]$ and therefore the shape test cannot be applied.

where the index i labels energy bins, q_I is the iodine quenching factor for which we take $q_I = 0.09$,[3] $F_I(E_{\rm nr})$ is the Helm form factor for iodine, and $f_I = m_{\rm I}/(m_{\rm Na} + m_{\rm I})$. In each energy bin we assume $A_i^{\rm obs}$ is constant, and thus in each bin we numerically integrate $(dv/dE_{\rm nr})h(E_{\rm nr})/F_{\rm I}^2(E_{\rm nr})$ over the bin width.

For the first integral on the r.h.s. of eq. (4.2) there is an ambiguity, since the interval $[u_{\rm min}, u_{\rm med}]$ corresponds to two regions in energy: $[E_{\rm med}, E_{\rm min}]$ or $[E_{\rm min}, E_2]$. If the inelastic DM hypothesis under consideration is correct, both energy intervals should give the same value of the integral. We can use this observation to test the hypothesis that the signal is due to inelastic DM scattering by requiring that the two integrals agree within experimental errors. In the following, we will call this the "shape test". Let us denote the integrals corresponding to the two energy intervals by I_a and I_b and their experimental errors by σ_a and σ_b, correspondingly. In figure 3 we show the difference weighted by the error as obtained from DAMA data:

$$\frac{|I_a - I_b|}{\sqrt{\sigma_a^2 + \sigma_b^2}}\,. \tag{4.4}$$

We observe that a strip in the parameter space in δ and m_χ is already excluded by this requirement at more than 3σ in a completely halo-independent way, just requiring a spectral shape of the signal consistent with the inelastic scattering hypothesis. In cases where the two values are consistent within errors we use for the integral the weighted average of the two values. In figure 3, I_a and I_b are evaluated for the choice of $h(v) = v - u_{\rm min}$. The shape

[3]For DM masses that we consider one can safely neglect scattering on sodium. Note also that the channeling fraction of iodine in NaI is likely to be very small and can be neglected [36].

JCAP07(2013)049

test is only slightly different for $h(v) = 1$ which is the case for the trivial bound explained later in eq. (4.7).

In order to evaluate the r.h.s. of the inequality in eq. (3.7), we need to calculate an integral over the experimental upper bound $\tilde{\eta}_{\rm bnd}(v_m)$ on the unmodulated signal, with

$$\tilde{\eta}(v_m) \equiv \frac{\sigma_p \rho_\chi}{2 m_\chi \mu_{\chi p}^2} \eta_0(v_m) \,, \tag{4.5}$$

where σ_p is the cross section on a nucleon and $\mu_{\chi p}$ is the DM-nucleon reduced mass. $\tilde{\eta}$ has units of events/kg/day/keV. In using eqs. (4.3) and (4.5) we have assumed an A^2 dependence of the scattering cross section on the nucleus with mass number A. We use the method discussed in ref. [25] (see also [20]) to evaluate $\tilde{\eta}_{\rm bnd}(v_m)$ for the inelastic case. Namely, we use the fact that $\tilde{\eta}(v_m)$ is a falling function, and that the minimal number of events is obtained for $\tilde{\eta}$ constant and equal to $\tilde{\eta}(v_m)$ up to v_m and zero for larger values of v_m. Therefore, for a given v_m we have a lower bound on the predicted number of events in an interval of observed energies $[E_1, E_2]$, $N^{\rm pred}_{[E_1,E_2]} > \mu(v_m)$ with

$$\mu(v_m) = M T A^2 \tilde{\eta}(v_m) \int_{E_-}^{E_+} dE_{\rm nr} F_A^2(E_{\rm nr}) G_{[E_1,E_2]}(E_{\rm nr}) \,, \tag{4.6}$$

where $G_{[E_1,E_2]}(E_{\rm nr})$ is the detector response function which describes the contribution of events with the nuclear-recoil energy $E_{\rm nr}$ to the observed energy interval $[E_1, E_2]$. M and T are the detector mass and exposure time, respectively. Notice that $\mu(v_m)$ for the elastic case is given in eq. (10) of ref. [25] and in that case the integral is computed between 0 and $E(v_m)$ which corresponds to velocities below a fixed v_m. For the inelastic case, we have two solutions E_+ and E_- for each v_m, and the region in velocity space below v_m is precisely, the region $E_- < E_{\rm nr} < E_+$.

Assuming an experiment observes $N^{\rm obs}_{[E_1,E_2]}$ events in the interval $[E_1, E_2]$, we can obtain an upper bound on $\tilde{\eta}(v_m)$ for a fixed v_m at a confidence level CL by requiring that the probability of obtaining $N^{\rm obs}_{[E_1,E_2]}$ events or less for a Poisson mean of $\mu(v_m)$ is equal to $1-{\rm CL}$. The upper bound obtained in this way is $\tilde{\eta}_{\rm bnd}(v_m)$ and can then be used in eq. (3.7) and numerically integrated over $[u_{\rm min}, u_{\rm max}]$ to constrain the modulation amplitude. We use the data from XENON100 [8] where the $E_{\rm nr}$ interval $[6.61, 43.04]\,$keV is binned into four bins. In each bin we calculate the probability of obtaining $N^{\rm obs}_{[E_1,E_2]}$ events or less for a Poisson mean of $\mu(v_m)$ as described above, and then multiply the probability of the four bins to obtain the overall probability, giving finally the actually observed event distribution. Note, that since only the high energy range in Xenon is relevant, our results are not sensitive to uncertainties in the scintillation efficiency $\mathcal{L}_{\rm eff}$ at low energies. For the comparison of the DAMA and XENON100 data using eq. (3.7) we define the $[u_{\rm min}, u_{\rm max}]$ range as the overlap between v_m spaces corresponding to the DAMA iodine $[2, 4]\,$keVee range and the XENON100 $[6.61, 43.04]\,$keV range.[4]

In figure 4 we show the l.h.s. and r.h.s. of the bound from eq. (3.7) in red and black, respectively, as a function of m_χ for $\delta = 50\,$keV, $100\,$keV, $120\,$keV, and $150\,$keV. We calculate the integral over the annual modulation amplitude in the l.h.s. of eq. (3.7) as described above. The red dashed curves indicate the 1σ error on the integral. The upper limit on the r.h.s. of eq. (3.7) is calculated from the XENON100 3σ upper limit. We see that in most regions

[4] For most of the region in parameter space this joint interval is actually very close to the one coming from DAMA iodine $[2, 4]\,$keVee.

JCAP07(2013)049

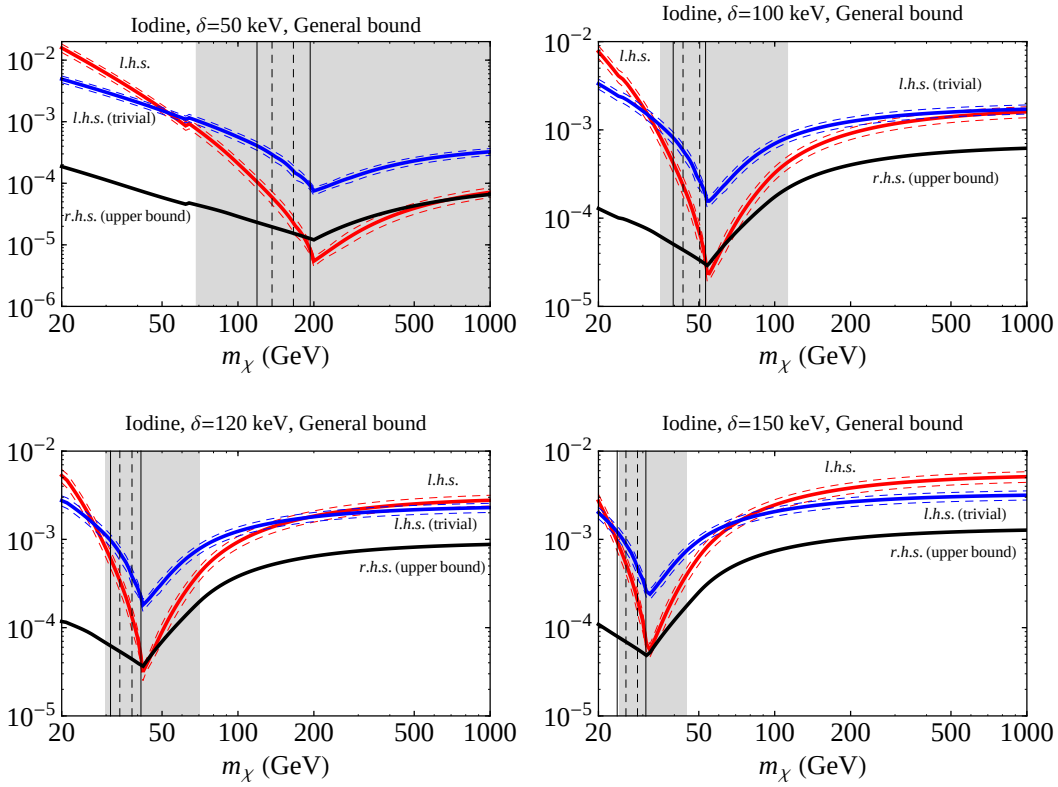

Figure 4. The bounds from eqs. (3.7) and (4.7) for DAMA data as a function of m_χ for $\delta = 50, 100, 120, 150$ keV. The red curve labeled "l.h.s." shows the integral on the l.h.s. of eq. (3.7), whereas the blue curve labeled "l.h.s. (trivial)" corresponds to the l.h.s. of the trivial bound in eq. (4.7). The dashed curves indicate the 1σ error. The black curve labeled "r.h.s. (upper bound)" is the same for (3.7) and (4.7) and has been obtained from the 3σ limit on $\eta_{\rm bnd}$ from XENON100 data. The units on the vertical axis are counts/kg/day/keV $(\mathrm{km/s})^2$. In the gray shaded regions we have $v_e/\Delta v > 0.7$; truncating the expansion may not be a good approximation and hence, the red curve should not be trusted in those regions, but instead the blue one can be used there. The solid (dashed) vertical lines indicate the regions where the two integrals relevant for the "shape test" differ by more than 2σ (3σ) according to eq. (4.4).

of the parameter space the bound is strongly violated, disfavoring an inelastic scattering interpretation of the DAMA signal halo-independently. Note that DM mass enters only via $\mu_{\chi A}$, so that $\mu_{\chi A} \simeq m_A$ for $m_\chi \gg m_A$, and eq. (4.1) becomes independent of m_χ. This is what we see in figure 4, where curves become flat for large m_χ and therefore the tension between XENON100 and DAMA cannot be diminished when going to larger DM masses.

The shaded regions in figure 4 are the regions where the expansion parameter $v_e/\Delta v$ is large (we take somewhat arbitrarily $v_e/\Delta v > 0.7$, cf. also figure 2). Hence, in the shaded regions the astrophysics independent bound on the modulation amplitude, eq. (3.7) (the red curves in figure 4), can receive $\mathcal{O}(1)$ corrections and should not be trusted. Interestingly, however, part of the region where the v_e expansion breaks down is disfavored by the internal consistency "shape test", eq. (4.4). We indicate the range in m_χ where the two integrals differ by more than 2σ and 3σ with vertical lines, cf. also figure 3.

JCAP07(2013)049

Finally we consider the "trivial bound", which is based on the simple fact valid for any positive function that the amplitude of the first harmonic has to be smaller than the constant part, i.e., $A_\eta \leq \eta_0$. To compare directly with eq. (3.7), we can write the trivial bound as,

$$\frac{v_e}{2}\left(3-\frac{u_{\rm min}^2}{u_{\rm max}^2}\right)\int_{u_{\rm min}}^{u_{\rm max}} dv A_\eta(v) < \frac{v_e}{2}\left(3-\frac{u_{\rm min}^2}{u_{\rm max}^2}\right)\int_{u_{\rm min}}^{u_{\rm max}} dv\, \eta_{\rm bnd}(v)\,. \tag{4.7}$$

The l.h.s. of this relation is shown as blue curve in figure 4 together with its 1σ error band. We observe again strong tension with the upper bound from XENON100 data. Clearly this bound is independent of any expansion parameter and is valid in the full parameter space. In the regions where the expansion is expected to break down (i.e., the grey shaded regions) this bound can be used to exclude the inelastic explanation for DAMA. From figure 4 we also observe that in the regions where the expansion in v_e is expected to be valid the modulation bound from eq. (3.7) becomes stronger (or at least comparable — for large m_χ) to the trivial bound.

5 Conclusions

Inelastic scattering [9] has originally been invoked to reconcile the DAMA annual modulation signal with bounds from other experiments. Using the kinematics of inelastic scattering the annual modulation amplitude can be enhanced compared to the time averaged rate. This is achieved at the expense of tuning the minimal velocity probed by the experiment so that it is close to the galactic escape velocity, which makes the signal rather sensitive to properties of the tails of the dark matter velocity distribution. Hence it is important to establish halo-independent methods for this scenario.

In this work we have generalized the comparison of dark matter direct detection experiments in v_m space [20, 21] to the case of inelastic scattering. This is non-trivial due to the non-unique relation between the recoil energy and v_m. Turning this complication into a virtue, we presented a consistency check based on the particular shape of the signal for inelastic scattering which we dubbed the "shape test", given in eq. (4.4) and figure 3. In certain regions of the parameter space the inelastic scattering hypothesis can be excluded simply based on the energy spectrum of the modulation signal, without referring to halo properties.

Furthermore, we have applied a bound on the annual modulation amplitude based on an expansion of the halo integral in the Earth's velocity v_e [28]. We have identified the relevant expansion parameter to be $v_e/\Delta v$, where Δv is the range in minimal velocities v_m probed in the experiment. For inelastic scattering, Δv can become of order v_e for part of the (m_χ, δ) parameter space, and then the bound cannot be applied. However, in those cases one can use the "trivial bound", requiring that the amplitude of the annual modulation has to be less than the bound on the unmodulated rate.

We were able to show that XENON100 strongly disfavors an interpretation of the DAMA modulation signal in terms of inelastic scattering, independent of assumptions on the properties of the local dark matter velocity distribution. Beyond the immediate problem of interpreting the DAMA signal, the methods developed in this manuscript will provide a valuable consistency check for an inelastic scattering interpretation of any future dark matter signal.

In our work we have focused on spin-independent contact interactions, where the differential scattering cross section takes the form of eq. (2.3). Our considerations generalize

JCAP07(2013)049

trivially to other interaction types which lead to a similar $1/v^2$ dependence (e.g., the spin-dependent inelastic scattering considered in [15]) but may feature a different dependence on $E_{\rm nr}$. Furthermore, the shape test and the trivial bound can be applied for any particle physics model where the differential cross section factorizes as $X(v)Y(E_{\rm nr})$, where X and Y are arbitrary functions of v and $E_{\rm nr}$, respectively. An example where such a factorization is not possible in general are magnetic interactions, e.g. [37]. In such cases generalized methods as presented recently in [38] may be invoked.

Acknowledgments

N.B., J.H.-G., and T.S. acknowledge support from the European Union FP7 ITN INVISIBLES (Marie Curie Actions, PITN-GA-2011-289442). J.H.-G. is supported by the MICINN under the FPU program. J.Z. was supported in part by the U.S. National Science Foundation under CAREER Grant PHY-1151392.

References

[1] M.W. Goodman and E. Witten, *Detectability of certain dark matter candidates*, *Phys. Rev.* **D 31** (1985) 3059 [INSPIRE].

[2] DAMA/LIBRA collaboration, R. Bernabei et al., *New results from DAMA/LIBRA*, *Eur. Phys. J.* **C 67** (2010) 39 [arXiv:1002.1028] [INSPIRE].

[3] A.K. Drukier, K. Freese and D.N. Spergel, *Detecting cold dark matter candidates*, *Phys. Rev.* **D 33** (1986) 3495 [INSPIRE].

[4] K. Freese, J.A. Frieman and A. Gould, *Signal modulation in cold dark matter detection*, *Phys. Rev.* **D 37** (1988) 3388 [INSPIRE].

[5] CDMS-II collaboration, Z. Ahmed et al., *Dark matter search results from the CDMS II experiment*, *Science* **327** (2010) 1619 [arXiv:0912.3592] [INSPIRE].

[6] CDMS-II collaboration, Z. Ahmed et al., *Results from a low-energy analysis of the CDMS II germanium data*, *Phys. Rev. Lett.* **106** (2011) 131302 [arXiv:1011.2482] [INSPIRE].

[7] XENON10 collaboration, J. Angle et al., *A search for light dark matter in XENON10 data*, *Phys. Rev. Lett.* **107** (2011) 051301 [arXiv:1104.3088] [INSPIRE].

[8] XENON100 collaboration, E. Aprile et al., *Dark matter results from 225 live days of XENON100 data*, *Phys. Rev. Lett.* **109** (2012) 181301 [arXiv:1207.5988] [INSPIRE].

[9] D. Tucker-Smith and N. Weiner, *Inelastic dark matter*, *Phys. Rev.* **D 64** (2001) 043502 [hep-ph/0101138] [INSPIRE].

[10] G. Angloher et al., *Results from 730 kg days of the CRESST-II dark matter search*, *Eur. Phys. J.* **C 72** (2012) 1971 [arXiv:1109.0702] [INSPIRE].

[11] J. Kopp, T. Schwetz and J. Zupan, *Light dark matter in the light of CRESST-II*, *JCAP* **03** (2012) 001 [arXiv:1110.2721] [INSPIRE].

[12] XENON100 collaboration, E. Aprile et al., *Implications on inelastic dark matter from 100 live days of XENON100 Data*, *Phys. Rev.* **D 84** (2011) 061101 [arXiv:1104.3121] [INSPIRE].

[13] S. Chang, G.D. Kribs, D. Tucker-Smith and N. Weiner, *Inelastic dark matter in light of DAMA/LIBRA*, *Phys. Rev.* **D 79** (2009) 043513 [arXiv:0807.2250] [INSPIRE].

[14] K. Schmidt-Hoberg and M.W. Winkler, *Improved constraints on inelastic dark matter*, *JCAP* **09** (2009) 010 [arXiv:0907.3940] [INSPIRE].

JCAP07(2013)049

[15] J. Kopp, T. Schwetz and J. Zupan, *Global interpretation of direct dark matter searches after CDMS-II results*, *JCAP* **02** (2010) 014 [arXiv:0912.4264] [INSPIRE].

[16] C. Arina, *Chasing a consistent picture for dark matter direct searches*, *Phys. Rev.* **D 86** (2012) 123527 [arXiv:1210.4011] [INSPIRE].

[17] S. Kim et al., *New limits on interactions between weakly interacting massive particles and nucleons obtained with CsI(Tl) crystal detectors*, *Phys. Rev. Lett.* **108** (2012) 181301 [arXiv:1204.2646] [INSPIRE].

[18] J. March-Russell, C. McCabe and M. McCullough, *Inelastic dark matter, non-standard halos and the DAMA/LIBRA results*, *JHEP* **05** (2009) 071 [arXiv:0812.1931] [INSPIRE].

[19] M. Lisanti, L.E. Strigari, J.G. Wacker and R.H. Wechsler, *The dark matter at the end of the galaxy*, *Phys. Rev.* **D 83** (2011) 023519 [arXiv:1010.4300] [INSPIRE].

[20] P.J. Fox, J. Liu and N. Weiner, *Integrating out astrophysical uncertainties*, *Phys. Rev.* **D 83** (2011) 103514 [arXiv:1011.1915] [INSPIRE].

[21] P.J. Fox, G.D. Kribs and T.M. Tait, *Interpreting dark matter direct detection independently of the local velocity and density distribution*, *Phys. Rev.* **D 83** (2011) 034007 [arXiv:1011.1910] [INSPIRE].

[22] C. McCabe, *DAMA and CoGeNT without astrophysical uncertainties*, *Phys. Rev.* **D 84** (2011) 043525 [arXiv:1107.0741] [INSPIRE].

[23] M.T. Frandsen, F. Kahlhoefer, C. McCabe, S. Sarkar and K. Schmidt-Hoberg, *Resolving astrophysical uncertainties in dark matter direct detection*, *JCAP* **01** (2012) 024 [arXiv:1111.0292] [INSPIRE].

[24] P. Gondolo and G.B. Gelmini, *Halo independent comparison of direct dark matter detection data*, *JCAP* **12** (2012) 015 [arXiv:1202.6359] [INSPIRE].

[25] J. Herrero-Garcia, T. Schwetz and J. Zupan, *Astrophysics independent bounds on the annual modulation of dark matter signals*, *Phys. Rev. Lett.* **109** (2012) 141301 [arXiv:1205.0134] [INSPIRE].

[26] M.T. Frandsen, F. Kahlhoefer, C. McCabe, S. Sarkar and K. Schmidt-Hoberg, *The unbearable lightness of being: CDMS versus XENON*, *JCAP* **07** (2013) 023 [arXiv:1304.6066] [INSPIRE].

[27] E. Del Nobile, G.B. Gelmini, P. Gondolo and J.-H. Huh, *Halo-independent analysis of direct detection data for light WIMPs*, arXiv:1304.6183 [INSPIRE].

[28] J. Herrero-Garcia, T. Schwetz and J. Zupan, *On the annual modulation signal in dark matter direct detection*, *JCAP* **03** (2012) 005 [arXiv:1112.1627] [INSPIRE].

[29] T. Bringmann, *Particle models and the small-scale structure of dark matter*, *New J. Phys.* **11** (2009) 105027 [arXiv:0903.0189] [INSPIRE].

[30] J. Diemand, B. Moore and J. Stadel, *Earth-mass dark-matter haloes as the first structures in the early universe*, *Nature* **433** (2005) 389 [astro-ph/0501589] [INSPIRE].

[31] M. Kuhlen, M. Lisanti and D.N. Spergel, *Direct detection of dark matter debris flows*, *Phys. Rev.* **D 86** (2012) 063505 [arXiv:1202.0007] [INSPIRE].

[32] K. Freese, M. Lisanti and C. Savage, *Annual modulation of dark matter: a review*, arXiv:1209.3339 [INSPIRE].

[33] G. Gelmini and P. Gondolo, *WIMP annual modulation with opposite phase in Late-Infall halo models*, *Phys. Rev.* **D 64** (2001) 023504 [hep-ph/0012315] [INSPIRE].

[34] A.M. Green, *Effect of realistic astrophysical inputs on the phase and shape of the WIMP annual modulation signal*, *Phys. Rev.* **D 68** (2003) 023004 [*Erratum ibid.* **D 69** (2004) 109902] [astro-ph/0304446] [INSPIRE].

JCAP07(2013)049

[35] N. Bozorgnia, J. Herrero-Garcia, T. Schwetz and J. Zupan, in preparation.

[36] N. Bozorgnia, G.B. Gelmini and P. Gondolo, *Channeling in direct dark matter detection I: channeling fraction in NaI (Tl) crystals*, *JCAP* **11** (2010) 019 [arXiv:1006.3110] [INSPIRE].

[37] S. Chang, N. Weiner and I. Yavin, *Magnetic inelastic dark matter*, *Phys. Rev.* **D 82** (2010) 125011 [arXiv:1007.4200] [INSPIRE].

[38] E. Del Nobile, G. Gelmini, P. Gondolo and J.-H. Huh, *Generalized halo independent comparison of direct dark matter detection data*, arXiv:1306.5273 [INSPIRE].

JCAP07(2013)049

Philosophical reflection

Since I have use of reason, I have always been asking myself questions about the world and wanted to learn everything about Nature. Some of them went so deep inside my mind that really obsessed me and sometimes made me feel *lost*. The thoughts, extended from childhood to nowadays, which I could call *the dialogue of my life*, are something like this:

- What is *all* this?
- You mean the world, etc...?
- Yes... all this complexity we see around us.... the world... I know it is a planet inside a spiral galaxy, just like many others of the billions that are out there, in a Universe that is flat, expanding, in fact accelerating... but apart from this, we don't know much...
- We know a lot, what do you mean?
- Come on, you did not even read the introduction...!! We know about 5% of the energy content of the Universe! We are here in a Universe whose more abundant ingredients, like dark energy or dark matter we have not detected, we have no idea what makes most of it...
- OK, one step at a time... what bothers you?
- Why all this... what are we... I mean, I know we are a human beings, not so different from other animals: made out of carbon through millions of years of evolution, conscious about our existence, and more intelligent than other mammals, with some abstract thinking... We have just evolved from inert matter, probably from some primary amino-acids that were made thanks to lightning... We are alive in the sense that we are born, we build ourselves with inert matter, atoms that are most of them made up in the stars, we reproduce so the species survives, we die and we become inert again... but.... where do we come from?

- That one I know, from the Big Bang ∼15.000.000.000 years ago, and from there on... before no time can be defined... In fact, we have a decent understanding of what happened from $\sim 10^{-10}$ seconds after it until now, which looks quite amazing... although it is true that in energy scale, we are several orders of magnitude below the Planck mass....

- but I think it is an allowed to question to ask why.... why all this?

- Why? Come on...!! You just ask how!!! Otherwise you should go to the philosophy school then and do some bla bla bla...

- You mean a physicist should not look for the reason why things happen, be happy with just a phenomenological description of how things work...? I believe the separation between *why* and *how* is not so well defined... and I want to use the scientific method, test my theories and reject them if proven to be false!!

- OK... You know, we are just the result of evolution... let's say 4.000.000.000 years ago life started, random mutations and evolution get the fittest to survive, reproduce and therefore to evolve and we are here, with our brothers the chimpanzees... so we have just the brain and senses needed to understand how some things work to be able to survive, live a couple of years, but not much more... In fact some people seem to have just the brain to *pass* the day :)...

- I guess that is the reason why when deadlines approach my brain works better, because then it is no longer a matter of curiosity but of survival... :) but really, why does everything exist?

- The why questions seem beyond our capacities... I guess we ask where do all atoms come from? from stars... and why do stars shine? and we can find an answer... because of nuclear fusion... but why are there protons? Because of QCD's phase transition... and Helium nuclei? Nucleosynthesis in the Early Universe, 3 minutes after the Big Bang... and when do Hydrogen atoms form? at recombination, below Hydrogen's binding energy... in fact the CMB is a *snapshot* of 380.000 years after the Big Bang, when protons and electrons combined to form hydrogen, that is a pretty amazing *picture* of the Big Bang... and quarks and leptons? Probably some GUT, SO(10)... and three families? some flavour symmetry... but why these symmetries? String Theory... and so on... but why does the Universe *exist*?

- I deeply think there is a logic in all this... Quantum fluctuations of some field... we have even recently discovered gravitational waves from inflation! We are speaking about times as early as $\sim 10^{-36}$ seconds... in any case, it is true that without knowing what are dark matter and dark energy, and the inflationary model, and a quantum theory of gravity, we seem to be far from this question....

- so you really think that everything can be described in a mathematical way...

- Mathematics are just a language, a tool... I don't believe in a deep meaning of a perfect Platonic triangle... we invent mathematics, some do describe Nature extremely well, some are good approximations of it and some have nothing to do with it... but there always seem to be a *why* question to which we have no clue...

- So we give up and enjoy life...

- What!!??

- We said it was going to be hard, we have begun the soccer match with the leg injured, just one eye, no contact lenses and with a headache, but for sure there is a logic in all this mess, a pattern, a symmetry that got broken by quantum fluctuations in the Big Bang and gave all this apparent non-sense... (don't ask me *why* that symmetry please...) but don't be pessimistic, we know a lot, even if it is true that we don't know most of it... from a working perspective it is good news: there are many things to investigate...

- Yes, you are right... So what do we do?

- We continue... being smarter... working harder.... we should build an enormous accelerator, precise satellites, super-pure underground experiments... As you know, one can do physics in several different ways:

  - Build experiments without a particular motivation, trying to see if Nature reveals any of its mysteries.
  - Based on some theoretical and/or experimental motivation, propose a complete new theoretical framework, with a strong mathematical background needed, and try to test it, probably in the very long run, as you are in the frontier of theory/experiment.

  - Try to explain some experimental result which is not understood, proposing a new model with new particles, interactions... which hopefully will give signals in other experiments, so it can be tested in the near future.
  - and so on...

  Choose your preferred way, and go for it...

- OK, I like the idea of proposing testable models, and trying to understand strange experimental results...
- So in which topic would you like to do your research? The time in History is important... maybe we don't have the knowledge, or it is not the time, to solve the flavour puzzle... or to unify gravity and quantum physics, remember that not even Einstein could, and that guy was kind of smart... and these theories can be difficult to test... Neutrinos have recently been discovered to have masses and we still don't know how they get them...
- That sounds really interesting...!
- But keep and eye on dark matter, it could be the next one to be discovered. Its experimental situation looks pretty much like the confusing situation with neutrino oscillations some years ago...
- That sounds also great!
- Good luck!

Agradecimientos

Nunca habría podido realizar esta tesis sin la educación, guía y ayuda que muchas personas me han brindado. Algunos no han participado directamente, pero mi salud mental y estado de ánimo depende de ellos, y repercute directamente en la ciencia que hago, así que todo el mundo que aquí aparece, y otra mucha gente que me habré dejado, ¡me ha ayudado de una manera u otra!

Quiero empezar por mis padres, para los que mi educación ha sido y es lo más importante. En concreto, desde su experiencia, me han dado buenos consejos, como que tan importante o más que que rodearte de gente competente, es hacerlo de buenas personas. Creo que de mi madre he sacado como virtudes científicas la pragmaticidad, la eficiencia, la enorme capacidad de trabajo cuando estamos motivados, el ser *echado para adelante* y mi capacidad de socialización, y de mi padre la capacidad de abstracción, la imaginación, la profundización a largo plazo en un tema, la inteligencia e interés a la hora de aprender algo nuevo, y el intentar siempre ver el bosque sin quedarse únicamente en los árboles, buscando la perspectiva y la visión de conjunto. La mezcla ideal no es fácil de conseguir, todo tiene pros y contras, y a veces se peca de correr, y otras de divagar... ¡pero estoy contento de la lotería genética!

A mis tías quiero agradecerles que, aunque nunca he conseguido que entiendan lo que hago, siempre me han apoyado, y ponían velas en los exámenes. También quiero agradecer a mis tíos y primos, por apoyarme, interesarse y animarme, y porque siempre me encuentro muy a gusto con ellos. En especial a mi tío Alejandro, por interesarse mucho por la física, y por decirme en el bachiller (más allá de que se compinchara con mis padres y otros tíos míos para que hiciera medicina) que física no era una carrera, era *la* carrera. Y también quiero recordar a mi tío Ramón, con el que conversaba de ciencia en las comidas familiares, y al que se le echa de menos.

En segundo lugar quiero agradecer a mis directores de tesis, Arcadi y Nuria, que creo que me han guiado con acierto en esta andadura. Con ellos el trato ha sido siempre más que bueno y fácil, y las puertas de sus despachos

siempre han estado abiertas. De ambos he aprendido muchas cosas. Además quiero agradecerles la lectura de esta tesis y las sugerencias que me han hecho.

De Nuria espero haber aprendido su seriedad y rigor científicos, su espíritu crítico, por ejemplo analizando en profundidad un artículo, y su detallismo al escribir un paper, pensando con cuidado cada frase, y le agradezco su buena dirección. Además siempre se ha preocupado por las mil cosas que conlleva hacer una tesis (y que parece que no están, pero que están), desde el millón de burocracias torturadoras a las decisiones de estancias, de dar charlas, de conferencias, visados, informes, memorias.. y un largo etc.

De Arcadi me conformo con que se me haya pegado algo de su capacidad matemática e intuición física, y de su tesón y resistencia al abandono, *el picarse* hasta que se resuelve la maldita integral o lo que sea. Le quiero agradecer las charlas de física en la pizarra de su despacho, y las miles de dudas que siempre me ha resuelto, incluyendo entre ellas una buena dosis de informáticas, así como su preocupación en las distintas facetas asociadas a la realización de una tesis.

En fin, ¡muchas gracias a los dos!

Y mención especial también a Thomas, el cual me acogió en Heidelberg con los brazos abiertos, y me introdujo en un muy buen tema de candente actualidad. Con él he tenido la oportunidad de seguir colaborando y espero seguir haciéndolo en mi nueva andadura. Ojalá se haya producido cierta ósmosis hacia mi persona de su increíble capacidad en todo lo relacionado con el trabajo científico. Para mí ha sido casi como un tercer supervisor, y no puedo más que agradecérselo.

También quiero agradecer a André la posibilidad de haber ido a Chicago, estancia que me resultó muy provechosa en todos los aspectos. Respecto a la física me permitió introducirme en el mundo de las teorías efectivas, que me han resultado muy interesantes. Además quiero agradecerle la ayuda que me brindó para dar charlas, por ejemplo en Fermilab, donde disfruté mucho del grupo tan activo que hay en física.

A todos ellos quiero además agradecerles sus cartas de recomendación a la hora de solicitar postdoc, que he conseguido.

Quiero también agradecer a los miembros del tribunal la lectura de esta tesis y las sugerencias que me han hecho. En especial a Sergio y Laura, que me han dicho una buena cantidad de typos y de útiles sugerencias.

Y también hacer una mención especial al resto de personas con las que he podido colaborar, Alberto, Jure, Nassim, Andrew y Miguel, con los que he trabajado muy a gusto.

Especialmente agradecido estoy a Alberto, que siempre ha estado allí voluntarioso, más que disponible para resolverme dudas de todo tipo, especialmente latexianas, de consola, de mac... etc.

Acto seguido quiero nombrar a mi grupo: a Pilar, Carlos y Olga, por las ayudas de todo tipo y las conversaciones mantenidas, y porque siempre me han tratado como uno más. Sobre todo quiero agradecerles todo lo que he disfrutado atendiendo a las Trobadas, hablando de física con ellos de tú a tú... ha sido un placer. Y a Carlos también agradecerle las divertidas rutas gastronómicas en las conferencias.

Del departamento quiero mencionar especialmente a Vicente Vento y a Óscar, con los que he compartido asignatura y ha sido muy fácil y sencillo, y siempre me han ayudado. A Vicente también le agradezco su carisma, las risas y la vida que le da al departamento.

Al resto del departamento y del IFIC, en los que me he sentido como en casa. Ha sido un privilegio y una suerte el haber estado aquí con vosotros haciendo el máster y el Doctorado.

También quiero destacar la ayuda, consejos, y charlas de física de un gran número de colegas (y amigos) del mundo de la física: Mattias, Enrique, que conocí en Moriond, Laura, Philipp, Yasutaka, Kher Sham... etc, con los que me lo pasé muy bien en Heidelberg, y una larga lista de colegas y amigos físicos, a bote pronto: Ana Rodrǵuez, Juan González, Bogna, Joan, Miki y Miguel (Cargese estuvo genial), Rodrigo, Florian, Jacobo, Pilar, Juan Racker, Jordi Salvado idem en Florencia, Martín en Argonne, Ignacio, Elena, Valentina en Durham, Avelino, Javier Redondo, Walter y los Madrid-Bayern exitosos, Tommy, Belén Gavela, Sergio Palomares... etc.

Dicho ésto, quiero remontarme a mis principios en la ciencia. Y creo que hay dos nombres propios que me han marcado en Primaria-Secundaria, y en el Bachillerato, y que me han llevado por el camino correcto. El primero es mi primera profesora de matemáticas y de ciencias (aunque es química) María Pilar Alegre[1], la cual me hizo entender lo que era el rigor, aprendí mucho y vi qué era la ciencia, aunque fuera orientada más a la química y la formulación.

El segundo nombre propio en orden cronológico es Miguel Ángel Per, mi profesor de física en el bachiller, físico teórico, y el que creo que me dió el empujón definitivo para estudiar física: lo explicaba todo tan bien, que con atender en clase, que me encantaba, y con una lectura de los apuntes y un par de ejercicios ibas al examen y sacabas un 10. Además le hacías preguntas, razonaba, y a veces incluso se paraba a pensar, dudaba... una novedad para

[1]No quiero dejar de agradecer a Javier su paciencia conmigo, como me decía cuando no callaba en clase, *un hijo único*, y a Elena su empeño en que escribiera bien: me haría escribir varias decenas de cuadernillos Rubio. También a María Pilar Gómez, que era puro corazón.

mí.[2] También llegaba a clase, veía una barbaridad[3] de otro profesor cuyo nombre no diré y cuya preparación y esfuerzo no comentaré, y lo corregía. Allí por fin me di cuenta de que había salida más allá de la memoria: ¡el razonamiento! ¡Y que encima llevaba menos tiempo y era más gratificante e inapelable, universal! Además me apoyó para el premio final de bachillerato, y años después en la Universidad hablamos y me animó a que siguiera en la física.

De la facultad de Zaragoza, quiero agradecer especialmente a Manuel Asorey, por darme la oportunidad de ir a Southampton, ayudarme en todo, y por sus consejos más allá de la física. A José Luis Cortés, con el que disfruté muchísimo en Mecánica Cuántica, y con el que hablé y me ayudó a orientarme para hacer una tesis. A Vicente Azcoiti, por hacer de Relatividad General algo sencillo y un disfrute, y por el 10 ;). Al resto de profesores que me han enseñado cosas, como Fernando Falceto, Antonio Seguí, María Luisa Sarsa, Jesús Atencia (por sus clases de física de primero), Jorge Puimedón, Morellón, Rebolledo (por sus cartas para ir a un curso de verano), Juan Vallés, Forniés (porque electromagnetismo la disfruté mucho), García Vinuesa (por hablarnos de posibilidades de futuro y ser accesible), a Ramón Pla (por corregirme solicitudes en inglés)...

De Southampton solo tengo buenos recuerdos. Quiero agradecer a Nick Evans la asignatura que más he disfrutado en mi vida, Particle Physics, cada hora de clase era un auténtico placer. Recuerdo leerme los apuntes antes de ir allí, como quien va al cine, a disfrutar como un enano. También a Steve King por sus didácticas clases, a Alexander Belyaev por ofrecerme la oportunidad de que me quedara, a Beatriz de Carlos, cuyo examen sólo logramos hacer los tres españoles, y por charlas más allá de la física, y en general a toda la Universidad y los profesores, que daban apuntes perfectos antes de que empezara el curso, que te permitían atender y no copiar cual chimpancé rápido y mal, e incluso leértelos antes de ir a clase y poder ir con dudas pensadas, y que ponían los exámenes antes del curso, de forma que sabían lo que tenían que explicar, ¡y en el examen preguntaban cosas que habían dado o comentado en clase!

También quiero agradecer a José González el tiempo que disfruté en Madrid gracias a la Beca de Introducción a la Investigación del CSIC, fue una gran experiencia y resultó muy provechosa.

También a mis compañeros de la carrera, Micha, Noe y Ceci. Al primero por sus llamadas para comentar dudas del día de antes y por ser uno de mis

[2] Como una vez que le pregunté cómo se medía la entropía de gases y estuvo un rato pensando...

[3] ¡Que las ondas penetraban o no cuerpos dependiendo de su amplitud!

mejores amigos, a Noe por ser una buena compañía tanto en la carrera como en Southampton y por supuesto fuera de la física. Y especialmente a Ceci, mil gracias por no se cuántos apuntes que me has pasado, por preparar exámenes juntos, por comentar dudas etc. Creo que todos fuimos un buen equipo. Y a Jacobo por los buenos ratos en Southampton.

Quiero mencionar ahora a mis amigos. A los de Zaragoza, en especial a Juan Artigas, con el que mantuvimos mil conversaciones los primeros tiempos de carrera y nos apoyamos mutuamente. A Víctor, porque llevamos vidas paralelas en todo desde los cuatro años, hemos compartido mil cosas y es como un hermano para mí. Al resto, por los buenos ratos pasados: a Checo, por las mil risas y por su amistad, a Chemi, que aun cree que hago química, y por las anécdotas, como cuando me quitó mi examen (en mitad del examen al ir a preguntar al profesor) ¡y yo no lo encontraba!, a Flo por hacer que las teclas de mi mac vayan mal, al rematar de cabeza un cubata al ir a coger algo del suelo, cuando les estaba torturando con una charla divulgativa de física en Salou, a Héctor por interesarse por la física, aunque solo se le haya quedado por algún motivo la teoría del Big Rip (o Gran Desgarro), y porque gracias a él he aprendido técnicas que no me explican en la carrera, como *la del aguante*, *la de la huida* o la del *revoloteo*, a Pepe por el tiempo en Madrid cuando estuve de estancia y le ocupaba su estante en la nevera con pasta para la semana entera, a Mateo por las risas con sus bolis bic enciclopédicos y los exámenes para los que necesitan dos horas de estudio y acababan no presentándose, y por seguir preguntándome "pero lo que haces... ¿para qué sirve?" y yo no conseguir explicárselo, y a Ramiro por ser un gran jugador de póker y ponérmelo difícil, y por las mcuhas risas, a Guti por nuestras salidas de fiesta, por aconsejarme que me opere el tabique y porque cada vez que recuerdo lo de "estoy en Modo" a las 7 de la mañana estando en Salou me va a dar algo... a Alejandra por nuestras conversaciones... al resto del grupo... a Chicho, Laura, Iñaki, María etc etc... gracias.... A David y Alex, por las charlas técnicas sobre el póker.... y a todos los demás.

A los de Valencia. A Alberto, por ser un gran amigo, por todo, por las mil conversaciones que hemos tenido, por haber estado ahí.... A Clarilla, por ser una de las mejores personas que conozco y una gran amiga. A Javi, por ser una gran persona, por las risas, por las fiestas, por los ratos de teoría y análisis de probabilidad del póker en la pizarra de tu despacho... A Oli, tras saber la teoría, porque gracias a él aprendí a jugar al póker de verdad, con depuradas técnicas como *la de la grúa* o la del *all-in sin ver cartas*, y por los mil ratos pasados de fiesta y nuestras anécdotas... A Antonio, por los ratos disfrutados juntos tanto en el IFIC como fuera, y por las conversaciones con unas cervezas, y también por ayudarme con alguna que otra duda informática... A Gammerman, por tu movimentación hasta la

conquista y por las anécdotas.... a Vido, por nuestras conversaciones y por ser entrañable, y porque además hiciste que recuperara la fe, a Montse, por la ilusión y por todo... y por tu amistad, que deseo continúe en el futuro... A Mira, por ser divertida y genial... ¡aunque a veces no nos deje dormir! ;) A Joaquín, por el rescate tras el naufragio, y por las historias disfrutadas juntos... a Beni, por las conversaciones profundas que disfruto, y por las risas y los buenos momentos, y por abrirme los ojos al póker de verdad al jugar contra ti y al hablarme de un libro, y a Diana, por estar siempre de buen humor, con una sonrisa en la cara... a Carmen y al resto por los buenos momentos que hemos pasado... A David Castelló, por ser mi primer amigo en Valencia, por las pizzas de los jueves de mi primer año, porque recién llegado me introdujiste en tu círculo valenciano... a Ivana, por habérnoslo pasado muy bien y por tus detalles... a Andrea, por las risas, y por recordarme que las *resistencias* en serie y en paralelo son muy diferentes :) ... a Agustín, por nuestras conversaciones y su buena compañía en las comidas del IFIC, a Francesca, aunque tenga poca fé en mis posibilidades ;), a María, aunque te hayas ido, por ser una gran amiga con la que lloro de risa... a Carl, por las cenas en el Kin-Ma y nuestras conversaciones... a Ebe, por nuestras largas conversaciones de café en el IFIC, y por ser una confidente espectacular... a Miguel, más allá de la física, por tu sentido del humor particular que ameniza las comidas, y por nuestras conversaciones políticas... a Joan (y Oli, claro), por los ratos de póker cash en casino y por enseñarme a floatear, a Rubén, Nuria, Aaron (con el que he compartido algunas conferencias, y por leerse el capítulo de cosmología y sugerirme algunas pequeños cambios), Alex Celis, Alberto Filipuzzi, Elena, Manu, Francesc, Juan Racker, Marija, Marisa, Marga, Luis, Adrián, Rafa, Raquel, Japepe, Joel ... etc por hacer más divertido el trabajo y por lo que hemos compartido juntos.

A los amigos del colegio (Diego, Álvaro, Pedro, Miguel, Laura, Ana...) y más recientemente al equipo de fútbol, al de frontón, al de los torneos de póker de los viernes... por darle diversión a la rutina...

A mis amigos del pueblo... gracias porque siempre que voy parece que nos vimos ayer, desde las cabañas en la prehistoria, pasando por los partidos de fútbol, las rutas en bici, el Ronda, los baños en el río, el local, las múltiples fiestas y risas en pueblos y en Jaca y muchísimas otras vivencias... En fin, siempre disfruto volviendo a las raíces.

A (algunos de) mis compis de piso a lo largo de éstos años, como Tanit, por su tenacidad con los problemas e inteligencia, y porque siempre estás de buen humor, a Lola, por los desfases y nuestras charlas en el sofá de la terraza, a David y a Aritz con los que la convivencia es tan fácil... y a la vecina, sin la cual habría muchas más fiestas en mi casa ¡y por lo tanto menos trabajo!

A mis amigos de Chicago, a Luiza, por todo y por venirte a Seattle conmigo, a Alejandra, por ser una buena amiga, a Tommasso, porque nos entendemos a la perfección, y por nuestras historias paralelas en Chicago... a Gabi, porque eres una grande y me acogiste en tu grupo como uno más, a Luca y a Antonella por los ratos divertidos, a Ben por tu inteligencia social e intuición, sabiendo cosas de mí antes que yo mismo... y a Samara por nuestras conversaciones... gracias a vosotros mi paso por Chicago fue increíble...

Los que me he dejado y creéis estar, ¡seguro que estáis!

Para finalizar, quiero agradecer al *difunto* Ministerio de Educación, Ciencia e Innovación (MICINN)[4] el permitirme realizar la tesis con una beca FPU y dos estancias de investigación en el extranjero, y en general por apostar por la investigación y el conocimiento, así como a los distintos proyectos que me han permitido financiar la asistencia a escuelas, congresos y conferencias: de la Unión Europea FP7 ITN INVISIBLES, MRTN-CT- 2006-035482 (FLAVIAnet); de MINECO: FPA-2007-60323, FPA2011-29678-C02-01 y de la Generalitat Valenciana: PROMETEO/2009/116.

[4]Ahora *ha descendido de categoría* a Secretaría de Estado de Investigación, Desarrollo e Innovación, perteneciente al Ministerio de Economía y Competitividad.

Algunas críticas y sugerencias

Desde mi humildad y experiencia quiero comentar algunos puntos que en mi opinión son más que mejorables en el funcionamiento de la educación y el sistema científico en general, y el español en particular.

Primero debo decir que muchos de mis profesores nos obligaban en muchas ocasiones a memorizar sin sentido. Hago aquí un llamamiento, al mundo educativo: no hagan perder el tiempo a los estudiantes memorizando horrores que van a olvidar tras el examen, enséñenles a pensar, argumentar, imaginar... ojalá no hubiera tenido que aprenderme semejantes ladrillos... el que necesite saber algo de memoria lo estudiará en su momento (por ejemplo en Derecho o Medicina) y siempre puede acudir a las referencias. Practicar y ejercitar la memoria en una dosis prudente puede ser discutible, basar el sistema en recitar la lección cual loro que no sabe ni lo que dice, no. Lo importante es el razonamiento y el conocimiento, no la erudición. Lo fundamental es la pregunta, no la respuesta.

Y hago un segundo llamamiento de algo que me ha enervado desde el día uno de mi Doctorado (realmente incluso antes, al pedir becas), que me ha frustrado, que mi cabeza no logra comprender: por favor, señores que organizan las cosas, políticos y burócratas, ¿saben ustedes que nos ahogan en burocracias estúpidas? Es una auténtica barbaridad. No puedo estar haciendo memorias cada tres meses, para viajes, estancias, al volver, de beca, de contrato... y todas con papeles físicos. Como mi amigo David diría, tienen ustedes que tener empapelado un par de cuartos con fotocopias de mi DNI. No puede ser que se dedique el 20% del tiempo a burocracias que no son discriminantes, no aportan nada más que pérdida de tiempo: las haces, nadie las lee, y ya está, aceptan a todos. Para dar clases, un papelito. Irte de viaje, otro, volver, otro, adelanto, otro, expediente compulsado, certificado pago tasas, certificado centro receptor, adscriptor, idoneidad, informe gastos previstos, informe dinero en cuenta, de estar en el periodo de investigación del doctorado, programa trabajo, factura original, otro papel, pasar a contrato otro, empadronamiento para no sé qué, vida laboral, CV, sexenios directores, sus CVs, sus papers, su informe firmado por el director de turno, título

licenciatura, idomas, cursos Doctorado, pago cursos, calificaciones, título máster, inscripción al proyecto, papers físicamente, papeles congresos, papeles charlas, memoria del grupo, otra burocracia, memoria del IFIC, otra vez a poner todo, actas, informes de no sé qué, que el vicerrector firme el 12 de cada mes, que también el director del departamento, todos los papeles sellados a Madrid ... ahora todo ésto en inglés, español, valenciano y para un postdoc en Italia en italiano... cojonudo...

¿¡De verdad es necesario todo esto!? ¿No es suficiente con que pida la beca entregando todo telemáticamente y si me la dan, ya está, me dejan investigar y dar clases? ¿Es necesario rellenar informes que no discriminan, que los aprueban a todo el mundo y solo me hacen perder el tiempo en lugar de investigar? Que es más difícil presentarte bien a Selectividad (día, hora, pegatinas, colores, no firmar, escribir por una cara, etc etc) que hacer bien el examen, e ídem con la tesis... que David tuvo que hacer un pdf de 4 hojas para aclararse con la burocracia... que le piden matrícula en el doctorado, inscripciones, informes de 6 personas (no sé cuántas mujeres, no sé cuántos de la universidad, no sé cuántos de fuera), y además de esto, ¡le piden hasta la partida de nacimiento pare recoger el título! Por favor, que ha nacido... creedme... puede que la probabilidad de que nos haya engañado durante 30 años no sea estrictamente nula, pero vamos a jugárnosla, va, ¡¡¡aunque sólo sea por esta vez....!!! La última gran burocracia absurda, para un contrato, es pedirme un certificado de *no* disponer del título de Doctor, un título de no tener el título, sería de risa si no fuera porque lo necesito de verdad, y a ver cómo se consigue... Y de nuevo otra vez me piden el título de Licenciatura (cuando he hecho el máster, estoy inscrito en el Doctorado etc.), que les tendré que llevar tras descolgarlo de la pared, con marco y todo. En serio, intenten reducir la burocracia hasta el mínimo posible, por favor.

Y digo ésto yo que soy un *mindundi*, y ya constato como año a año los papeleos que debo hacer crecen exponencialmente, no me puedo imaginar ni quiero pensar lo que tiene que hacer un profesor, un catedrático, un investigador principal de proyecto, un director de departamento o el director de un instituto. ¿De verdad hay que ahogar a la gente más brillante en papeles?

Y un tercer canto al aire, aunque suene extraño: publicar demasiado debería estar penalizado... casi debería haber un máximo de papers con los que alguien puede inundar el arxiv anualmente... Estamos inundados de información, crece exponencialmente, cuesta estar al día, y más aún separar la paja del trigo. Muchos papers no dicen objetivamente nada nuevo; no podemos valorar la ciencia a peso, hay que encontrar otro baremo (tampoco sólo las citas)...

Espero que alguien pueda hacer algo respecto de estos tres puntos, que

en mi modesta opinión son más que importantes... si no, al menos me he podido desahogar. Y espero que en España se siga (o mejor dicho, *se vuelva*) a apostar por la ciencia, el conocimiento y la innovación como únicas vías para el progreso y bienestar humanos. Fin.